

Development of membranes for low and intermediate temperature polymer electrolyte membrane fuel cell

A thesis submitted for the degree of

Doctor of Philosophy

by

Chenxi Xu

Supervisor: Professor Keith Scott

Dr. Eileen Yu



School of Chemical Engineering and Advanced Materials

Newcastle University

June 2013

Abstract

Proton exchange membrane fuel cells (PEMFCs) are promising electrochemical energy conversion devices, which are based on high cost materials such as Nafion[®] membranes. The high cost and limited availability of noble metals such as Pt hinder the commercialisation of PEMFCs. The research described in this thesis focused on the development of composite materials and functionalised polymer membranes for intermediate temperature PEMFCs that operate in the temperature range of 120 to 200°C. A higher operating temperature would enhance the kinetics of the cell compared to a perfluorinated polymer membrane based cell and provide a greater opportunity to use non-noble metal electrocatalysts.

Inorganic–organic composite electrolyte membranes were fabricated from Cs substituted heteropolyacids (CsHPAs) and polybenzimidazole (PBI) for application in intermediate temperature hydrogen fuel cells. Four caesium salts of heteropolyacid, ($Cs_xH_{3-x}PMo_{12}O_{40}$ (CsPOMo), $Cs_xH_{3-x}PW_{12}O_{40}$ (CsPOW), $Cs_xH_{4-x}SiMo_{12}O_{40}$ (CsSiOMo) and $Cs_xH_{4-x}SiW_{12}O_{40}$ (CsSiOW)), and an ionic liquid heteropolyacid were used to form composite membranes with PBI. The membranes were characterised by using SEM, FTIR and XRD. The CsHPA powders were nano-size as shown in the XRD and SEM data. The CsHPA/PBI composite membranes, loaded with H_3PO_4 had high conductivity, greater than that of a phosphoric acid loaded PBI membrane. Cs substituted heteropolyacid salt showed better enhancement of conductivity than that provided from ionic liquid heteropolyacid salt. The conductivity increased with an increase in the percentage of powder in the composite. The 30% CsPOMo/PBI/ H_3PO_4 exhibited a conductivity of 0.12 S cm^{-1} under anhydrous conditions although its mechanical strength was the poorest, but still promising with a value of 40 MPa. The performance of the hydrogen fuel cell with composite membranes was better than that with a phosphoric acid-doped PBI membrane under the same conditions. The CsPOMo gave the best power density, of around 0.6 W cm^{-2} with oxygen at atmospheric pressure.

A novel method was used to prepare poly (ethylene oxide)/graphite oxide (PEO/GO) composite membrane aimed for low temperature polymer electrolyte membrane fuel cells without any chemical modification. The membrane thickness was 80 μm with the GO content was 0.5 wt. %. SEM images showed that the PEO/GO membrane was a condensed composite material without structure defects. Small angle XRD for the resultant membrane results showed that the d-spacing reflection (001) of GO in PEO matrix was shifted from

$2\theta=11^\circ$ to 4.5° as the PEO molecules intercalated into the GO layers during the membrane preparation process. FTIR tests showed that the vibration near 1700 cm^{-1} was attributed to the -COOH groups. The ionic conductivity of this PEO/GO membrane increased from 0.086 S cm^{-1} at 25°C to 0.134 S cm^{-1} at 60°C and 100% relative humidity. The DC electrical resistance of this membrane was higher than $20\text{ M}\Omega$ at room temperature and 100% relative humidity. Polarisation curves in a single cell with this membrane gave a maximum power density of 53 mW cm^{-2} at temperature around 60°C , although an optimised catalyst layer composition was not used.

Polybenzimidazole/graphite oxide (GO /PBI), sulphonated graphite oxide/PBI and ionic liquid GO/PBI composite membranes were prepared for high temperature polymer electrolyte membrane fuel cells. The membranes were loaded with phosphoric acid to provide suitable proton conductivity. The PBI/GO and PBI/SGO membranes were characterised by XRD which showed that the d-spacing reflection (001) of SGO in PBI matrix was shifted from $2\theta=11^\circ$, meaning that the PBI molecules were intercalated into the SGO layers during the membrane preparation. A low acid loading reduced the free acid in the membranes which avoided water loss and thus conductivity loss. The ionic conductivities of the GO /PBI and SGO/PBI and ILGO/PBI membranes, with low acid loading, were 0.027 S cm^{-1} , 0.052 S cm^{-1} and 0.025 S cm^{-1} at 175°C and 0% humidity. Fuel cell performance with SGO/PBI membranes gave a maximum power density of 600 mW cm^{-2} at 175°C .

A quaternary ammonium PBI was synthesised as a membrane for applications in intermediate temperature ($100\text{-}200^\circ\text{C}$) hydrogen fuel cells. The QPBI membrane was loaded with phosphoric acid (PA) to provide suitable proton conductivity and compared to that of a similar PA loading of the pristine PBI membrane. The resulting membrane material was characterised in terms of composition, structure and morphology by NMR, FTIR, SEM, and EDX. The proton conductivity of the membrane was 0.051 S cm^{-1} at 150°C and a PA acid loading of 3.5 PRU (amount of H_3PO_4 per repeat unit of polymer QPBI). The fuel cell performance with the membrane gave a peak power density of 440 mW cm^{-2} and 240 mW cm^{-2} at 175°C using oxygen and air, respectively.

Inorganic–organic composite electrolyte membranes were fabricated from $Cs_xH_{3-x}PMo_{12}O_{40}$, CsPOMo and quaternary diazabicyclo-octane polysulfone (QDPSU) using a polytetrafluoroethylene (PTFE) porous polymer matrix for applications in intermediate temperature (100-200°C) hydrogen fuel cells. The CsPOMo/QDPSU/PTFE composite membrane was made proton conducting using a relatively low phosphoric acid loading to provide the membrane conductivity without compromising the mechanical strength to a great extent. A casting method was used to build a thin and robust composite membrane. The resulting membrane materials were characterised in terms of composition, structure and morphology by EDX, FTIR and SEM. The proton conductivity of the membrane was 0.04 S cm^{-1} with a PA loading of 1.8 PRU (amount of H_3PO_4 per repeat unit of polymer QDPSU). The fuel cell performance with the membrane gave a peak power density of 240 mW cm^{-2} , at $150\text{ }^\circ\text{C}$ and atmospheric pressure.

A composite material for phosphoric acid (PA) loaded membrane was prepared using a porous polytetrafluoroethylene (PTFE) thin film. N, N-Dimethylhexadecylamine partially quaternised poly (vinyl benzyl chloride) (qPVBzCl⁺) was synthesised as the substrate for the phosphoric acid loaded polymer membrane. The qPVBzCl⁺ was filled into the interconnected pores of a PTFE thin film to prepare the PTFE/qPVBzCl⁺ membrane. A SEM data indicated that the pores were filled with the qPVBzCl⁺. The PA loading was calculated to be on average 4.67~5.12 per repeat unit. TGA results showed that the composite membrane's was stable at intermediate temperatures of $100\text{ }^\circ\text{C}$ to $200\text{ }^\circ\text{C}$. The composite membrane's tensile stress was 56.23 MPa, and Young's Modulus was 0.25GPa. The fractured elongation was 23%. The conductivity of the composite membrane after PA addition (PTFE/qPVBzCl⁺/ H_3PO_4) increased from 0.085 S cm^{-1} to 0.1 S cm^{-1} from $105\text{ }^\circ\text{C}$ to $180\text{ }^\circ\text{C}$. The peak power density of the H_2/O_2 fuel cell, at $175\text{ }^\circ\text{C}$ under low humidity conditions (<1%), with the PTFE/qPVBzCl⁺/ H_3PO_4 membranes was 360 mW cm^{-2} .

Acknowledgement

Over the last three years I have been blessed with the opportunity to work with people in the fuel cell group who provided me encouragement, guidance and help unconditionally. I would like this occasion to thank and acknowledge some individuals who especially stood out.

First and foremost thank you, Professor Keith Scott, my supervisor and mentor, who offered this fantastic opportunity to work on this project. Your earnest guide and edification has helped to improve my research ability and your patience and generosity have become profound and beautiful impressions in my heart, which will be valuable mind treasures in my whole life. I am truly grateful for all these.

Dr. Eileen Hao Yu, my second supervisor, who also provided a lot of support both technical and moral with great encouragement.

I am very thankful Prof. Qingfeng Li who offered me opportunity working in DTU and gave me a lot of guidance and encouragement both in research and daily life during I have been visiting in Denmark.

I would like to thank the UK EPSRC Supergen program for the financial support.

Thanks to my parents, who always encourage and support me when I make any decision in my life. Thanks for forgiving not being able to often accompany them.

Thanks to Dr Xu Wu who taught me so much knowledge and technology both on research and communication, and shared his idea with me. I am thanking for Dr. Xu Wang who provided me the QDPSU material and taught me fill the material into PTFE. Thanks to Dr. Yuancheng Cao who taught me the synthesis Graphite oxide and provided me dimethylhexadecylamine quaternized poly (vinyl benzyl chloride)/PTFE membrane. Dr Cao also helped me a lot on polymer synthesis. I would like to say thanks to Dr. Mohamed Monlouk who managed lab safety and was helpful about necessary materials. I am thankful for Mr. Lei Xing who joins our group later but always encourage me. Thanks to Ravi who provided sulfonate Graphite oxide. Many thanks to lab mates Aris, Vinod, Ravi, Aiser Ukrit and so on. Thanks to Professor Niels J. Bjerrum, Mr. Chao Pan, Mr. Jingshua Yang, Dr. Lars N. Cleemann, Dr. Jens Oluf Jensen give me a lot help during in Denmark. Thanks to all the facilities that support my PHD thesis.

Table of Content

Abstract	I
Acknowledgement	IV
Table of content	V
List of Figures	IX
List of Schemes	XIV
List of Tables	XV
Abbreviations and Symbols	V
Chapter 1. Introduction and Objectives	1
1.1 Overview	1
1.2 Project Objective	2
references	4
Chapter 2. Literature Review	6
2.1 Fuel Cell	6
2.2 Proton exchange membrane fuel cell (PEMFC)	10
2.3 Performance measures of Fuel cells	12
2.4 Intermediate temperature PEMFC	13
2.5 Electrolytes	14
2.5.1 Proton conducting materials	14
2.5.1.1 Perfluorosulphonic acid (PFSA) polymer membranes	14
2.5.1.2 Polybenzimidazole	18
2.5.1.3 Quaternary polymer and PTFE support composite membranes for PEMFC	26
2.5.2 Inorganic filler for composite membranes	30
2.5.2.1 Heteropolyacid and Polyoxometalate/polymer composite	30
2.5.2.2 Graphite oxide used in composite polymer membranes	36
2.6 Electrode	39
2.7 Conclusions and perspectives	42
References	43

Chapter 3. Theoretical	59
3.1 Thermodynamic and kinetic for the fuel cell	59
3.1.1 Thermodynamic	59
3.1.2 Electrochemical kinetic	61
3.2 Proton conducting mechanism	64
3.3 Percolation theory	65
References	69
Chapter 4: Experiment	71
4.1 Membrane preparation	71
4.1.1 PBI membrane preparation	71
4.1.2 Cs and BmIm substitute Heteropolyacid	71
4.1.3 Preparation of graphite oxide and functional graphite oxide	72
4.1.4 PEO/GO membrane preparation	73
4.1.5 PBI/GO membrane preparation	74
4.1.6 Synthesis of quaternary PBI	74
4.1.7 Caesium Salt of Heteropolyacids/Quaternary diazabicyclo-octane Polysulfone/PTFE composite membranes	75
4.1.8 dimethylhexadecylamine quaternized poly (vinyl benzyl chloride)/PTFE composite membrane	77
4.2 Sample Characterization and instruments	77
4.2.1 Conductivity measurement	77
4.2.2 Electrode preparation	79
4.2.3 Membrane electrode assemblies (MEA)	80
4.2.4 Fuel cell performance test	81
4.2.5 Mechanical Strength	81
4.2.6 Scanning electron microscope (SEM) and Energy dispersive X-ray spectroscopy (EDX)	83
4.2.7 X-ray diffraction (XRD)	84
4.2.8 Fourier Transform Infrared (FTIR)	87
4.2.9 Nuclear Magnetic Resonance (NMR)	89
References	90

Chapter 5: Caesium and ionic liquid substituted Heteropolyacid/PBI composite membrane	92
5.1 Introduction	92
5.2 Results and discussion	93
5.2.1 Pristine PBI membrane as a Benchmark and acid loading to membrane	93
5.2.2 SEM	96
5.2.3 FT-IR	98
5.2.4 XRD	100
5.2.5 Conductivity	104
5.2.6 Tensile test	112
5.2.7 Fuel cell test	113
5.3 Conclusions	118
References	119
Chapter 6: Graphite oxide/polymer composite membrane	121
6.1 Introduction	121
6.2 GO/PEO composite membrane	123
6.2.1 Results and Discussion	123
6.2.2. Conclusions	130
6.3 GO/PBI and functionalized GO/PBI composite membranes	130
6.3.1. Results and discussion	131
6.3.2 Conclusions	142
References	143
Chapter 7 Functionalized PBI	145
7.1. Introduction	145
7.2 Results and discussion	145
7.3 Conclusion	154
References	155
Chapter 8 Poly (tetrafluoroethylene) support composite membranes	156
8.1 Introduction	156

8.2 Caesium Salt of Heteropolyacids/Quaternary diazabicyclo-octane	
Polysulfone/PTFE composite membranes	157
8.2.1 Results and Discussion	157
8.2.2 Conclusions	164
8.3 Dimethylhexadecylamine quaternized poly (vinyl benzyl chloride)/PTFE	
composite membrane	165
8.3.1 Results and discussion	165
8.3.2 Conclusions	169
References	171
Chapter 9 Conclusion and perspectives	173
9.1 Conclusions	173
9.2 Future research recommendations	174
References	176
Appendix: List of Publications	177

List of Figures

Chapter 2

Figure 2-1, Comparison of fuel cell performance with other energy conversion systems	7
Figure 2-2, Schematic picture of a PEMFC fuel cell	10
Figure 2-3, Structure of a single MEA (GDL: gas diffusion layer, CL: catalyst Layer, PEM: proton exchange membrane)	11
Figure 2-4, Various voltage losses and resulting polarization curve of an operating fuel cell	13
Figure 2-5, a) Teflon backbone and aromatic side group, b) polyphenylene backbone and pendant fluorosulfonic acid, c) some typical sulfonated aromatic polymers	15
Figure 2-6, Chemical structure of Nafion.	16
Figure 2-7. Proton conduction for PBI membranes, 1) from N-site to another, 2) from N-site to phosphoric acid molecular, 3) via the acid chain, 4) via water molecular	25
Figure 2-8, in plane and the cross section Proton conductivity of the PTFE/PBI composite membrane 3 doping level, and Relative humidity 8.4%	29
Figure 2-9, Polarization and power density curves of a PEMFC with PTFE/PBI composite membranes with H ₂ /O ₂ at 170 °C under 1 bar	29
Figure 2-10, The structure of heteropolyacid: (a) primary (Keggin) structure; (b) secondary (hydrated) structure	31
Figure 2-11, (a) polarization and power density curves of a PEMFC operated at 150 °C atmospheric pressure; (b) polarization and power density curves of a PEMFC operated 150 °C, 1 bar	35
Figure 2-12, Crystal structure of graphite	37
Figure 2-13, The structure of functionalized graphite oxide incorporation with nafion	39

Chapter 3

3-1 Plot of Tafel equation	63
Figure 3-1, Model of percolation, conductive beads (grey), insulation beads (white)	66
Figure 3-2, Typical dependence of conductivity on filler content	68

Chapter 4

Figure 4-1, conductivity measurement system	78
Figure 4-2, Four point probe method to measure the in plane conductivity	79

Figure 4-3, The three phase boundary for porous catalyst layer	80
Figure 4-4, Fuel cell test system	81
Figure 4-5, the tensile test with the dog-bone sample	82
Figure 4-6, Geometry of SEM	84
Figure 4-7, Illustration of Bragg's law	85
Figure 4-8, a harmonic oscillator with two masses	88
Chapter 5	
Figure 5-1, acid doping level of PBI membrane in different phosphoric acid concentration at room temperature about 50 h	94
Figure 5-2, Doping level of the bonded and free phosphoric acid in PBI as a function of the acid concentration	95
Figure 5-3, SEM images of CsPOMo, CsPOW, CsSiOMo, and CsSiOW	96
Figure 5-4, SEM images of membrane cross-sections. (a) PBI/H ₃ PO ₄ (b) 30 wt% CsPOW/PBI, (c) 30 wt% CsSiOMo/PBI (d) 30 wt% CsSiOMo/PBI/ H ₃ PO ₄	97
Figure 5-5. Infrared spectra of a) CsHPA powders b) PBI and CsHPA/PBI composite membrane	99
Figure 5-6, XRD patterns of Caesium salts of heteropolyacid powders	102
Figure 5-7, XRD patterns of PBI membrane, CsPOW/PBI membrane, CsSiOMo/PBI membrane and CsSiOMo/PBI doped membrane with H ₃ PO ₄	103
Figure 5-8, conductivities of PBI, 30 wt% CsPOMo/PBI and 30 wt% BmIm/PBI composite membrane doped with 10 mol/L H ₃ PO ₄ with doping level of 6 under anhydrous conditions	104
Figure 5-9, conductivities of PBI, 30 wt% (CsPOMo:BmIm= 1:3, 1:1, and 3:1)/PBI composite membrane doped with 10 mol/L H ₃ PO ₄ with doping level of 6 under anhydrous conditions.	105
Figure 5-10, the conductivity of CsPOMo powder under anhydrous and humidity conditions	106
Figure 5-11, conductivities of different ratio Cs-heteropolyacid in PBI membrane doped with H ₃ PO ₄ with doping level of 4.5 under anhydrous conditions	109
Figure 5-12, conductivities of 30 wt. % CsHPA /PBI composite membrane doped with H ₃ PO ₄ with doping level of 4.5 under anhydrous conditions.	111
Figure 5-13a, Polarization and power density curves of a PEMFC operated at 150 °C	113

with H ₂ /O ₂ atmospheric pressure	
Figure 5-13b, Polarization and power density curves of a PEMFC operated at 150 °C with H ₂ /Air atmospheric pressure	114
Figure 5-14 (a) IR corrected polarization curves of PBI and CsHPA-PBI membrane; (b) Tafel plots obtained from polarization curves (I is current density)	116
Figure 5-15, the PBI membrane polarization curves of different cathode electrode layer at 150 °C	117
Chapter 6	
Figure 6-1, schematic of Graphite Oxide (GO) structure	122
Figure 6-2 (a) the illustration of PEO/GO membrane, SEM morphology of PEO/GO membrane with 0.5 wt% GO (b) the surface (c) and cross-section	124
Figure 6-3 Powder XRD spectra of Graphite (a), Graphite Oxide (b), PEO (c) and PEO/GO membrane (d).	126
Figure 6-4, FTIR spectrum of Graphite (a), Graphite Oxide (b) and PEO/GO membrane (c)	127
Figure 6-5 Conductivity of PEO/GO membrane at relative humidity of 100% from 25 °C to 60 °C	128
Figure 6-6, Polarization and power density curves of PEO/GO membrane in fuel cell test. The Pt loading was 0.7 mg/cm ² and H ₂ and O ₂ was used in the test without back pressure at 16 °C, 30°C, and 60°C	129
Figure 6-7, SEM images of GO/PBI/PA and SGO/PBI/PA, ILGO/PBI/PA	131
Figure 6-8, Infrared spectra of Graphite, GO, and SGO	132
Figure 6-9, Conductivities of composite membranes loaded with H ₃ PO ₄ PRU of 1.9 under anhydrous condition	134
Figure 6-10. Arrhenius plot of PBI, 2 wt. % GO/PBI and 2 wt. % SGO/PBI composite membrane loaded with H ₃ PO ₄ with acid loading of 1.9 PRU under anhydrous condition	135
Figure 6-11, Conductivities of PBI and ILGO/PBI composite membranes loaded with similar PRU of 1.9 and 3.6 under anhydrous condition	136
Figure 6-12 Polarization and power density curves of a fuel cell operated at 175 °C with (a) H ₂ /O ₂ atmospheric pressure and (b) H ₂ /Air atmospheric pressure.	138
Figure 6-13 Polarization and power density curves of a fuel cell operated at 175 °C	140

with (a) H₂/O₂ atmospheric pressure.

Figure 6-14 Voltage response of a 12 h fuel cell life test under a constant voltage of - 500 mV vs OCV at 150 °C with H₂/O₂ condition 141

Chapter 7

Figure 7-1, ¹H NMR spectra of QPBI 146

Figure 7-2, FT-IR spectra of QPBI 146

Figure 7-3, SEM images of QPBI and EDX analysis for QPBI; before and after H₃PO₄ treatment. 148

Figure 7-4, Variation in H₃PO₄ doping level of PBI and QPBI membranes in different H₃PO₄ concentrations at room temperature after 7 days 149

Figure 7-5, Conductivities of PBI and QPBI membrane loaded with H₃PO₄. PRU of 3.6 and 3.5 respectively under anhydrous conditions 150

Figure 7-6, Polarization and power density curves of a fuel cell operated at 175 °C with H₂/O₂ at pressure 151

Figure 7-7, Polarization and power density curves of a fuel cell operated at 175 °C with H₂/Air atmospheric pressure 152

Figure 7-8 (a) IR corrected polarization curves of PBI and QPBI membrane; (b) Tafel plots obtained from polarization curves (I is current density). 154

Chapter 8

Figure 8-1, SEM of a) CsPOMo/QDPSU/PTFE/H₃PO₄ composite membrane and b) PTFE 157

Figure 8-2. EDX analysis of CsPOMo/QDPSU/PTFE/H₃PO₄ composite membrane. a) Cs, b) S, c) F, d) P, e) Mo 158

Figure 8-3, Infrared spectra of CsPOMo/PSU/PTFE/H₃PO₄ composite membrane 159

Figure 8-4, Conductivities of CsPOMo/PSU/PTFE composite membrane and PBI membrane loaded with H₃PO₄ (PRU 1.8) under relative humidity <1%. 160

Figure 8-5, Polarization and power density curves of a fuel cell operated at 150 °C with (a) H₂/O₂ and (b) H₂/air atmospheric pressure. Pt loading: cathode 0.4 mg cm⁻²; anode 0.2 mg cm⁻²; no gas humidity, H₃PO₄ PRU: 1.8, membrane thickness 28 μm. Gas rate: anode: 40 dm³ min⁻¹; cathode: 70 dm³ min⁻¹. 161

Figure 8-6, Polarization curves of CsPOMo/QDPSU/PTFE and PBI fuel cell operated 162

at 150 °C with H₂/O₂. Atmospheric pressure, no gas humidity

- Figure 8-7, a) IR corrected polarization curves of CsPOMo/PSU/PTFE b) Tafel plots 163
obtained from polarization curves in b). I is current density
- Figure 8-8, TGA analysis of the H₃PO₄ doped PTFE/qPVBz/Cl⁻ composite membrane 165
- Figure 8-9, Stress-strain curves of the PTFE porous membrane, H₃PO₄ doped 166
PTFE/qPVBzCl⁻ composite membrane and H₃PO₄ loaded qPVB/Cl⁻
- Figure 8-10. Proton conductivity-temperature relationship for the H₃PO₄ loaded 167
PTFE/qPVBzCl⁻ membrane
- Figure 8-11, Polarization curves of H₃PO₄ loaded PTFE/qPVBzCl⁻ membrane. H₂/O₂ 168
was used without back pressure; Pt/C (0.5 mg cm⁻²).
- Figure 8-12, IR corrected V-I polarization curves (A) and Tafel slopes (B) for different 169
operation temperatures

List of Schemes

Chapter 2

Scheme 2-1 Poly 2,2'-m-(phenylene)-5,5'-bibenzimidazole	18
Scheme 2-2 The two-stage process for PBI synthesis	19
Scheme 2-3 The single stage process for PBI synthesis	19
Scheme 2-4 The PPA process for PBI synthesis	20

Chapter 4

Scheme 4.1 Illustration of the preparation of ILGO	73
Scheme 4.2 Synthesis of the QPBIs	75
Scheme 4.3, Preparation of the CsPOMo/QDPSU/PTFE membrane	76

List of Tables

Chapter 2

Table 2-1, categories of fuel cell by electrolyte	9
Table 2-2, Structures of PBI variants	21
Table 2-3 reviews on the application of heteropolyacids in the solid electrolyte of fuel cells	32

Chapter 3

Table 3-1 Enthalpies and Entropies of formation for fuel cell reactants and products at 25 °C and 1 atm	60
Table 3-2, The percolation threshold for the various lattices	66

Chapter 4

Table 4-1, Expressions for d spacing in the different crystal systems	85
---	----

Chapter 5

Table 5-1. Particles size of four caesium powders	100
Table 5-2, Conductivities of CsHPA /PBI composite membrane imbibed with H ₃ PO ₄ . Acid amount of 4.5 RPU under anhydrous condition at 150 °C. The conductivity of the PBI membrane is 0.047 S cm ⁻¹ at the same conditions	109
Table 5-3, Mechanical strength of 30 wt% CsHPA acid/PBI membrane	112

Chapter 6

Table 6-1, the activation energy and the conductivity of membrane at 175 °C	136
---	-----

Chapter 7

Table 7-1, Volume swelling and mechanical strength of PBI and QPBI membrane	150
---	-----

Abbreviations and Symbols Used in this Thesis

A	Cross-section area
	Current density
	Absorbance
	Frequency factor
ABPBI	Poly(2,5-benzimidazole)
AFCs	Alkaline fuel cells
CL	Catalyst layer
CsPHA	caesium salts heteropolyacid
CsPOMo	$Cs_xH_{3-x}PMo_{12}O_{40}$
CsPOW	$Cs_xH_{3-x}PW_{12}O_{40}$
CsSiOMo	$Cs_xH_{4-x}SiMo_{12}O_{40}$
CsSiOW	$Cs_xH_{4-x}SiW_{12}O_{40}$
DL	Doping level
DMAc	Dimethylacetamide
DMF	Dimethylformamide
DMSO	Dimethyl sulfoxide
EDX	Energy-dispersive X-ray spectroscopy
F	Faraday's constant
FTIR	Fourier transformed infrared spectra
FC	Fuel cell
GDL	Gas diffusion layer
GO	Graphite oxide
HPA	Heteropolyacid
I	Intensity in the sample spectrum
	nuclear spin
ITFCs	Intermediate temperature fuel cells
IL	Ionic liquid
m	Mass of a unit cell
M	Molecular weight
MCFCs	Molten carbonate fuel cells
MEA	Membrane electrode assemblies
NHE	Normal hydrogen electrode

Abbreviations and Symbols Used in this Thesis

P	Pressure
PA	Phosphoric acid
PAFCs	Phosphoric acid fuel cells
PBI	Polybenzimidazole
PEEK	polyether ether ketone
PEMFCs	Proton exchange membrane fuel cells
PEO	polyethylene oxide
PRU	Per repeat unit
PSU	polysulfone
PTFE	Polytetrafluoroethylene
PWA	H3PW12O40
QPBI	Quaternary polybenzimidazole
QDPSU	Quaternary diazabicyclo-octane polysulfone
QPVBz	Quaterixed poly (vinyl benzyl chloride)
RH	Relative humidity
SEM	Scanning Electron Microscope
SGO	Sulfonic graphite oxide
SOFCs	Solid oxide fuel cells
T	Temperature
	Transmittance
TGA	Thermogravimetry analysis
XRD	X-ray diffraction analysis
V	Voltage
W	Wavenumber
α_a	Transfer coefficient of the reduction reaction
α_c	Transfer coefficient of the oxidation reaction
B_M	the width in radians of diffraction peaks of the sample
B_S	the width in radians of standard peak at half height
C_A	Concentration of A
C_B	Concentration of B
E_r	Reversible potential
E_0^0	Standard reference potential

Abbreviations and Symbols Used in this Thesis

ΔG^*	Relative energy
ΔH	Enthalpy
H_0	Magnetic field intensity
k	force constant for the bond standard rate constant
i_0	Exchange current density
h	Planck constant
n	Number of electrons
θ	Incident angle
λ	Wavelength of the light
ν	Vibration frequency
μ	Reduced mass
γ	Gyromagnetic ratio
I_0	Intensity in the background spectrum
η	Efficiency
ν_f	Rate of the forward process
ν_b	Rate of the reverse process
σ	Conductivity

Units

Energy = Force \times Distance = Work

1 atm = 1013 mb

1 bar = 10^5 N m⁻² = 10^5 Pa

1 S m⁻¹ = 0.01 S cm⁻¹

1 A cm⁻² = 1000 mA cm⁻²

1 W cm⁻² = 1000 mW cm⁻²

1 eV = 1.602×10^{-19} J

Chapter 1 Introduction and Objectives

1.1 Overview

Fuel cells have been developed over 100 years as candidates as portable source of power for light duty vehicles and buildings and as replacement for rechargeable batteries. The use of polymer membranes as electrolytes has received tremendous impetus in recent years.

Polymer electrolyte membrane Fuel Cells (PEMFC) have been considered as a suitable alternative to internal combustion engines because of their high power density, compared to other fuel cells, higher energy conversion efficiency, low emission levels, and being environmental friendly [2]. Now, the membrane costs 20-30% over the whole fuel cell system, so the development of membranes becomes a key challenge for applying fuel cell into industry and business. My work gave more focus on development of membranes for PEM fuel cell, especially at temperature range of 100-200 °C.

Although great success has been achieved with perfluorosulphonic acid (PFSA) polymer membrane (e.g. Nafion[®]), there are still some challenges that restrict commercialisation and development of PEMFC such as:

- High materials costs of membrane, catalysts and bipolar plates [2],
- Low tolerance to fuel impurities such as sulphur and carbon monoxide [3],
- Complex system construction and operation with respect to water and thermal management [4]

One of the solutions to improve PEMFCs technology is to develop new polymers or composite polymer electrolyte to reduce the membrane costs and elevate the operation temperature (more than 100 °C). Especially, most of the above shortcomings are associated with the low operation temperature, so development of some new polymer materials which exhibit stability and high conductivity in the absence of liquid water (more than 100 °C) may improve the overall fuel cell characteristics and overcome the shortcomings [1, 2].

Acid loaded polymer membranes are considered as promising electrolytes for use at temperatures between 100-200 °C. Polybenzimidazole (PBI) is a relatively low cost (\$70-100/lb) non-perfluorinated basic polymer (pKa=5.5) easily imbibed with strong acids to form a single phase polymer electrolyte [5, 6]. Xing et al. [7] compared the conductivity of PBI membrane doped in various acids, and found that the conductivities were in the order of

$\text{H}_2\text{SO}_4 > \text{H}_3\text{PO}_4 > \text{HClO}_4 > \text{HNO}_3 > \text{HCl}$. However H_3PO_4 offers greater thermal, chemical and electrochemical stability than using H_2SO_4 as PBI membrane was not stable in H_2SO_4 at elevated temperature.

Inorganic/polymer composite membranes with polymer as the host matrix were considered as a way to improve the conductivity and thermal stability. Typically examples included $\text{Zr}(\text{HPO}_4)_2$ [8, 9], phosphotungstic acid ($\text{H}_3\text{PW}_{12}\text{O}_{40}$, PWA) [10] and boron phosphate (BPO_4) [11]. The combinations of inorganic components with polymers offered a route to improved membranes with desired properties of conductivity and stability. The CsPOMo powders were used as addition catalyst element to optimising the electrode, and investigated the effect of CsHPA powder in the catalyst.

1.2 Project Objective

This work aimed to develop new solid state proton conducting electrolytes and investigate their fuel cell electrochemistry. This not only promised new operating parameters that would be better suited to PEMFC applications, but also offered important technology inputs to the more established technologies operating both for low ($< 100\text{ }^\circ\text{C}$) and intermediate temperature ($100\text{-}200\text{ }^\circ\text{C}$) ranges.

The program was comprised of the following goals:

- Synthesis and characterisation of inorganic filler combined with polymer matrix to enhance the conductivity or other properties
- Synthesis and characterisation of functionalised PBI and other polymer to improve the conductivity and fuel cell performance.

This thesis consisted of eight chapters listed as below:

Chapter 1, an introduction to the subjects of the research and objectives

Chapter 2, a literature review introduces fuel cells, especially the PEMFC, the polymer electrolyte membrane materials, composite membrane for PEMFC and characterization method and fuel cell performance.

Chapter 3, introduction the theory related to the fuel cell and membranes

Chapter 4, described experiments and instruments used in this work.

Chapter 5, the preparation and characterization of Cs-heteropolyacid, ionic liquid heteropolyacid/PBI composite membrane for PEMFC

Chapter 6, Graphite Oxide (GO) and functional GO polymer composite membrane for PEMFC

Chapter 7, synthesis and characterization of functionalised PBI membrane for intermediate PEMFC

Chapter 8, quaternary polysulfone/PTFE membrane for intermediate fuel cell

Chapter 9, conclusion of the study were presented which form the basis for the recommendations for future work.

References

1. Smitha, B., Sridhar, S., Khan, A.A. *Solid polymer electrolyte membranes for fuel cell applications—a review*, Journal of Membrane Science, 2005, 259, 10–26
2. Li, Q., He, R., Jensen, J.O., Bjerrum, N.J. *PBI-based polymer membranes for high temperature fuel cells - Preparation, characterization and fuel cell demonstration*, Fuel Cells 2004, 4 (3) , 147-159
3. Li, Q.F., He, R.H., Gao, J.O., and Bjerrum, N.J. *The CO poisoning effect in PEMFCs operational at temperatures up to 200 °C*, Journal of the electrochemical society, 2003, 150 (12) 1599-1605
4. Samms, S.R. and Savinell R. F. *Kinetics of methanol-steam reformation in an internal reforming fuel cell*, Journal of power sources, 2002, 112(1), 13-29
5. Wang, J.T., Savinell, R.F., Wainright, J., Litt, M. and Yu, H. *A H₂/O₂ feul cell using acid doped Polybenzimidazole as polymer electrolyte*. Electrochimica Acta, 1996, 41 (2), 193-197.
6. Mamlouk, M. *Investigation of high temperature polymer electrolyte membrane fuel cells*, PHD thesis, 2008.
7. Xing, B.Z. and Savadogo, O., *the effect of acid doping on the conductivity of Polybenzimidazole (PBI)*. Journal of new materials for electrochemical systems, 1999, 2(2), 95-101
8. Yang, C., Srinivasan, S., Bocarsly, A.B., Tulyani, S., Benziger, J.B. *A comparison of physical properties and fuel cell performance of Nafion and zirconium phosphate/Nafion composite membranes*, Journal of Membrane Science, 2004 237 (1-2) ,145-161
9. He, R., Li, Q., Xiao, G., Bjerrum, N.J. *Proton conductivity of phosphoric acid doped polybenzimidazole and its composites with inorganic proton conductors* , Journal of Membrane Science, 2003, 226, 169–184.
10. Staiti, P., Minutoli, M., Hocevar, S. *Membranes based on phosphotungstic acid and polybenzimidazole for fuel cell application*, J. Power Sources, 2000, 90, 231–235.

11. Zaidi, S.M.J., *Preparation and characterization of composite membranes using blends of SPEEK/PBI with boron phosphate*, *Electrochim. Acta*, 2005, 50, 4771–4777.

Chapter 2: Literature Review

2.1 Fuel Cells

Hydrogen is a high energy density and carbon emission-free fuel. An energy system based on hydrogen and hydrogen generation could provide a renewable and sustainable energy system referred to as the 'Hydrogen economy'. A great amount of effort has been devoted to the research and development of fuel cells as part of the 'Hydrogen Economy' in recent decades.

The fuel cell (fc) is an device which produces electrical energy from an electrochemical reaction. The discovery of fuel cells can be dated back to 1839 when Sir William Grove developed his prototype fuel cells, in which sulphuric acid was used as the electrolyte [1]. Progress in fuel cell development was limited until the 1950s when space application research was required. The first practical fuel cell application was initially developed by General Electric who used FC as a power supply for the Gemini Earth-orbiting program in the early 1960s [2]. Since then terrestrial usage of fuel cells has been limited due to the large utilisation of noble metals which has restricted the development of fuel cells.

The fundamental physical structure of a fuel cell consists of an electrolyte layer in contact with a porous anode and cathode on either side. The efficiency of a fuel cell is normally higher than that of traditional combustion devices (around 40%-60%) because fuel cells are not constrained by Carnot limitation. Figure 2-1 shows better fuel cell efficiency than any other energy conversion system.

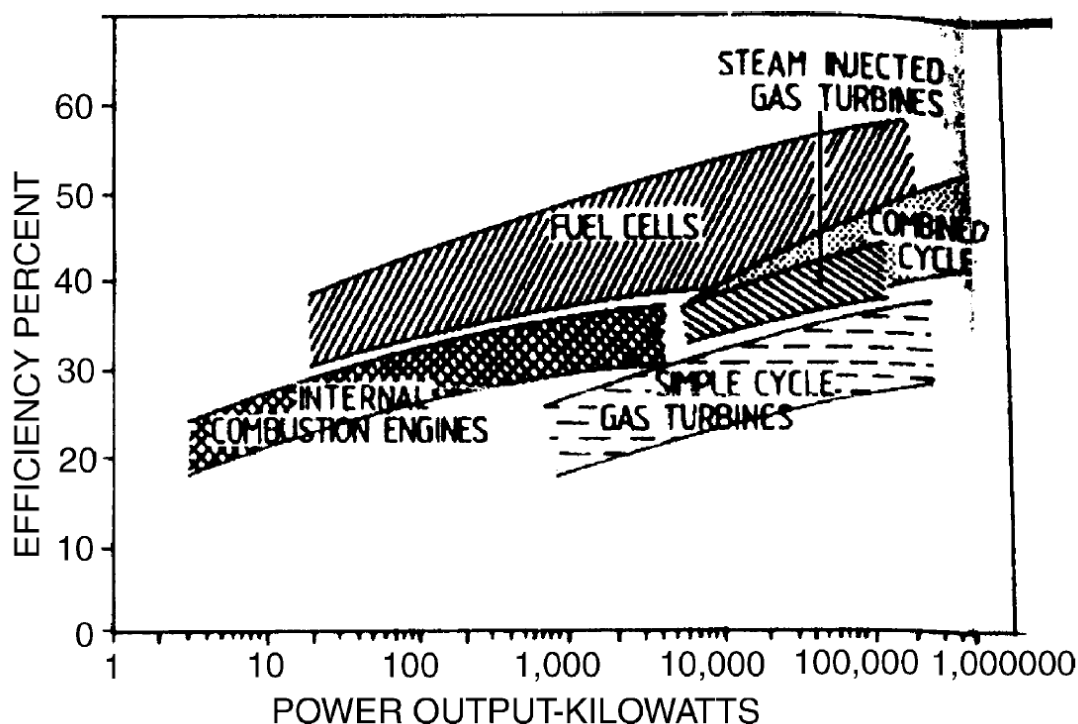


Figure 2-1 Comparison of fuel cell performance with other energy conversion systems [3]

Fuel cells are environmentally friendly as they normally use hydrogen as fuel and oxygen (air) as an oxidant, thereby producing water as the final product. Production of pollutants such as nitric oxides are avoided as no thermal combustion of a fuel with air occurs. The added advantages are the low noise and high reliability of fuel cells. Recently fuel cells have been considered as suitable alternatives to internal combustion engines for power applications and have attracted more and more research attention. [4-7]

Fuel cells can be classified according to the type of electrolytes used: into molten carbonate fuel cells, solid oxide fuel cells, alkaline fuel cells, phosphoric acid fuel cells and proton exchange membrane fuel cells. They can also be divided into high temperature fuel cells ($>500^{\circ}\text{C}$), intermediate temperature fuel cells ($100\text{-}500^{\circ}\text{C}$) and low temperature fuel cells ($<100^{\circ}\text{C}$) [4-7]. The classification of fuel cells and cell reactions is shown in Table 2.1.

Fuel cells have good potential as power sources, especially in remote locations, such as spacecrafts, remote weather stations, rural locations, and in certain military applications. Fuel cells could provide constant electric power to houses, office buildings and factories and can be used in cars, on buses, ships, portable and small scale systems, and many other applications [4-7].

Table 2-1 Categories of fuel cells by electrolytes

Fuel cells	Electrolyte	Work temperature (°C)	Reaction
Alkaline fuel cells (AFC)	KOH	<120	Anode: $2\text{H}_2 + 4\text{OH}^- \rightarrow 4\text{H}_2\text{O} + 4\text{e}^-$ Cathode: $\text{O}_2 + 2\text{H}_2\text{O} + 4\text{e}^- \rightarrow 4\text{OH}^-$ Overall: $2\text{H}_2 + \text{O}_2 \rightarrow 2\text{H}_2\text{O}$
Phosphoric acid fuel cells (PAFC)	H_3PO_4	100-200	Anode: $\text{H}_2 \rightarrow 2\text{H}^+ + 2\text{e}^-$ Cathode: $\text{O}_2 + 4\text{H}^+ + 4\text{e}^- \rightarrow 2\text{H}_2\text{O}$ Overall: $2\text{H}_2 + \text{O}_2 \rightarrow 2\text{H}_2\text{O}$
Molten carbonate fuel cells (MCFC)	Immobilised liquid molten carbonates	~650	Anode: $\text{H}_2 + \text{CO}_3^{2-} \rightarrow \text{CO}_2 + \text{H}_2\text{O} + 2\text{e}^-$ Cathode: $\text{O}_2 + 2\text{CO}_2 + 4\text{e}^- \rightarrow 2\text{CO}_3^{2-}$ Overall: $2\text{H}_2 + \text{O}_2 + 2\text{CO}_2$ (cathode) $\rightarrow 2\text{H}_2\text{O} + 2\text{CO}_2$ (anode)
Solid oxide fuel cells (SOFC)	Solid oxide	550-1000	Anode: $\text{H}_2 + \text{O}^{2-} \rightarrow 2\text{H}_2\text{O} + 2\text{e}^-$ Cathode: $\text{O}_2 + 4\text{e}^- \rightarrow 2\text{O}^{2-}$ Overall: $2\text{H}_2 + \text{O}_2 \rightarrow 2\text{H}_2\text{O}$
Polymer electrolyte membrane fuel cells (PEMFC)	Perfluorosulphonic acid membrane or Polybenzimidazole	<100 100-200	Anode: $2\text{H}_2 \rightarrow 4\text{H}^+ + 4\text{e}^-$ Cathode: $\text{O}_2 + 4\text{H}^+ + 4\text{e}^- \rightarrow 2\text{H}_2\text{O}$ Overall: $2\text{H}_2 + \text{O}_2 \rightarrow 2\text{H}_2\text{O}$

2.2 Proton Exchange Membrane Fuel Cell (PEMFC)

The PEM fuel cell has been under development for a long time. However, the evolution of membranes for fuel cell applications started as early as 1959 [3], and during recent years there has been an increasing interest in PEMFCs due to their high energy conversion efficiency, high power density, low emissions, and long life [4]. PEMFCs are considered to be suitable for commercial transport and portable applications [4, 6]. In the 1970s, Du Pont developed a novel membrane based on a sulphonated tetrafluorethylene polymer called “Nafion[®]” which was the most widely used and investigated for the PEMFC system [3].

The principle of PEMFC operation can be explained by the following reactions 1 to 3 and Figure 2-2 [4].

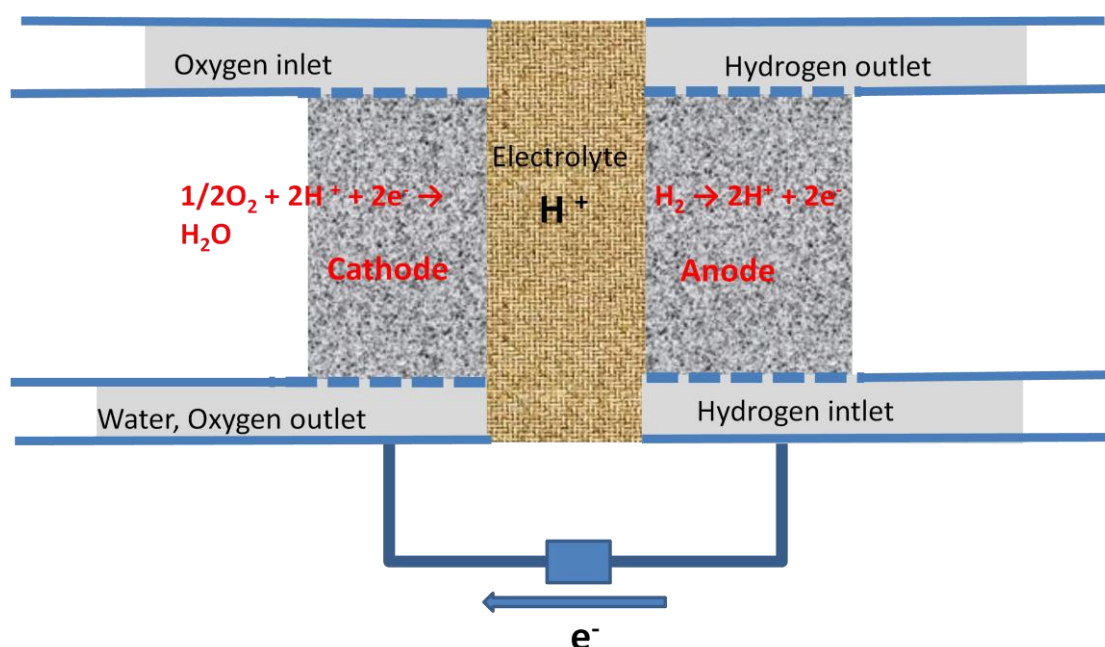
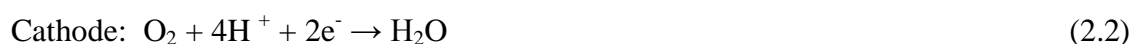


Figure 2-2 Schematic picture of a PEMFC fuel cell

The PEMFC is formed by a solid membrane between catalyst layers, two gas diffusion layers and electrodes. The membrane is a very important part of a PEMFC, and should be an electronic insulator as well as a proton conductor. Also, the membrane separates the oxidant and fuel. At the anode, hydrogen is electro-oxidised to protons and electrons which pass through the membrane and the external circuit, respectively. The oxygen reduction reaction occurs at the cathode and produces water as the final product. Both reactants react at separate catalyst layers (CL). The gas diffusion layer (GDL) provides voids for gas transfer to the catalyst layers and also electronic conductivity for flow of electrons from the catalyst layers (Figure 2-3).

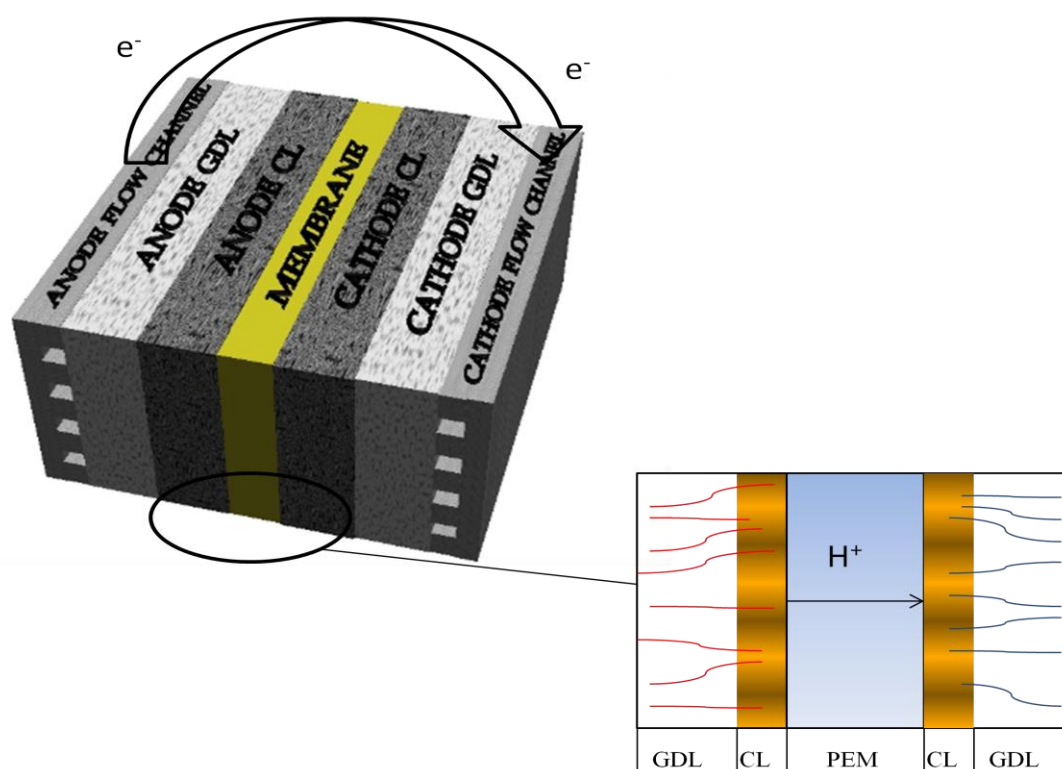


Figure 2-3 Structure of a single MEA (GDL: gas diffusion layer, CL: Catalyst layer, PEM: proton exchange membrane)

2.3 Performance measures of Fuel cells

A polarisation curve (Figure 2-4) is the most important characteristic of a fuel cell and its performance. Voltage losses in an operational fuel cell are caused by several factors such as [8, 9]:

- Slow kinetics of the electrochemical reactions (activation polarisation).
- Internal electrical and ionic resistance.
- Mass transport limitations of reactants to reaction sites Internal (stray) currents.
- Crossover of reactants.

The voltage loss is mainly divided into three parts. The first part (mainly at low current densities) is activation polarisation controlled by the oxygen and hydrogen reaction rate on the electrodes indicating catalyst effectiveness. The second part (at intermediate current densities) is mainly attributed to the resistance of membrane electrode assembly (MEA), so better proton conductivity of electrolytes should reduce the voltage loss in this part. The last part is controlled by mass transport and is caused by concentration polarisation (gas transport loss) which is mainly associated with the oxygen reduction reaction (ORR) rate in the PEMFC.

The output power density (in mW cm^{-2}) which is calculated from the product of cell voltage and the current density at this voltage is an important characteristic of a fuel cell and its performance. One of the goals of PEMFCs is to achieve high power density) (notionally $> 1 \text{ W cm}^{-2}$), using a low catalyst loading ($\sim 0.1 \text{ mg cm}^{-2}$) to reduce the cost of a fuel cell. The United States Department of Transportation (DOT) published a target price of vehicle fuel cells at \$30/kW for transportation applications with 5,000 hour lifespan (150,000 miles) and the ability to function over the full range of vehicle operating conditions (40°C to 80°C), and production volume of 500,000 per year in 2010 [9]. For stationary systems, the acceptable price is \$400–\$750/kW for commercialisation with more than 40,000 hours of reliable operation for market acceptance [9].

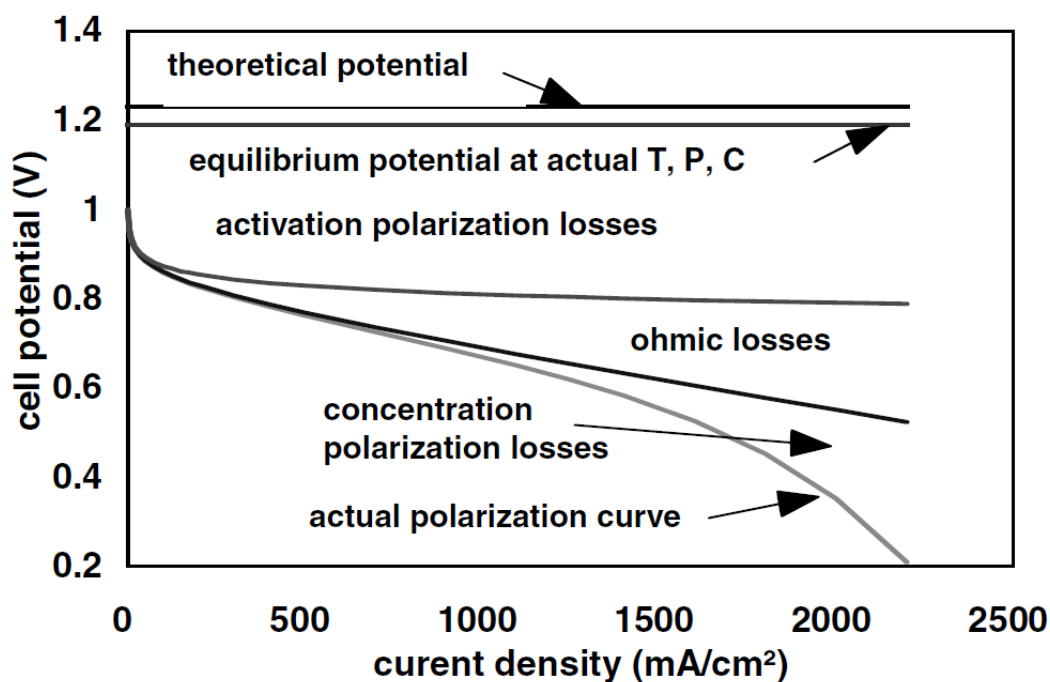


Figure 2-4 Various voltage losses and the resulting polarisation curve of an operating fuel cell [8]

2.4 Intermediate temperature PEMFC

As discussed in Chapter 1 most of the shortcomings associated with low-temperature PEMFC technology can potentially be solved or avoided by developing alternative membranes that operate at temperatures higher than 100 °C. As a result, in recent years, application of fuel cells in the intermediate temperature range of 100–400 °C has attracted increasing interest [10-12]. Compared with low temperature PEMFC, the intermediate temperature PEMFC (ITPEMFC) potentially offers some significant advantages such as:

1. The kinetics for both electrode reactions will be enhanced [12, 13].
2. Reducing catalyst poisoning on the anode caused by CO for example. This high CO tolerance makes it possible for a fuel cell to use hydrogen directly from a steam reformer and simplifies the CO cleanup system [12, 13]. The CO

tolerance will be dramatically enhanced, from 10-20 ppm of CO at 80 °C, to 1000 ppm at 130 °C, and up to 30000 ppm at 200 °C [13]. Thereby improving the efficiency of the fuel cell [11].

3. Avoiding fuel cell flooding by the product water.
4. A simplified cooling system [12].
5. Making it more feasible to use a non-noble metal catalyst [14].

The PEMFC is expected to give the overall power system advanced features including higher efficiency, smaller size, lower weight, simple construction and operation, and lower capital and operational cost. High reliability, less maintenance, and better transient response capacities can be expected as the potential features of the intermediate temperature PEMFC technology [13]. Therefore, the development of ITPEMFC is of great importance for fuel cell research and development.

The development of conducting membranes above 100°C operation includes (i) modified PFSA membranes, (ii) alternative sulfonated polymers and their composite membranes, and (iii) acid-base polymer and their composite membranes [12].

2.5 Electrolytes

The membrane provides the proton transport, electronic insulation between the two electrodes and prevents gas permeation. The membrane thus must provide high ionic conductivity, good chemical resistance, good thermal stability, and low gas transport.

2.5.1 Proton conducting materials

2.5.1.1 Perfluorosulphonic acid (PFSA) polymer membranes

According to the proton conduction mechanism, the proton conduction membranes can be classified into three main groups:

1. The perfluoroalkyl backbone (such as aromatic) and stable side group acid pendants (e.g. sulfonic acids group Fig. 2-5 a).
2. Polymers with an aromatic backbone and side group, like $-\text{CF}_2-\text{SO}_3\text{H}$ or $-\text{CF}_2-\text{CF}_2-\text{SO}_3\text{H}$, which can provide higher proton conductivity due to increase of side group acidity as shown in Fig. 2-5 b.
3. Incorporation of a sulfonic acid group into aromatic polymers, such as sulfonated polybenzimidazole, polyimides, and polyphenylene as shown in Fig. 2-5 c.

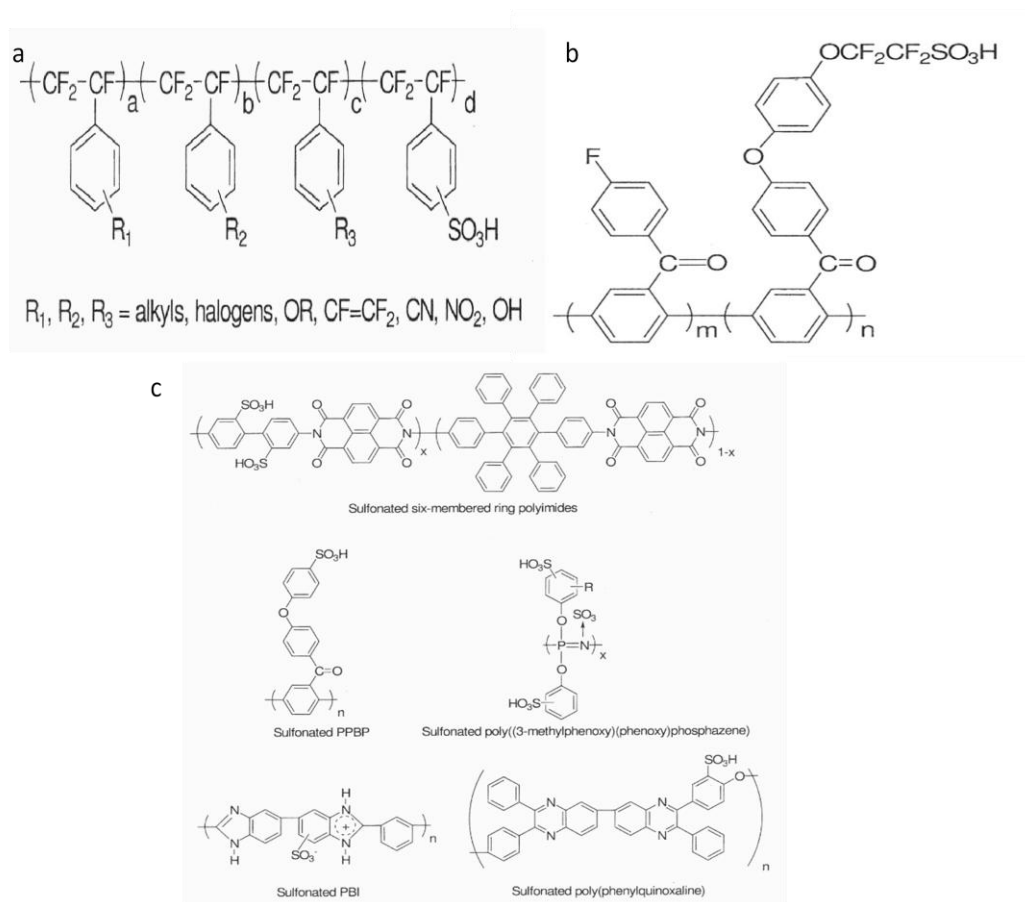


Figure 2-5 a) Teflon backbone and aromatic side group, b) polyphenylene backbone and pendant fluorosulfonic acid, c) some typical sulfonated aromatic polymers [6]

The best known example of membrane for PEMFC is perfluorosulfonic acid polymer membrane (Nafion[®]) produced by Dupont Inc., which is used at a low temperature due to its hydrated requirement. The mobility of protons in water through Nafion[®] membranes is extremely high because of the fast reorientation between water molecules. Therefore, water plays a vital role in the proton conduction processes. These types of proton conductors usually possess internal open structures (layers, channels) so that water molecules are maintained and “free” to move.

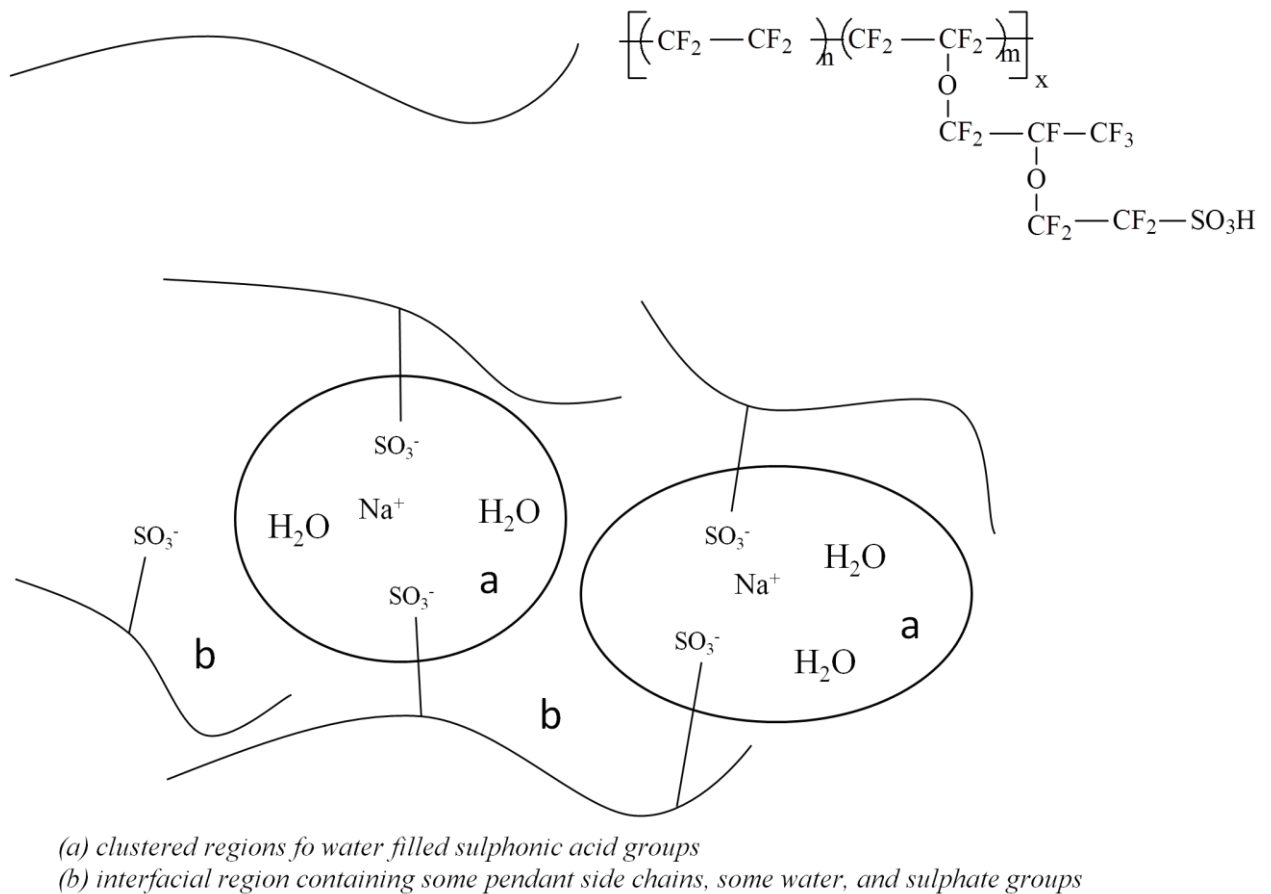


Figure 2-6 Chemical structure of Nafion[®]

The fluorinated backbones are hydrophobic and lead to the formation of the continuous network of channels where hydrophilic sulfonic groups form an aqueous domain. The

aqueous domain contains only protons as mobile species in addition to water molecules, and protons are charge-balanced by immobilised anionic sulfonic groups. This specific structure allows fast exchange and migration of protons and therefore high proton conductivity can be obtained [15]. In the Nafion[®] structure, the charge units are anions, typically sulfonic groups (-SO₃⁻). The sulfonated hydrocarbon polymers provides a conventional way for ionic conducting via attached charged units and release to another charged group, as shown in Figure 2-6.

However there are some disadvantages to restricting the use of Nafion[®] as a polymer electrolyte [6].

1. The high cost of membrane, US\$ 700 per square meter [19].
2. Requirements of supporting equipment, such as humidity supply systems to provide water for the membrane.
3. The polymers proton conductivity is highly water dependent therefore operating temperatures need to be less than 100°C.

Several approaches have been made to modify the PFSA membranes so as to overcome the shortcomings of the last 30 years. These approaches include [3, 12]:

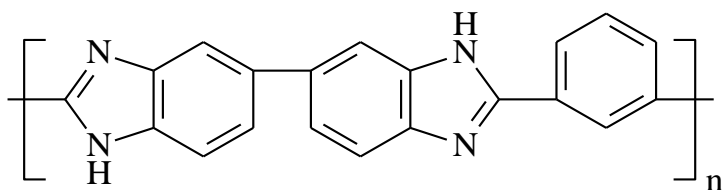
- Replacement of water with low volatile or non-aqueous media such as phosphoric acid, ionic liquid
- Impregnation with hygroscopic oxide nanoparticles, e.g. SiO₂
- Impregnation with solid inorganic proton conductors, e.g. heteropolyacids, and zirconium phosphate
- Development of aromatic and hydrocarbon polymers functionalised with sulphuric groups, such as sulfonated polystyrene, sulfonated polysulfone, and sulfonated polyimide

- Development of acid base polymer complexes. The polymers have basic properties and can easily react with strong acids by establishing hydrogen bonds

2.5.1.2 Polybenzimidazole

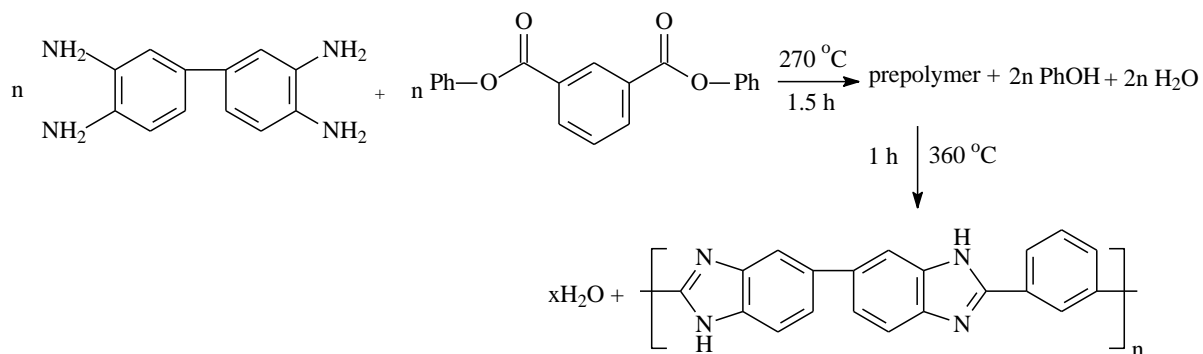
Phosphoric acid has a good conductivity and thermal stability, and its use is well known in phosphoric acid fuel cells (PAFC) for intermediate temperatures of 175–220 °C [20]. However, the conventional PAFC has certain disadvantages such as the fact that phosphoric acid electrolytes can have limited immobilisation in certain matrices. Therefore, attempts to apply phosphoric acid to certain materials (e.g. polymer membrane), through chemical bonding, has attracted much interest [21]. The phosphoric acid loaded polybenzimidazole (PBI) is the best known example which has produced reasonably successful membranes for fuel cells, with excellent thermo-chemical stability and good conductivity.

Polybenzimidazole (PBI) refers to amorphous thermoplastic polymers with linear heterocyclic polymers containing benzimidazole nuclei as a repeat unit. It has a high thermal stability (glass transition temperature, $T_g = 425 - 436$ °C), excellent chemical resistance, retention of stiffness and toughness, and good membrane-forming properties. [21, 22] PBI membranes can be impregnated with variable amounts of phosphoric acid to yield proton-conducting membranes that can work at temperatures up to 200 °C. As a speciality polymer PBI is used as textile fibres for a wide range of high temperature applications and refers to a commercial product under the trademark Celazole[®] (Scheme 2-1) [22].



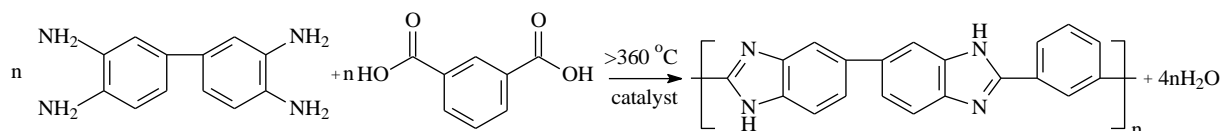
Scheme 2-1 Poly 2, 2'-m-(phenylene)-5,5'-bibenzimidazole

PBI, in wholly aromatic form, were first synthesised by Vogel and Marvel in 1961 [23]. A two stage process was developed to produce PBI with tetraminobiphenyl (TAB) and diphenyl isophthalate (DPIP) as monomers, as shown in Scheme 2-2 [23].



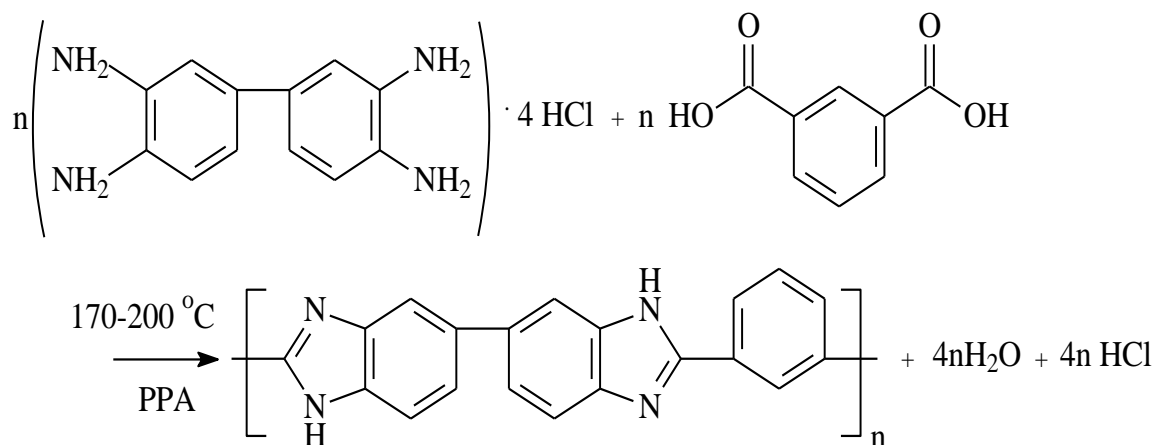
Scheme 2-2 Two-stage process for PBI synthesis

Choe [24, 25] developed a single stage method to synthesise high molecular PBI through using the isophthalic acid (IPA) to replace DPIP in the presence of catalysts of organo-phosphorus and silicon compounds (Scheme 2-3).



Scheme 2-3 Single stage process for PBI synthesis

PBI can also be synthesised in homogeneous solutions with solvents such as polyphosphoric acid (PPA) [26] (Scheme 2-4). This method is an excellent route for preparing laboratory or small scale polymers as it requires only a moderate temperature (170–200 °C) and uses more stable monomers (TAB stabilised by tetra hydrochloride) [26].



Scheme 2-4 PPA process for PBI synthesis

Other solvents rather than PPA have been used for the homogeneous synthesis of PBI, such as molten sulpholane or diphenyl sulphone [27], and a mixture of phosphorus pentoxide (P_2O_5) and methanesulphonic acid (MSA) [28, 29].

After poly [2, 2-p-(phenylene)-5, 5-benzimidazole] (pPBI, Scheme 2-1) was synthesised in 1961 [23], the extensive work on synthetically modified PBI of varied structures, which consist of bis (3, 4-tetraaminodiphenyl) containing ether, sulphone, ketone and aliphatic groups and various bis(phenoxy-carbonyl) acid derivatives is shown in Table 2.

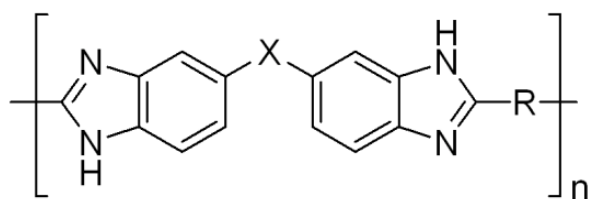
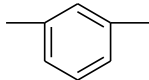
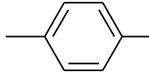
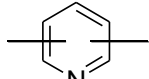
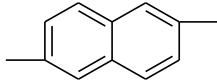
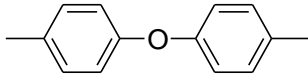
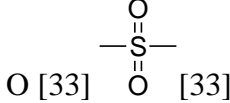
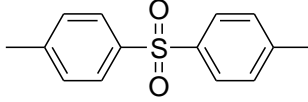
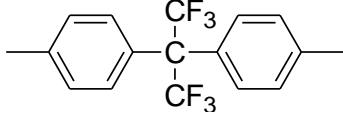
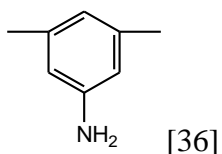
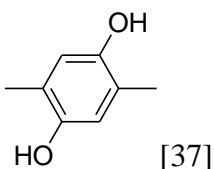


Table 2-2 Structures of PBI variants

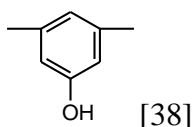
	R	X
m-PBI	 [30]	
p-PBI	 [30]	
Py-PBI	 [31]	
Naphthalin-PBI	 [32]	
O-PBI/ OO-PBI/ SO ₂ -O-PBI	 [33]	
SO ₂ -PBI	 [34]	
F6-PBI	 [35]	

NH₂-PBI

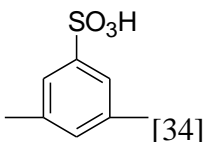
2OH-PBI



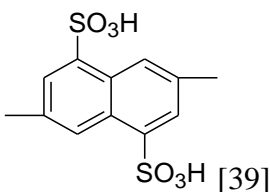
OH-PBI



Sulphonated PBI



Sulphonated naphthalin-PBI



Some groups such as ether linkages [40, 41] sulfone, fluorine [42], N-phenyl 1, 2, 4-triazole group [43] and perfluorocyclobutyl [44] were introduced into PBIs to reduce the intermolecular forces between the polymer chains. This was in order to overcome the restricted polymer solubility as well as to improve other physicochemical properties of acid-doped PBI electrolytes. The thermal stability, oxidation resistance, and water absorption were increased.

Varieties of diacids or sulphonated diacids were used to prepare PBI with modified structures, such as 4, 4-(hexafluoroisopropylidene)bis(benzoic acid) [45], (4,8-disulphonyl-2,6-naphthalenedicarboxylic acid [46] or 5-sulphoisophthalic acid [47].

Recently and interestingly, Xu et al. [48, 49] synthesised a series of amine-terminated hyperbranched PBI with good mechanical properties with the help of cross-linkers.

Poly (2, 5-polybenzimidazole) (AB-PBI) has a simpler structure to PBI without the connecting phenyl rings and therefore a high concentration of the basic sites in the structure.

As NH groups in the imidazole rings became chemically reactive, the PBI could first react with an alkali hydride (e.g. LiH, NaH) to produce a polybenzimidazole poly-anion, and then react with an alkyl, aryl or alkenyl methyl halide such as hydroxyethyl [50], sulfoalkyl [51, 52], and cyanoethyl [53]. The N-substituted PBI may increase the polymer spacing or decrease the polymer packing when a group is introduced, resulting in high acid-doping levels and therefore high proton conductivity [35]. Xavier Glipa et al.[54] grafted the benzylosulfonate groups on the imidazole nitrogen in PBI and controlled the degree of sulfonation through the amount of sulfonated grafting agent used. The sulfonated groups benefited proton conductivity, water uptake, and acid sorption. Prabakran R. Sukumar et al. [55] reported two functionalised PBI. One was phosphoric acid (PA) functionalised onto PBI via N-alkylation which showed good proton conductivity. Increasing the degree of modification of PA resulted in an improvement in conductivity, but a loss of mechanical stability. The other one was vinyl phosphonic acid (VPA) cross-linked onto PBI to form the PBI/PVPA networks. These materials showed improved solubility and very good film-forming properties as well as a high degree of grafting of VPA enhancing proton conductivity.

There were two direct casting methods used for membrane fabrication, either from a phosphoric acid and trifluoroacetic acid (TFA) mixture (called TFA-cast) or from a polyphosphoric acid (PPA, called PPA-cast) [22]. PBI also dissolved in a few organic

solvents, such as *N,N*-dimethylacetamide (DMAc), *N,N*-dimethylformamide (DMF), *N*-methylpyrrolidone (NMP) [22, 23]. Typically, DMAc was chosen as a suitable solvent.

The conduction mechanisms indicated that higher conductivity will be achieved when loaded with acid. DMAc-cast membrane should be loaded with acids to achieve high conductivity. Many acids were investigated by researchers to find the suitable acid, such as H₃PO₄, H₂SO₄, HClO₄, HNO₃, HBr, etc [22]. As described in Chapter 1, phosphoric acid was better for PBI membrane loading as it is amphoteric with both the proton donor and proton acceptor groups to form dynamic hydrogen bond networks [22, 23]. The other advantages were good thermal stability and low vapour pressure at higher temperatures [22]. Generally, the higher acid doping level resulted in higher conductivity for the PBI membrane, but it decreased the mechanical strength which was also influenced by the PBI molecular weight [23]. When the PBI was loaded with acid, the selection of acid doping level should take both the conductivity and mechanical strength into account. For DMAc-cast membranes, doping level of 5-6 was considered suitable [23].

The proton conduction mechanisms for PBI were studied by many researchers and there were four possible mechanisms proposed, as shown schematically in Figure 2-7 [29].

1. Proton directly hopping from one N site to another when it is non-doped. This procedure contributes little to conductivity.
2. At low doping level (less than 2), proton hopping from the N-H site to a phosphoric acid anion.
3. Proton hopping along the H₃PO₄/H₂PO₄⁻ chain at high doping level (~6), the free acid provides the major conductivity.
4. Humidity will also increase conductivity, because protons can hop via water molecules.

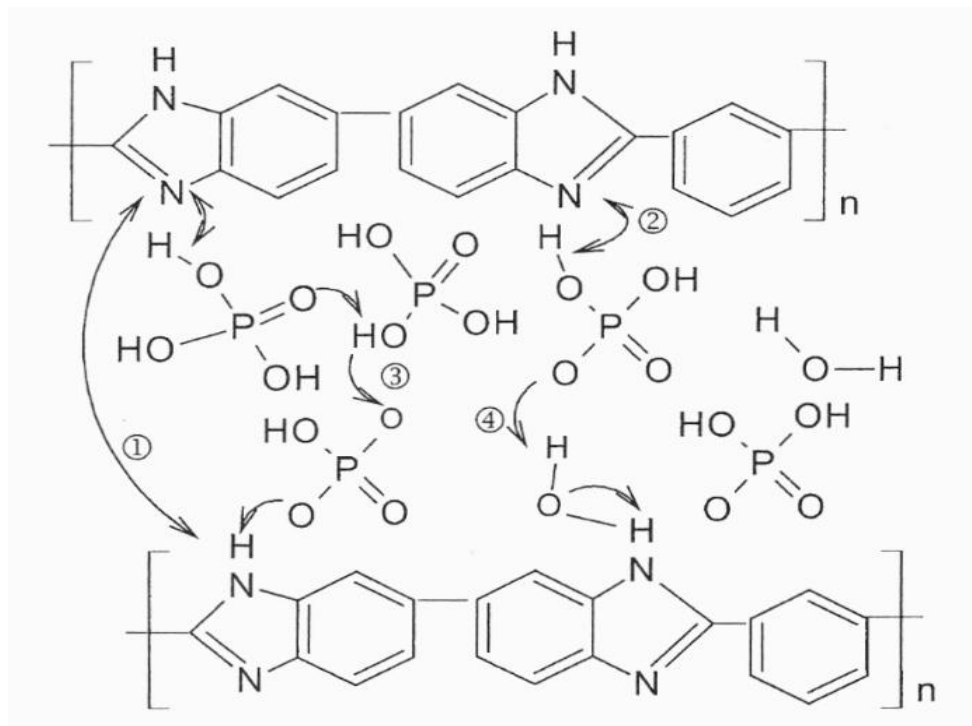


Figure 2-7 Proton conduction for PBI membranes, 1) from N-site to another, 2) from N-site to phosphoric acid molecular, 3) via the acid chain, 4) via water molecular [29].

As Kawahara et al. [56] reported, the PBI membrane with a PA doping level of 1.9 under anhydrous conditions at temperatures up to 160 °C, the conductivity varied from 10^{-9} - 10^{-5} S cm^{-1} . Even under humidified conditions and at 200 °C, the conductivity did not exceed 10^{-2} S cm^{-1} with low PA doping levels (less than 3) [57, 58]. When excess PA was present in the membrane (i.e. at a PA doping level of 4-6, At 200 °C, the conductivity for the PBI with PA doping levels of 4-6 has been reported to be about $4-7 \times 10^{-2}$ S cm^{-1} [59]

The dry PBI membrane had a small elongation at break of around 1–3%, and a tensile strength of 60–70 MPa at room temperature. When saturated with water, the elongation and tensile strength increased to about 7–10% and 100–160MPa, respectively [58]. When phosphoric acid was introduced into the polymer structure at a low acid-doping level range, there was no significant change of modulus or tensile strength of the PBI [59]. However, the strength of the PBI membrane would decrease due to free acid reducing intermolecular forces.

[60] The strength was also strongly influenced by the average molecular weight and casting method [61].

The membrane in a PEM fuel cell was also a separator of reactants. Hence, the gas permeability of the membrane was an important parameter to take into account. PBI membranes results showed low gas permeability for both hydrogen and oxygen (2×10^{-13} and $5 \times 10^{-15} \text{ mol cm}^{-1} \text{ s}^{-1} \text{ bar}^{-1}$, respectively [62]). At elevated temperatures, from 80 to 180 °C, He et al. [63] reported a hydrogen permeability of $1.6\text{--}4.3 \times 10^{-12} \text{ mol cm}^{-1} \text{ s}^{-1} \text{ bar}^{-1}$ and an oxygen permeability of $5\text{--}10 \times 10^{-14} \text{ mol cm}^{-1} \text{ s}^{-1} \text{ bar}^{-1}$ [63]. PA doped PBI membrane (doping level of 6) was 2-3 times higher than the non-doped membrane at 120-180 °C, because PA swelling of the polymer matrix and separation of the polymer chains [61].

Besides PBI, there were also some widely investigated materials including sulfonation of polysulfones (PSF) or polyethersulfone (PES) [64,65], polyetheretherketone (PEEK) [66, 67], polyimides (PI) [68, 69], polyphenylenes (PP) [70], polyphenylenesulfide (PPS) [71], etc, in developing polymer electrolytes for fuel cells. These materials were also considered as suitable membranes which could provide acceptable conductivity for proton transfer.

2.5.1.3 Quaternary polymer and PTFE support composite membranes for PEMFC

According to a good bonding with phosphoric acid and stable in the operating condition of ITFCs, quaternary ammonium group bonding to polymer materials that had high glass transition temperature and chemical stability were investigated [20].

Poly (phthalazine ether sulfone ketone) (PPESK) is a material that has good mechanical strength, chemical resistance and a high glass transition temperature (263–305°C) [72]. The quaternized poly (phthalazinone ethersulfone ketone) (QAPPESK) membranes doped with 4 times mole ratio of H_3PO_4 gave fuel cell performance 0.85 W/cm^2 with H_2/O_2 at 150°C and 0.1 MPa. This performance was stable for more than 100 hours [72].

Li et al. [20] developed a novel polymer quaternized polysulfone (QNPSU) poly ($\text{R}_1\text{R}_2\text{R}_3$)– N^+ doped with H_3PO_4 for intermediate temperature PEMFC. This membrane was synthesised from polysulfone and $\text{ClCH}_2\text{OCH}_2\text{CH}_3$ and after loading with H_3PO_4 gave high proton conductivity (0.12 S cm^{-1}) at 160°C as well as giving a good performance in fuel cells with a peak power density more than 0.7 Wcm^{-2} at 150 °C and 1bar pressure. X. Wang et al. [73] synthesised a quaternary 1, 4-diazabicyclo-[2.2.2] octanes (DABCO) polysulfone (QDPSU) with different degrees of substitution (DS). The higher DS of quaternary group resulted in higher conductivity but lower mechanical property. The DS 106 one was optimised as achieving a high power density output of 400 mWcm^{-2} at 150 °C and atmospheric pressure.

Good mechanical strength is an important property for the membrane, which will benefits the working period in the fuel cells. However, it is a challenge for most polymer materials to chase both the high conductivity and good mechanical property, especially after doping with H_3PO_4 . Polytetrafluoroethylene (PTFE) is a hydrophobic material with high mechanical strength and could be used under 300 °C over a long period. The thin porous PTFE films were used as a support framework to enhance the mechanical strength requirement.

Li et al. [74] also reported polytetrafluoroethylene/zirconium/phosphate ($\text{PTFE}/\text{ZrP}_2\text{O}_7 \cdot x\text{HPO}_3$) composite membranes for an intermediate temperature of 120 to

200°C. They filled the $\text{ZrP}_2\text{O}_7 \cdot x\text{HPO}_3$ sol as the proton conductor into a porous PTFE as the membrane-supporting structure. This membrane had high proton conductivity, greater than 0.1 S cm^{-1} at anhydrous condition, and a good mechanical strength of 10.25 MPa, indicating that this composite membrane was a promising material for the intermediate temperature PEMFC. Li et al. [75] also tried to immobilising PBI into porous PTFE film to form the composite membranes. The mechanical strength of the membrane was good, exhibiting a maximum load of 35.19 MPa, After doping with the phosphoric acid, the PTFE/PBI composite membrane had a proton conductivity of 0.3 S cm^{-1} at a relative humidity of 8.4% and 180 °C with a doping level of 3 (Fig. 2-8) [75]. This conductivity was much higher than the pristine PBI doped with phosphoric acid. The peak power density was over 1.2 W cm^{-2} with oxygen at 1 bar overpressure and the current densities were over 3 A cm^{-2} (shown in Figure 2-9). Even with H_2/air condition, the peak power densities of 0.6 W cm^{-2} are achieved at 1 bar overpressure [75]. The PTFE/PBI/ H_3PO_4 composite membrane did not exhibit significant degradation after 50 hours of intermittent operation at 150 °C. PTFE supported composite membrane balanced the cell performance, mechanical property, and durability. This kind of membrane provided a way to fit the requirement of intermediate temperature PEMFCs for the vehicles application [75].

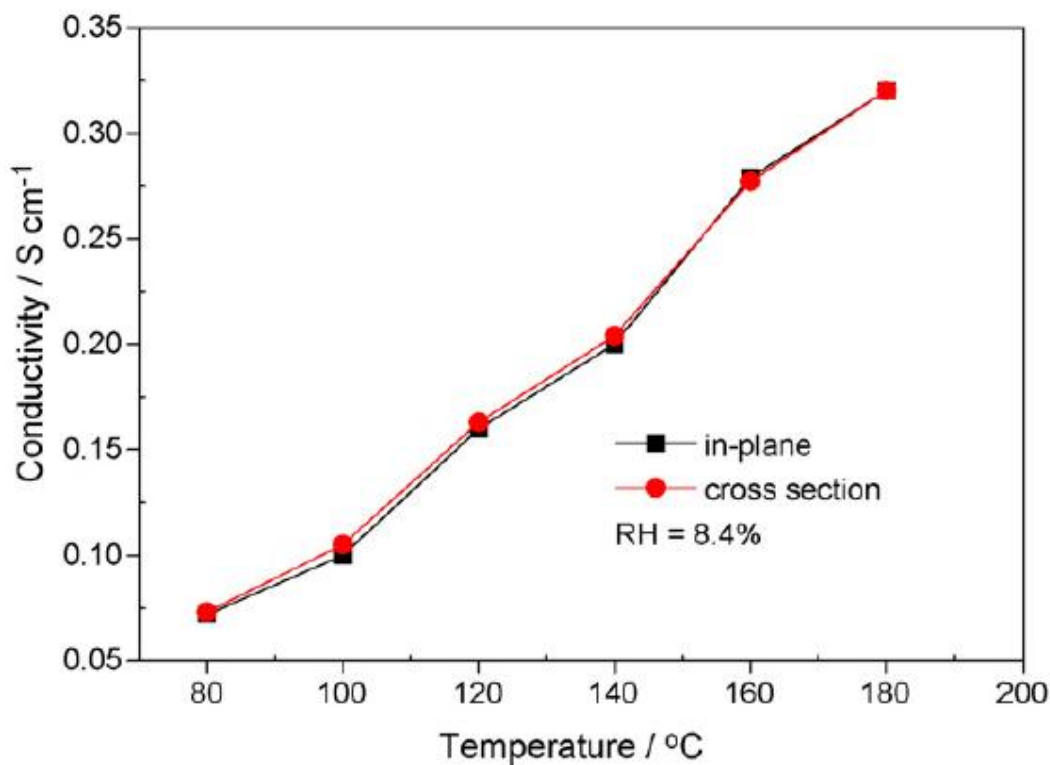


Figure 2-8 In plane and the cross section Proton conductivity of the PTFE/PBI composite membrane 3 doping level, and Relative humidity 8.4% [75]

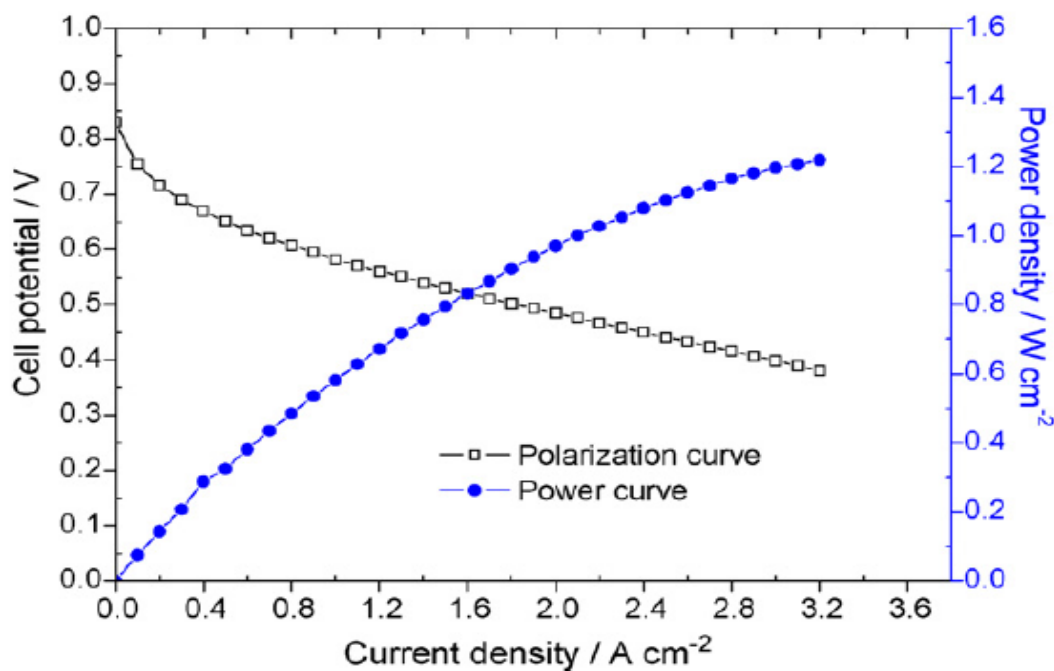


Figure 2-9 Polarisation (adapt diag. above) and power density curves of a PEMFC with PTFE/PBI composite membranes with H_2/O_2 at 170°C under 1 bar pressure [75]

Da Hye Choi et al. [76] prepared sulfonated poly (fluorinated arylene ether) (SDF-F)/poly (N-vinylimidazole) (PVI) and PTFE layered membranes. The new layered membranes had a sandwich structure with PTFE between the SDF-F/ PVI layers. This PTFE membrane also had a high-proton conductivity of $2.20 \times 10^{-2} \text{ S cm}^{-1}$ at 150 °C anhydrous condition, and good mechanical strength by using a porous PTFE film. A peak power density was 317 mW cm^{-2} at a cell voltage of 0.6V at 190°C. The new SDF-F/ PVI and PTFE layered membranes show stable performances for 150 hours. Another example for PTFE composite membrane was $\text{NH}_4\text{PO}_3/\text{PTFE}$ reported by Jiang, Y. et al. [77]. This composite membrane showed good conductivity under 250 °C, so the thermal stability was an advantage for PTFE support membranes as well.

2.5.2 Inorganic filler for composite membranes

2.5.2.1 Heteropolyacid and Polyoxometalate/polymer composite

Incorporating inorganic proton conductors into a polymer matrix can help to improve conductivity, retain water, and increase the operating temperature limit.

Heteropolyacid (HPA) is formed as nano-sized metal–oxygen anion clusters with unique variety in structure and strong acidity. HPAs and their salts are generally considered to be one of the most acidic materials in solids with high conductivity and thermally stable. This has attracted much attention [78–80], HPA compounds include a metal (such as tungsten, molybdenum or vanadium), oxygen, acidic hydrogen atoms, and an element generally from the p-block (such as silicon, phosphorus) [81, 82]. HPAs have different hydrated structures (Keggin and Dawson Structures), and the Keggin structure ($\text{H}_n\text{XM}_{12}\text{O}_{40}$) is well known consisting of a central atom in a tetrahedral arrangement of oxygen atoms surrounded by 12 oxygen octahedra connected with tungsten or molybdenum due to its ease of preparation and strong acidity [80-82]. HPA molecules bridge water moieties through formation of

hydronium ions such as H^+ , H_3O^+ , $H_5O_2^+$ (Figure 2-10), so HPAs react with the water of hydration, which is generally bound loosely in the structure for high proton conductivity [81]. This is the reason that the conductivity of the Keggin units HPAs relate to the number of water molecules, which are determined by the relative humidity and temperature. So HPAs are attracted as inorganic modifiers in polymer matrix to improve conductivity and thermal stability for PEMFC. Table 2-3 lists some matrix with HPA.

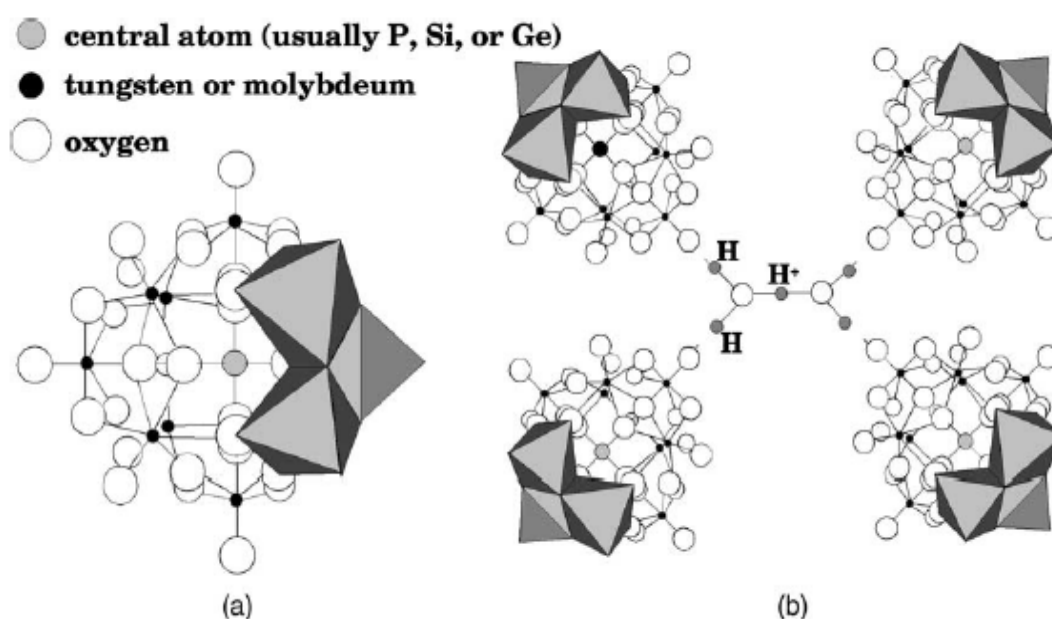


Figure 2-10 Structure of heteropolyacid: (a) primary (Keggin) structure; (b) secondary (hydrated) structure [81]

Table 2-3 reviews on the application of heteropolyacids in the solid electrolyte of fuel cells

Matrix	Heteropolyacid	Additional inorganic	Reference
Nafion	PWA/SiWA	SiO ₂	83-89
Nafion	Cs ⁺ , NH ⁴⁺ , Rb ⁺ and TI ⁺ PWA		90
Nafion/poly(tetraflouroethylene) (PTFE)	Cs _{2.5} H _{0.5} PW ₁₂ O ₄₀		91
Sulfonated polyether ether ketone (SPEEK)	PWA or SWA	CsHSO ₄	92
Poly(ethylene glycol) (PEG)	H ₈ SiW ₁₁ O ₃₉		93
Sulfonated polyimides (SPI)	PWA		94
Sulfonated poly(arylene ether ketone)/polyaniline (SPAES/PANI)	PWA		95
Poly(vinyl alcohol)/polyacrylamide (PVA/PAM)	Cs _{2.5} H _{0.5} PW ₁₂ O ₄₀ Cs _{2.5} H _{0.5} PMo ₁₂ O ₄₀		96
Polybenzimidazole (PBI)	PWA or SWA	CsHSO ₄	97

Gomez-Romero et al. [81] reported that a hybrid organic–inorganic material formed by phosphomolybdic acid (H₃PMo₁₂O₄₀, denoted here as PMo₁₂) and poly (2, 5-benzimidazole) (ABPBI) were cast in the form of membranes from methanesulfonic acid (MSA) solutions. This composite membrane was impregnated with phosphoric acid. An ABPBI–45% PMo₁₂ membrane impregnated in a 68% phosphoric acid solution reached a proton conductivity of 0.03 S/cm at 185 °C un-humidification. This composite membrane presented higher

conductivity than the pristine ABPBI polymer membranes impregnated and tested under the same conditions, and was stable even up to 200 °C [81].

Heterotungstic acid (phosphotungstic acid (PWA, $H_3PW_{12}O_{40} \cdot nH_2O$) and silicotungstic acid (SiWA, $H_4SiW_{12}O_{40} \cdot nH_2O$) provided good mechanical strength [58]. However, the composite membranes showed lower conductivity at higher temperature than pristine PBI membranes due to their higher demand for humidity [58]. P. Staiti et al. [98] tried to combine SiO_2 with heteropolyacid to provide a stable structure for the heteropolyacid, avoiding its dissolution in water. Silicotungstic acid and silica/PBI (SiWA- SiO_2 /PBI) composite membrane had higher conductivity in comparison with that of the PBI membrane. Anil Verma et al. [99] reported on the development of the heteropolyacid/PBI membrane in the fuel cell. They pre-treated PWA and SiWA with a water and NaOH solution and found that the pre-treated HPA membrane showed higher conductivity than the untreated HPA membrane. 40%SiWA/PBI showed a higher conductivity of 0.1774 S/cm at 150°C. The SiWA/PBI membrane performed better than the PWA/PBI membrane in the fuel cell. Open circuit voltages (OCV) of the 40% SiWA/PBI composite membrane reached a peak point at 120°C, and decreased with the temperature increasing. Therefore, the HPA/PBI membrane showed higher conductivity and better fuel cell performance, but there were still limitations for HPA/PBI in using the higher temperature PEMFC. Another problem was the relatively high crossover of the HPA/PBI membrane.

An addition of heteropolyacid into sulfonated polymer for higher temperature PEMFC was reported, such as heteropolyacid /sulfonated poly (arylene ether sulfone) [100], Heteropolyacid /Sulfonated Poly (ether ether ketone sulfone) (SPEEK) Composite Membranes [101]. A higher degree of sulfonation of sulfonated polymer will make a stronger interaction between HPA particles and polymer backbone.

Water solubility was a limitation for heteropolyacid use in the PEMFC, because water was a final product which will take the heteropolyacid out through flowing, leading to the properties decreasing and the membrane to break. The addition of CsHPA inorganic to the Nafion[®] matrix also enhanced the water content, and the CsHPA may provide the additional surface functional sites to facilitate proton transport in anhydrous conditions. However, it was a limitation that the CsHPA covering the Nafion[®] clusters and shielding the Nafion sulfonic groups, resulting in decrease of the activity of hydrophilic sulfonic groups. The covering effect for the CsPOW particle was stronger than that for the CsPOMo particle, so CsPOMo/Nafion provided a better conductivity than CsPOW/Nafion[®] [102].

Li et al. [80] reported a caesium-heteropolyacid (CsHPA) /PBI membrane. In their report, the material $\text{Cs}_{2.5}\text{H}_{0.5}\text{PMo}_{12}\text{O}_{40}$ (CsPOM) which was synthesised from Cs_2CO_3 and $\text{H}_3\text{PMo}_{12}\text{O}_{40}$ was insoluble in the water. CsPOM/PBI membranes gave a much higher conductivity (even up to 0.25 S/cm) than the pristine PBI membrane. For the fuel cell performance, the power density of CsPOM/PBI reached the peak point of 0.7 W/cm², and OCV were around 0.95V. The CsPOM/PBI composite membrane was stable above 200 °C and thus was suitable for intermediate temperature PEMFC.

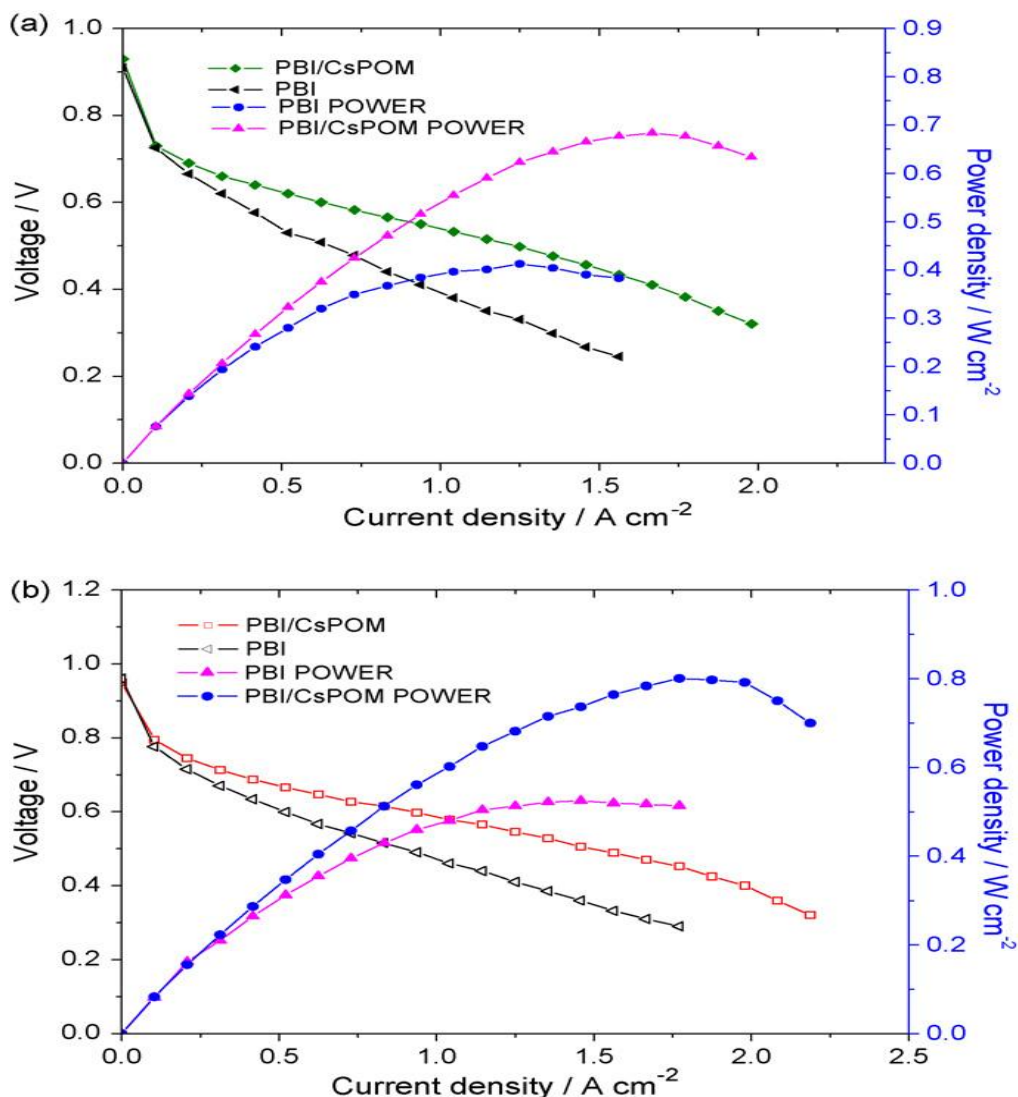


Figure 2-11 (a) polarisation and power density curves of a PEMFC operated at 150 °C atmospheric pressure; (b) polarisation and power density curves of a PEMFC operated at 150 °C, 1 bar pressure. [103]

Ionic liquids (ILs) are organic salts which exhibit a low melting temperature (<100 °C). They consist of only ions; their properties are strikingly different from those of molecular liquids. ILs have been widely used by electrochemists for a long time, as a result of their high ionic conductivity (within 10^{-4} to 10^{-2} S cm⁻¹ around room temperature) and their wide electrochemical potential window (which can be as high as 5.7 V between Pt electrodes) [104,

105]. ILs present advantages such as improved safety and a higher operating temperature range for the membrane, so Ionic liquid combined with polymer materials could be considered used over 100 °C. The membranes H₃PO₄/PMIH₂PO₄/PBI have acceptable ionic conductivity of up to $2.0 \times 10^{-3} \text{ S cm}^{-1}$ at 150 °C and under anhydrous conditions [105]. The IL substitute Heteropolyacids are also a good optimising way to use in the membrane [104-106].

2.5.2.2 Graphite oxide used in composite polymer membranes

From the 18th century, graphite, which is recognised as an allotrope of carbon, is remarkable for the large variety of materials that can be produced from its basic form [107- 109]. Graphite is a composite material containing series of stacked parallel layers of hexagonal planes which are parallel to each other in a three-dimensional structure with arranged carbon atoms in a planar condensed ring system, and the bond has a short length (0.141 nm) [107-109]. The chemical bonds are covalent with sp² hybridisation, and six σ bonds form carbon hexagons with a remaining *p* orbital, of which two neighbouring carbon atoms form a π orbital [107- 109]. Due to the trigonal sp² bonding of carbon atoms, graphite can be used to produce diverse materials such as extremely strong fibers, gas-tight barriers, and gas absorbers [109]. Although the bond between the carbon atoms within a layer is stronger than the bond of diamonds, the force between the two layers of graphite is weak [107- 109]. Graphite invariably contains defects, such as vacancies due to a missing atom, and stacking faults. Figure 2-12 is the graphite structure. The other graphite structure is rhombohedral which is thermodynamically unstable and considered as an extended stacking fault of hexagonal graphite [109].

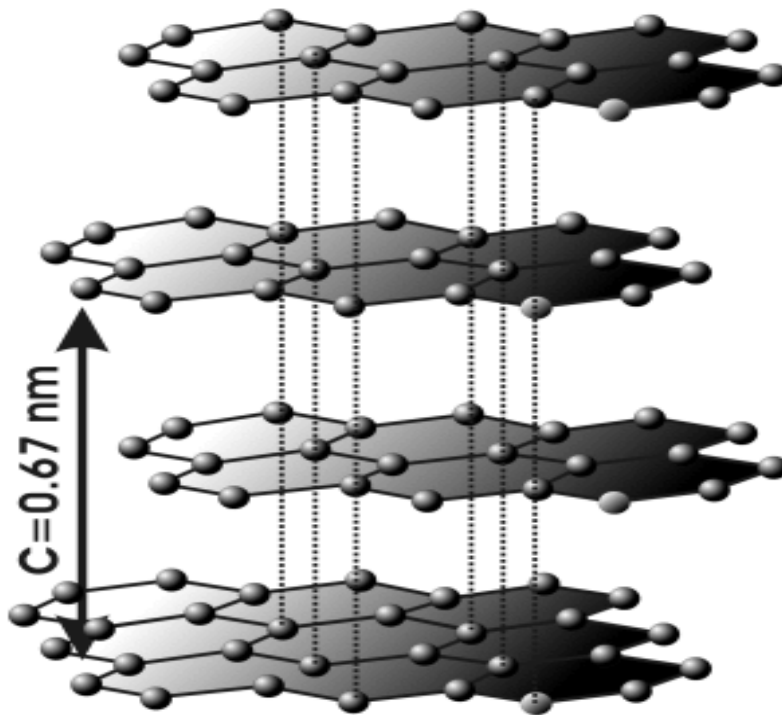


Figure 2-12 Crystal structure of graphite [107]

Graphite as an electrical conductor is one of the allotropes of carbon consisting of layers of hexagonally arranged carbon atoms in a planar condensed ring system, so it can be used as the material in the electrodes of an electrical arc lamp [107- 109]. Graphite is considered to be an up-to-date topic in modern material science and extensive research and developments have been devoted to the use of graphite as fillers to produce a variety of high-performance nanocomposites for applications. Graphite as reinforcing fibers for composites can improve the performance of a matrix or achieve new properties due to its low density, excellent mechanical strength, thermal stability, and electrical and thermal conductivity [110].

Graphite oxide (GO), which is oxidized from graphite, not only contains most good properties of graphite, but also improves some properties because of increased O and N atoms. The preparation of graphene oxide was reported in 1859 by a British chemist, B. C. Brodie [111], while investigating the structure of graphite and later Hummer and Offeman

developed an oxidation method [112]. Hummer's method is widely used to prepare the graphite oxide.

Thin sheets of graphite oxide (GO) have recently emerged as a new carbon-based nanoscale material. The solubility of GO in water and other solvents allows it to be deposited uniformly onto wide ranging substrates in the form of thin films. The structure of GO is often simplistically assumed to be a graphene sheet bonded to oxygen in the form of carboxyl, hydroxyl or epoxy groups. [113-116].

Functionalised graphite oxide (FGO) is not only easily incorporated and homogeneously distributed into various matrices, but also improves the hydrophilicity and proton conductivity. Functionalised groups such as 3-mercaptopropyl trimethoxysilane (MPTMS) [117], $-\text{SO}^{3-}$ [115] added into graphite oxide were incorporated with the Nafion[®]. The functionalised graphite controlled the state of water by means of nanoscale manipulation of the physical geometry and chemical functionality of ionic channels. The confinement of bound water within the reorganised nanochannels of composite membranes enhanced proton conductivity at high temperature and the low activation energy for ionic conduction [118]. Also, the increase of F-GO nanofiller loading extended the number of available ion exchange sites per cluster, resulting in the increment of proton mobility in the membrane at high temperatures and low humidity values [117].

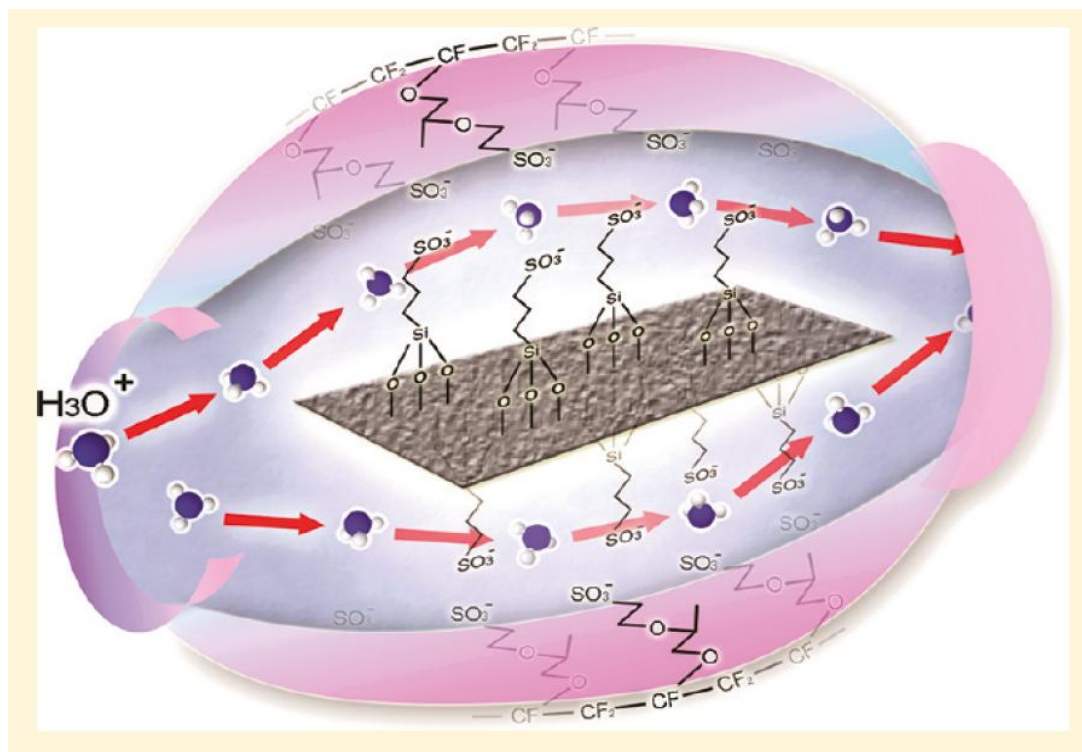


Figure 2-13 Structure of functionalised graphite oxide incorporation with Nafion[®] [117].

As Zarrin, H. Et al. [117] Reported, the Nafion[®] incorporation with FGO showed good fuel cell performance at an elevated temperature (120 °C). The peak power density for 10 wt % FGO/ Nafion was 0.15 W cm⁻², approximately 3.6 times higher than that of recast Nafion (0.042 W cm⁻²). This indicated that incorporation of the FGO filler was beneficial to structural and mechanical properties of electrolytes.

2.6 Electrode

A PEM fuel cell electrode is essentially a thin catalyst layer pressed between the membrane and porous electrically conductive substrate (e.g. carbon paper). The electrochemical reactions take place on the catalyst surface in this layer [8]. Pt based catalysts are most successful and common catalysts developed in either research or commercial scale. The electro-catalysts used in the PEMFCs are usually based on Pt or its alloy for both anode and cathode. There are three different participants in electrochemical reactions, electrons, protons

and gaseous-liquid reaction, which take place on the catalyst surface. Protons travel through the ionomer and electron transfer through the electrically conductive substrate, so it is essential to have an intimate contact between the catalyst and the ionomer. The electrode should be porous to allow both gases to reach the reaction sites and the product water to be removed to prevent the flood [8, 119].

To minimize potential losses in the cell caused by limitation in the rate of proton transport and gas permeation, the electrode layer should be reasonable thin. The metal active surface area is expected to be larger to provide enough reaction sites, so the Pt particles should be appropriately small. The key to improving the PEMFC performance is to increase Pt effective usage in the catalyst layer, and ionomer added into layer is a useful way [8]. The combination of ionomer membrane and catalyst layers is called membrane electrode assembly (MEA). One way to prepare the MEA is to deposit the catalyst layer including ionomer to the porous substrate and then hot press it to the membrane. The other method is to apply the catalyst directly to the membrane and then press the substrate. Several methods, such as spreading, spraying, and painting, are used for deposition of a catalyst layer to the membrane or the substrate [8].

Typically in the intermediate temperature PEMFC, a binder has been used to enhance the contact of the catalyst to the electrode. The binder fixes the catalyst particles within a layered structure and enables some degree of electronic conductivity between particles and also provides the access of gas into the structure. Nafion[®] ionomers were usually used as a binder in low temperature PEMFC. The Nafion[®] ionomers were normally covered in a thin layer which had thickness in the range of 0.5 to 3 nm depending on a balance between the proton

mobility and oxygen solubility through the layer [121-123]. PTFE is also typically used as binder in the intermediate temperature PEMFC.

Qi et al. [124] recommended a Nafion ionomer of 30% for electrodes with a platinum loading of 0.2-0.35 mg cm⁻¹. Proton migration was improved due to the higher ionomer content, but oxygen transport was compromised by decrease in the porosity. Compared with a uniform Nafion[®] distribution having a different content of Nafion[®] in the catalyst layer compared with the GDL towards membrane will result in a better performance [125].

Seland et al. [125] reported that a Pt loading of 0.36 mg cm⁻² and 0.6 mg cm⁻² accompanied by acid loading of 0.8-1.2 mg cm⁻² are optimum. Scott et al. [126] reported the use of a colloidal ionomer in the catalyst ink which enhanced performance compared with the use of a standard ionomer solution. Kongstein et al. [127] also reported non homogenous platinum distribution that 50% Pt/C loading close to the membrane and 20% Pt/C close to GDL with total loading of 0.6 mg cm⁻². This electrode showed advantages over normal 0.6 mg cm⁻² 50% Pt/C. Pan [128] suggesting that PBI and acid loading used in catalyst layer could be 0.7 and 2.8-3.5 mg cm⁻¹, respectively. Wang et al. [129] concluded that the preparation method and ionomer content of PBI had severe impact.

Based on our groups' previous work, the PBI ionomer used in the catalyst ink showed a similar performance to that with only PTFE added as binder. Hence a 30 wt% PTFE in the Pt/C catalyst ink for the both anode and cathode was found to be optimal. MEA was prepared by depositing the catalyst layer to the porous substrate and then pressed on to the membrane

2.7 Conclusions and perspectives

The PEMFC is considered to be an optimising potential power supply application. The electrolyte as a core issue for PEMFC should have good proton conductivity, mechanical properties, durability, and low cost. So, the development of innovation materials with beneficial properties is attracting much attention. The development of the membrane used for higher temperatures (over 100°C) will especially play a major role in energy research and application. The whole PEMFC system will be simplified over 100°C and the cost will be reduced due to the low cost of the membrane and catalyst. So, this will improve the commercialisation of the PEMFC. Three ways are considered so as to develop the membrane materials: i) using the inorganic filler with polymer to improve the performance, ii) modifying the PBI materials by grafting the functional group, iii) combining the PTFE mechanics with high conductivity polymer to elevate the fuel cell performance.

References:

1. Bacon, F.T. and Fry T. M. *Review Lecture: the development and practical application of fuel cells*. Proceedings of the royal society of London. Series A, Mathematical and physical sciences, **1973**, 334(1599), 427-452
2. Bent S. *Hydrogen and Fuel Cells: emerging technologies and applications*, **2005**, Elsevier Inc.: London, P113-153
3. Smitha, B., Sridhar, S., Khan, A.A., *Solid polymer electrolyte membranes for fuel cell applications - A review*, Journal of Membrane Science, **2005**, 259 (1-2) , 10-26
4. Leo J. M. J. Blomen, and Michael N. Mugerwa, *Fuel cell system*, **1993**, PLENUM Press: New York, P73-115
5. Mehta V and Cooper J S. *Review and analysis of PEM fuel cell design and manufacturing*, J. Power Sources, **2003**, 114 32-53
6. Liu B. *Membranes for Energy conversion*, volume 2, Chapter 1, Edited by Klaus-Viktor Peninemann and Suzana Pereira Nunes **2008**, Wiley-VCH publishing, Germany P1-39
7. Mamlouk, M. *Investigation of High Temperature Polymer Electrolyte Membrane Fuel Cells*, PHD thesis, Newcastle University, P50-60, **2008**, P17-32
8. Frano Barbir, *Fuel Cell Technology*, 1st Edition., 2006, springer, Germany
9. Fuel Cell Section of the Program's Multi-Year Research, Development, and Demonstration Plan, 2011
10. Norby, T. *The promise of protonics*, Nature, **2001**, 410, 877-878

11. Yang, C.; Costamagna, P.; Srinivasan, S.; Benziger, J.; Bocarsly, A. B. *Approaches and technical challenges to high temperature operation of proton exchange membrane fuel cells*, Journal of Power Sources, **2001**, 103, 1
12. Li, Q., He, R., Jensen, J.O., and Bjerrum, N.J. *PBI-based polymer membranes for high temperature fuel cells - Preparation, characterization and fuel cell demonstration*, Fuel Cells, **2004**, 4 (3) , 147-159
13. Li, Q., He, R., Jensen, J.O., and Bjerrum, N.J. *Approaches and Recent Development of Polymer Electrolyte Membranes for Fuel Cells Operating above 100 °C*, Chemistry of Materials, **2003**, 15, 4896-4915
14. Li, M., Shao, Z., Scott, K. *A high conductivity $Cs_{2.5}H_{0.5}PMo_{12}O_{40}$ /polybenzimidazole (PBI)/ H_3PO_4 composite membrane for proton-exchange membrane fuel cells operating at high temperature*. Journal of Power Sources, **2008**, 183(1), 69-75
15. K. D. Kreuer, S. J. Paddison, E. Spohr, M. Schuster, *Transport in Proton Conductors for Fuel-Cell Applications: Simulations, Elementary Reactions, and Phenomenology*, Chemical Review, **2004**, 104, 4637-4678
16. Xiaoxiang Xu, *Development of new proton conducting materials for intermediate temperature fuel cells*, PHD thesis, St, Andrews University, **2010**, P5-30
17. P. Colomban, *Proton conductors solid, membranes and gels-materials and devices*, Cambridge University Press, **1992**, New York
18. Dippel, Th., Kreuer, K.D., Lassègues, J.C., Rodriguez, D., *proton conductivity in fused phosphoric acid; A $^1H/^{31}P$ PFG-NMR and QNS study*, Solid State Ionics, **1993**, 61 (1-3) , 41-46
19. X. Gilpa, M. Hogarth, Department of Trade and Industry (UK) Homepage, November 2, **2001**.

20. Li, M., Scott, K. Wu, X., *A poly (R₁R₂R₃)-N⁺/H₃PO₄ composite membrane for phosphoric acid polymer electrolyte membrane fuel cells*, Journal of Power Sources, **2009**, 194(2): 811-814
21. Xu, C., Wu, X., Wang, X., Mamlouk, M., Scott, K., *Composite membranes of polybenzimidazole and caesium-salts-of- heteropolyacids for intermediate temperature fuel cells*, Journal of Materials Chemistry, **2011**, 21 (16) , 6014-6019
22. Li, Q., J. O. Jensen, Savinell, R. F. and Bjerrum, N. J., *High temperature proton exchange membranes based on polybenzimidazoles for fuel cells*. Progress in Polymer Science, **2009**, 34(5), 449-477
23. Vogel H, Marvel CS., *Polybenzimidazoles, new thermally stable polymers*, Journal of Polymer Science, **1961**; 50:511–39
24. Choe EW. *Single-stage melt polymerization process for the production of high molecular weight polybenzimidazole* (Celanese Corporation). US patent, **1982**, 4,312,976.
25. Choe EW, Choe DD. *Polybenzimidazoles (overview)*. In: Salamone JC, editor. *Polymeric materials encyclopedia*, vol. 7. New York: CRC Press; **1996**, 5619–38.
26. Iwakura Y, Imai Y, Uno K. *Polyphenylenebenzimidazoles*. Journal of Polymer Science **1964**, 2A, 2605–2615
27. Hedberg FL, Marvel CS. *New single-step process for Polybenzimidazole synthesis*, Journal of Polymer Science, **1974**, 12, 1823–1828.
28. Eaton PE, Carlson GR, Lee JT. *Phosphorus pentoxide-methanesulphonic acid—convenient alternative to polyphosphoric acid*. Journal of Organic Chemistry **1973**, 38, 4071–3.

29. Li Q, Jensen J. *Membranes for Energy conversion*, volume 2, Chapter 3, Edited by Klaus-Viktor Peinemann and Suzana Pereira Nunes, **2008**, Wiley-VCH publishing, Germany
30. Kim T., Lim T., Lee J, *High-temperature fuel cell membranes based on mechanically stable para-ordered polybenzimidazole prepared by direct casting*, Journal of Power Sources, **2007**, 172, 172–179
31. Arindam S., Sandip G., Sudhangshu M., Tushar J., *Structurally isomeric monomers Directed copolymerization of polybenzimidazoles and their properties*, Polymer, **2010**, 5,1 5929-5941
32. Carollo A, Quartarone E, Tomasi C, Mustarelli P, Belotti F, Magistris A, Maestroni F, Parachini M, Garlaschelli L, Righetti PP. *Developments of new proton conducting membranes based on different polybenzimidazole structures for fuel cells applications*. Journal of Power Sources, **2006**,160, 175-180.
33. Li Q, Jensen O. *Membranes for high temperature PEMFC based on acid-doped polybenzimidazoles*. In: Peinemann KV, Nunes SP, editors. *Membranes for energy conversion*, vol. 6. Wiley-VCH; **2007**, P61-89.
34. Qing S., Huang W, Yan D. *Synthesis and characterization of thermally stable sulphonated polybenzimidazoles*. European Polymer Journal, **2005**; 41:1589-1595
35. Kumbharkar S, Karadkar P, Kharul U. Enhancement of gas permeation properties of polybenzimidazoles by systematic structure architecture. Journal of Membrane Science **2006**,286,161-169
36. Xu N, Guo X., Fand J., Xu H., Yin J., *Synthesis of Novel Polybenzimidazoles with Pendant Amino Groups and the Formation of their Crosslinked Membranes for Medium Temperature Fuel Cell Applications*, Journal of Polymer Science: Part A: Polymer Chemistry, **2009**, 47, 6992–7002

37. Yu S, Xiao L, Benicewicz BC. *Durability studies of PBI-based high temperature PEMFCs*. Fuel Cells, **2008**, 8, 156-174.
38. Chuang S., Hsu S., Liu Y., *Synthesis and properties of fluorine-containing polybenzimidazole/silica nanocomposite membranes for proton exchange membrane fuel cells*, Journal of Membrane Science, **2007**, 305, 353–363
39. Tan N., Xiao G., Yan D., Sun G., *Preparation and properties of polybenzimidazoles with sulfophenylsulfonyl pendant groups for proton exchange membranes*, Journal of Membrane Science, **2010**, 353, 51–59
40. Kim T., Kim S., Lim T., Lee, J., *Synthesis and properties of poly(aryl ether benzimidazole) copolymers for high-temperature fuel cell membranes*, Journal of Membrane Science, **2008**, 323, 362–370
41. Dai H., Zhang H., Zhong H., Jin H., Li X., Xiao S., and Mai Z., *Properties of Polymer Electrolyte Membranes Based on Poly(Aryl Ether Benzimidazole) and Sulphonated Poly(Aryl Ether Benzimidazole) for High Temperature PEMFCs*, Fuel Cells, **2010**, 10, 5, 754–761
42. Pu H, Wang L., Pan H., Wan D., *Synthesis and Characterization of Fluorine-Containing Polybenzimidazole for Proton Conducting Membranes in Fuel Cells*, Journal of Polymer Science: Part A: Polymer Chemistry, **2010**, 48, 2115–2122
43. Poterkar R., Kulkarni M., Kulkarni R., Vernekar S., *Polybenzimidazoles Tethered with N-Phenyl 1,2,4-Triazole Units as Polymer Electrolytes for Fuel Cells*, Journal of Polymer Science: Part A: Polymer Chemistry, **2009**, 47, 2289–2303
44. Qian G., Dennis W. Smith Jr., Brian C., *Synthesis and characterization of high molecular weight perfluorocyclobutylcontaining polybenzimidazoles (PFCB–PBI) for high temperature polymer electrolyte membrane fuel cells*, Polymer, **2009**, 50, 3911–3916

45. Chuang S, Hsu S, Hsu C. *Synthesis and properties of fluorine-containing polybenzimidazole/montmorillonite nanocomposite membranes for direct methanol fuel cell applications*. Journal of Power Sources, **2007**, 168, 172-177.
46. Qing S, Huang W, Yan D. *Synthesis and characterization of thermally stable sulfonated polybenzimidazoles obtained from 3,3'-disulphonyl-4,4' dicarboxyldiphenylsulphone*. Journal of Polymer Science A: Polymer Chemistry, **2005**, 43, 4363-4372.
47. Mader J. and Benicewicz B., *Synthesis and Properties of Segmented Block Copolymers of Functionalised Polybenzimidazoles for High-Temperature PEM Fuel Cells*, Fuel Cells, **2011**, 11, 2, 222–237
48. Xu H, Chen K, Guo X, Fang J, Yin J. *Synthesis of hyperbranched polybenzimidazoles and their membrane formation*. Journal of Membrane Science, **2007**, 288, 255–60.
49. Xu H, Chen K, Guo X, Fang J, Yin J. *Synthesis and properties of hyperbranched polybenzimidazoles via A(2) + B-3 approach*. J Polymer Science A: Polymer Chemistry **2007**, 45, 11508.
50. Bower EA, Rafalko JJ. *Process for modifying Polybenzimidazole polymers with ethylene carbonates* (Celanese Corporation). US patent, **1986**, 4,599,388
51. Sansone MJ, Gupta B, Stackman RW. *Sulfoalkylation of Polybenzimidazole* (Hoechst Celanese). US patent, **1989**, 4,814,399.
52. Sansone MJ, Gupta B, Forbes CE, Kwiatek MS. *Sulfalkylation of hydroxyethylated polybenzimidazole polymers* (Hoechst Celanese). US patent, **1991**, 4,997,892.
53. Sansone MJ. *Cyanoethylation of hydroxyethylated Polybenzimidazole polymers* (Hoechst Celanese). US patent, **1989**, 4,868,249.

54. Glipa X., Haddad M., Jones D., Roziere J., *Synthesis and characterisation of sulfonated polybenzimidazole: a highly conducting proton exchange polymer*, *Solid State Ionics*, **1997**, 97, 323–331
55. Sukumar P., Wu W., Markova D., Unsal O., Klapper M., Mullen K., *Functionalized Poly(benzimidazole)s as Membrane Materials for Fuel Cells*, **2007** 208(19-20), 2258-2267
56. Kawahara M., Rikukawa M., Sanui K., *Relationship between absorbed water and proton conductivity in sulfopropylated poly(benzimidazole)*, *Polymers for Advanced Technologies*, **2000**, 11, 544-547.
57. Li Q., Hjuler H., Bjerrum N., *Phosphoric acid doped polybenzimidazole membranes: Physiochemical characterization and fuel cell applications*, *Journal of Applied Electrochemistry*, **2001**, 31, 773-779
58. He R, Li Q, Xiao G, Bjerrum N. *Proton conductivity of phosphoric acid doped polybenzimidazole and its composites with inorganic proton conductors*. *Journal of Membrane Science*, **2003**, 226,169–184
59. Li Q, He R, Jensen J, Bjerrum N. *PBI-based polymer membranes for high temperature fuel cells—preparation, characterization and fuel cell demonstration*. *Fuel Cells*, **2004**, 4,147–59.
60. Litt M, Ameri R, Wang Y, Savinell R, Wainwright J. *Polybenzimidazoles/ phosphoric acid solid polymer electrolytes: mechanical and electrical properties*. *Materials Research Society Symposium Proceedings*, **1999**, 548, 313–23.
61. Xiao L, Zhang H, Scanlon E, Ramanathan L, Choe EW, Rogers D, Apple T., and Benicewicz B. *High-temperature polybenzimidazole fuel cell membranes via a sol–gel process*. *Chemistry of Materials*, **2005**, 17, 5328–33

62. Kumbharkar S, Karadkar P, Kharul U. *Enhancement of gas permeation properties of polybenzimidazoles by systematic structure architecture*. Journal of Membrane Science **2006**, 286, 161–9.
63. He R, Li Q, Bach A, Jensen J, Bjerrum N. *Physicochemical properties of phosphoric acid doped polybenzimidazole membranes for fuel cells*. Journal of Membrane Science, **2006**, 277, 38–45.
64. Nolte, R., Ledjeff, K., Bauer, M., Mulhaupt, R., *Partially sulfonated poly(arylene ether sulfone) - A versatile proton conducting membrane material for modern energy conversion technologies* , Journal of Membrane Science, **1993**, 83 (2) , 211-220
65. Manea, C., Mulder, M., *Characterization of polymer blends of polyethersulfone/sulfonated polysulfone and polyethersulfone/sulfonated polyetheretherketone for direct methanol fuel cell applications*, Journal of Membrane Science, **2002**, 206 (1-2) , pp. 443-453
66. Zaidi, S.M.J., Mikhailenko, S.D., Robertson, G.P., Guiver, M.D., Kaliaguine, S., *Proton conducting composite membranes from polyether ether ketone and heteropolyacids for fuel cell applications*, Journal of Membrane Science, **2000**, 173 (1), 17-34
67. Xing, P., Robertson, G.P., Guiver, M.D., Mikhailenko, S.D., Wang, K., Kaliaguine, S., *Synthesis and characterization of sulfonated poly(ether ether ketone) for proton exchange membranes*, Journal of Membrane Science, **2004**, 229 (1-2) , pp. 95-106
68. Fang, J., Guo, X., Harada, S., Watari, T., Tanaka, K., Kita, H., Okamoto, K.-I., *Novel sulfonated polyimides as polyelectrolytes for fuel cell application: 1. Synthesis, proton conductivity, and water stability of polyimides from 4,4'-diaminodiphenyl ether-2,2'-disulfonic acid*, Macromolecules, **2002**, 35 (24) , pp. 9022-9028

69. Miyatake, K., Zhou, H., Matsuo, T., Uchida, H., Watanabe, M., *Proton conductive polyimide electrolytes containing trifluoromethyl groups: Synthesis, properties, and DMFC performance*, *Macromolecules*, **2004**, 37 (13), 4961-4966
70. Hickner, M.A., Fujimoto, C.H., Cornelius, C.J., *Transport in sulfonated poly(phenylene)s: Proton conductivity, permeability, and the state of water*, *Polymer*, **2006**, 47 (11), 4238-4244
71. Yang, T., Shi, P., *Study on the mesocarbon microbeads/polyphenylene sulfide composite bipolar plates applied for proton exchange membrane fuel cells*, *Journal of Power Sources*, **2008**, 175 (1), 390-396
72. Li M, Zhang H., and Shao Z, *Quaternized Poly(phthalazinone ether sulfone ketone) Membrane Doped with H₃PO₄ for High-Temperature PEMFC Operation*, *Electrochemical and Solid-State Letters*, **2006**, 9 (2), A60-A63
73. Wang X., Xu C, Golding B., Sadeghi M., Cao Y, Scott K., *A novel phosphoric acid loaded quaternary 1,4-diazabicyclo- [2.2.2]-octane polysulfone membrane for intermediate temperature fuel cells*, *International journal of hydrogen energy*, **2011**, 36, 8550-8556
74. Li M. and Scott K., *A Polymer Electrolyte Membrane Fuel Cell Based on Zirconium Phosphate and Phosphoric Acid*, *Electrochemical and Solid-State Letters*, **2009**, 12(12) B171-B175
75. Li M., Scott K., *A polymer electrolyte membrane for high temperature fuel cells to fit vehicle applications*, *Electrochimica Acta*, **2010**, 55, 2123–2128
76. Choi D., Lee J., Kwon O., Kim; Kim J., Kim K., *Sulfonated poly (fluorinated arylene ether)s/poly(N-vinylimidazole) blend polymer and PTFE layered membrane for operating PEMFC at high temperature*, *Journal of Power Sources*, **2008**, 178(2), 677-682

77. Jiang, Y., Xu, X., Lan, R., Zhang, L., Tao, S., *Stability and conductivity study of NH₄PO₃-PTFE composites at intermediate temperatures*, Journal of Alloys and Compounds, **2009**, 480 (2) , 874-877
78. Kozhevnikov I., *Catalysts for fine chemical synthesis*, in: *Catalysis by Polyoxometalates*, vol. 2, John Wiley & Sons, Chichester, **2002**, P9-59
79. Baker L., Glick D., Present general status of understanding of heteropoly electrolytes and a tracing of some major highlights in the history of their elucidation, Chemical Review, **1998**, 98, 3-49.
80. Vuillaume P., Mokrini A., Siu A., Theberge K., Robitaille L., *Heteropolyacid/saponite-like clay complexes and their blends in amphiphilic SEBS*, European Polymer Journal, **2009**, 45, 1641–1651.
81. Gómez-Romero, P., Asensio, J.A., Borrós, S., *Hybrid proton-conducting membranes for polymer electrolyte fuel cells: Phosphomolybdic acid doped poly (2, 5-benzimidazole) - (ABPBI-H₃PMO₁₂O₄₀)*. Electrochimica Acta, **2005**, 50 (24), 4715-4720
82. Vogel H, and Marvel C, *Polybenzimidazoles, new thermally stable polymers*, Journal of Polymer Science, **1961**, 50:511-39
83. H. Tian, O. Savadogo, *Silicotungstic acid Nafion composite membrane for proton-exchange membrane fuel cell operation at high temperature*, Journal of New Materials for Electrochemical Systems, **2006**, 9, 61-71.
84. V. Ramani, H.R. Kunz, J.M. Fenton, *Effect of particle size reduction on the conductivity of Nafion/phosphotungstic acid composite membranes*, Journal of Membrane Science, **2005**, 266, 110-114.
85. Z.-G. Shao, P. Joghee, I.-M. Hsing, *Preparation and characterization of hybrid Nafion–silica membrane doped with phosphotungstic acid for high temperature operation of proton exchange membrane fuel cells*, Journal of Membrane Science, **2004**, 229, 43-51.

86. Z.-G. Shao, H. Xu, M. Li, I.-M. Hsing, *Hybrid Nafion–inorganic oxides membrane doped with heteropolyacids for high temperature operation of proton exchange membrane fuel cell*, *Solid State Ionics*, **2006**, 177, 779-785.
87. W. Xu, T. Lu, C. Liu, W. Xing, *Low methanol permeable composite Nafion/silica/PWA membranes for low temperature direct methanol fuel cells*, *Electrochimica Acta*, **2005**, 50, 3280-3285.
88. A. Mahreni, A.B. Mohamad, A.A.H. Kadhum, W.R.W. Daud, S.E. Iyuke, *Nafion/silicon oxide/phosphotungstic acid nanocomposite membrane with enhanced proton conductivity*, *Journal of Membrane Science*, **2009**, 327, 32-40.
89. X.-M. Yan, P. Mei, Y. Mi, L. Gao, S. Qin, *Proton exchange membrane with hydrophilic capillaries for elevated temperature PEM fuel cells*, *Electrochemistry Communications*, **2009**, 11, 71-74.
90. V. Ramani, H.R. Kunz, J.M. Fenton, *Stabilized heteropolyacid/Nafion composite membranes for elevated temperature/low relative humidity PEFC operation*, *Electrochimica Acta*, **2005**, 50, 1181-1187.
91. M. Li, Z.-G. Shao, H. Zhang, Y. Zhang, X. Zhu, B. Yi, *Self-humidifying $C_{52.5}H_{0.5}PW_{12}O_{40}$ /Nafion/PTFE composite membrane for proton exchange membrane fuel cells*, *Electrochemical and Solid-State Letters*, **2006**, 9, A92–A95.
92. S.Y. Oh, T. Yoshida, G. Kawamura, H. Muto, M. Sakai, A. Matsuda, *Proton conductivity and fuel cell property of composite electrolyte consisting of Csubstituted Csubstituted heteropoly acids and sulfonated poly(ether–ether ketone)*, *Journal of Power Sources*, **2010**, 195, 5822–5828.
93. D.R. Vernon, F. Meng, S.F. Dec, D.L. Williamson, J.A. Turner, A.M. Herring, *Synthesis, characterization, and conductivity measurements of hybrid membranes containing a*

- mono-lacunary heteropolyacid for PEM fuel cell applications*, Journal of Power Sources, **2005**, 139, 141–151.
94. W. Jang, S. Choi, S. Lee, Y. Shul, H. Han, Characterizations and stability of polyimidephosphotungstic acid composite electrolyte membranes for fuel cell, Polymer Degradation and Stability, **2007**, 92, 1289–1296.
95. C. Zhao, H. Lin, Q. Zhang, H. Na, Layer-by-layer self-assembly of polyaniline on sulfonated poly(arylene ether ketone) membrane with high proton conductivity and low methanol crossover, International Journal of Hydrogen Energy, **2010**, 35, 10482–10488.
96. M. Helen, B. Viswanathan, S. Srinivasa Murthy, Poly(vinyl alcohol)–polyacrylamide blends with cesium salts of heteropolyacid as a polymer electrolyte for direct methanol fuel cell applications, Journal of Applied Polymer Science, **2010**, 116, 3437–3447.
97. S.-Y. Oh, T. Yoshida, G. Kawamura, H. Muto, M. Sakai, A. Matsuda, *Inorganic–organic composite electrolytes consisting of polybenzimidazole and Cs-substituted heteropoly acids and their application for medium temperature fuel cells*, Journal of Materials Chemistry, **2010**, 20, 6359–6366.
98. Staiti, P. and M. Minutoli, *Influence of composition and acid treatment on proton conduction of composite polybenzimidazole membranes*. Journal of Power Sources, **2001**, 94(1), 9-13
99. Verma, A. and Scott K., *Development of high-temperature PEMFC based on heteropolyacids and polybenzimidazole*. Journal of Solid State Electrochemistry, **2010**, 14(2), 213-219
100. Kim Y., Wanga F, Hicknera M., Zawodzinski T., McGrath J., *Fabrication and characterization of heteropolyacid ($H_3PW_{12}O_{40}$)/directly polymerized sulfonated poly(arylene ether sulfone) copolymer composite membranes for higher temperature fuel cell applications*, Journal of Membrane Science, **2003**, 212(1-2), 263-282

101. Wang Z., Ni H., Zhao C., LI X., Fu T., Na H., *Investigation of sulfonated poly (ether ether ketone sulfone)/heteropolyacid composite membranes for high temperature fuel cell applications*, Journal of Polymer Science, Part B: Polymer Physics, **2006**, 44(14), 1967-1978
102. Amirinejada M., Madaenia S., Rafieeb E., Amirinejad S., *Cesium hydrogen salt of heteropolyacids/Nafion nanocomposite membranes for proton exchange membrane fuel cells*, Journal of Membrane Science, **2011**, 377, 89– 98
103. Li, M., Shao Z., Scott K., *A high conductivity $Cs_{2.5}H_{0.5}PMo_{12}O_{40}$ /polybenzimidazole (PBI)/ H_3PO_4 composite membrane for proton-exchange membrane fuel cells operating at high temperature*, Journal of Power Sources, **2008**, 183(1), 69-75
104. Le Bideau, J., Viau, L., Vioux, A., *Ionogels, ionic liquid based hybrid materials*, Chemical Society Reviews, **2011**, 40 (2) , pp. 907-925
105. Ye H., Huang, J., Xu, J.J., Kodiweera, N.K.A.C., Jayakody, J.R.P., Greenbaum, S.G., *New membranes based on ionic liquids for PEM fuel cells at elevated temperatures*, Journal of Power Sources, **2008**, 178 (2) , pp. 651-660
106. Lin, B., Cheng, S., Qiu, L., Yan, F., Shang, S., Lu, J. *Protic ionic liquid-based hybrid proton-conducting membranes for anhydrous proton exchange membrane application*, Chemistry of Materials, **2010**, 22 (5) , pp. 1807-1813
107. P. Delhaes, *Graphite and Precursors*. CRC Press, **2001**, ISBN:9056992287
108. Peter M., *Carbon Fibers and their Composites*, CRC Press, **2005** ISBN: 9780824709839

109. Pierson H., *Handbook of Carbon, Graphite, Diamond and Fullerenes*, Nypes Publication, U.S., **1993** ISBN: 9780815513391
110. Jin J., Song M., and Pan F., *A DSC study of effect of carbon nanotubes on crystallisation behaviour of poly(ethylene oxide)*, *Thermochimica Acta*, **2007**, 456,25–31
111. Brodie B., *On the Atomic Weight of Graphite*, *Philos. Trans. R. Soc. London*, **1859**, 149, 249–259
112. Hummers W., and Offeman R., *Preparation of Graphitic Oxide*, *Journal of the American Chemical Society*, **1958**, 80, 6, 1339
113. Dikin, D., Stankovich, S., Zimney, E., Piner, R., Dommett, G., Evmenenko, G., Nguyen, S., Ruoff, R., *Preparation and characterization of graphene oxide paper*, *Nature*, **2007**, 448, 457-460.
114. Mkhoyan, K.; Contryman, A.; Silcox, J.; Stewart, D.; Eda, G.; Mattevi, C.; Miller, S.; Chhowalla, M., *Atomic and electronic structure of graphene-oxide*, *Nano Letters*, **2009**, 9, 1058-1063
115. Yu, A.; Roes, I.; Davies, A.; Chen, Z. *Ultrathin, transparent, and flexible graphene films for supercapacitor application*, *Applied Physics Letters*, **2010**, 96, 253105.
116. Stankovich, S., Dikin, D., Dommett, G., Kohlhaas, K., Zimney, E., Stach, E., Piner, R., Nguyen, S., Ruoff, R., *Graphene-based composite materials*, *Nature*, **2006**, 442, 282-286
117. Zarrin, H., Higgins, D., Jun, Y., Chen, Z., Fowler, M., *Functionalized graphene oxide nanocomposite membrane for low humidity and high temperature proton exchange membrane fuel cells*, *Journal of Physical Chemistry C*, **2011**, 115 (42) , 20774-20781
118. Choi, B.G., Hong, J., Park, Y.C., Jung, D.H., Hong, W.H., Hammond, P.T., Park, H., *Innovative polymer nanocomposite electrolytes: Nanoscale manipulation of ion channels by functionalized graphenes*, *ACS Nano*, **2011**, 5 (6) , 5167-517

119. Vielstivh W., Lamm A., and Gasteiger H., *Handbook of Fuel cells: Fundamentals Technology and Applications*, Volume 3, **2003**, John Wiley & Sons Ltd., UK
120. Lee, S.J., S. Mukerjee, J. McBreen, Y. W. Rho, Y. T. Kho, and T. H. Lee, *Effects of Nafion impregnation on performance of PEMFC electrode*, *Electrochimica Acta*, **1998**, 43 (24) 3693-3701.
121. Ralph, T. R. and M. P. Hogarth, *Catalysis for low temperature fuel cells*, *Platinum Metals rev*, **2002**, 46 (1), 3-14
122. Tada, T. *Handbook of Fuel Cells: Fundamentals, Technology and Applications*, John Wiley& Sons, UK, **2003**
123. Qi Z.G., and A. Kaufman, *Low Pt loading high performance cathodes for PEM fuel cells*, *Journal of Power Sources*, **2003**, 113 (1), 37-43
124. Song, D. T., Q. P. Wang, Z. S. Liu, M. Eikerling, Z. Xie, T. Navessin, and S. Holdcroft, *A method for optimising distributions of Nafion and Pt in cathode catalyst layers of PEM fuel cells*, *Electrochimica Acta*, **2005**, 50 (16-17)
125. Seland, F., Berning T., Borresen, B., and Tunold R., *Improving the performance of high temperature PEM fuel cells based on PBI electrolyte*. *Journal of Power Sources*, **2006**, 160 (1), 27-36
126. Scott K. and Manlounk M. *High temperature polymer electrolyte membrane fuel cell*. *Battery bimonthly*, **2006**, 36 (5), 11
127. Kongstein O., Berning T., Borresen B., Seland F., and Tunold R., *Polymer electrolyte fuel cells based on phosphoric acid doped Polybenzimidazole (PBI) membranes*, *Energy*, **2007**, 32 (4), 418-422
128. Pan, C., Q. Li, J. Q. Jensen, R. He, L. N. Cleemann, M. S. Nilsson, N. J. Bjerrum, and Q. Zeng, *preparation and operation of gas diffusion electrodes for high-temperature proton exchange membrane fuel cells*, *Journal of Power Sources*, **2007**, 172, 278-286

129. Wang, J. T., R. F. Savinell, J. Wainright, M Litt, H Yu, *A H_2/O_2 fuel cell using acid doped Polybenzimidazole as polymer electrolyte*, *Electrochimica Acta*, **1996**, 41(2), 193

Chapter 3: Theoretical

It is an important step to understand and comprehend the basic theories about electrochemistry, fuel cell, materials and etc. This chapter introduced fuel cell thermodynamic, electrochemical kinetic, proton conductance and mechanism, and percolation theory. The operation of fuel cells includes electrochemical reactions which follow the thermodynamic and kinetic principle that was introduced in this chapter. The proton conducting mechanism and the percolation theory indicate the way to improve the proton conductivity.

3.1 Thermodynamic and kinetic for the fuel cell

3.1.1 Thermodynamic

The reaction in a hydrogen/oxygen PEM fuel cell corresponds to a chemical process, which contains two separate electrochemical reactions at the anode and the cathode [1, 2].



The same number of electrons, n , must be exchanged in both reactions to balance of the overall reaction. The Gibbs free energy of the reactions is given by:

$$\begin{aligned} \Delta G &= -nFE = \Delta H - T\Delta S \\ \Delta G(l) &= \Delta H - T\Delta S = -286.01 - 298.15 \times \left(0.06996 - 0.13066 - \frac{1}{2} \times 0.20517 \right) \\ &= -237.34 \text{ kJ mol}^{-1} \\ \Delta G(g) &= \Delta H - T\Delta S = -241.98 - 298.15 \times \left(0.18884 - 0.13066 - \frac{1}{2} \times 0.20517 \right) \\ &= -228.74 \text{ kJ mol}^{-1} \end{aligned} \quad (3.4)$$

Where n is the number of electrons involved in the above reaction, F is the Faraday constant (96,485 Coulombs/electron-mol), E is the cell voltage, ΔH is the Enthalpy, T is the temperature, and ΔS is the entropy. The table 3-1 showed the enthalpies and entropies of

materials, which could be used to calculate the ΔG under different conditions through eq. 3.4.

Table 3-1 Enthalpies and Entropies of formation for fuel cell reactants and products at 25 °C and 1 atm [1]

	ΔH (kJ mol ⁻¹)	ΔS (kJ mol ⁻¹ K ⁻¹)
H ₂	0	0.13066
O ₂	0	0.20517
H ₂ O (liquid)	-286.02	0.06996
H ₂ O (vapor, gas)	-241.98	0.18884

Assuming that all of the Gibbs free energy can be converted into electrical energy, the maximum possible theoretical efficiency of a fuel cell is the ratio between the Gibbs free energy and Enthalpy [8]:

$$\eta = \frac{\Delta G}{\Delta H} = \frac{237.34}{286.02} \times 100\% = 83\% \quad (3.5)$$

The efficiency of PEMFC is much higher than other energy conversion systems at low temperatures which are limited by the Carnot cycle which are normally 20%-40% in the temperature range from 100-200 °C [1, 2].

The theoretical cell potential at 25°C and atmospheric pressure is:

$$E_0 = \frac{-\Delta G}{nF} = \frac{237.34}{2 \times 96485} = 1.229V \quad (3.6)$$

Under non standard conditions the equilibrium potential is expressed by the Nernst equation [3], For the hydrogen and oxygen reaction, the cell potential is a function of operating temperature and pressure [2, 3].

$$E = E_0 + \frac{RT}{nF} \ln \left[\frac{a_{H_2} a_{O_2}^{0.5}}{a_{H_2O}} \right] \quad (3.7)$$

Where, a, is the activity or the ratio between the partial pressures of reactants (H₂ and O₂) or product (H₂O) and atmospheric pressure (for liquid water product $a_{H_2O} = 1$).

Actual cell potential is a function of temperature and pressure as presented by equ. 3.8:

$$E_{T,P} = -\left(\frac{\Delta H}{nF} - \frac{T\Delta S}{nF}\right) + \frac{RT}{nF} \ln \left[\frac{P_{H_2}(P_{O_2})^{0.5}}{P_{H_2O}} \right] \quad (3.8)$$

Typically the PBI based fuel cells operated above 100 °C, so the potential was considered to fit the gaseous water condition that achieve around 1.18V theoretically by ignoring all the other affection.

Practical equilibrium or open circuit potentials are affected by other factors. Crossover of hydrogen from anode to cathode and oxygen from cathode to anode create a mixed potentials leading to a reduction of the open cycle potential. In addition, the coverage of platinum electro-catalyst surfaces with oxides and impurities, and the corrosion of the carbon electrode supports would influence the equilibrium potential. So in experimental tests, the open cycle voltage typically was in the range of 0.8-0.9V depending on operating conditions [3-5].

3.1.2 Electrochemical kinetics

Consider two substances, A and B with a simple unimolecular elementary reaction [3]



The reaction rate is described by

$$\begin{aligned} v_f &= k_f C_A & \& & v_b &= k_b C_B \\ v_{net} &= v_f - v_b = k_f C_A - k_b C_B \end{aligned} \quad (3.10)$$

Where v_f and v_b are the rate of the forward and reverse process, k_f and k_b are the rate constant, C_A and C_B are the concentration.

The Arrhenius equation describes the temperature rate constants, which is expressed as:

$$k = A e^{-E_a/RT}$$

$$(3.11)$$

Where E_a is the activation energy, A is the frequency factor. The exponential term represents the probability of using thermal energy to surmount an energy barrier E_a [3].

If the potential is changed by ΔE to a new value, E , the relative energy changes from ΔG^* to ΔG by $-F\Delta E = -F(E - E_r)$, so the Gibbs free energy of reduction and oxidation could be presents as:

$$\text{Reduction reaction: } \Delta G = \Delta G^* + \alpha_a F \Delta E$$

$$\text{Oxidation reaction: } \Delta G = \Delta G^* - \alpha_c F \Delta E$$

$$(3.12)$$

Where α_a is the transfer coefficient of the reduction reaction and α_c is the transfer coefficient of the oxidation reaction. The transfer coefficient is a measure of the symmetry of the energy barrier. Furthermore, according to the Arrhenius equation, the reaction rate is given as

$$\text{Reduction reaction: } k_f = k_{f,0} e^{-\alpha_a F \Delta E / RT}$$

$$\text{Oxidation reaction: } k_b = k_{b,0} e^{\alpha_c F \Delta E / RT}$$

$$(3.13)$$

At equilibrium of the reaction, equation 3.10 gives

$$i_0 = nF C_A k_{f,0} e^{-\alpha_a F \Delta E / RT} = nF C_B k_{b,0} e^{\alpha_c F \Delta E / RT}$$

$$(3.14)$$

i_0 is the exchange current, and the net current is equal to zero at equilibrium, E_r is the reversible potential.

Consider a special equilibrium condition with a solution, which $C_A = C_B = C$, $k_f = k_b = k$ called the standard rate constant. Combinin g equations 3.10 and 3.14, gives

$$i = i_0 \left\{ \exp \left[\frac{\alpha_a n F (E - E_r)}{RT} \right] - \exp \left[- \frac{\alpha_c n F (E - E_r)}{RT} \right] \right\}$$

$$i_0 = nFkC$$

$$(3.15)$$

At large overpotentials, such as those at the fuel cell cathode, ignoring mass transport limitations, the B-V equation becomes

$$\eta = E - E_r = \frac{RT}{\alpha_c F} \ln \left(\frac{i}{i_0} \right) \quad (3.15)$$

Furthermore, this equation can be simplified as 3.16 when $e^{-\alpha_a F \Delta E / RT} \gg e^{\alpha_c F \Delta E / RT}$

$$\eta = a + b \log i \quad (3.16)$$

This equation is the Tafel equation (fig. 3-1), where, $a = -2.3 \frac{RT}{\eta F} \log i_0$, and $b = 2.3 \frac{RT}{\eta F}$, b is the Tafel Slope. Through a plot of the overpotential versus logarithm of the current density, information regarding the reaction kinetics is obtained. 1) i_0 is obtained from the linear part of the curve extrapolated to the current density axis, 2) the slope of the linear part of the graph gives the value of b , and the transfer coefficient can be calculated.

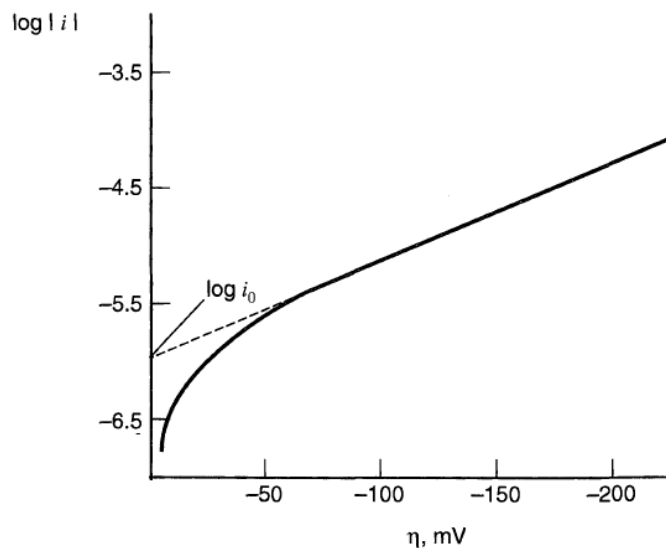


Figure 3-1 Plot of Tafel equation [3]

The kinetics of ORR on Pt in acid has been well studied over ten decades. The Tafel slope of ORR at the low current density region in acid is typically, $b = -2.3RT/F$. The calculated value is around 100 mV dec^{-1} for Pt/PBI- H_3PO_4 system (3 H_3PO_4 per imidazole) at $150 \text{ }^\circ\text{C}$ [13].

3.2 Proton conducting mechanism

As the simplest case of water, proton transfer takes place in a structure such as H_3O_4^+ and H_5O_2^+ instead of transfer within extended hydrogen-bonded water chains [6, 7]. One possible reason is that the hydrogen bond formed as H_3O^+ needs more energy which is unfavourable for fast proton transfer process [6], and the proton transfer from one molecule to the other molecule through hydrogen bond which can be explained by hopping mechanism. Another important point is that the diffusion of protonated water molecules makes some contribution to the total proton conductivity [6]. However, the proton defect concentration of water remains too low ($10^{-7} \text{ mol dm}^{-3}$) leading to a low proton conduct as a diffusion view. So introducing some proton defects is a good method to enhance proton conductivity of water that could be provided as defined in equation (3.17) below.

$$\sigma = \frac{cDz^2F^2}{RT} \quad (3.17)$$

Where σ is the conductivity of ion, c is the concentration of the ion, D is its diffusion coefficient, z is the charge on ion, F is the Faraday constant and R is the gas constant [7, 8].

The mechanism for proton conduction of H_3PO_4 remains the same, i.e. Grotthuss type that an 'excess' proton or protonic defect diffuses through the hydrogen bond network of water molecules or other hydrogen-bonded liquids through the formation or cleavage of covalent bonds. The high proton conductivity could be ascribed to the extremely high proton mobility which involves proton transfer between phosphate species and some structural rearrangements [6-8]. Diffusion constant was affected by several factors shown in eq. 3.18 [8]

$$D = \frac{kT}{6\pi\eta R} \quad (3.18)$$

Where D is the diffusion constant, k is the Boltzmann constant, T is the temperature and η is the viscosity [8].

3.3 Percolation theory

Percolation represents the basic model for a structurally disordered system. Percolation theory is a simple model displaying a phase transition. Although this theory was frequently used to explain the carbon-black network and the DC conductivity of the semiconducting material. For the composite membrane, the proton conductive come from the conductor particles, and the polymer matrix could be considered the insulator. So the proton conductivity of composite membrane could also be explained by percolation theory.

If it is assumed that the composite materials is a square lattice, the conductive filler particles (e.g. cesium heteropolyacid, graphite oxide) as conductor and polymer matrix (e.g. PBI) as insulator, current can only flow between nearest neighbour conductor sites as shown in fig 3-2. Each site is occupied randomly with probability p by the conductive fillers and empty space is $(1 - p)$ [9-11].

When there are few conduction paths which give a low probability p connecting the opposite edges of lattices, the composite materials are isolated. With an increasing volume fraction, more links between edges are established thereby increasing the conductivity. Therefore a threshold concentration p_c exists where for the first time a conduction path is established in which the current can percolate from one edge to the other. At large values of p , the mixture is conductive as many conducting paths exists [9-11]. The table 3-2 refers to the threshold of the content of conducting particles.

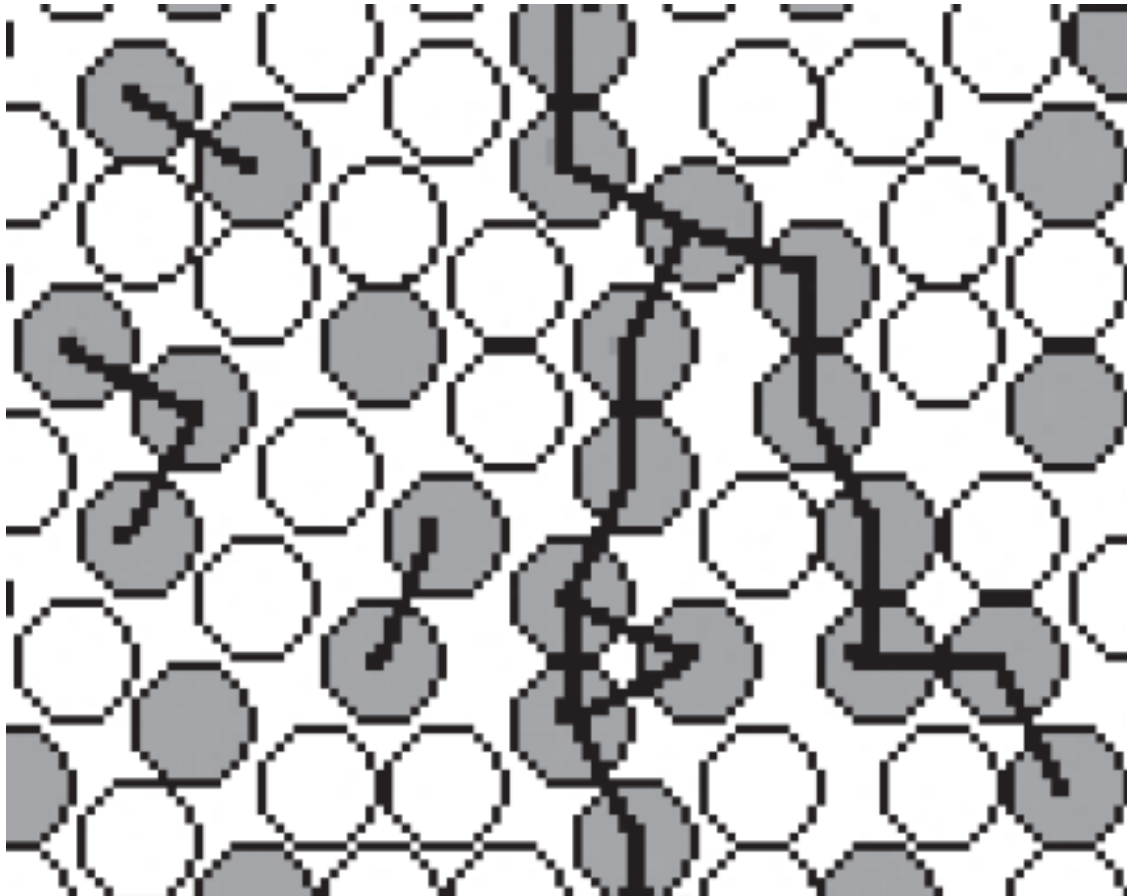


Figure 3-2. Model of percolation, conductive beads (grey), insolation beads (white) [9].

Table 3-2, The percolation threshold for the various lattices [12]

Lattice	Site	Bond
1d	1	1
2d Hexagonal	0.692	0.6527
2d Square	0.592746	0.5
2d Triangular	0.5	0.34729
3d Diamond	0.43	0.388
3d Cubic	0.3116	0.2488
3d Body Centered Cubic	0.246	0.1803
3d Face Centered Cubic	0.198	0.119

The threshold (p_c) is the critical value of the occupation probability and is different in different lattice structures. For a 1d lattice with an infinite number of sites as a line. Each site has a conductivity site p occupied, and insulate parts as $1-p$. Hence, only when percolation threshold $p_c = 1$ is achieved, that is each conductivity site touches at least one by one, the conducting path could be established. For 2d and 3d structures, the value p_c is shown in Table 3-2 [9-12]. The connectivity of sites on the lattice is known as site percolation, and the edges of the sites occupied known as the bond percolation.

For a composite material composed of conducting sites (taking copper particles as an example) and non-conducting sites (particles of insulating material). When a voltage is applied across such a composite material, current only goes through the the copper particles sites. There exists a limit volume fraction of conducting sites (percolation threshold) f_0 , and this threshold obeys the scaling law in the form [12-14]

$$\begin{aligned} \sigma &\propto (f - f_0)^\beta, & f &\geq f_0 \\ \sigma &= 0, & f &< f_0 \end{aligned} \tag{3.19}$$

Where σ is the relative conductivity and f is the volume fraction of conducting sites. The exponent β is a universal constant which depends only on spatial dimensions and is applicable to any percolation system regardless of its chemical, mechanical, structural morphological and statistical properties. For a three-dimensional system, β has been reported to range between 1.3 and 1.7 [13, 14]

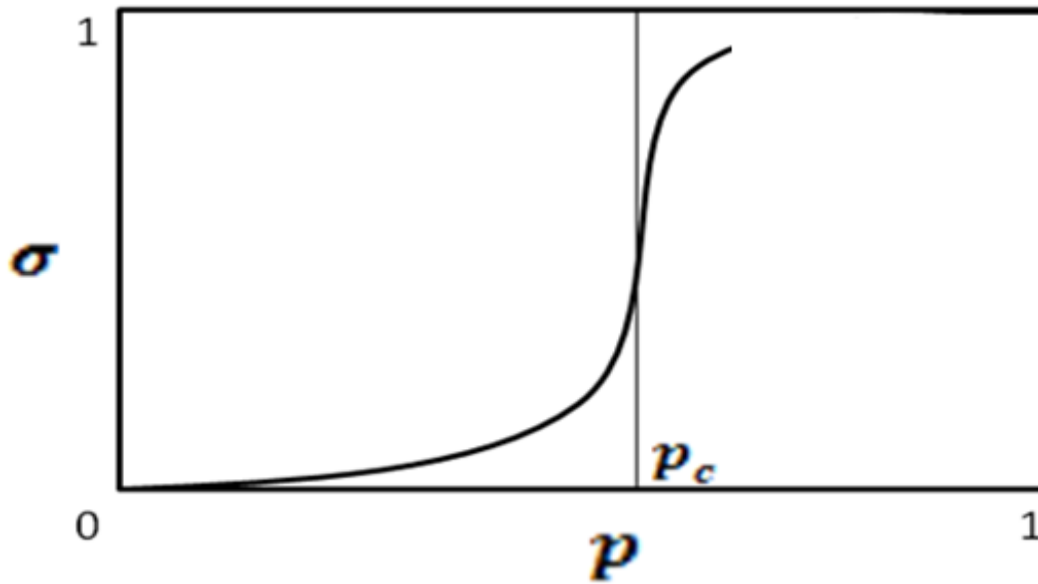


Figure 3-3, Typical dependence of conductivity on filler content.

For composite materials (the filler dispersed in the polymer matrix) loaded with water or phosphoric acid, the polymer also shows a conductivity. The effect of conductivity which arise from the hydrophilicity of the membrane should also be considered [13]. So the composite proton conductivity with low filler loadings well below the percolation threshold is mainly the result of transport processes within the polymer host matrix [15, 16]. When the filler reaches the percolation threshold at which the first conducting infinite cluster is formed in the infinite lattice, the value of conductivity increases rapidly over several orders of magnitude. In this case, the conducting filler particles touch each other, and that the conduction of charge occurs through the continuous structure of the chain of filler particles in the polymer matrix. So these two factors will assist the conductivity of the composite membrane, and the conductivity is increased as (fig. 3-3)

$$\sigma \propto (p - p_c)^n, \quad p \geq p_c \quad (3.20)$$

Where the exponent n is a parameter between 1.65 and 2 for three dimensional lattices [6]

References:

1. F. Barbir, PEM Fuel Cells - Overview, in N.M. Sammes (ed.), *Fuel Cell Technology: Reaching Towards Commercialization*, Springer-Verlag, London, 2006, pp.27-52
2. Vielstivh W., Lamm A., and Gasteiger H., *Handbook of Fuel cells: Fundamentals Technology and Applications*, Volume 3, **2003**, John Wiley & Sons Ltd., UK ISBN: 0471499269
3. Bard, A.J., *Electrochemical methods: fundamental and applications*, second edition, John wiley & Sons Inc., **2001**, US, ISBN: 0471043729
4. Bent S. *Hydrogen and Fuel Cells: emerging technologies and applications*, **2005**, Elsevier Inc.: London, ISBN: 978-0-12-655281-2
5. Leo J. M. J. Blomen, and Michael N. Mugerwa, *Fuel cell system*, **1993**, PLENUM Press: New York
6. K. D. Kreuer, S. J. Paddison, E. Spohr, M. Schuster, *Transport in Proton Conductors for Fuel-Cell Applications: Simulations, Elementary Reactions, and Phenomenology*, Chem. Rev. **2004**, 104 4637-4678
7. Xiaoxiang Xu, *Development of new proton conducting materials for intermediate temperature fuel cells*, PHD thesis, St, Andrews University, **2010**
8. Dippel, Th., Kreuer, K.D., Lassègues, J.C., Rodriguez, D., *proton conductivity in fused phosphoric acid; A ¹H/³¹P PFG-NMR and QNS study*, Solid State Ionics, **1993**, 61 (1-3) , 41-46
9. Jäger, K. and Lindbom, L., *The Continuing Evolution of Semiconductive Materials for Power Cable Applications*, IEEE Electrical Insulation Magazine, **2005**, 21, 1, 20-34
10. McLachlan, D., *Analytical Functions for the dc and ac Conductivity of Conductor-Insulator Composites*, Journal of Electroceramics, 2000, 5, 2, 93-110
11. Manuela H., Francoise E., *Electrical conductivity of carbon black-polyethylene composites Experimental evidence of the change of cluster connectivity in the PTC effect*, **2001**, Carbon, 39, 375-382
12. D. Stauffer, *Introduction to percolation theory*, Taylor and Francis, London, **1985**, ISBN-10: 0748402535

13. Xu Tongwena, Yang Weihua, He Binglin, *Ionic conductivity threshold in sulfonated poly (phenylene oxide) matrices: a combination of three-phase model and percolation theory*, *Chemical Engineering Science*, **2001**, 56, 5343–5350
14. Nelson, D. R., *Recent developments in phase transitions and critical phenomena*, *Nature*, **1979**, 269, 379–383.
15. Ye.P. Mamunya, V.V. Davydenko, P. Pissis, E.V. Lebedev, *Electrical and thermal conductivity of polymers filled with metal powders*, *European Polymer Journal*, **2002**, 38, 9, 1887 – 1897
16. R. Struè mpler, and J. Glatz-reichenbach, *Conducting Polymer Composites*, *Journal of Electroceramics*, **1999**, 3, 4, 329-346

Chapter 4: Experimental

This chapter described the experiment and instruments used in this project as well as some basic principles in relation to the experiment. The introduction included the materials synthesis, membrane preparation and characterisation, and the fuel cell test.

4.1 Membrane preparation

4.1.1 PBI membrane preparation

PBI powder was purchased from Caled Between inc. PBI powder (intrinsic viscosity $IV=0.7-0.9$ dl/g) was dissolved in N, N-dimethylacetamide (DMAc) with vigorous stirring in a three neck bottle at $130-160^{\circ}\text{C}$ for 24 hours. Then the solution was put in the centrifuge for 10 minutes at a speed of 4000 r/min. to separate the solution and the undissolved powder.

In general, directly casting PBI from a DMAc solution made it more rubbery and soft but had a higher conductivity [1-3], so a higher molecular weight polymer was required for a direct casting method to achieve enough mechanical strength. In this project, the membranes were based on a direct casting method. The solution was poured onto a flat glass and kept in an oven at 80°C for 4 hours and 120°C for 8 hours so that the DMAc evaporated and formed the membrane. The thickness of membrane was controlled by a doctor blade.

4.1.2 Cs and BmIm substitute Heteropolyacid

$\text{Cs}_x\text{H}_{3-x}\text{PW}_{12}\text{O}_{40}$ was prepared from $\text{H}_3\text{PW}_{12}\text{O}_{40}$ (Aldrich) and Cs_2CO_3 (Aldrich) according to published procedures [4]. In this procedure a solution of 0.407 g (0.00125 mol) Cs_2CO_3 which was dissolved in 10 cm^3 (ml) deionised water was added to a solution of 2.88 g (0.001 mol) $\text{H}_3\text{PW}_{12}\text{O}_{40}$ dissolved in 30 ml deionised water to achieve the ratio of 1.25:1 (mol:mol). The resulting precipitate was recovered from the solution by evaporation at 60°C , rinsed in deionised water, and filtered three times. The other three CsHPA acids, CsPOMo, CsSiOMo, and CsSiOW, were prepared using a similar procedure. BmImPOMo was synthesised from 0.218 g (0.00125 mol) 1-Butyl-3-methylimidazolium chloride and 1.825 g (0.001 mol) phosphomolybdic acid by following the same procedure. Different ratio of Cs and BmIm was controlled by molecular weight added when it reacted with Heteropolyacid

CsHPAs composite membranes were prepared as follows. CsHPA powders were dispersed in a PBI/DMAc (N, N-dimethylacetamide) solution with a mass ratio of 10%, 20% or 30%. The CsHPA/PBI composite membranes were cast by evaporating the DMAc solvent at 120 °C for 12 hours. Finally, the composite membrane was immersed in H₃PO₄ aqueous solution (11 mol dm⁻³ (M)) for 96 hours at 25 °C, for loading with acid.

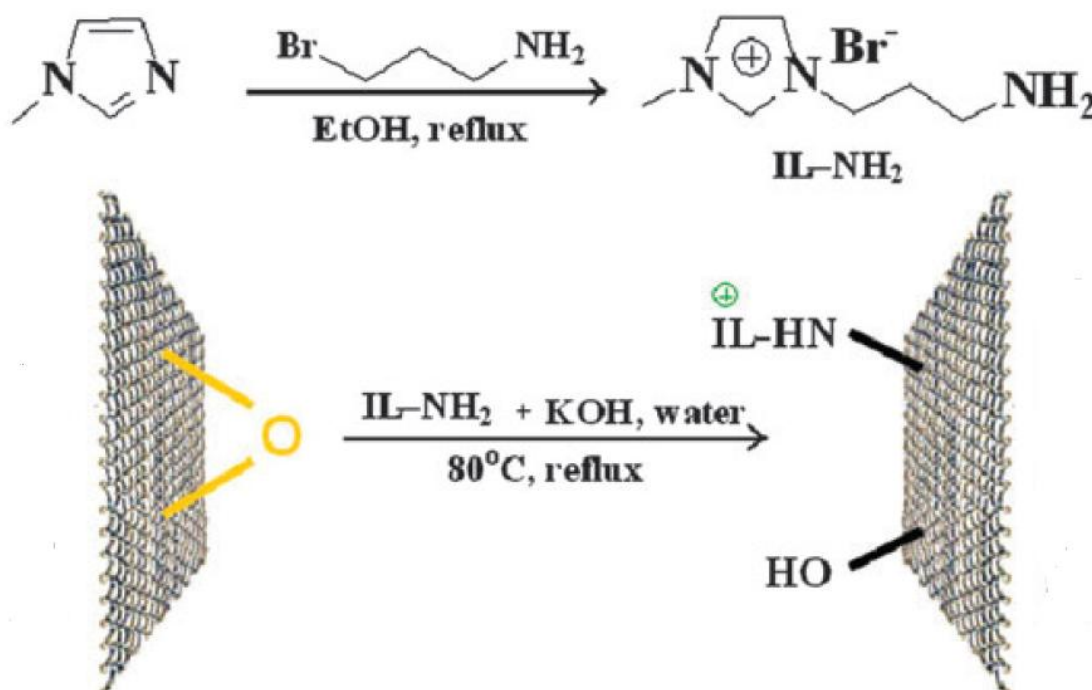
4.1.3 Preparation of graphite oxide and functional graphite oxide

A graphite oxide (GO) sheet was synthesised from graphite (Shandong Qingdao graphite company (China)) by oxidation with KMnO₄ in concentrated H₂SO₄ according to the Hummers method [5]. A graphite sheet, which was placed in cold (0 °C) concentrated H₂SO₄, and KMnO₄ powder was added gradually by stirring and cooling to ensure a temperature below 20 °C. This mixture was stirred at 35 ± 3 °C for 30 minutes, and then the temperature was increased to 98 °C and 150 ml distilled water was added slowly. This temperature was maintained for 15 minutes. The reaction was then terminated by the addition of a large amount of distilled water and 30 % H₂O₂ solution. Finally, the mixture was filtered and rinsed with 5% aqueous HCl solution until the sulphate could not be detected with BaCl₂, and then it was dried under a vacuum at 50 °C [5].

Sulphonated graphite oxide was prepared using chlorosulphonic acid. 100 mg of graphite oxide was dissolved in 30 cm³ (ml) of DMAc with vigorous stirring for 1 hour. 5 ml of chloro- sulfonic acid was added, drop by drop, with continuous stirring for 1 hour. The mixture was then centrifuged and washed with deionised water and air-dried for 10 hours at 50 °C. The membrane thickness was 40 µm and approximately 70 µm after being imbibed with phosphoric acid.

3-bromopropylamine hydrobromide (4.4000 g, 0.02 mol) and 1-methylimidazole (1.58 ml, 0.02 mol) were added to 50 ml ethanol in a three neck bottle, forming a colourless solution which was refluxed under nitrogen for 24 hours. The resulting turbid mixture was purified by re-crystallization from ethanol, with ethyl acetate as anti-solvent. Finally, the resulting white powder was dried oven dried at 60 °C.

Ionic liquids graphite oxide (ILGO) was synthesised by an epoxide ring-opening reaction between graphite oxide (GO) and the 1-(3-aminopropyl)-3- methylimidazolium bromide (IL-NH₂) shown in scheme 5-1. Firstly, 0.05 g (8.9×10^{-4} mol) KOH was added into the 50ml of GO homogeneous and transparent dispersion in water (5×10^{-4} g/ml) and then the mixture was subjected to ultrasonication for 30 minutes. Secondly, IL-NH₂ (0.05 g) was added into a mixture solution for another 1hour of ultrasonication, and then the turbid mixture was transferred into a three neck bottle by vigorously stirring at 80 °C for 24 hours. The resulting p-CCG was subsequently centrifuged, washed with ethanol and water, and air-dried [6].



Scheme 4.1 Illustration of the preparation of ILGO [6]

4.1.4 PEO/GO membrane preparation

5 g PEO was first completely dissolved in 10 ml of distilled water in a round-bottom flask and then 2 ml (0.5 g/ml) of graphite oxide solution was added into the flask while stirring for 2 hours to obtain the resultant PEO/GO solution (0.5 wt%). The PEO/GO solution was then poured onto the prepared glass slides mould (10 mm x 10 mm) which was kept at room temperature for 48 hours until the membrane was solid. The membrane was peeled from the

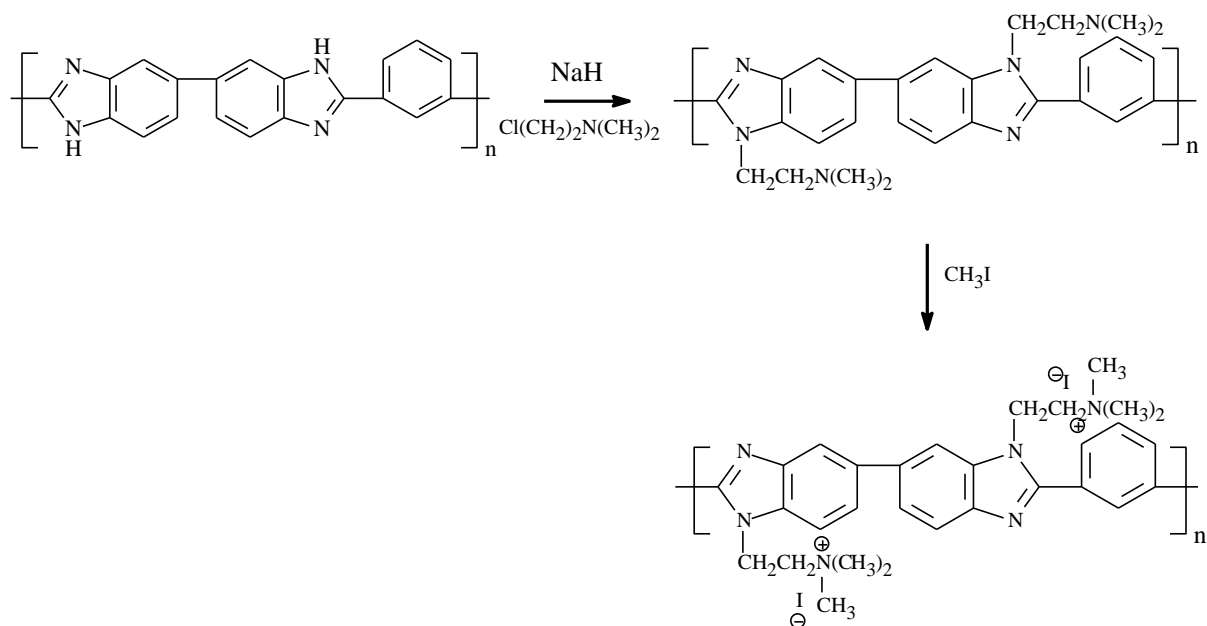
mould and dried for 12 hours at room temperature before undergoing characterisation and being used in fuel cell tests. PEO blank membranes were prepared under the same conditions.

4.1.5 PBI/GO membrane preparation

GO/PBI composite membranes were prepared as follows. GO sheets were dispersed in a PBI/N, N-dimethylacetamide (DMAc) solution with a mass ratio of 2 wt. %. The GO/PBI composite membranes were cast by evaporating the DMAc solvent at 120 °C for 12 hours. Finally, the composite membrane was immersed in aqueous H₃PO₄ solution (2M) for several days at 25 °C. Unless otherwise specified, phosphoric acid loadings in this paper were defined as number of H₃PO₄ molecules per repeat unit (PRU) of PBI in the membrane.

4.1.6 Synthesis of quaternary PBI

In a three neck bottom flask, 1g Poly(2,20-m-(phenylene)-5,50-bibenzimidazole) (PBI) powder was dissolved in 100 ml of Dimethyl sulfoxide (DMSO) with vigorous stirring for 6 hours at 160 °C to form a uniform solution. After cooling down to 60-80 °C, 0.15 g (0.00625 mol) Sodium hydride (NaH) was added into the solution which was charged under N₂ atmosphere for 24 hours. At this stage, a deep blood red colour developed. 1.5 g (0.0104 mol) 2-Chloro-N, N-dimethylethylamine hydrochloride was added into the solution for another 24 hours reaction. The solution was precipitated from deionised water. The resulting precipitate was filtered and rinsed with deionised water several times and dried at 100 °C overnight. The dried precipitate was dissolved in DMAc again and iodomethane (CH₃I) was added, being kept at 30-40 °C for 24 hours. The resulting solution was precipitated and rinsed with deionised water. The resulting precipitate was redissolved in DMAc to cast on a glass plate and the DMAc solvent evaporated at 120 °C for 12 hours [7, 8].



Scheme 4.2 Synthesis of the QPBIs

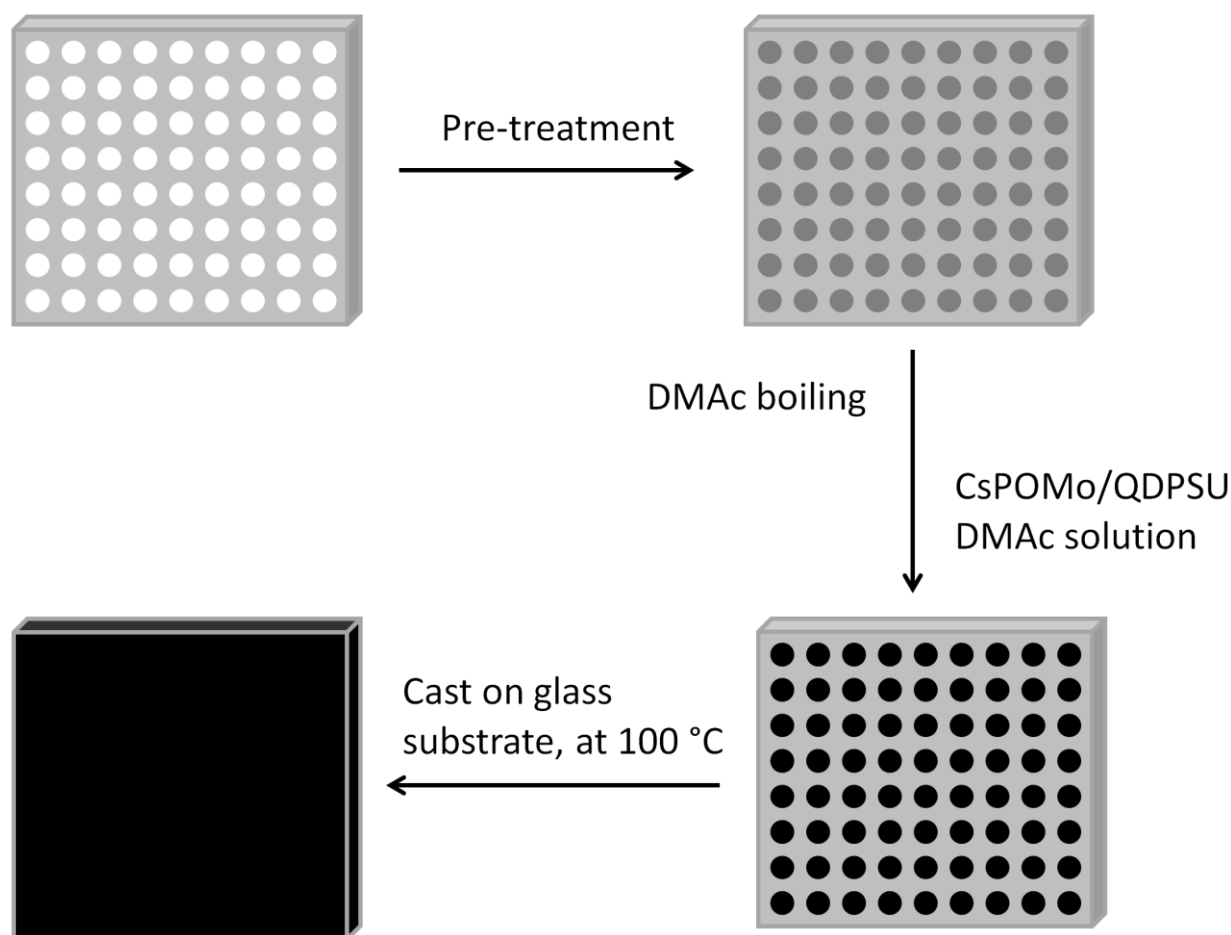
4.1.7 Caesium Salt of Heteropolyacids/Quaternary diazabicyclo-octane

Polysulfone/PTFE composite membranes

Cs_xH_{3-x}PMo₁₂O₄₀ was prepared according to procedures discussed previously. Quaternary diazabicyclo-octane Polysulfone (QDPSU) was made as described in previous work provided by Dr Wang [9]. Briefly, the chloromethylated polysulfone (CM-PSU) was synthesised through the Friedel-Crafts reaction. 10 g polysulfone (2.26×10^{-3} mol) (P-1700, Udel) was dissolved in 400 ml 1, 2-dichloroethane. 6.78 g (2.26×10^{-2} mol) paraformaldehyde and 24.6 g (2.26×10^{-2} mol) trimethylchlorosilane were added to the solution with magnetic stirring. Stannic chloride 1.178 g (4.52×10^{-3} mol) was added drop-wise and the reaction was carried out for 12 hours at 50 °C. The CM-PSU was formed as a white precipitate in ethanol (99.9 %) to remove the excess reactants. The CM-PSU and 1, 4-diazabicyclo [2.2.2] octane (DABCO) was mixed in DMAc in a molar ratio of 1:5, with vigorous stirring at 80 °C for 14 hours, whereupon the final product was precipitated using diethyl ether and dried in a vacuum. CsPOMo was dissolved in QDPSU/DMAc solution at a weight ratio of 30 wt% to form the resultant.

The PTFE membrane used in this work was obtained from a Membrane Solution (US). It was 25 μm in thickness and had a porosity of 82 % and a pore size between 0.2-0.3 μm. The hydrophobic PTFE sheet was pre-treated, to enable incorporation of the QDPSU polymer

solution, using the method of Li et al [10]. This involved treatment with seven parts H_2SO_4 (98 wt% aqueous solution Aldrich) and three parts H_2O_2 (30 wt% aqueous solution Aldrich) at 80°C for 1 hour. Following this, the porous PTFE was rinsed with copious amounts of deionised water and further treated by immersion in a solution containing one part aqueous NaOH (1.0 mol dm^{-3}) solution, one part H_2O_2 (30 wt% aqueous solution), and five parts deionised water at 70°C for 30 minutes, followed by rinsing with copious amounts of DI water. The pre-treated PTFE sheet was boiled in DMAc for 10 minutes and then immersed in 3 wt % CsPOMo/QDPSU solution for 10 minutes and placed on an optical glass plate and left for 6 hours at 60°C to form the CsPOM/QDPSU/PTFE membrane.



Scheme 4.3 Preparation of the CsPOMo/QDPSU/PTFE membrane

The membrane was immersed in $2.0\text{ M H}_3\text{PO}_4$ at room temperature for 3 days. The theoretical amount of “bonded acid” corresponded to 2.0 molecules of PA per repeat unit of

QDPSU with nitrogen sites for hydrogen bonding. Thus with a 2.0 M PA, the acid content will be less and was measured at 1.8 PRU. The data in this work was compared against a PBI membrane (30 μm in thickness) which was prepared by a casting method as described previously [11].

4.1.8 Dimethylhexadecylamine quaternized poly (vinyl benzyl chloride)/PTFE composite membrane

Dimethylhexadecylamine quaternized poly (vinyl benzyl chloride) (qPVBzCl⁺) was provided by Dr Cao. PTFE porous films (10 cm x 10 cm) were first sonicated for 1 hour in ethanol and then acetone. These films were then air-dried. After these treatments, the PTFE films were weighed individually and then immersed into diluted qPVB/Cl⁻ ionomer solution for 30 minutes and then air-dried. They were then immersed once again into the qPVB/Cl⁻ ionomer solution for 30 minutes before air-drying. This process was repeated several times before being weighed and the qPVB/Cl⁻ ionomer percentage was calculated from the weight differences. The calculated weight of the qPVB/Cl⁻ ionomer in the PTFE was 71% over the original PTFE membrane weight. Then the qPVB/Cl⁻ ionomer filled PTFE membranes were immersed into 11 mol dm⁻³ (M) H₃PO₄ solution for 2 days.

4.2 Sample characterisation and instruments

4.2.1 Conductivity measurement

The conductivity of the membranes was measured using a four-point probe method with a Frequency Response Analyser (Voltech TF2000, UK) as shown in Figure 4-1. The four-point method involves four equally spaced probes in contact with the measured material: two of the probes were used to source the current whilst the other two were used to measure the voltage drop. There are two main methods to test the conductivity. One is four point method to test in-plane conductivity of membrane and the other one is two point method for through plane conductivity. The reason for using the four-point method rather than the two-point method was that the four-point method can eliminate the probe resistance and the resistance between the probe and the membrane surface, so the four point method is more accurate to test the conductivity of the membrane (shown in Fig. 4-2). A rectangular membrane sample (10 mm

width \times 50 mm length) was placed across four platinum foils (probes) with equal spacing of 5 mm. AC impedance measurements were carried out between frequencies of 1 and 20 kHz amplitude of 40. To ensure the membrane reached a steady state, the membranes were held at the desired conditions for 2 hours before testing, and measurements were taken at 30 minute intervals. At the low temperature, the humidity was provided from the N₂ gas which passes a water tank and was measured by the humidifier. Above 100 °C, the humidity was considered less than 1% at atmosphere pressure.



Figure 4-1 Conductivity measurement system

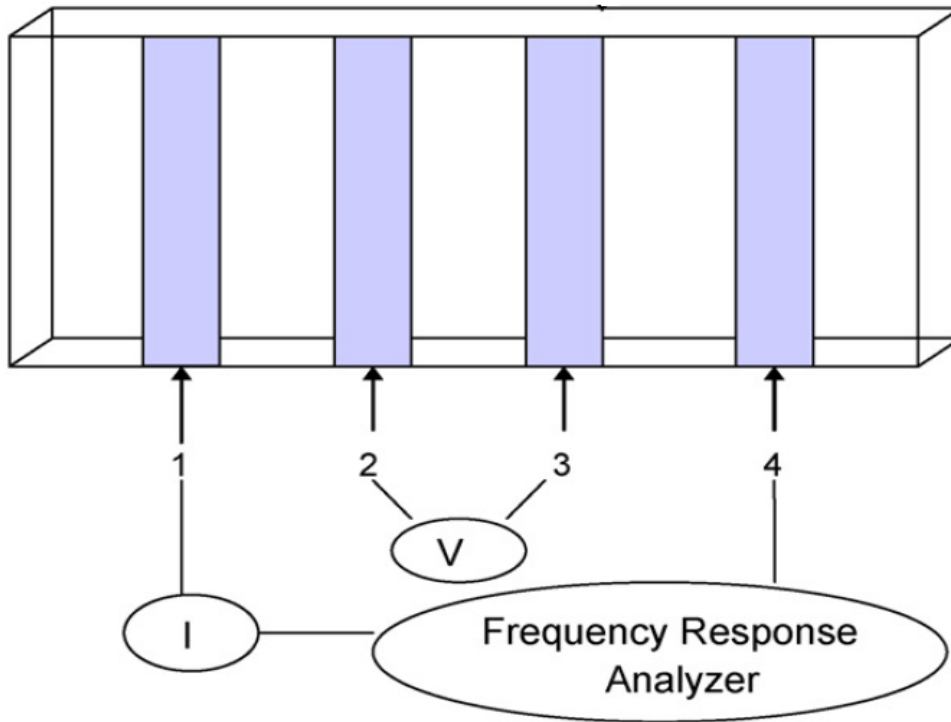


Figure 4-2 Four-point probe method to measure the in-plane conductivity [4]

4.2.2 Electrode preparation

Catalysts used in the PEMFC were usually based on platinum or its alloys for both anode and cathode. Polytetrafluoroethylene (PTFE) was used as a binder which fixes the catalyst particles within a layered structure and enabled some degree of electronic conductivity and gas path into the structure. Catalyst inks were prepared by blending carbon-supported catalysts (50 wt. % Pt/C, Alfa Aesar) and polytetrafluoroethylene (PTFE) solution (60 wt% Aldrich) in a water–ethanol mixture under ultrasonic vibration for 60 min. [2]. Based on previous work in our lab, the PTFE was optimised as 30 wt% of the catalyst.

Gas diffusion electrodes (carbon paper) incorporated with a wet proofed micro-porous layer (H2315 T10AC1), obtained from Freudenberg (FFCCT, Germany), were used as substrates to deposit the catalyst layer for both anode and cathode. The catalyst inks were sprayed onto the micro-porous gas diffusion layer, at 90 °C, and then the electrodes were held at a temperature of 100 °C for 2 hours. To calculate the Pt loading, the carbon paper was weighed before and after spray. 10 µl 2 M PA acid was added to the surface of the electrodes by

means of a micropipette and electrodes were kept in an oven, at 80 °C, for 1 hour to dry the water residue.

4.2.3 Membrane electrode assemblies (MEA)

Membrane electrode assemblies (MEA) were made by pressing the anode and cathode onto the membranes at 0.1 ton/cm² pressure for 5 minutes. The electrochemical reaction took place at the three phase boundary by the ionomer, solid and void phases. The catalyst was covered in a thin layer of electrolyte ionomer, which balances the proton mobility and oxygen solubility through the layer. For the PBI membrane, the PTFE was used to hold the phosphoric acid and to enhance porosity.

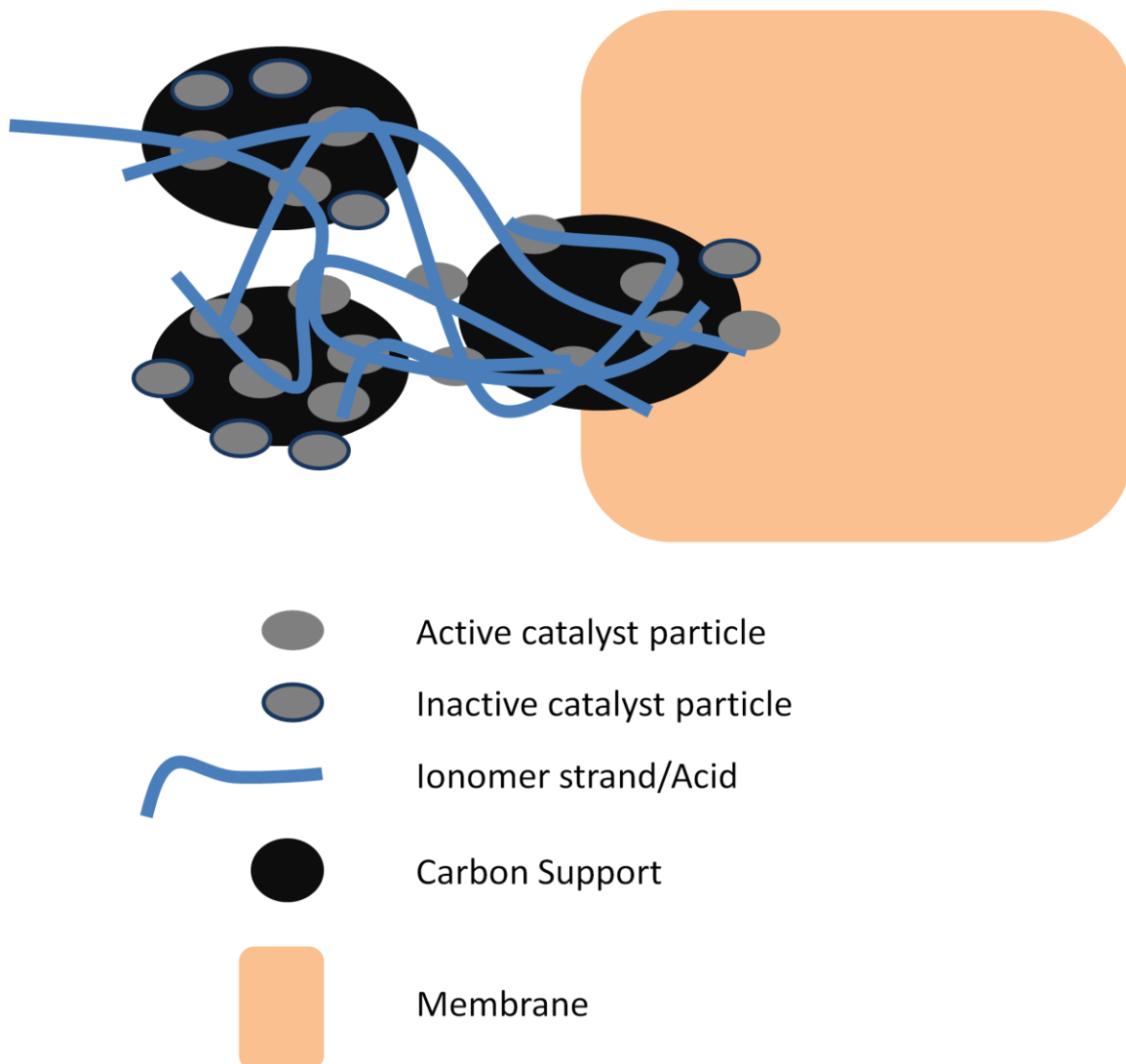


Figure 4-3 The three phase boundary for porous catalyst layer

4.2.4 Fuel Cell Performance Test

The MEA was set in contact with high-density graphite blocks impregnated with phenolic resin, and the active electrode area covered the parallel gas flow channels area (1 cm^2). Electric cartridge heaters were mounted at the rear of the graphite blocks to maintain the desired temperature which was monitored by thermocouples and controlled by a temperature controller. Gold-plated steel bolts were screwed into the blocks to allow electrical contact. H_2 and O_2/air were fed to the cell at flow rates of 0.2 and 0.5 dl/min respectively. The whole fuel cell test rig was shown in Figure 4-4.

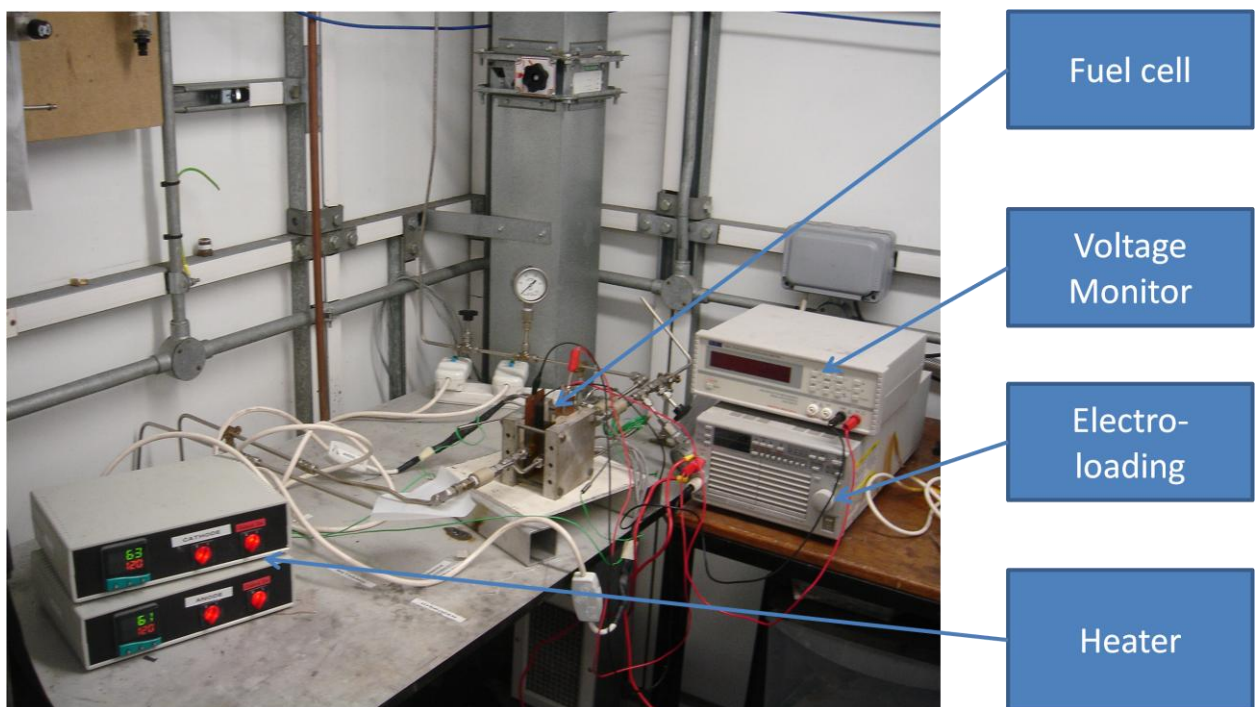


Figure 4-4 Fuel cell test system

4.2.5 Mechanical Strength

The strength of a material is an ability to withstand an applied stress without failure. The intensity of the internal forces is called stress, while deformation of the material is called strain. The stresses acting on the material cause deformation of the material. The applied stress may be tensile, compressive, or shear. Tensile stress is the stress state caused by an applied load that tends to elongate the material in the axis of the applied load, so the mechanical strength of membranes is showed as tensile strength.

Most materials under a small stress showed elasticity which a material could return to its previous shape after stress is released, and this reversible deformation was called elastic deformation. The initial portion of the stress-strain curve is linear. The maximum point of this linear slope is called the yield point and indicates the onset of plastic deformation. The corresponding stress and elongation are called yield strength and elongation at yield. At higher stress, the deformation cannot be covered after the stress removed, and it is called plastic deformation. Further elongation leads to an abrupt increase in stress and the ultimate rupture of the material. The stress at break point of the material is ultimate strength. The stress-strain behaviour of a polymeric material depends on various parameters such as molecular characteristics, microstructure, strain-rate and temperature.

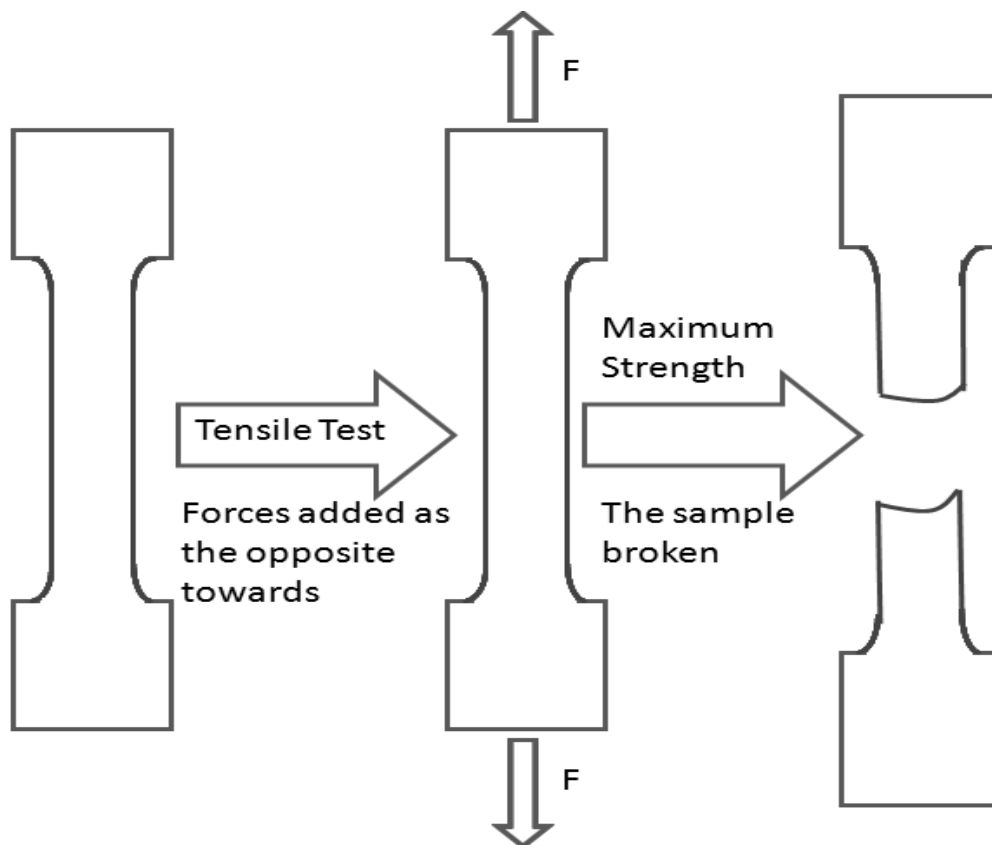


Figure 4-5, the tensile test with the dog-bone sample.

The membrane was cut into a dog-bone shape before testing the mechanical strength. The tensile strength of the membranes was measured using a vertical filament stretching instrument. The forces were added through clipping a part of the sample, and go towards the opposite way with the constant speed. Finally, the force was recorded when the sample broken as the figure 4-5 shown. The tensile stress is the force per unit area acting on a plane

transverse to the applied load, and it is a fundamental measure of the internal forces within the material. Measurements were performed with a constant separating speed of 10 mm min⁻¹ in unhumidified air. Maximum Tensile stress is expressed by equation (4.1)

$$\sigma = \frac{F}{A} \quad (4.1)$$

Where F is the force at point of membrane broken, A is the cross-section area, the width is 20mm, and thickness is 50 μm .

For the acid doping membrane, due to the plasticizing effect of PA, the mechanical properties of PA doped membrane was strongly correlated to the PA doping level of the membrane. At PA doping levels below 2, the strong ionic interactions present had been shown to increase the cohesion in the membrane, resulting in increased modulus and toughness. When excess acid (PA doping level is higher than 2) was present in the membrane, the mechanical strength was dramatically reduced [1]. Cross-linking and added enforcement of membrane materials were two promising approaches to allow for high PA doping levels and thus higher proton conductivity without sacrificing mechanical strength [1].

4.2.6 Scanning Electron Microscope (SEM) and Energy dispersive X-ray spectroscopy (EDX)

The Scanning Electron Microscope (SEM) is capable of producing high-resolution images which have a characteristic three-dimensional appearance of a sample surface. JSM-5300LV (Japan) Scanning Electron Microscope was used when a morphological investigation was required for the project. In SEM, electrons are thermionically emitted from a tungsten or lanthanum hexaboride (LaB₆) cathode and are accelerated towards an anode; alternatively, electrons can be emitted via field emission (FE). The electron beam, which has an energy ranging from a few hundred eV to 100 keV, passes through pairs of scanning coils in the objective lens. When the primary electron beam interacts with the sample, the electrons lose energy by repeated scattering and absorption within the interaction volume, which depends on the beam accelerating voltage the atomic number of the specimen and the specimen's density, extending from less than 100 nm to around 5 μm into the surface [12, 13].

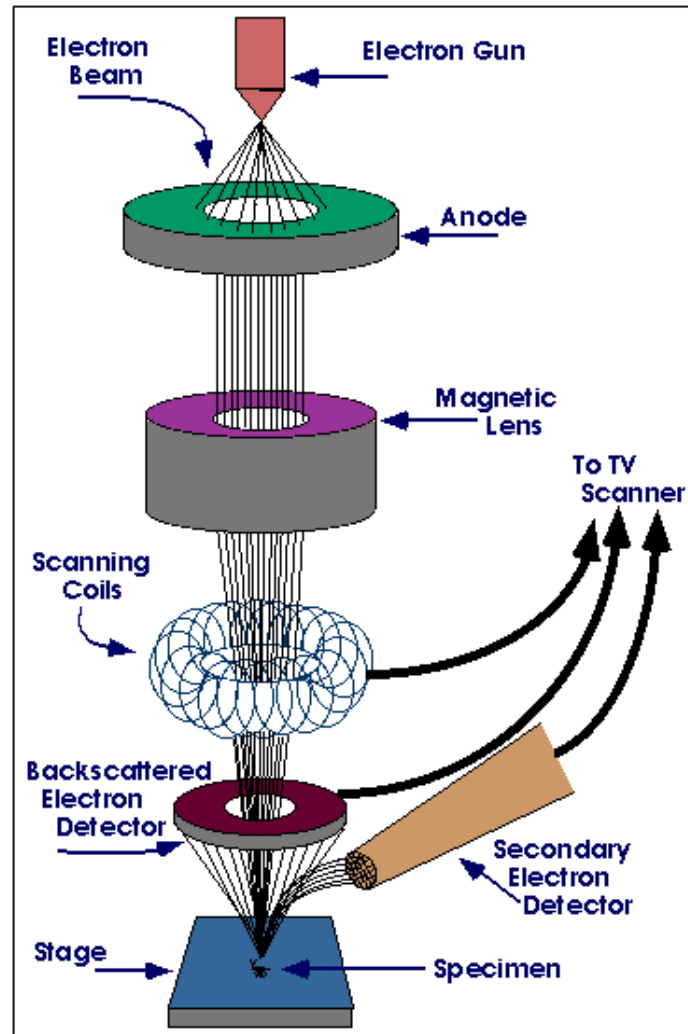


Figure 4-6, Geometry of SEM [14]

Energy dispersive X-ray spectroscopy (EDX) analysis system is used for elemental analysis of samples. EDX relies on interactions between incident charged particles such as electrons and the sample. In principle, a high energy incident beam will knock out an electron in an inner shell of atoms in the sample, creating an electron hole where the electron was. Then an electron from an outer, higher-energy shell will fill that hole and release the energy differences between these two shells in the form of an X-ray. Since the energy differences between electron shells are closely related to the atomic structure, the emitting X-ray shall be a characteristic of an atom, which allows the elemental composition of the specimen to be measured. The systems provide limited detection of elements below C in the periodic table. The detection limit is around 0.1% depending on the element [12, 13].

4.2.7 X-ray diffraction (XRD)

XRD is a method to determine the atomic and molecular structure of a crystal. When an X-ray beam hits an atom, the electrons around the atom start to oscillate with the same frequency as the incoming beam. In almost all directions interference is destructive, but the atoms in a crystal are arranged in a regular pattern, leading to a constructive interference in some directions. Hence, a diffracted beam may be described as a beam composed of a large number of scattered rays mutually reinforcing one another. The number and positions (2θ) of the reflections depend on the cell parameters, crystal class, lattice type and wavelength used to collect the data [15, 16].

Crystals are solid substances in which the atoms, molecules or ions are arranged in an orderly repeating pattern extending in all three spatial dimensions. X-ray scattering techniques reveal information about the crystallographic structure, chemical composition, and physical properties of materials and thin films. The basis of these techniques is through observing the scattered intensity of an x-ray beam hitting a sample as a function of incident and scattered angle, polarization, and wavelength [15, 16]. A simple and straightforward way to describe crystal diffraction is Bragg's Law:

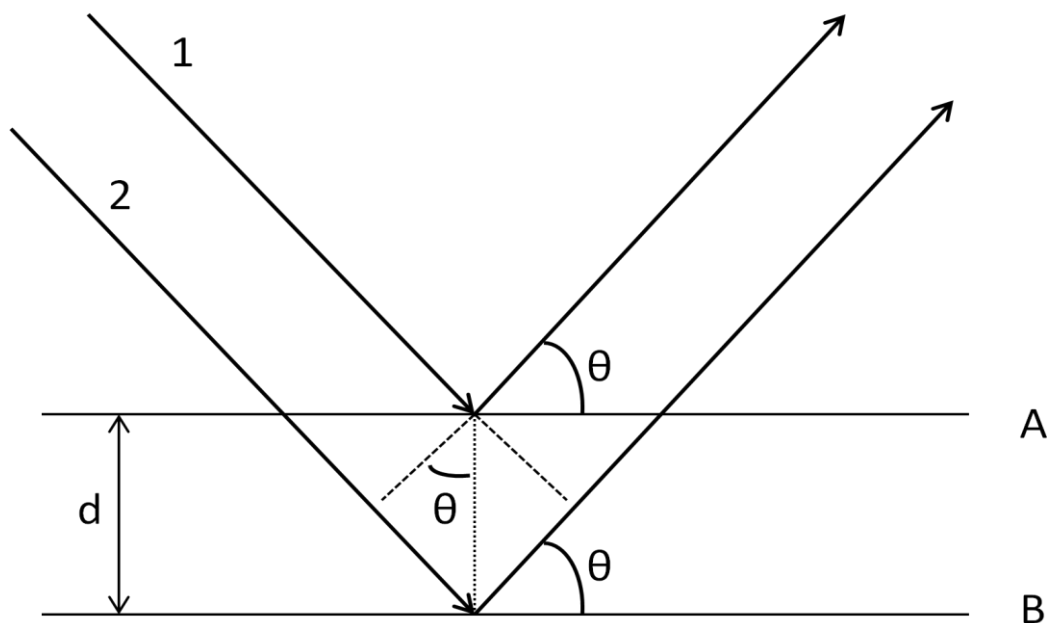


Figure 4-7, Illustration of Bragg's law

It treats one layer of atoms (A and B) in crystal as a plane and the smallest unit to diffract incident light. If the emergent light 1'' and 2'' are in phase, the equation is:

$$2d \sin \theta = n\lambda \quad (4.2)$$

Where d is the distance between adjacent atom planes, θ is the incident angle and λ is the wavelength of the light, n is normal kept equal to 1.

The distance between adjacent atomic planes d can be obtained from Bragg's Law and can be used to calculate the unit cell parameters of a crystal. For a three dimensional unit cell, three indices are shown as h , k , and l , the Miller indices are usually written (h, k, l) , d -spacing for any set of planes are shown in Table 4.1, which depends on crystal system [15]

Table 4-1, Expressions for d spacing in the different crystal systems [15]

Crystal system	Expression for d
Cubic	$\frac{1}{d^2} = \frac{h^2 + k^2 + l^2}{a^2}$
Tetragonal	$\frac{1}{d^2} = \frac{h^2 + k^2}{a^2} + \frac{l^2}{c^2}$
Orthorhombic	$\frac{1}{d^2} = \frac{h^2}{a^2} + \frac{k^2}{b^2} + \frac{l^2}{c^2}$
Hexagonal	$\frac{1}{d^2} = \frac{4}{3} \left[\frac{h^2 + hk + k^2}{a^2} \right] + \frac{l^2}{c^2}$
Monoclinic	$\frac{1}{d^2} = \frac{1}{\sin^2 \beta} \left[\frac{h^2}{a^2} + \frac{k^2 \sin^2 \beta}{b^2} + \frac{l^2}{c^2} - \frac{2hl \cos \beta}{ac} \right]$

Useful information that X-ray powder diffraction can also give the particle size by utilising Scherrer equation:

$$\tau = \frac{0.9\lambda}{\sqrt{B_M^2 - B_S^2} \cos \theta} \quad (4.3)$$

Where τ is the crystallite size; λ is the X-ray wavelength (0.1540598 nm), θ is the Bragg angle (half the measured diffraction angle), B_M and B_S are the width in radians of diffraction peaks of the sample and the standard at half height. The standard peak width is obtained from a highly crystalline sample [15, 16].

The crystal structures of different powders were analysed by X-ray diffraction (XRD, PANalytical X'Pert Pro Diffractometer), with scan range of 5–70° over 2 hours. A Stoe STADI/P powder diffractometer was used in transmission mode. Incident radiation was generated using a CuK α 1 source ($\lambda = 1.540598 \text{ \AA}$) with curved Germanium as a monochromator.

4.2.8 Fourier Transform Infrared (FTIR)

Fourier transform spectroscopy is a measurement technique using time-domain measurements of the electromagnetic radiation or other type of radiation. Infrared Spectroscopy is the absorption measurement of the IR electromagnetic waves within different frequencies. Electromagnetic waves used in infrared spectroscopy have frequencies ranging from 1.9×10^{13} to 1.2×10^{14} Hz, corresponding to photon energies ranging from 0.078 to 0.5 eV from the Plank relation (Bohr equation 4.4) [17, 18].

$$E = h\nu \tag{4.4}$$

Where h is the Planck constant ($h = 6.626 \times 10^{-34} \text{ J s}$) and ν is the frequency

Another important property of a light wave is its wavenumber (W). The wavenumber measures the number of cycles a wave undergoes per unit length [17]. For an example, a spectrum of a peak at 3000 cm^{-1} , it means the sample absorbed infrared light that underwent 3000 cycles per unit length [17, 18].

Absorbance measures the amount of light absorbed by a sample, and the absorbance spectrum of a sample is calculated from the equation 4.5 [17, 18]:

$$A = \log(I_0/I) \tag{4.5}$$

Where A is absorbance, I_0 is the intensity in the background spectrum, and I is the intensity in the sample spectrum. Transmittance (%T), which measures the percentage of light transmitted by a sample, can also be plotted in units.

$$\begin{aligned} A &= \log(1/T) \\ \log \%T &= 2 - A \end{aligned} \tag{4.6}$$

For a typical IR spectrum, samples are exposed to a beam of infrared light and transmitted light is collected which reveals the absorption of the samples. From their characteristic absorption frequencies, different functional groups can be quickly identified.

The vibrations of two covalently bonded atoms could be simplified and treated as a harmonic oscillator with 2 masses (atoms) linked by a spring (Figure 4-8).



Figure 4-8: a harmonic oscillator with two masses

In this simple model, Hooke's Law could be used to approximate and understand stretching frequencies (equation 4.7) [17, 18].

$$v = \frac{1}{2\pi} \sqrt{\frac{k}{\mu}} \quad (4.7)$$

Where v is the vibration frequency, k is the force constant for the bond, μ is the reduced mass of A-B systems (equation 4.8):

$$\mu = \frac{m_A m_B}{m_A + m_B} \quad (4.8)$$

Where m_A and m_B are mass of A and B atoms.

In a Fourier transform infrared instrument, the complex curve, which can translate into the infrared spectrum, is an interferogram, or the sum of the constructive and destructive interferences. An interferogram is generated from the unique optics of an FT-IR instrument. In FTIR, the most important components are a moveable mirror, which is responsible for the quality of the interferogram, and a beam splitter, which splits the IR beam 50/50 to the fixed and moveable mirrors and then recombines the beams after being reflected at each mirror.

4.2.9 Nuclear Magnetic Resonance (NMR)

Nuclear magnetic resonance (NMR) is a physical phenomenon in which magnetic nuclei in a magnetic field absorb and re-emit electromagnetic radiation. This energy is at a specific resonance frequency which depends on the strength of the magnetic field and the magnetic properties of the isotope of the atoms. The most commonly studied nuclei are ^1H and ^{13}C .

Atomic nucleus involved in NMR possess a quantized property is called nuclear spin (I) which has values of 1, 1/2, 1, 3/2, etc. the value of nuclei spin depends on the mass number and the atomic number of the nuclei. When $I = 0$, (^{12}C , ^{16}O , ^{32}S , etc.), they have no spin angular momentum and thus no magnetic moment. The nuclear magnetic moment μ is given as 4.9 [19]:

$$\mu = \gamma I \frac{h}{2\pi} \quad (4.9)$$

Where h is the Planck's constant and γ is a constant for each particular nucleus.

The angular momentum of a spinning nucleus is a function of its spin quantum number which can have either integer or half-integer values. When a nucleus placed in a uniform magnetic field, magnetic field intensity is H_0 , a nucleus of spin I only has $2I + 1$ possible orientations, which could be characterized by a set of magnetic quantum numbers m . The energy of spin is shown in equation 4.10 [19].

$$E = -\gamma h m \frac{H_0}{2\pi} \quad (4.10)$$

For an example of ^1H nucleus, $I = 1/2$, and $m = \pm 1/2$, so the energy of spin could be $E = \pm \mu H_0$, the difference of two energy is [19]

$$\Delta E = 2\mu H_0 = h\nu_0 \quad (4.11)$$

Where ν_0 is the frequency of electromagnetic radiation of ^1H .

When the frequency of magnetic field $\nu = \nu_0$, the nuclear magnetic resonance is happened.

In this project, ^1H NMR (400 MHz) was performed with DMSO- d_6 as the solvent and tetramethylsilane (TMS) as the internal reference.

References:

1. Li Q, He R, Jensen J, Bjerrum N. *PBI-based polymer membranes for high temperature fuel cells—preparation, characterization and fuel cell demonstration*. Fuel Cells, **2004**, 4,147–59
2. Mamlouk, M. *Investigation of High Temperature Polymer Electrolyte Membrane Fuel Cells*, PhD thesis, **2008**
3. Wu, X. *Developmenr of High Temperature PEMFC and High Temperature PEMWE*. PHD thesis, **2011**
4. Li, M., Shao, Z., Scott, K. *A high conductivity Cs_{2.5}H_{0.5}PMo₁₂O₄₀/polybenzimidazole (PBI)/H₃PO₄ composite membrane for proton-exchange membrane fuel cells operating at high temperature*. Journal of Power Sources, **2008**, 183(1), 69-75
5. W.S. Hummers Jr, and R.E. Offeman, *Preparation of graphitic oxide*, Chemical Socirty, **1958**, 80 (6), 1339
6. Yang, H., Shan, C., Li, F., Han, D., Zhang, Q., Niu, L, *Covalent functionalization of polydisperse chemically-converted graphene sheets with amine-terminated ionic liquid*, Chemical Communications, **2009**, (26) , pp. 3880-3882
7. Wen Z., Tang Y., Wang B., Wang H., *Study on synthesis and quaternary ammoniation of ABPBI*, China National Polymer academic conference, **2009**.
8. Xia, Z., Yuan, S., Jiang, G., Guo, X., Fang, J., Liu, L., Qiao, J., Yin, J., *Polybenzimidazoles with pendant quaternary ammonium groups as potential anion exchange membranes for fuel cells*, Journal of Membrane Science, **2012**, 390-391 , 152-159
9. Wang, X; Xu, C.; Golding, B.T.; Sadeghi, M.; Cao, Y.; Scott, K. *A novel phosphoric acid doped quaternary 1, 4-diazabicyclo-[2.2.2]-octane polysulfone membrane for intermediate temperature fuel cells*, Int. J. hydrogen energy, **2011**, 36, 14, 8550-8556
10. Li, M., Scott, K., *A polytetrafluoroethylene/quaternized polysulfone membrane for high temperature polymer electrolyte membrane fuel cells*, Journal of Power Sources, **2011**, 196 (4) , 1894-1898
11. Xu, C.; Cao, Y.; Kumar, R.; Wu, X.; Wang, X; Scott, K. *A polybenzimidazole/sulfonated graphite oxide composite membrane for high*

- temperature polymer electrolyte membrane fuel cells*, J. Mater. Chem., **2011**, 21, 6014.
12. Goldstein, J., *Scanning electron microscopy and x-ray microanalysis*, Kluwer Academic/Plenum Publishers, **2003**.
 13. Reimer, L. *Scanning electron microscopy: physics of image formation and microanalysis*, Springer, **1998**.
 14. B. Voutou and E. Stefanaki, *Electron Microscopy: The Basics*, Physics of Advanced Materials Winter School, **2008**
 15. Weller M. T., *Inorganic materials chemistry*, Oxford University Press, **1994**, Oxford, ISBN: 0198557981
 16. Liebhafsky L., Pfeiffer H. G., Winslow E. H., and Zeman P. D., *X-rays, electrons, and analytical chemistry*, John Wiley & Sons Inc., **1972**, Canada ISBN: 0471534285
 17. Smith B. C., *Fundamentals of fourier transform infrared spectroscopy*, CRC press, **2011**, Boca Raton, US. ISBN:0849324610
 18. Stuart B., *Infrared spectroscopy: fundamentals and applications*, John Wiley & Sons, **2004**, UK ISBN: 9780470854280
 19. K. Hatada, and T. Kitayama, *NMR Spectroscopy of polymers*, Springer-Verlag Berlin Heidelberg, **2004**, New York ISBN: 075140005

Chapter 5: Caesium and Ionic Liquid Substituted Heteropolyacid/PBI Composite Membrane

5.1 Introduction

In this chapter, four caesium salts heteropolyacid, ($Cs_xH_{3-x}PMo_{12}O_{40}$ (CsPOMo), $Cs_xH_{3-x}PW_{12}O_{40}$ (CsPOW), $Cs_xH_{4-x}SiMo_{12}O_{40}$ (CsSiOMo), $Cs_xH_{4-x}SiW_{12}O_{40}$ (CsSiOW)), and ionic liquid heteropolyacid to form composite membranes with PBI, were synthesised. Their conductivity and fuel cell performance with phosphoric loading were investigated.

In water, all protons of heteropolyacids were dissociated. Heteropolyacids were stronger than typical inorganic acids, including H_2SO_4 , HBr, HCl, HNO_3 , and $HClO_4$. These differences could be attributed to larger heteropoly anions than the inorganic acids, leading to a lower strength of bonding between the proton and heteropoly anions [1-10].

Heteropolyacid has a low surface area ($5\text{ m}^2\text{ g}^{-1}$) and is highly soluble in water [5]. Therefore, substitution of protons by alkaline cations produced interesting effects on the surface area and made them insoluble in water. Salts with large monovalent ions, such as Cs^+ , resulted in unique changes in the surface area and hence in the amount of acidic site on the surface and a maximum for $Cs_xH_{3-x}PW_{12}O_{40}$ compounds with $x = 2.5$. $Cs_{2.5}H_{0.5}PW_{12}O_{40}$ showed significantly higher activities than $H_3PW_{12}O_{40}$ [5]. The $Cs_xH_{3-x}PW_{12}O_{40}$ compounds were synthesised by a titration method [11]. During this process, Cs_3 crystallites were initially formed followed by the adsorption of $H_3PW_{12}O_{40}$ on the surface of Cs_3 [5].

The surface area of Cs-Heteropolyacid increased when the Cs content x from 2 to 3 and decreased when $0 < x < 2$, and a maximum number of acidic sites on the surface (surface acidity) showed at $x = 2.5$ [12]. The ionic liquid (1-Butyl-3-methylimidazolium chloride) was also synthesised with phosphomolybdic acid to form BmIm-heteropolyacid salts and compared to Cs-heteropolyacid.

Recently, the $Cs_{2.5}H_{0.5}PMo_{12}O_{40}$ (CsPOM) /PBI membrane was used in a PEMFC. The CsPOM/PBI membrane gave a much higher conductivity (even up to 0.25 S/cm) than the pristine PBI membrane. For the fuel cell with CsPOM/PBI, gave a peak power density was

0.7 W cm^{-2} , and the OCV was around 0.95V [14]. By comparing $\text{Cs}_x\text{H}_{3-x}\text{PMo}_{12}\text{O}_{40}$ (CsPOMo), $\text{Cs}_x\text{H}_{3-x}\text{PW}_{12}\text{O}_{40}$ (CsPOW), $\text{Cs}_x\text{H}_{4-x}\text{SiMo}_{12}\text{O}_{40}$ (CsSiOMo) and $\text{Cs}_x\text{H}_{4-x}\text{SiW}_{12}\text{O}_{40}$ (CsSiOW), CsHPA/PBI composite membranes gave the best conductivity and superior performance. The P form of the CsHPA provided higher conductivity, as composite membranes, than those of the CsHPA with Si atom, although the mechanical strength was inferior [11].

5. 2 Results and discussion

5.2.1 Pristine PBI membrane as a benchmark and acid loading to membrane

The water evaporated from the PBI membrane when it was over 100 °C, so acid needed to be combined with the membrane that provided the conductivity. As mentioned in the introduction of Chapter 1, phosphoric acid was the best acid to use amongst the acids. The PBI membrane was immersed in a certain amount of phosphoric acid for a few days. The conductivity increased with an increase in of PA loading, but the mechanical strength decreased.

The PA loading (doping level (DL)) was calculated from the membrane weight gain before and after doping:

$$DL = \frac{m_{after\ doping} - m_{before\ doping}}{m_{before\ doping}} \times \frac{M_{polymer}}{M_{acid}} \quad (5.1)$$

Where m is the weight of the membrane, and M is the molecular weight.

The DL was affected by the following factors:

a) DL was a function of the concentration of acid shown in Figure 5-1 [15]. During the low concentration range, the DL increased rapidly with the acid concentration. In the range of 2-10 M concentration, the increase of DL was only slight [15, 16].

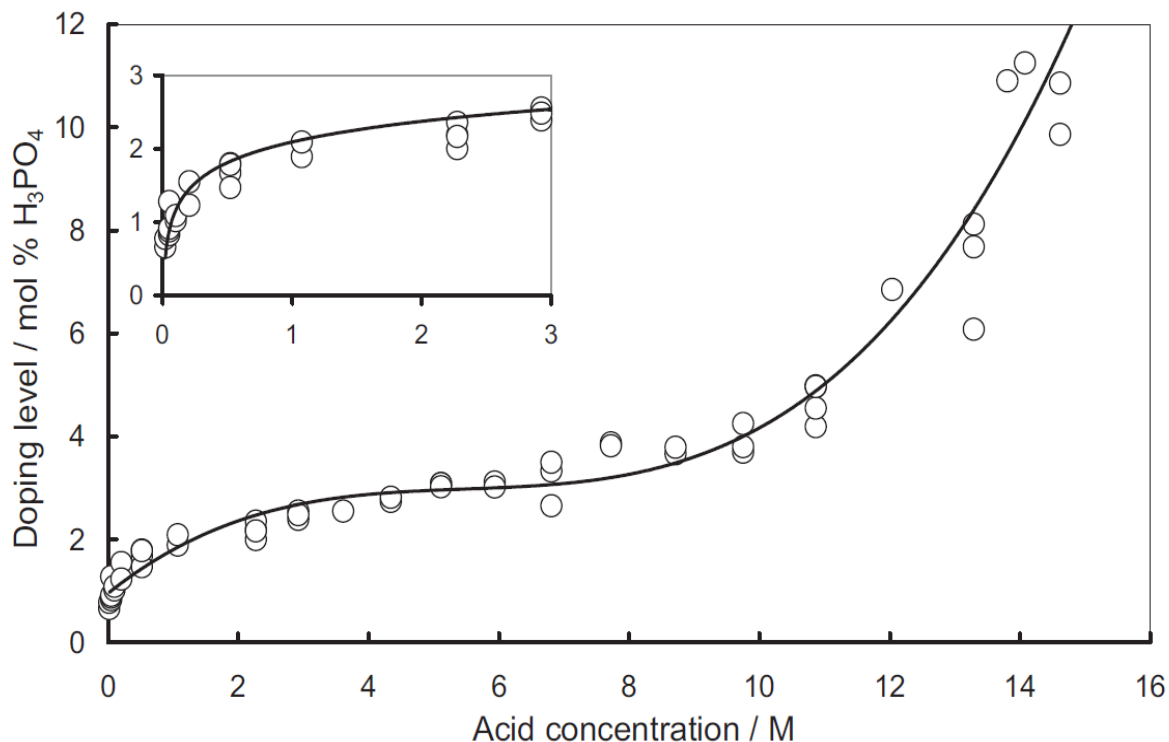


Figure 5-1 Acid doping level of PBI membrane in different phosphoric acid concentration at room temperature for about 50 hours [15]

b) Doping temperature: increasing the temperature would enhance acid diffusion in the polymer film. Elevating the temperature from 20 °C to 60 °C (11M acid concentration) increased the DL from 4.5 to 6.8 [17].

c) Time: the DL increased dramatically in the first few days (1-3 days), and kept a flat step for the following days (4-7 days), so this time the DL achieved a peak value indicating good conductivity. However, after the peak value was reached, the DL of the membrane decreased with extended loading time, because the molecular chain of PBI would swell and destroy by phosphoric acid, so the PBI hard to hold the acid in the structure after a long time dipping in the PA. [15].

d) The thicker the polymer film the larger equilibrium acid uptake, however, such equilibrium might take longer to achieve.

Due to the PBI structure, one PBI unit corresponded to around 2 molecules phosphoric acid called 'bonded acid', and excess acid is named 'free acid' (Figure 4-2) [15]. Based on Li et

al.'s paper [15], the medium molecular weight PBI membrane (IV 0.6-0.9 dl/g), the optimum doping level was around 5 for balance of the conductivity and mechanical properties. Figure 4-3 showed the PBI membrane before and after doping with phosphoric acid (11M).

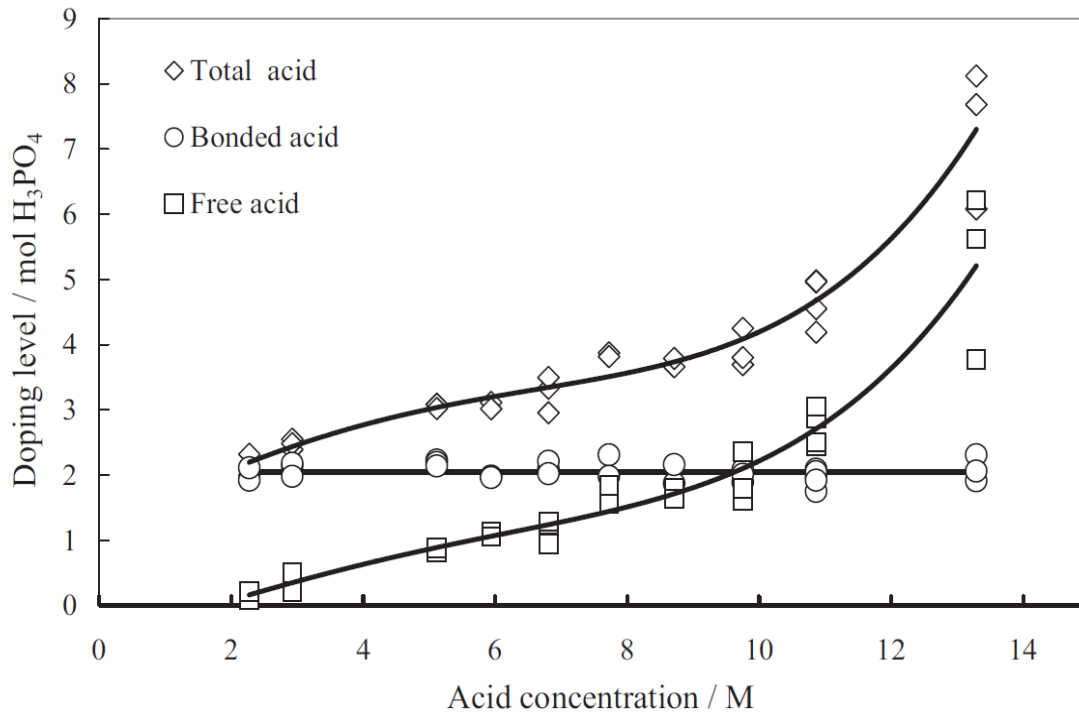


Figure 5-2 Doping level of the bonded and free phosphoric acid in PBI as a function of acid concentration [15]

5. 2.2 SEM

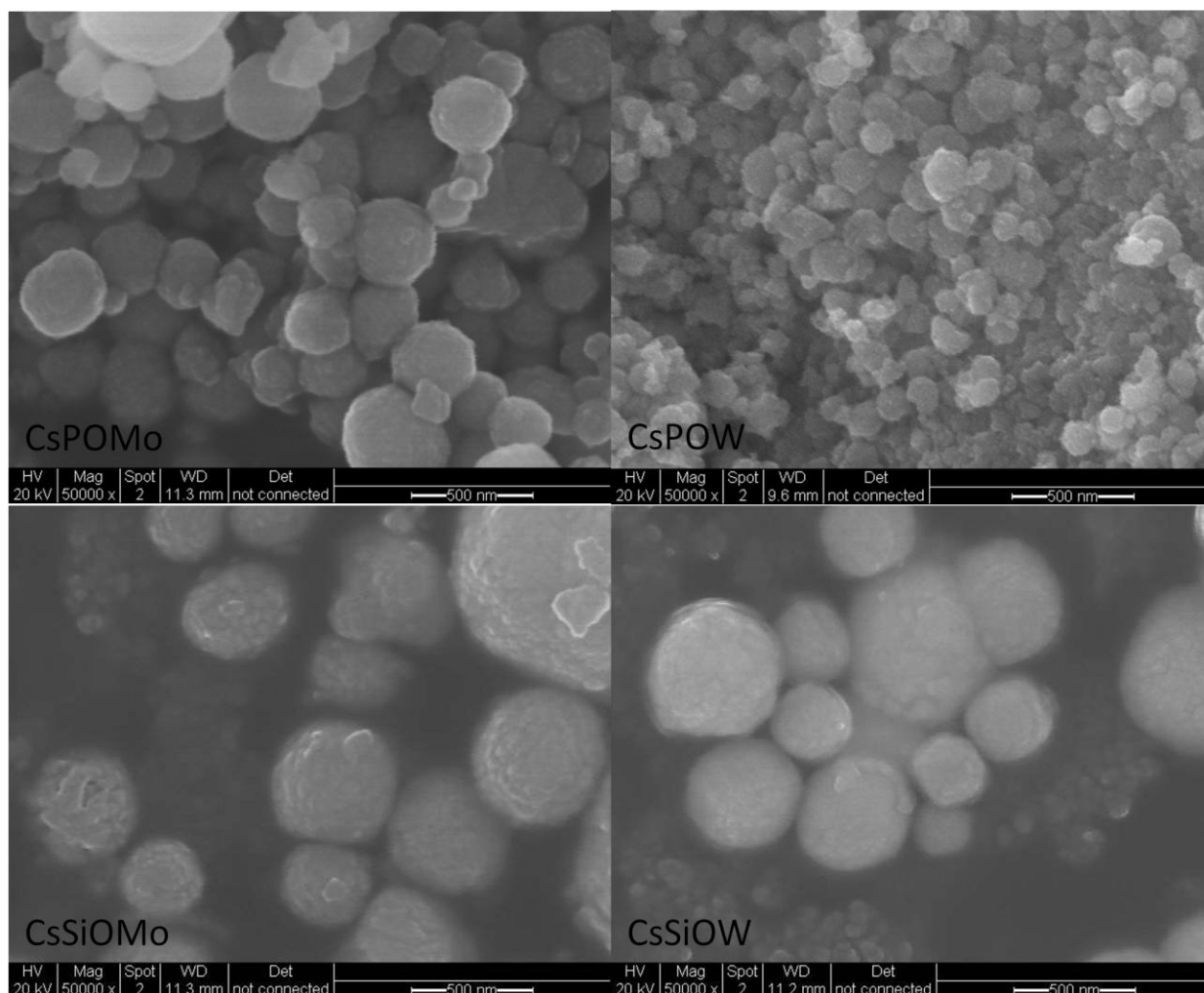


Figure 5-3 SEM images of CsPOMo, CsPOW, CsSiOMo, and CsSiOW

Fig. 5-3 showed SEM images of the four CsHPA powder particles. It could be seen that the morphology of the four powders was approximately spherical and they were formed micro size particles which are clusters of even smaller particles around 200-250 nm. The CsPOW and CsPOMo powders were smaller than the CsHPA powder with Si atoms. The smaller particles would provide more active surface area and potentially loading more acid that should be of benefit to the properties of the composite membranes. Clusters were formed in some cases with sizes between 300 and 500 nm.

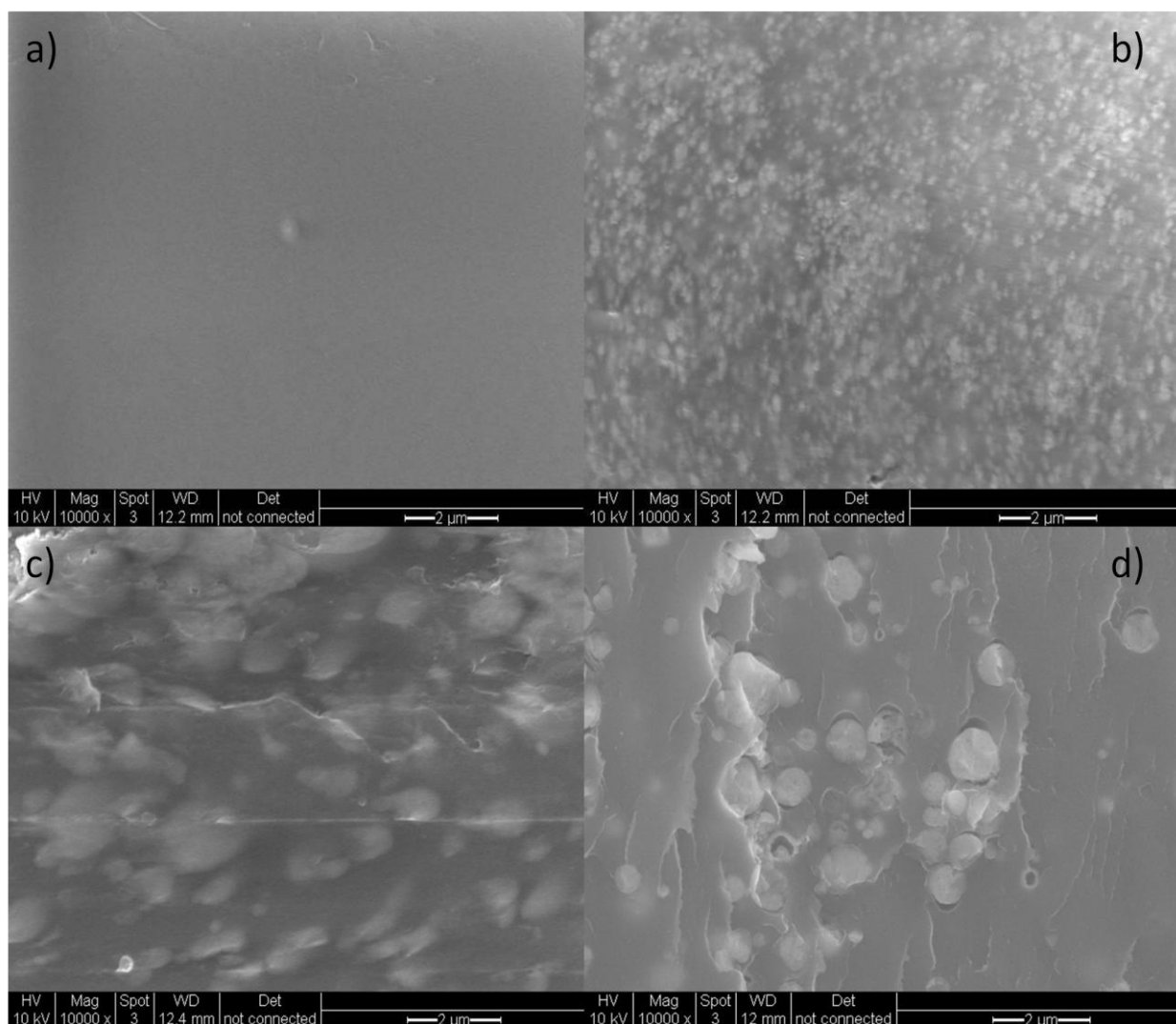


Figure 5-4 SEM images of membrane cross-sections (a) PBI/H₃PO₄ (b) 30 wt% CsPOW/PBI, (c) 30 wt% CsSiOMo/PBI (d) 30 wt% CsSiOMo/PBI/ H₃PO₄

Fig. 5-4 showed SEM images of the cross-section of the membranes. The powders, shown in the image of the CsPOM/PBI and CsSiOMo/PBI composite membranes, were interconnected in the composite membranes and dispersed homogeneously through the cross section of the membrane. Therefore, the conduction paths were established through the PBI matrix over the whole membrane and these conduction paths provide a possible interpretation for the high conductivity of the composite membrane, as will be discussed later.

5.2.3 FT-IR

All the infrared spectra of CsPOW powders (Fig. 4-5) showed four typical peaks in the 700–1200 cm^{-1} region. The characteristic vibration bands of P=O (1065cm^{-1}), Mo=O (960cm^{-1}), Mo–O_b–Mo (870cm^{-1}), Mo–O_c–Mo (770cm^{-1}) of CsPOMo were apparent and peak vibration bands of CsPOW shifted to a higher wave number with P=O (1080cm^{-1}), W=O (980cm^{-1}), W–O–W (885 cm^{-1} and 770 cm^{-1}) [13].

From the IR spectra of bare CsSiOMo and CsSiOW, it could be observed the peaks characteristic at 960 cm^{-1} for CsSiOMo and at 980 cm^{-1} for CsSiOW which indicate the vibrations of Si=O bonds. Compared to the peak bands of caesium salt of phosphor Heteropolyacid, Mo=O (900 cm^{-1}), W=O (920 cm^{-1}), in the caesium salt of silicon heteropolyacid were moved to the left. The spectrum of the PBI membrane indicated the N-H stretch near 3350cm^{-1} and the hydrogen-bonded N-H stretch at 3145cm^{-1} , and the benzimidazole characteristic absorption peaks were detected at 1608, 1560, 1442 and 800 cm^{-1} [13]. The peaks of P=O and W=O were showed in CsPOW/PBI membrane, indicating the CsPOW powder was successful mixed with the PBI membrane.

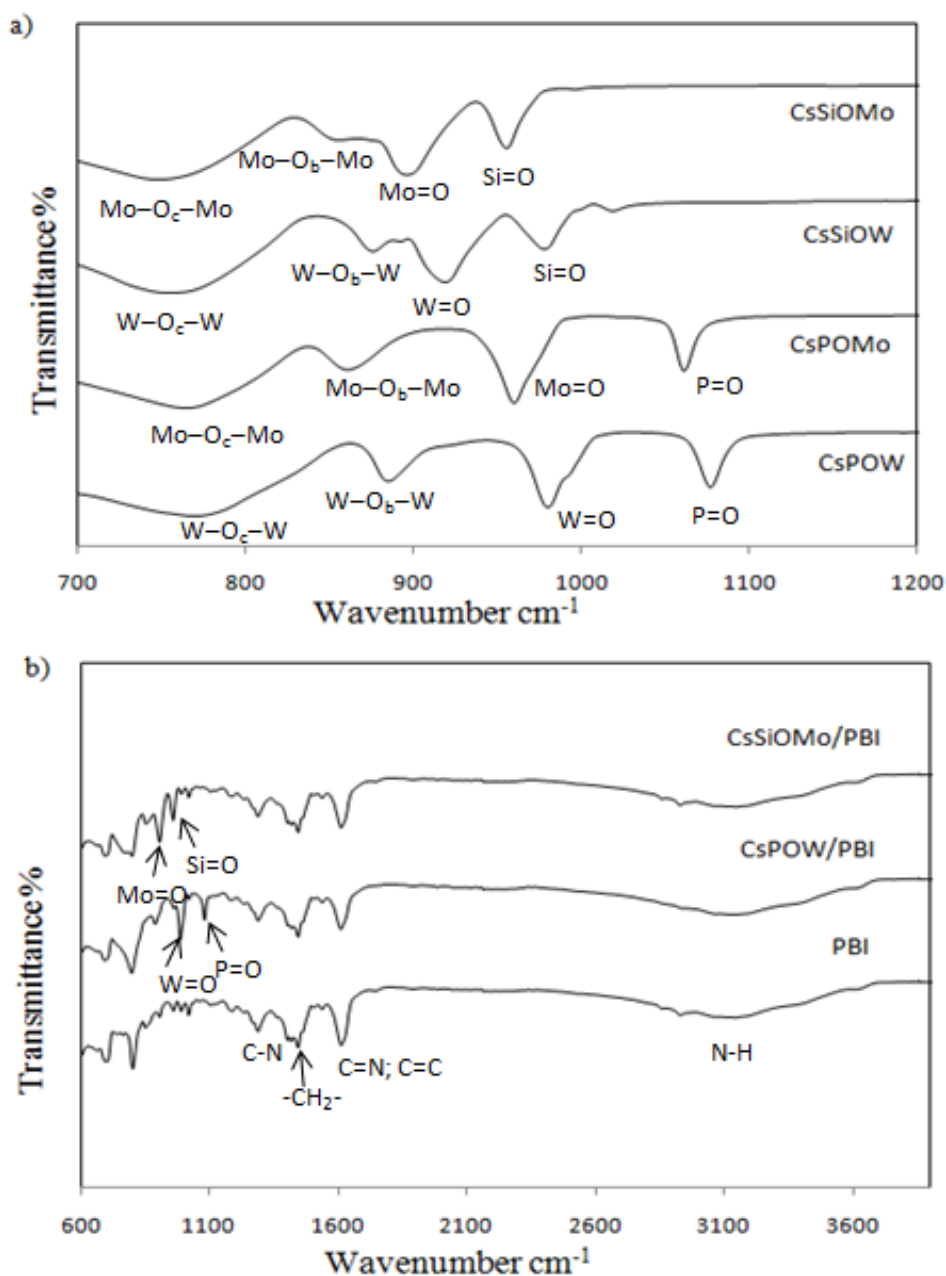


Figure 5-5 Infrared spectra of a) CsHPA powders b) PBI and CsHPA/PBI composite membranes. The peaks for the powders of CsSiOMo, and CsPOW are also shown in the PBI composite.

5.2.4 XRD

XRD patterns of four caesium salts of heteropolyacid powders were shown in Fig. 5-6. All samples gave XRD patterns identical to the crystalline structure. All peaks of powders existed at a similar position, indicating the same crystalline structure, and the most intense peaks were at around 26°. The XRD data indicates that the CsHPA powders formed cubic crystalline structures with. The CsSiOW as an example, the main peaks were fit to the Cesium silicon tungsten oxide hydrate comparison in JCPDS database. Also some small peaks may come from the structure of cesium tungsten oxide.

The size of the crystalline particles (Table 5-1) was calculated from the Scherrer equation:

$$\tau = \frac{K\lambda}{\sqrt{B_M^2 - B_S^2} \cos\theta} \quad (4.1)$$

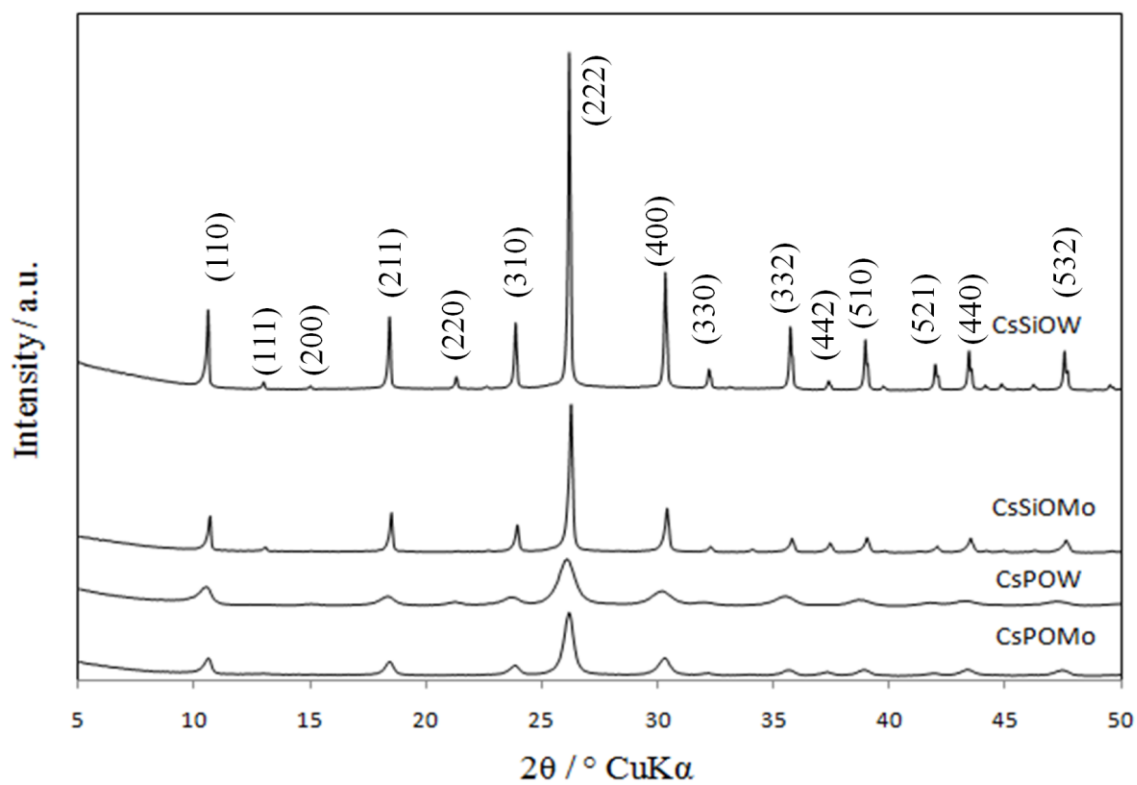
Where K is the shape factor normally as 0.9, λ is the x-ray wavelength, typically 0.15406 nm, β is the line broadening at half the maximum intensity in radians, and θ is the Bragg angle.

The CsPOW particle size was the smallest of all CsHPAs. The sizes of caesium salts of heteropolyacid powders with phosphor (11-18 nm) were smaller than those with silicon (70-136 nm), which was smaller than the size of observations particles from the SEM images. The crystal particles may be agglomerate to form the cluster that showed a larger size in SEM images than the results from Scherrer equation.

Table 5-1 Particles size of four caesium powders

	2θ °	$\sqrt{B_M^2 - B_S^2}$	τ /nm	Average size / nm
CsPOW	18.35	0.65	12.68	
	26.07	0.74	11.22	11.33
	30.16	0.83	10.1	
CsPOMo	18.42	0.4	21.48	18.73

	26.16	0.46	18.61	
	30.29	0.53	16.1	
CsSiOW	18.49	0.16	103.91	
	26.25	0.15	151.48	136.09
	30.40	0.15	152.87	
CsSiOMo	18.49	0.17	83.46	
	26.25	0.18	72.1	71.07
	30.39	0.2	57.64	



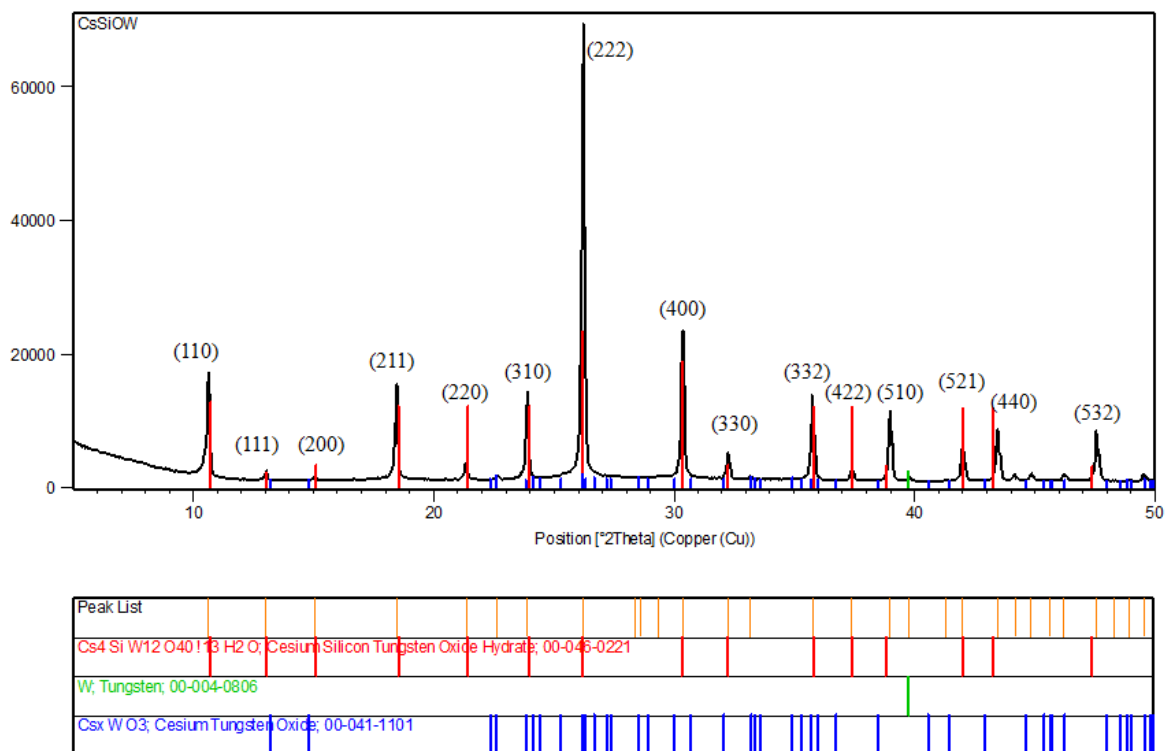
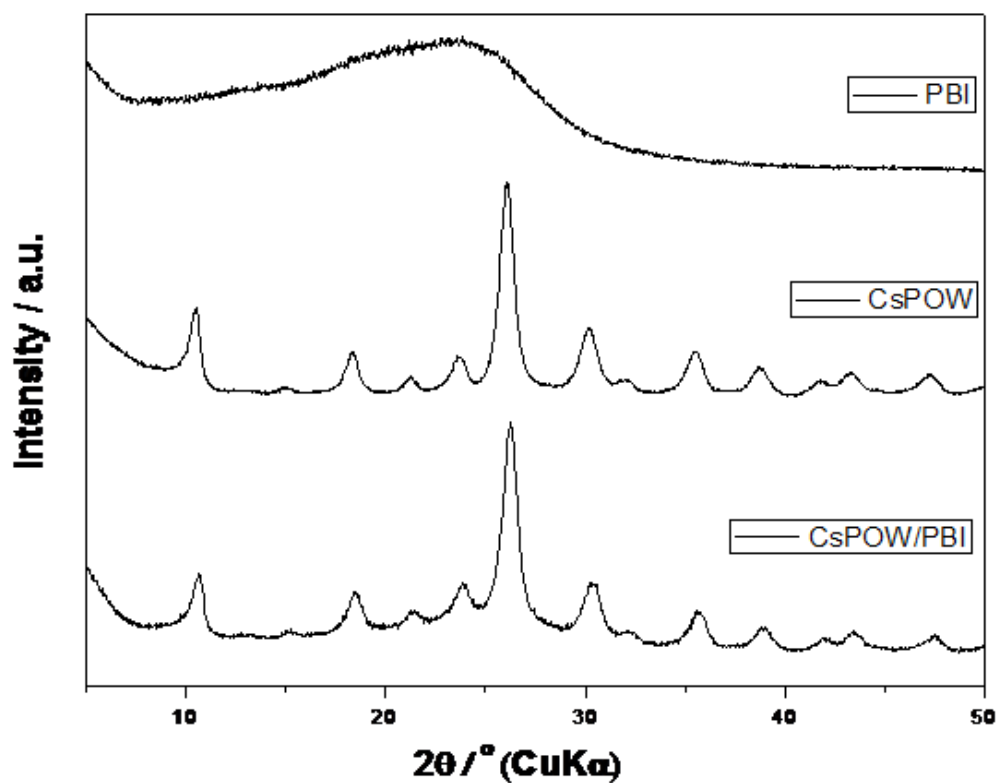


Figure 5-6 XRD patterns of Caesium salts of heteropolyacid powders



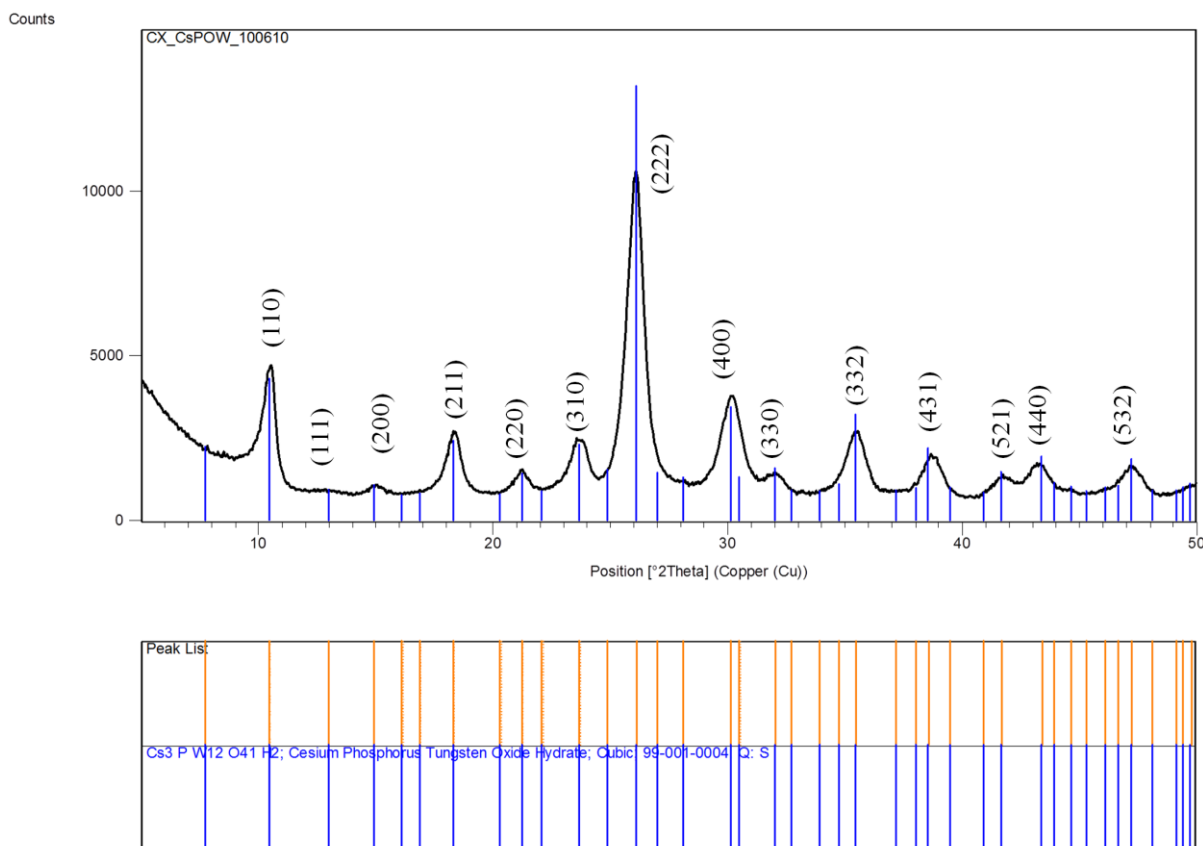


Figure 5-7 XRD patterns of PBI membrane, CsPOW powder, and CsPOW/PBI membrane

The X-ray diffraction pattern of the PBI membrane (Fig. 5-7) showed a broad peak at $2\theta=24^\circ$, associated with the convolution of an amorphous region and a crystalline region. The main sharp peaks of CsPOW fit to the reference of Caesium phosphorous tungsten oxide hydrate founded in Crystallographic Open Database. The peaks of CsPOW/PBI composite membranes were positioned almost at the same angle as that of the CsPOW, illustrating that the PBI did not affect the structure of the CsHPA after mixing [4].

5.2.5 Conductivity

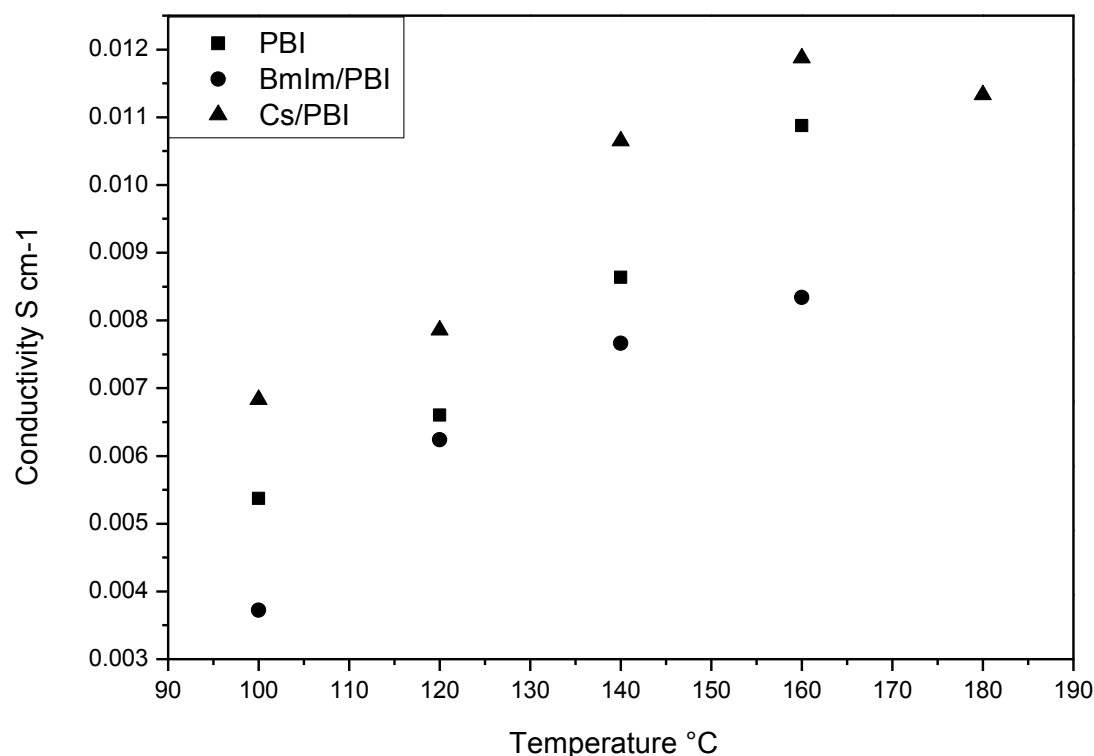


Figure 5-8 Conductivities of PBI, 30 wt% CsPOMo/PBI and 30 wt% BmIm/PBI composite membranes, doped with 10 mol/L H_3PO_4 with a doping level of 6 under anhydrous conditions. BmIm^+ was larger than Cs^+ , so the strength of bonding between the proton and heteropoly anions should be lower, which implied that the dissociation constants should be higher. Furthermore, greater degrees of delocalisation of the charge of the anion would lower the effective negative charge on its individual basic proton accepting centres, and thus weaken the attraction of the proton to the anion [21]. Therefore, the BmImPOMo was expected to provide a higher conductivity than the CsPOMo. However, as shown in Fig. 5-8, the BmImPOMo/PBI composite had lower conductivity even than the pristine PBI which implies that the BmImPOMo blocked the proton transition. This might be attributed to the Keggin structure not being formed due to the fact that the size of the BmIm was too large or the different ratio of the BmIm as required for the structure. Otherwise, it also may be attributed to block H_3PO_4 transport inner membrane by the large BmIm ion covering the H_3PO_4 cluster.

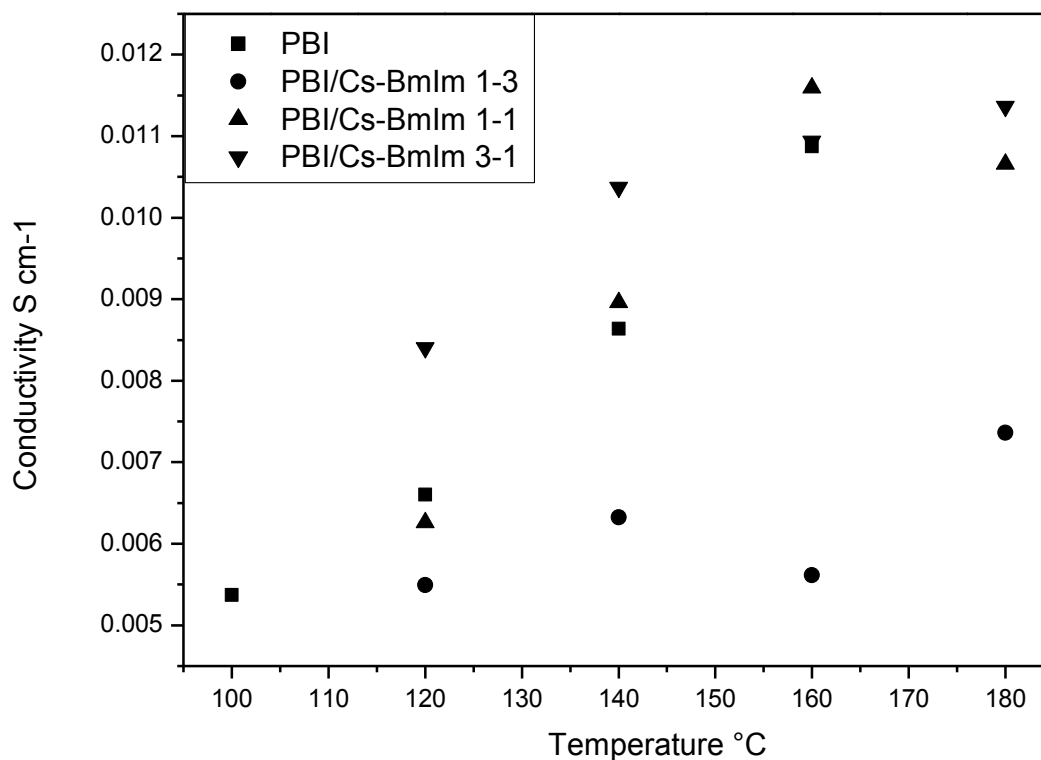


Figure 5-9 Conductivities of PBI, 30 wt% (CsPOMo:BmIm= 1:3, 1:1, and 3:1)/PBI composite membrane doped with 10 mol/L H_3PO_4 with doping level of 6 under anhydrous conditions

As shown in Fig. 5-9, when the Cs:BmIm approached 1:1, the composite membrane showed similar conductivity with the pristine PBI under the same condition. The conductivity increased by increasing the substitute of caesium in the composite membrane. These results were provided by Fig. 5-8 as well, indicating that the BmIm reduced conductivity in the PBI membrane. So, Caesium was optimised as the salt substitute of Heteropolyacid.

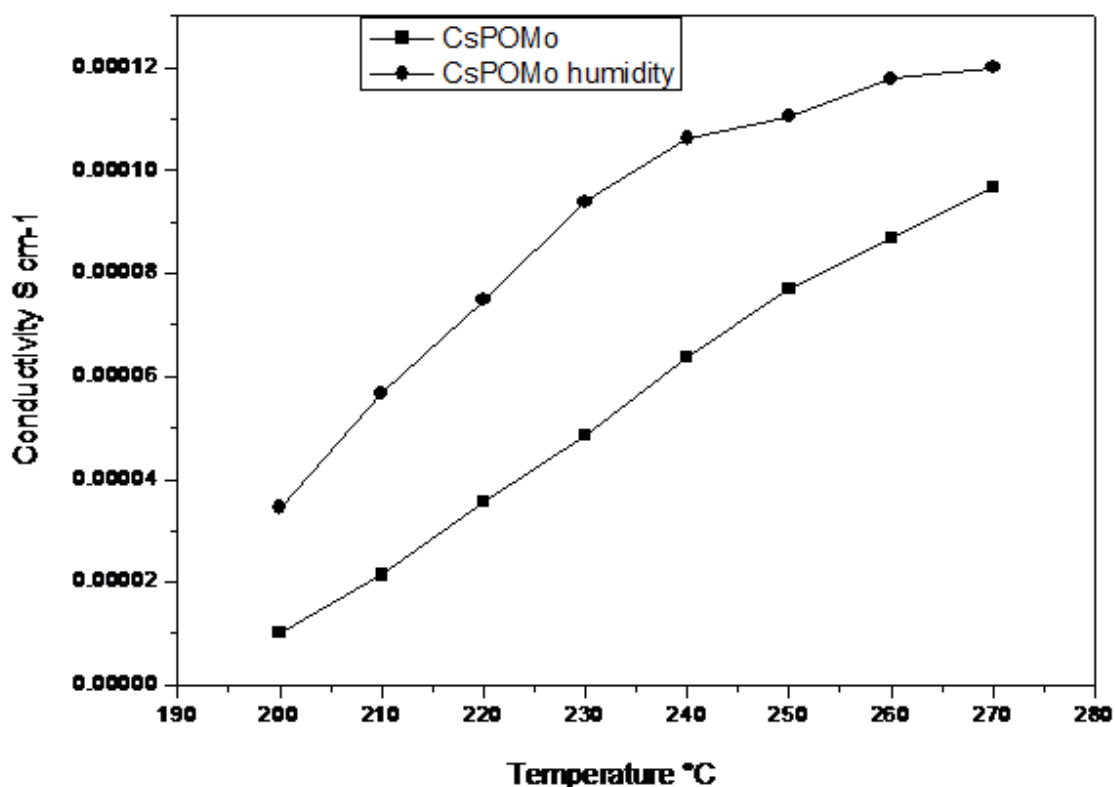
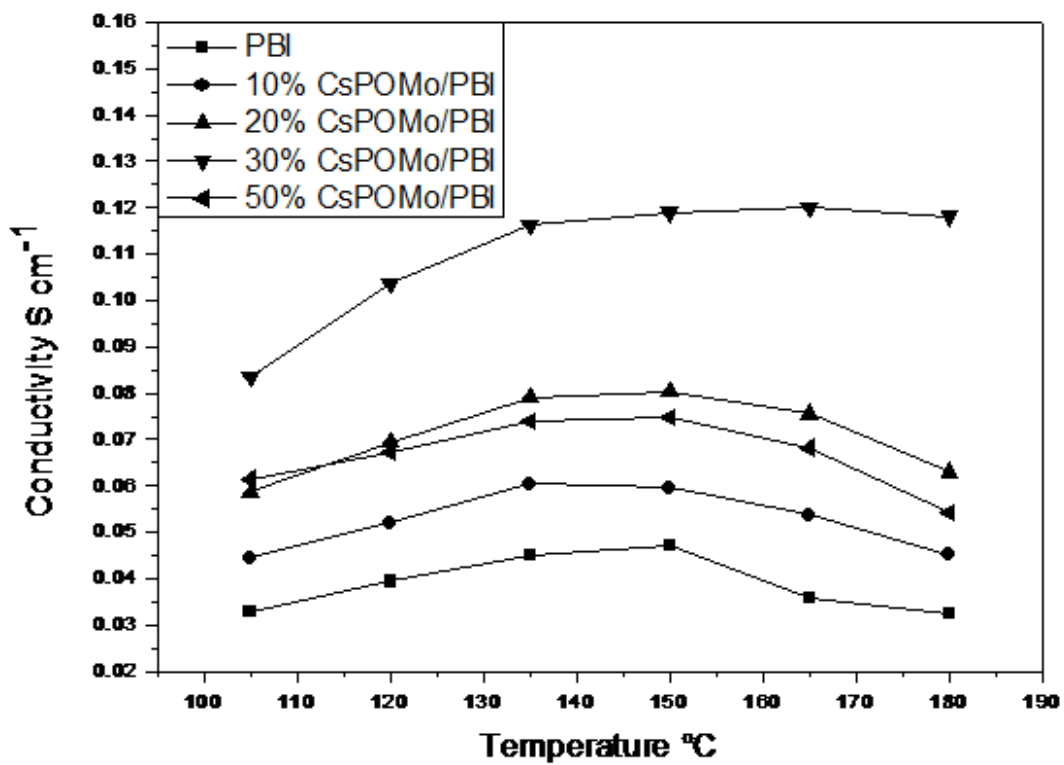
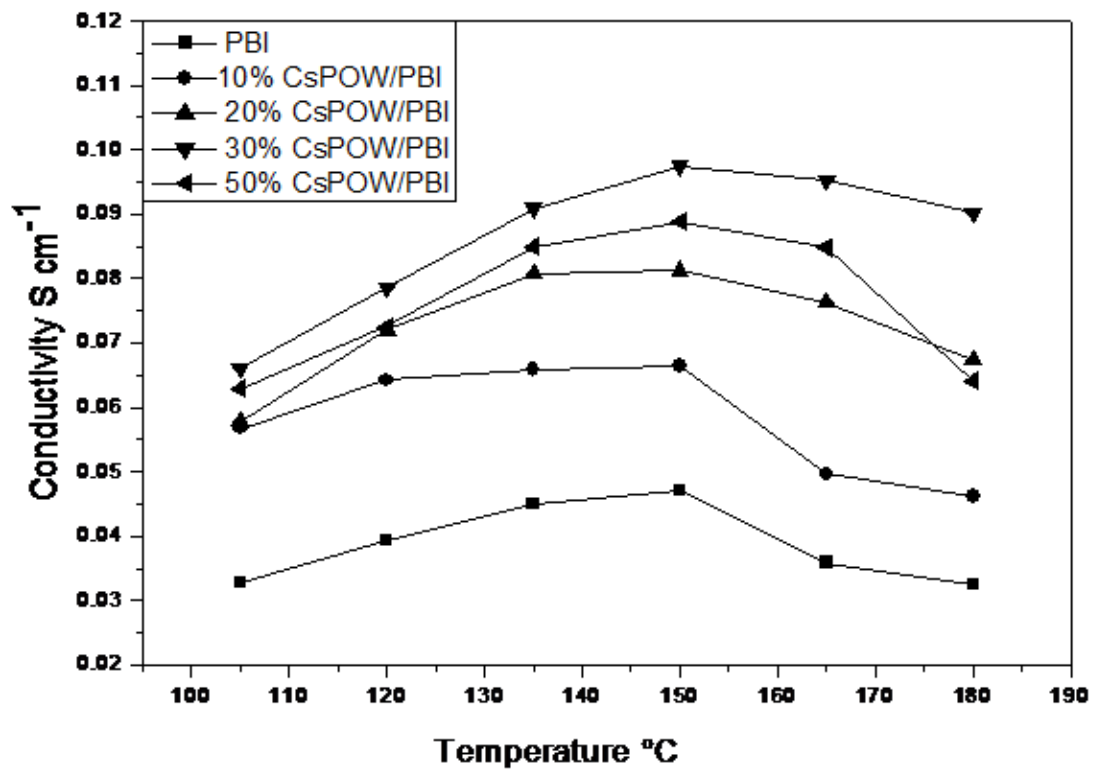


Figure 5-10 Conductivity of CsPOMo powder under anhydrous and humidity conditions

When lower than 190°C, the CsPOMo powder did not show conductivity under anhydrous and humidity conditions and it began to provide conduction from around 200°C. The humidity was provided by Nitrogen gas with a speed of 150 ml min⁻¹ going through the water tank at 90 °C, and the tube was 90 °C as well. The conductivity increased with the temperature increasing as shown in Fig 4-10. This conductivity might be caused by the H₂O being released from the CsHPA with a superprotonic phase formation as the similar conduction mechanism of CsH₂PO₄ under high temperature. When the humidity was added, the conductivity increased more than 2 times than that in the anhydrous conditions, so the water benefited the conductivity of the CsPOMo powder because it provided more H₂O for a protonic phase formation. However, the pure CsHPA powder did not provide prospected conductivity as expected.



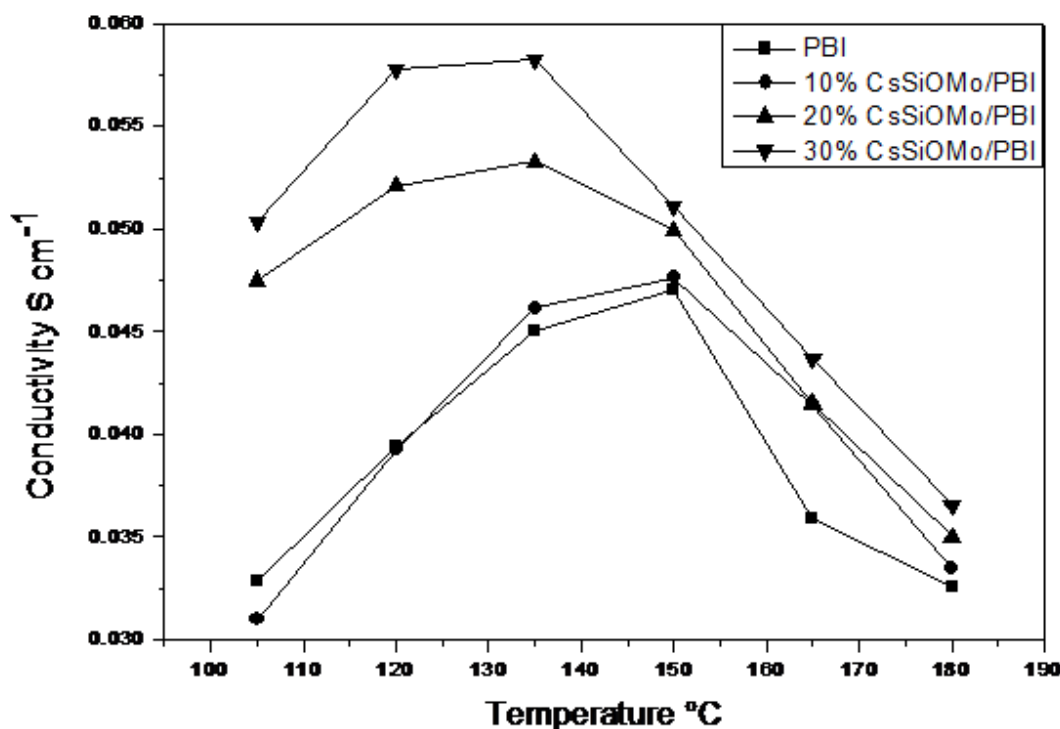
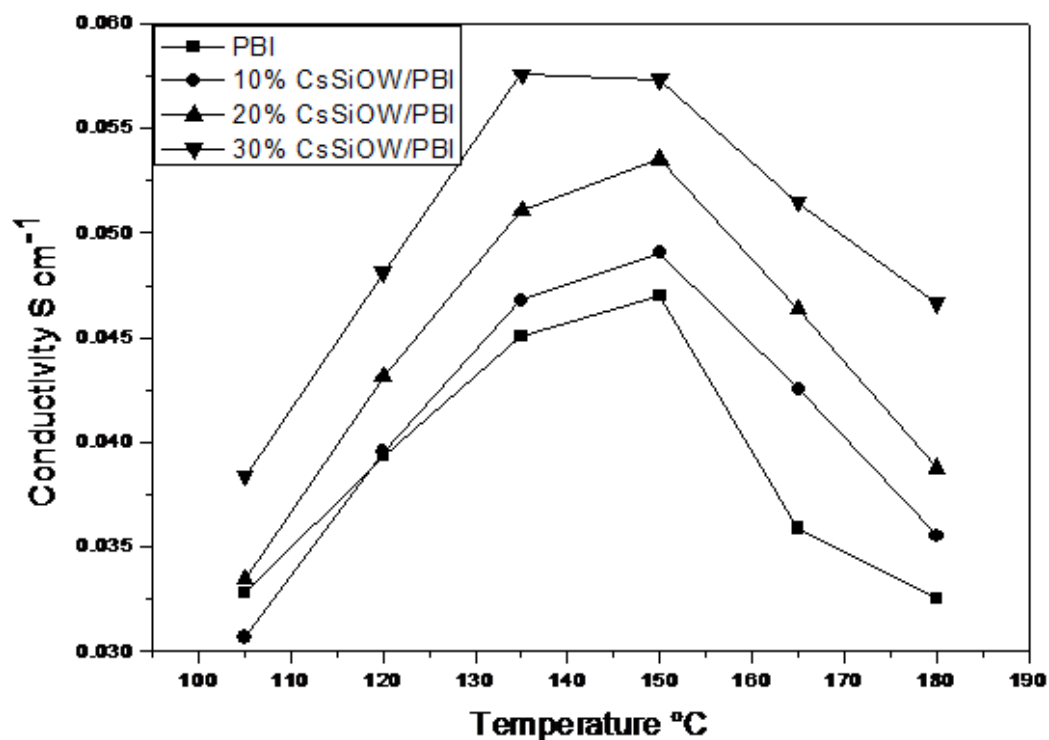


Figure 5-11 Conductivities of different ratio Cs-heteropolyacid in PBI membrane doped with H_3PO_4 with a doping level of 4.5 under anhydrous conditions

As shown in Fig. 5-11, the CsHPA/PBI composite showed a higher conductivity than the pristine PBI indicating the positive affection for conductivity of the CsHPA

Fig. 5-11 showed that the conductivity of Cs-heteropolyacid/PBI composite membranes increased with the ratio of the CsHPA rising from 10 wt% to 30 wt%. However, 50 wt% CsPOW or CsPOMo reduced the conductivity of the composite membrane compared to 30 wt% one. When, the CsHPA ratio was less than 30 wt%, CsHPAs HPAs act toward react with the water of hydration, which was generally loosely bound in the structure for high proton conductivity, but when it reached 50 wt%, the CsHPA powder might block the conduct path of PBI through H_3PO_4 .

Table 5-2 Conductivities of CsHPA /PBI composite membranes loaded with H_3PO_4 . Acid amounts of 4.5 RPU under anhydrous condition at 150 °C. The conductivity of the PBI membranes is $0.047 S cm^{-1}$ under the same conditions.

% of CsHPA	CsPOW ($S cm^{-1}$)	CsPOMo ($S cm^{-1}$)	CsSiOW ($S cm^{-1}$)	CsSiMo ($S cm^{-1}$)
10%	0.066	0.06	0.049	0.048
20%	0.081	0.08	0.054	0.05
30%	0.1	0.12	0.057	0.051

Table 5-2 showed the effect of the CsHPA content on the conductivities of the composite membranes. A greater content of CsHPA powders in the composite membrane improved the conductivity of the membrane. The conductivity of composite membranes was greater than that of the PBI membrane ($0.047 S cm^{-1}$) at the same conditions. This improvement of proton conductivity is caused by more conducting paths built by the CsPHA in the whole composite membrane according to the percolation theory. The protons not only transferred through the hydrogen bond, but also the CsHPA particles path from one side to the other. When the percentage of CsHPA powders is higher than the percolation threshold, the conductivity

improved sharply. Meanwhile, there were more proton defects provided by CsHPA in PA leading to higher proton conductivity.

For 30% CsSiOW or CsSiOMo/PBI membranes, the conductivities were around 0.055 S cm^{-1} and for 30% CsPOW and CsPOMo/PBI membranes they were around 0.1 S cm^{-1} . The relatively high conductivities of CsHPA/PBI/ H_3PO_4 composite membrane indicated that they were promising materials for intermediate temperature PPMFC applications. All membranes showed a similar variation in conductivity with the temperature as shown in Fig. 5-12, although conductivities were higher with a greater CsHPA content.

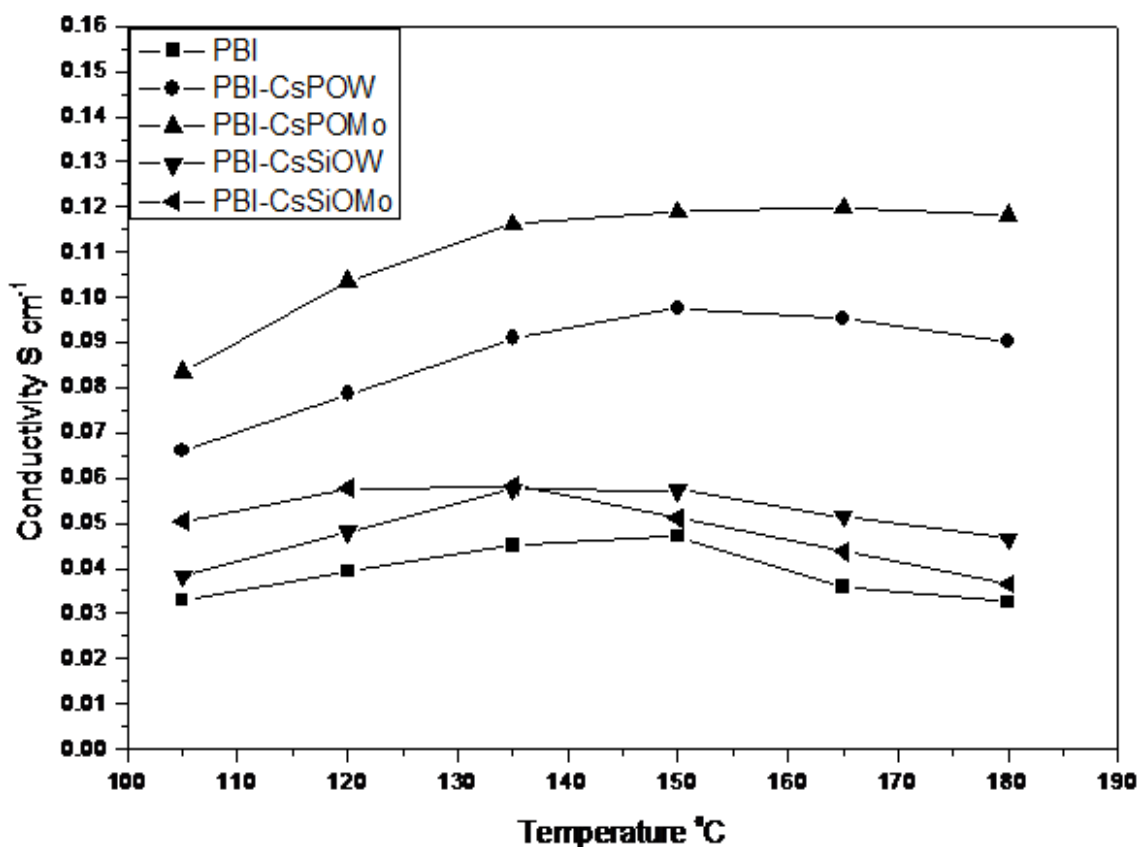


Figure 5-12 Conductivities of 30 wt. % CsHPA /PBI composite membrane doped with H_3PO_4 with a doping level of 4.5 under anhydrous conditions

Fig. 5-12 showed the conductivity data of the CsHPA/PBI membranes loaded with phosphoric acid (11 M) to achieve a doping level of 4.5 under anhydrous conditions. It was seen that the CsHPA based membranes had greater conductivity than the pristine PBI membrane. The conductivity of the PBI membrane was 0.047 S cm^{-1} at $150 \text{ }^\circ\text{C}$ under the

same conditions. This behaviour could be attributed to a combination of the good conductivities of the CsHPA powder in the PBI matrix. Overall the CsHPA powder improved the conductivity of PBI composite membranes.

The conductivities of CsPOW and CsPOMo were higher than those of CsSiOW and CsSiOMo, which could be attributed to the finer size and better acid uptake of phosphoric acid. This result was also in agreement with reported enthalpy of adsorption of ammonia ($\Delta H_{\text{ads}}^{\circ}$) calorimetry indicating that all Cs exchanging silicotungstates were weaker acids than their $\text{H}_3\text{PW}_{12}\text{O}_{40}$ counterparts. [19]. The conductivities decreased when the temperature exceeded 150 °C, because phosphoric acid could lose water through a condensation reaction to form pyrophosphate, above 140°C, which had lower conductivity [20]. The conductivities of CsSiOW and CsSiOMo were similar, and the highest conductivities, around 0.12 S cm⁻¹, were achieved with CsPOMo.

The higher conductivity of the Cs phosphotungstic acid based materials compared with the Cs silicotungstic acid materials agrees with the relative behaviour of these acids when formed as composites with PBI and loaded with phosphoric acid [7, 19]. For example the 30% acid solid containing membranes, with a phosphoric acid loading of 4.4 PRU, had conductivities of 0.033 and 0.029 S cm⁻¹ at 140 °C and 5% RH, for P and Si based materials respectively. In this work the conductivities of the solid acid/PBI composite membrane loaded with phosphoric acid were lower than that achieved with the PBI loaded with phosphoric acid without inorganic acid. The conductivity of this composite membrane depended critically on the water content or RH. At low humidity (1 %) the conductivities were less than 0.03 S cm⁻¹ for both Si and P based composite materials, significantly less than the conductivities of the Cs salt counterparts in this work. As yet the reason for the difference in conductivities of the P and Si based solid acid materials when formed as composites with PBI (acid loaded) was not known and was the subject of ongoing study, although particle size was one factor.

5. 2.6 Tensile test

Table 5-3, Mechanical strength of 30 wt% CsHPA acid/PBI membrane

	PBI	CsPOMo /PBI	CsPOW /PBI	CsSiOMo /PBI	CsSiOW /PBI
Maximum strength (MPa)	60	42	36.1	43.9	50.9

The mechanical strength of membranes without acid was measured at 42% relative humidity (RH) and room temperature (Table 5-3). All four composite membranes showed good mechanical strength although the mechanical strength of CsHPA/PBI composite membrane was weaker than that of the pristine PBI membrane and decreased with increased powder content (data not shown). This reduction in mechanical strength was indicative of the absence of physicochemical interaction between Cs-HPA and the PBI matrix [21]. The mechanical strengths of CsPOW and CsPOMo membranes were lower than those of CsSiOW and CsSiOMo. This indicated that the Si atom provided better mechanical properties although inferior conductivity than those of the P based salts.

5.2.7 Fuel cell test

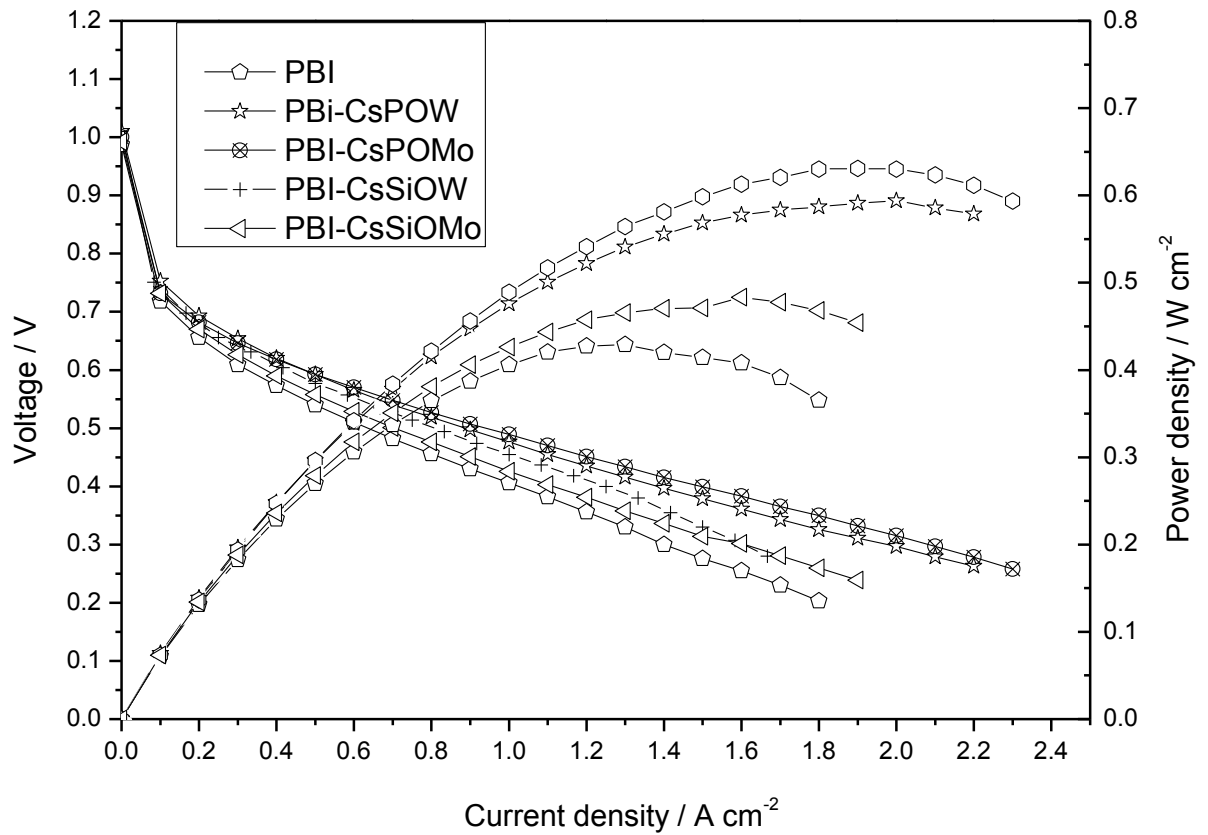


Figure 5-13a Polarisation and power density curves of a PEMFC operated at 150 °C with H_2/O_2 atmospheric pressure

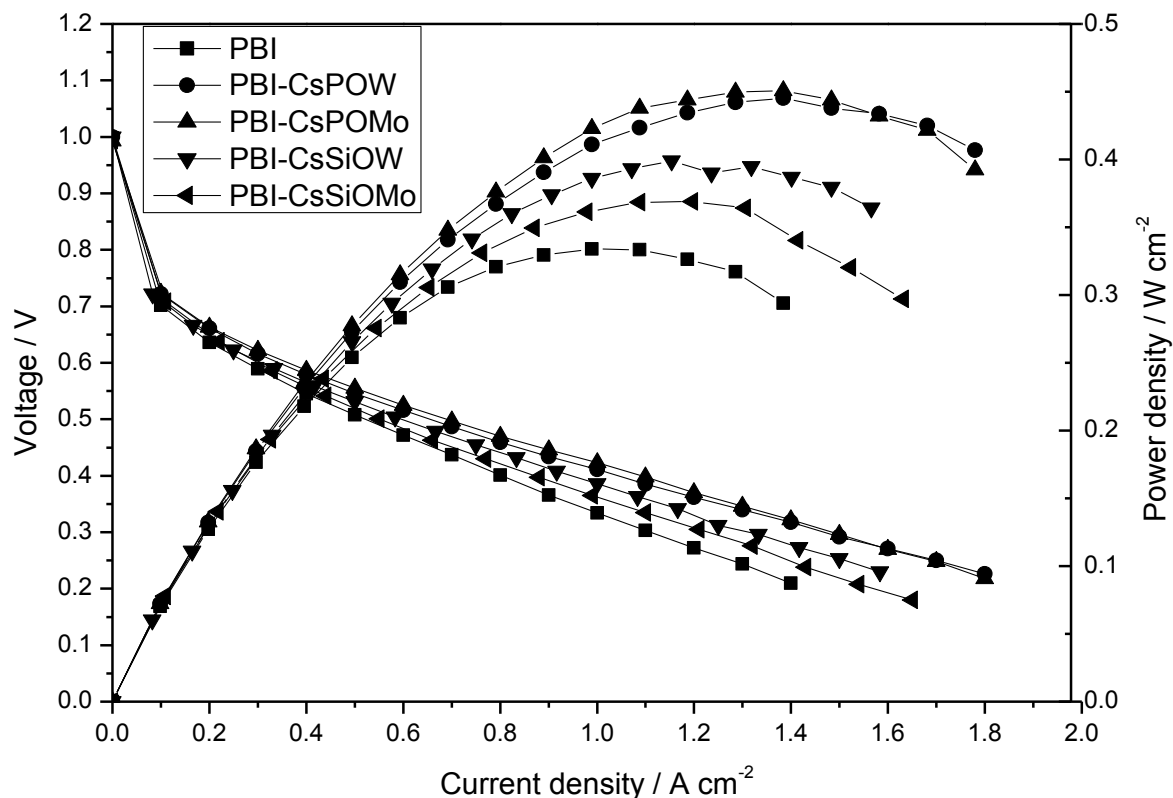


Figure 5-13b Polarisation and power density curves of a PEMFC operated at 150 °C with H₂/Air atmospheric pressure

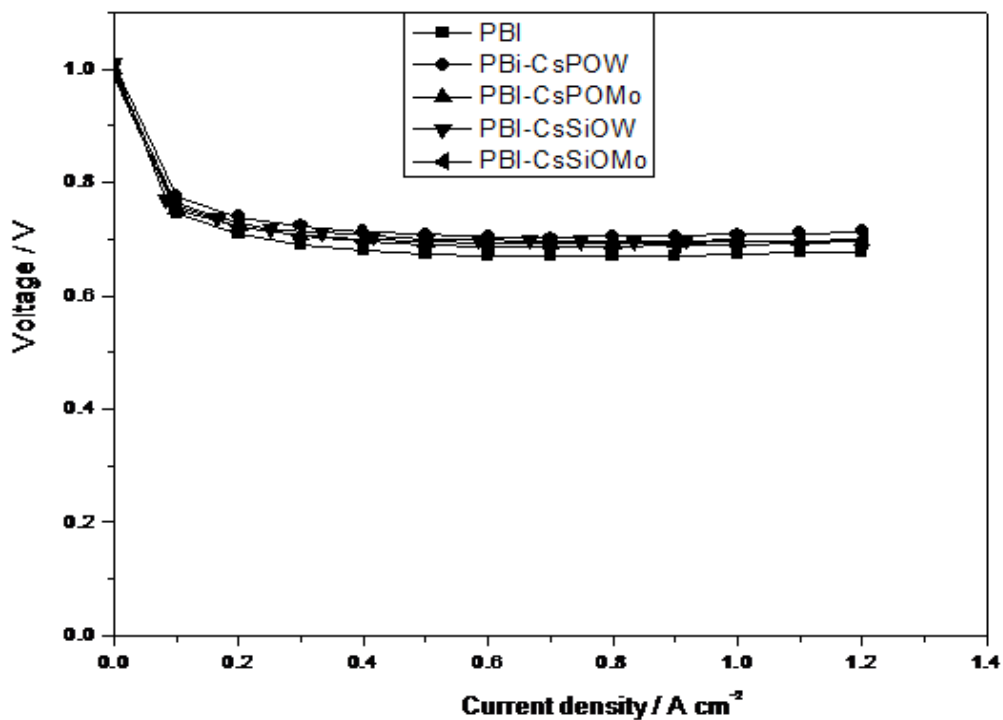
Fig.5-13 Comparison of CsHPA/PBI/H₃PO₄ composite membranes and PBI/H₃PO₄, in fuel cell performance Pt loading: cathode 0.7mg cm⁻²; anode 0.7mg cm⁻²; anhydrous condition, H₃PO₄ loading level: 4.5, gas rate: anode: 40 dm³ min⁻¹; cathode: 70 dm³ min⁻¹.

The polarisation and power density curves of the H₂/O₂ and H₂/air fuel cells obtained at 150 °C under anhydrous conditions for PBI and CsHPA/PBI membranes were shown in Fig. 8. The open circuit voltages (OCV) of all membranes were more than 0.95V, which indicates that the membranes have low gas permeability. If the gases go through the membrane directly, the hydrogen and oxygen reaction would happen on the one electrode, thus there is an electric cycle formed in the electrode rather than the whole fuel cell system leading to the OCV reduction. All the fuel cells exhibited significant activation polarisation, with overpotential of some 0.25 V at 0.1 A cm⁻². The performances of the cells with the CsHPA/PBI composite membranes were significantly better than that with the PBI membrane. Current densities of CsHPA/PBI at 0.4 V with oxygen were over 1 A cm⁻² at 150 °C. The CsPOW and CsPOMo

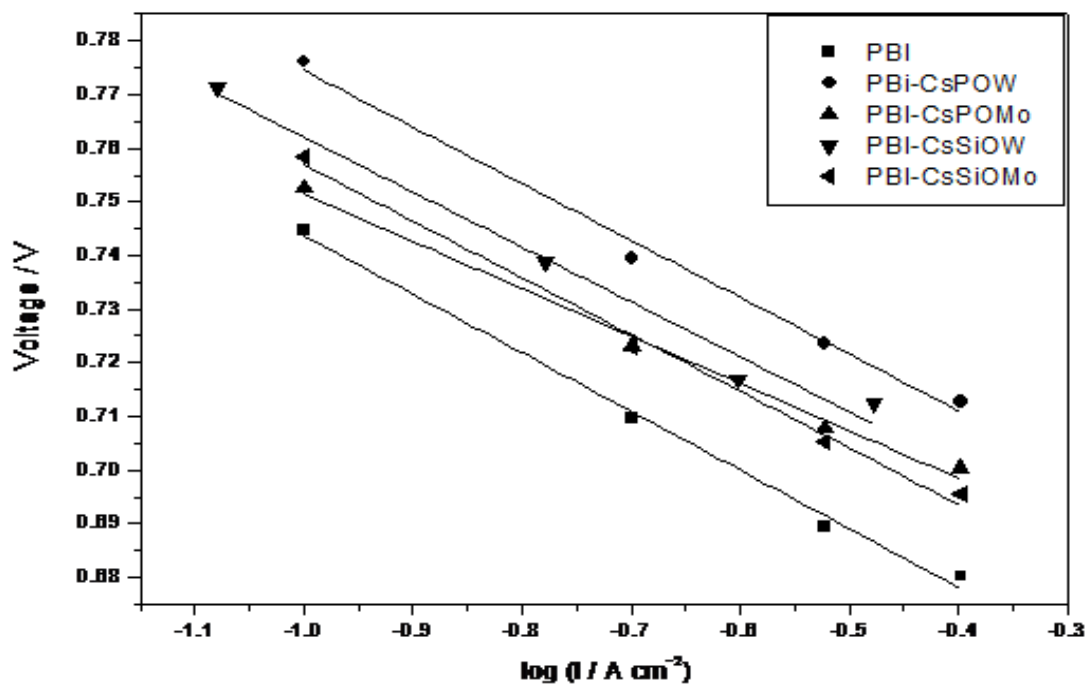
membranes gave better fuel cell performance than those of the CsHPA with Si atom. The peak power densities of PBI, CsPOW/PBI, CsPOMo/PBI, CsSiOW/PBI, and CsSiOMo/PBI were 0.43, 0.59, 0.63, 0.51, and 0.48 Wcm⁻², respectively. The result of CsPOMo/PBI was similar with the literature review which gave peak power densities of 700 mW cm⁻² [13]. The good performances were mainly attributed to the superior proton conductivity of the former and also the strong acid and water retention properties of the composite membrane.

With atmospheric air, the OCVs of membrane were more than 0.95 V. The peak power density with the PBI membrane was 0.334 W cm⁻² and cell voltages produced with the CsHPA composite membranes were greater than those with the PBI membrane at high-current densities. The CsPOMo gave a peak power density of 0.45 W cm⁻². CsHPA/PBI composite membranes achieved 1.6 A cm⁻² under air conditions at 150 °C. The CsHPA/PBI composite membranes were thus suitable for use with H₂/Air.

The internal resistance, as estimated from the voltage drop in the intermediate voltage range, gave a cell conductivity of around 0.03 S cm⁻¹ for the CsSiOMo membrane fuel cell. This conductivity was approximately half that of the membrane itself and indicates significant voltage loss in the electrode layers (and other cell components). Furthermore, as Fig. 8 shows, from current densities 0 to 0.1 Acm⁻² there was an approximate 250 mV voltage loss, indicating that the catalyst compositions in the MEA were not “optimal” for the fuel cell.



a)



b)

Figure 5-14 (a) IR corrected polarisation curves of PBI and CsHPA-PBI membrane; (b) Tafel plots obtained from polarisation curves (I is current density).

To investigate the kinetics performance of the electrodes in the fuel cell, the voltage losses associated with the membrane resistances and the contact resistances between the electrolyte and the electrodes were removed from the fuel cell polarization curve to provide called as IR correction. The Tafel slopes were calculated to indicate electrochemical kinetics behavior. Figure 5-14 showed IR corrected polarisation curves of the fuel cells operated with H₂/O₂ at 150 °C. IR correction was based on the combined resistance of membrane and electrode, measured from the slope of the cell voltage *vs.* current density at a high current density region (0.5–1.0 A cm⁻²).

In this region the voltage loss associated with electrode polarisation was small compared to that of the internal resistance. From the plot of the IR corrected voltage *vs.* log (current density I), the slope (Tafel type) of the line of PBI and CsHPA were around 100 mv per decade, The value was close to the literature reported values (100 mV dec⁻¹) on ORR electrodes for phosphoric acid loaded PBI fuel cells [22].

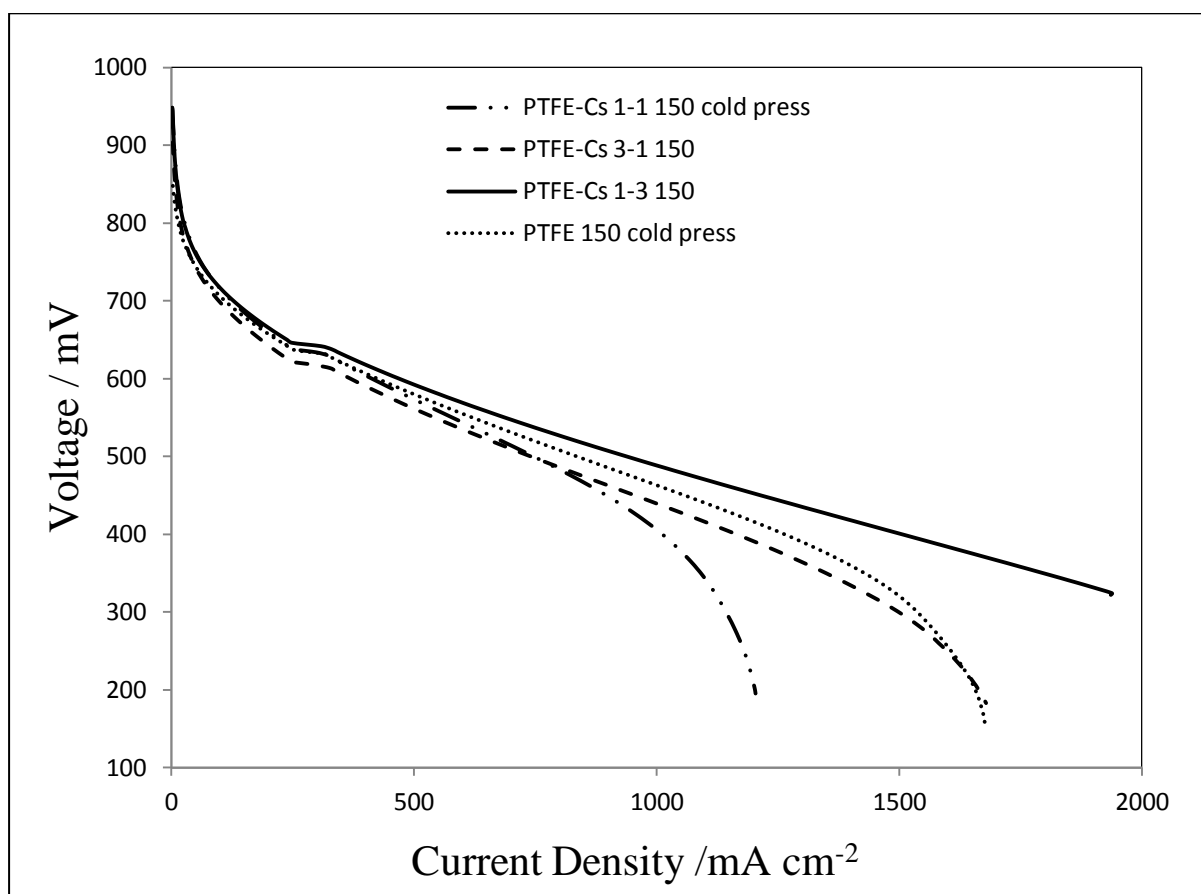


Figure 5-15 The PBI membrane polarisation curves of different cathode electrode layers at 150 °C

Overall, although the CsHPA/PBI composites were potential membranes for polymer phosphoric acid electrolyte membrane fuel cells, more studies were required to optimise the electrode catalyst layer composition and to establish suitable MEA preparation. As the best conductivity power among these four CsHPAs, the CsPOMo was added into the catalyst solution at different ratios to investigate the electrode catalyst layer composition. The anode electrode had 0.2 mg cm^{-2} Pt and 30 wt % PTFE. The membrane electrolyte was PBI with 4.5 PRU of PA. The Pt/C loading in the cathode was 0.6 mg cm^{-2} and the PTFE content was 20 wt % of Pt/C used, and CsPOMo was at the ratio of PTFE 1:3, 1:1, and 3:1, respectively. As shown in Figure 4-15, when the CsPOMo was added to the catalyst solution, the polarisation curve reduced and the lower voltage was shown at the same current density. There should be two opposite inflections of the CsPOMo powder to be used in the catalyst. One was to build the proton conducting path which benefited to the conductivity, and the other one was to block the gas to reach to the catalyst. When less CsPOMo powder added, the performance reduced which can be attributed to the CsPOMo powder blocked gas access to the catalyst surface. However with the CsPOMo content increasing to a value 3 times than that of the PTFE, a good proton transfer property of the CsPOMo powder started to exhibit due to the conduction path built.

5.3 Conclusions

Inorganic-organic composite electrolytes, made from CsHPA and PBI were prepared for use in phosphoric-acid polymer membrane fuel cells (PPMFC). The composite membranes, loaded with H_3PO_4 had higher conductivities than that of the phosphoric acid loaded PBI membrane. In fuel cell tests the CsHPA/PBI composite membranes gave superior performance to that of a PBI membrane. The P form of the CsHPA provided higher conductivity, as composite membranes, than those of CsHPA with Si atom, although the mechanical strength was inferior. The CsHPA showed better conductivity than BmImHPA, indicating that Cs was better as a salt substitute with Heteropolyacid. The data indicated that the PBI composites with CsHPA loaded with phosphoric acid could be potential membranes for intermediate PEMFC because of their high conductivity and fuel cell performance of $> 0.6 \text{ W cm}^{-2}$ with atmospheric pressure oxygen.

References

1. Kozhevnikov I., *Catalysts for fine chemical synthesis, in: Catalysis by Polyoxometalates*, **2002**, vol. 2, John Wiley & Sons, Chichester
2. Baker, L., Glick, D. *Present general status of understanding of heteropoly electrolytes and a tracing of some major highlights in the history of their elucidation*, Chemical Review, **1998**, 98, 3–49.
3. Vuillaume, P., Mokrini, A., Siu, A., Theberge, K., Robitaille, L., *Heteropolyacid/saponite-like clay complexes and their blends in amphiphilic SEBS*, European Polymer Journal, **2009**, 45, 1641–1651.
4. Romero P., Asensio J., Borrós S. *Hybrid proton-conducting membranes for polymer electrolyte fuel cells: Phosphomolybdic acid doped poly(2,5-benzimidazole) - (ABPBI- $H_3PMO_{12}O_{40}$)*, Electrochimica Acta, **2005**, 50, 4715–4720
5. Vogel H, and Marvel C., *Polybenzimidazoles, new thermally stable polymers*, Journal of Polymer Science, **1961**, 50:511-39
6. Okuhara T., *Water-tolerant solid acid catalysts*, Chemical Review, **2002**, 102, 3641–3666
7. He R, Li Q, Xiao G, Bjerrum N. *Proton conductivity of phosphoric acid doped polybenzimidazole and its composites with inorganic proton conductors*. Journal of Membrane Science, **2003**, 226,169–184
8. Staiti, P. and M. Minutoli, *Influence of composition and acid treatment on proton conduction of composite polybenzimidazole membranes*, Journal of Power Sources, **2001**, 94(1), 9-13
9. Kim, Y., Wang, F., Hickner, M. Zawodzinsk T., Mcgrath J., *Fabrication and characterization of heteropolyacid ($H_3PW_{12}O_{40}$)/directly polymerized sulfonated poly(arylene ether sulfone) copolymer composite membranes for higher temperature fuel cell applications*, Journal of Membrane Science, **2003**, 212(1-2),263-282
10. Wang, Z., Ni H., Zhao C., Li X., Fu T., Na H., *Investigation of sulfonated poly (ether ether ketone sulfone)/heteropolyacid composite membranes for high temperature fuel cell applications*, Journal of Polymer Science, Part B: Polymer Physics, **2006**, 44(14), 1967-1978
11. Xu, C., Wu, X., Wang, X., Mamlouk, M., Scott, K., *Composite membranes of polybenzimidazole and caesium-salts-of- heteropolyacids for intermediate temperature fuel cells*, Journal of Materials Chemistry, **2011**, 21 (16) , 6014-6019

12. Okuhara, T.; Watanabe, H.; Nishimura, T.; Inumaru, K.; Misono, M. *Microstructure of cesium hydrogen salts of 12-tungstophosphoric acid relevant to novel acid catalysis*, Chemistry of Materials, **2000**, 12, 2230.
13. Li, M., Shao Z., Scott K., *A high conductivity Cs_{2.5}H_{0.5}PMo₁₂O₄₀/polybenzimidazole (PBI)/H₃PO₄ composite membrane for proton-exchange membrane fuel cells operating at high temperature*. Journal of Power Sources, **2008**, 183(1), 69-75
14. Mamlouk M., and Scott K. *The effect of electrode parameters on performance of a phosphoric acid-doped PBI membrane fuel cell*, Int. J. of hydrogen energy, **2010**, 35, 784–793
15. Li Q, He R, Jensen J, Bjerrum N. *PBI-based polymer membranes for high temperature fuel cells—preparation, characterization and fuel cell demonstration*. Fuel Cells, **2004**, 4,147–59
16. Mamlouk, M. *Investigation of High Temperature Polymer Electrolyte Membrane Fuel Cells*, PHD thesis, **2008**
17. Wu, X. *Development of High Temperature PEMFC and High Temperature PEMWE*. PHD thesis, **2011**
18. Okuhara T., *Water-tolerant solid acid catalysts*, Chemical Review, **2002**, 102, 3641–3666.
19. Pesaresi L., Brown, D. Lee A., Monter J., Williams H., Wilson K., *Cs-doped H₄SiW₁₂O₄₀ catalysts for biodiesel applications*, Applied Catalysis A: General, **2009**, 360, 50–58
20. Lobato J., Cañizares P., Rodrigo M. and Linares J., *PBI-based polymer electrolyte membranes fuel cells, Temperature effects on cell performance and catalyst stability*, Electrochimica Acta, **2007**, 52(12), 3910-3920
21. Smitha, B., Sridhar, S. Khan A., *Proton conducting composite membranes from polysulfone and heteropolyacid for fuel cell applications*, J. of Polymer Science: Part B: Polymer Physics, **2005**, 43, 1538–1547
22. Liu, Z.; Wainright, J.S.; Savinell, R.F. *High-temperature polymer electrolytes for PEM fuel cells: Study of the oxygen reduction reaction (ORR) at a Pt–polymer electrolyte interface*. Chem. Eng. Sci. **2004**, 59, 4833–4838

Chapter 6: Graphite Oxide/Polymer Composite Membrane

Graphite oxide (GO) and functionalised GO were considered as good fillers to improve the conductivity of the membranes. GO and FGO were prepared and characterised in this chapter. They were combined with polymer matrix as composite membranes at a temperature ranging from room temperature to 200°C at a low PA doping level. The conductivity and performance of the composite membranes were studied to investigate the inflection of the GO and FGO to the membrane in the PEMFC.

6.1 Introduction

Graphite oxide (GO) consists of carbon, oxygen and hydrogen in variable ratios, which is exfoliated into individual graphite oxide nanoplatelets in water because of the hydrophilic oxygen groups attached to the graphite sheets [1]. Graphite oxide (GO) not only has most of the properties of graphite, but also has improved characteristics, such as better dispersion capability because of the increased number of O and N atoms. GO typically preserves the layer structure of the parent graphite, but the layers are buckled and the interlayer spacing is much larger than that of graphite [2-4]. GO is an insulator but controlled oxidation provides tunability of the electronic and mechanical properties, and the proton conductivity of a composite membrane is attributed to the hydrogen bonds in GO. The presence of different acidic functional groups like carboxylic acid, and epoxy oxygen, makes graphite oxide sheets strongly hydrophilic, which could provide more facile hopping of protons and hold more water [3-8].

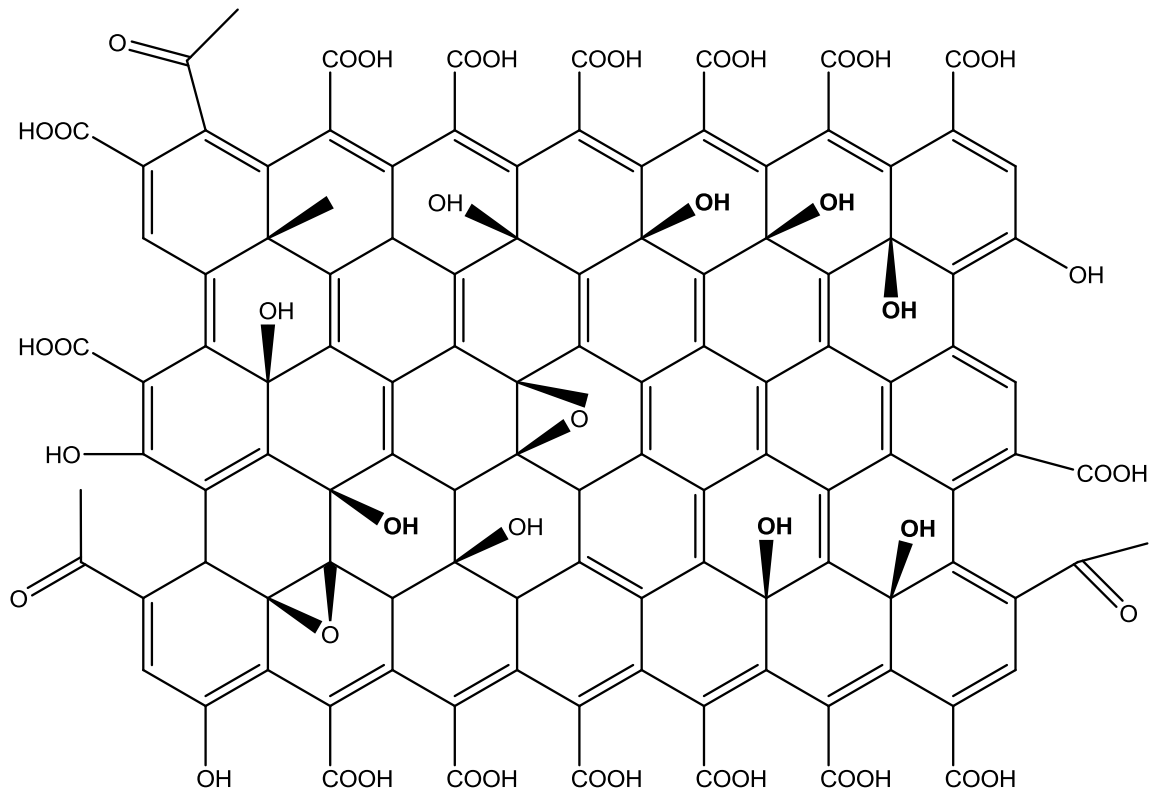


Figure 6-1 Schematic of Graphite Oxide (GO) structure

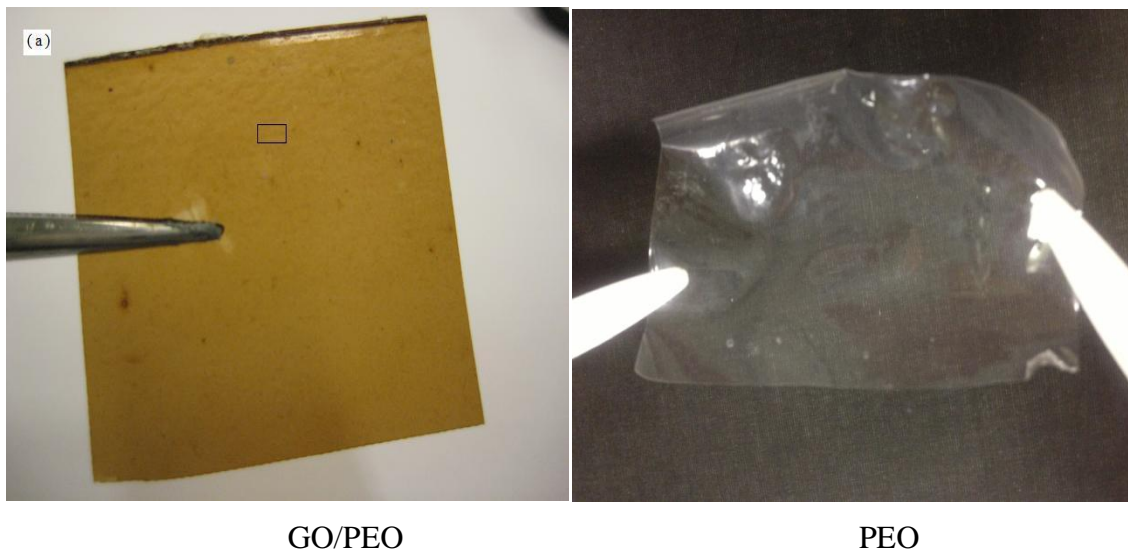
The typical model structure widely accepted for GO is shown in Fig. 6-1. Expandable graphites which are oxidised by sulphuric acid and potassium permanganate easily incorporate functional groups into its galleries, including carbonyl ($=\text{CO}$), hydroxyl ($-\text{OH}$), carboxyl ($-\text{COOH}$), phenol groups attached to both sides, and oxygen epoxide groups (bridging oxygen atoms) [2-4]. GO films are typically insulating, exhibiting sheet resistance (R_s) values of about $10^{12} \text{ V sq}^{-1}$ or higher, because of the absence of percolating pathways among sp^2 carbon clusters in GO which allow classical carrier transport [1]. However, GO when added to water, hydrolyzes to form thin platelets, which are negatively charged. The H^+ ions will be released from the carboxyl groups on the sheets of GO when humidified, and these groups make it suitable for various applications when improved conductivity is needed [1-3].

6.2 GO/PEO composite membrane

Graphite oxide (GO) was considered attractive for many applications owing to its unique thermal and mechanical properties. It was already reported that in combination with PFSA, the unique structure and high surface area of the GO could provide more proton transport channels and hold more water, which could be beneficial for the improvement of proton conductivity and the mechanical properties of the membranes. However, PFSA is costly, so graphite oxide had been investigated as inorganic fillers in a Poly-ethylene oxide composite membrane used for low temperature fuel cells.

6.2.1 Results and Discussion

The photo of the prepared PEO/GO membrane was shown in Fig. 6-2 (a). The pristine PEO membrane is transparent, but after mixed with GO, it changed to a yellow colour membrane as shown in Fig 6-2 (a). Poly (ethylene oxide) (PEO) was a widely used hydrophilic polymer with high tensile strength and flexibility. It also exhibited ion-transport behaviour when ionic salts were dissolved in it [9]. SEM images showed that the membrane was condensed composite materials without defects, such as air bubbles or pores (Figure 5-2 (b) and (c)). Such prepared membrane was around 80 μm in thickness and the GO in the PEO polymer matrix was the source of H^+ ions imparting ion conductivity.



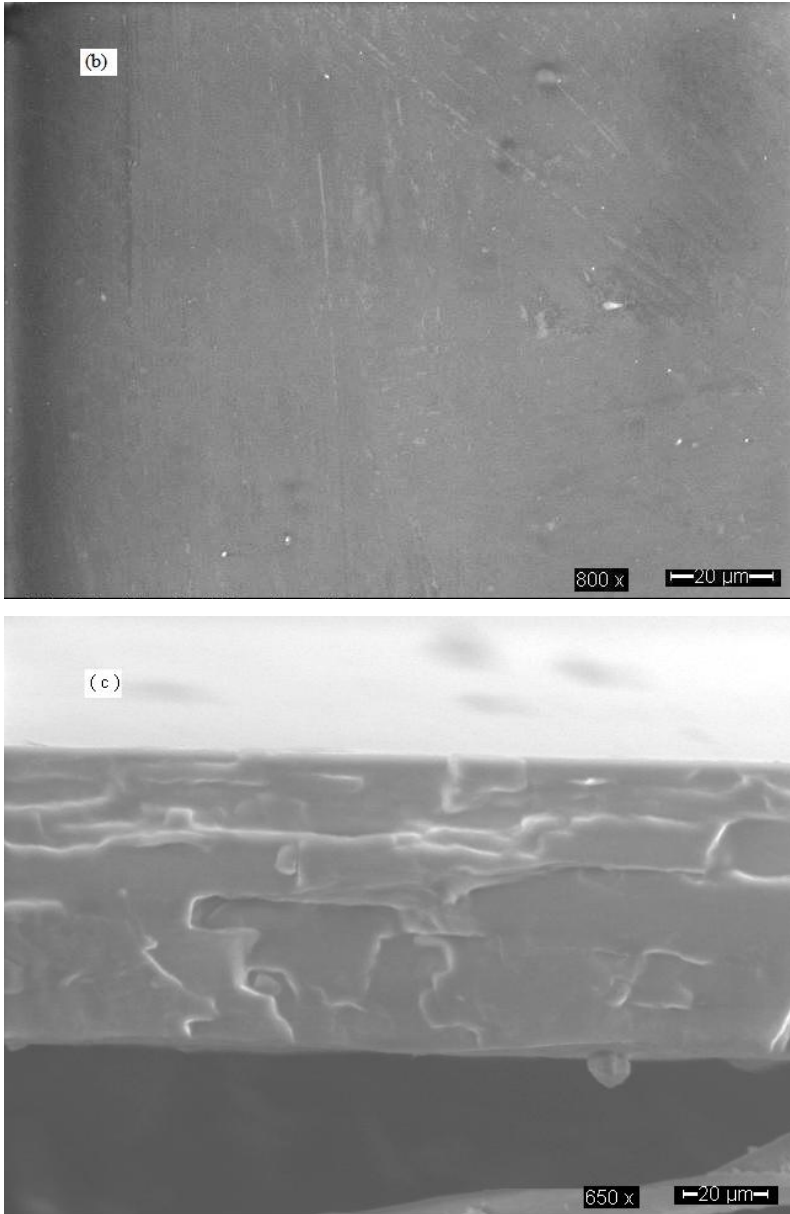
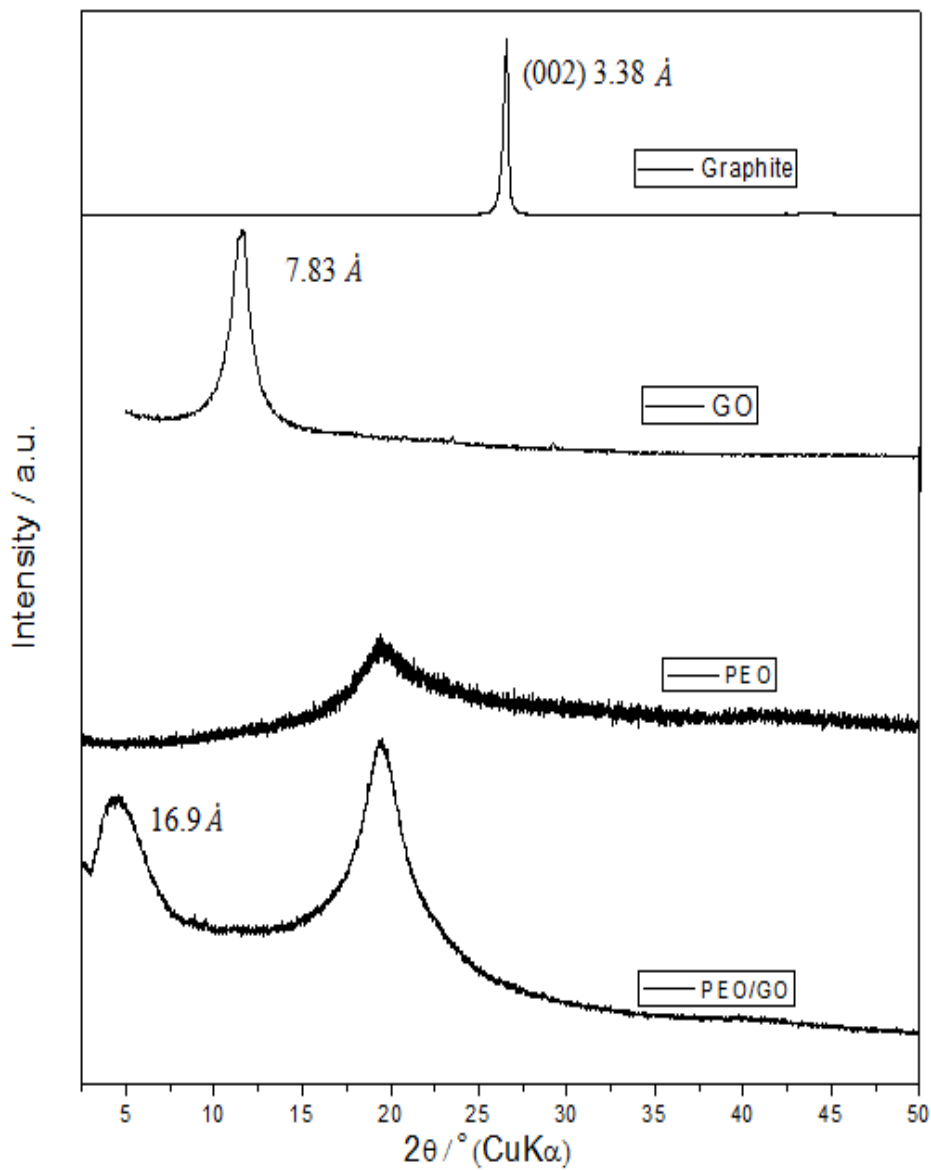


Figure 6-2 (a) the illustration of the PEO/GO and PEO membrane, SEM morphology of the PEO/GO membrane with 0.5 wt% GO (b) the surface (c) and cross-section

The membrane was tested by XRD. The GO layers in the PEO matrix and the data were shown in fig. 6-3. According to the reference standard graphite pattern from JCPDS data (ref. 00-041-1487), the peak indexed (002) at 26.38° , (100) at 42.2° , and (101) at 44.4° signify the crystalline structure of graphite showed in fig. 6-3. The graphite has a hexagonal structure, so the layer distance (d) could also be calculated from the equation of $\frac{1}{d^2} = \frac{4}{3} \left[\frac{h^2 + hk + k^2}{a^2} \right] + \frac{l^2}{c^2}$, for the sharpest peak (002), $h = 0, k = 0, l = 2, c = 6.7244$. The distinguishable (002) peak of graphite at 26.38° has an interplanar distance, $d_{(002)}$, of 3.38\AA .

This implies that graphite is a highly oriented carbon material. Meanwhile, the XRD pattern of GO shows an intense and sharp peak centered at 11.28° which corresponds to an interplanar distance of 7.83\AA . The increase of interplanar distance of the GO is due to the existence of oxygen functional groups. The GO is synthesized by chemical oxidation method, so it involves a number of chemical processes such as oxidation of carbon atoms at the periphery of the graphite matrix to form oxygen-containing groups including hydroxyl, carbonyl, or epoxy groups. So the acid-oxidized graphite shows a variable interplanar distance which depends on the synthesis method, air moisture, and other factors.



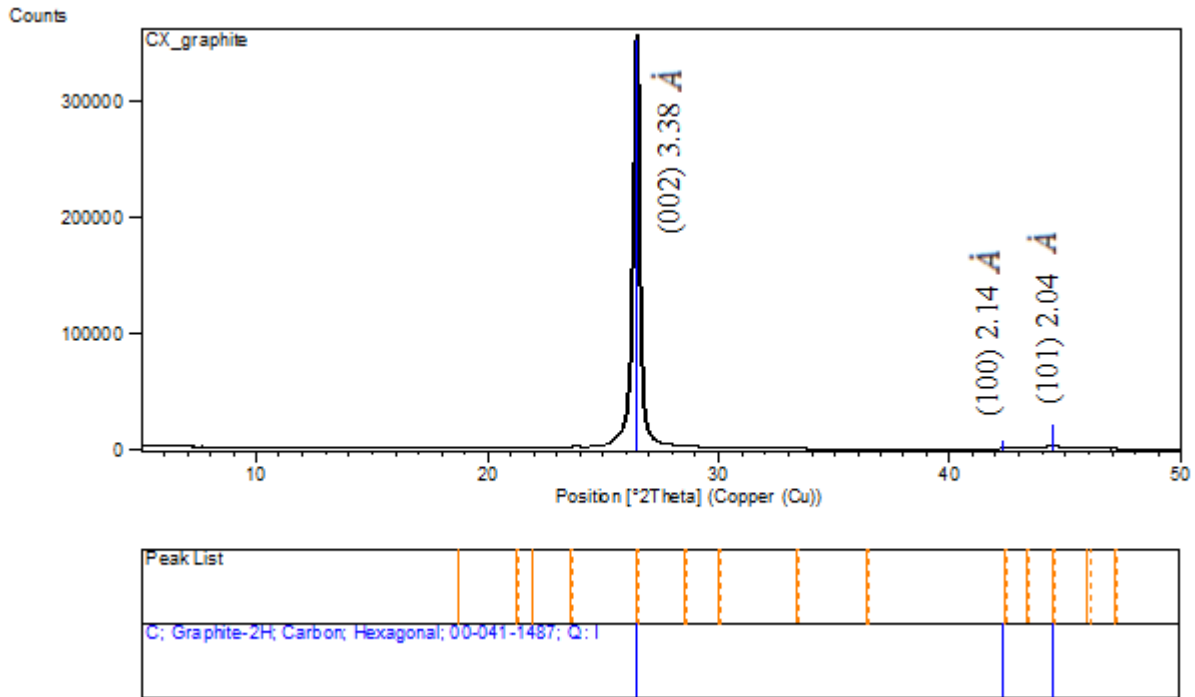


Figure 6-3, the explanation spectra of Graphite, Graphite Oxide, PEO, and PEO/GO membrane

Through comparing the XRD spectra of the PEO membrane and the PEO/GO membrane which were prepared under the same conditions, the reflection peak near $2\theta = 19.75^\circ$ contributed to the PEO matrix itself. The peak of PEO did not shift after mixing with GO, but a sharp peak appeared at $2\theta = 4.5^\circ$, this peak is caused by the GO. According to the Bragg's law: $d = \frac{n\lambda}{2 \sin \theta}$ when the θ shifted to the small value, the distance between the GO layer was expanded. The distance of the layer changed from 7.83\AA to the 16.9\AA indicated that the PEO molecules intercalated into the layers of the GO that the layer of GO was expanded. Also, this intercalation indicated that these two materials could mix during the membrane preparation process and they were highly compatible.

FTIR studies were undertaken to confirm the functional groups in the PEO/GO membrane and the results were shown in Figure 6-4. The FTIR spectrum of GO in fig. 6-4 showed CH_3^- (2926 cm^{-1}) and CH_2^- (2851). The C=O stretching vibrations in the carboxyl group as C=O is also visible around 1720 cm^{-1} . Oxygen functionalities in graphite oxide at 3300 cm^{-1} (O-H stretching vibrations), and evidence of the epoxide group can be seen at about 1032 cm^{-1} ,

representing C-O stretching vibrations, while no significant peak was found in graphite (Figure 6-4). Comparing the FTIR of PEO and GO/PEO, the peaks are in the similar position, because the identify peaks such as C=O and C-O are both existed in PEO and GO. However, after mixing of GO and PEO, the PEO should insert into the GO layer that leading the layer distance increased which was evidenced in Fig 6-3. These confirmed that graphite powder was oxidised successfully. The FTIR spectrum of the PEO/GO membrane included all the GO vibrations which indicated the presence of proton releasing groups in the membrane. These results depicted OH and other functionalities, such as COOH groups, in the resultant PEO/GO membrane.

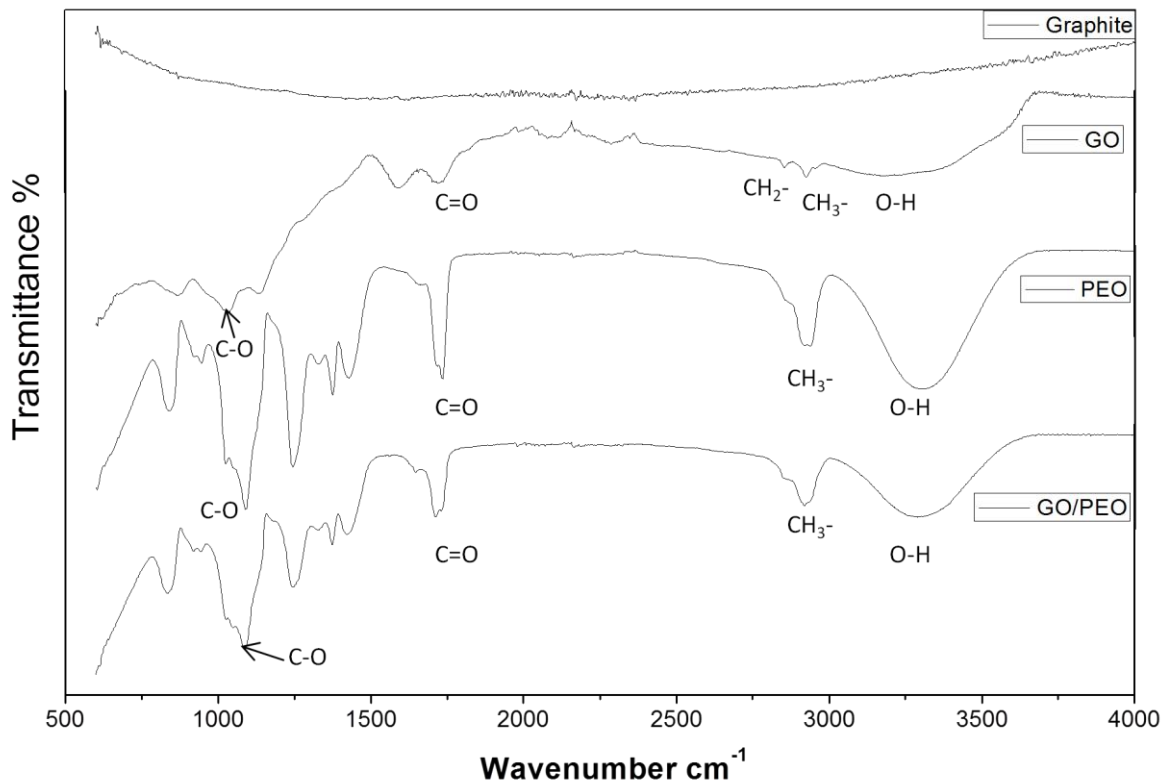


Figure 6-4 FTIR spectrum of Graphite (a), Graphite Oxide (b) and PEO/GO membrane (c)

The conductivity of the PEO/GO composite membrane increased from 0.086 S cm^{-1} to 0.134 S cm^{-1} from $25 \text{ }^\circ\text{C}$ to $60 \text{ }^\circ\text{C}$, at a relative humidity of 100% as shown in Figure 5-5. The ionic conductivity continued to increase at temperatures above $60 \text{ }^\circ\text{C}$, but the membrane became soft during the test, which is a limitation of the PEO polymer. Therefore, the optimum operating temperature would be around $60 \text{ }^\circ\text{C}$ with the current membrane for applications in a PEMFC. A higher temperature resulted in higher conductivity and reduced membrane tensile

strength and mechanical property because of the low glass transition temperature of the PEO. The pristine PEO membrane did not show ionic conductivity under the same conditions. So the conductivity of the GO/PEO composite membrane comes from GO that provided the ionic conduction path which was dependent on the H^+ released from the COOH, OH groups and which helped the absorption and retention of more water. These results indicated that GO and temperature played an important role in conductivity.

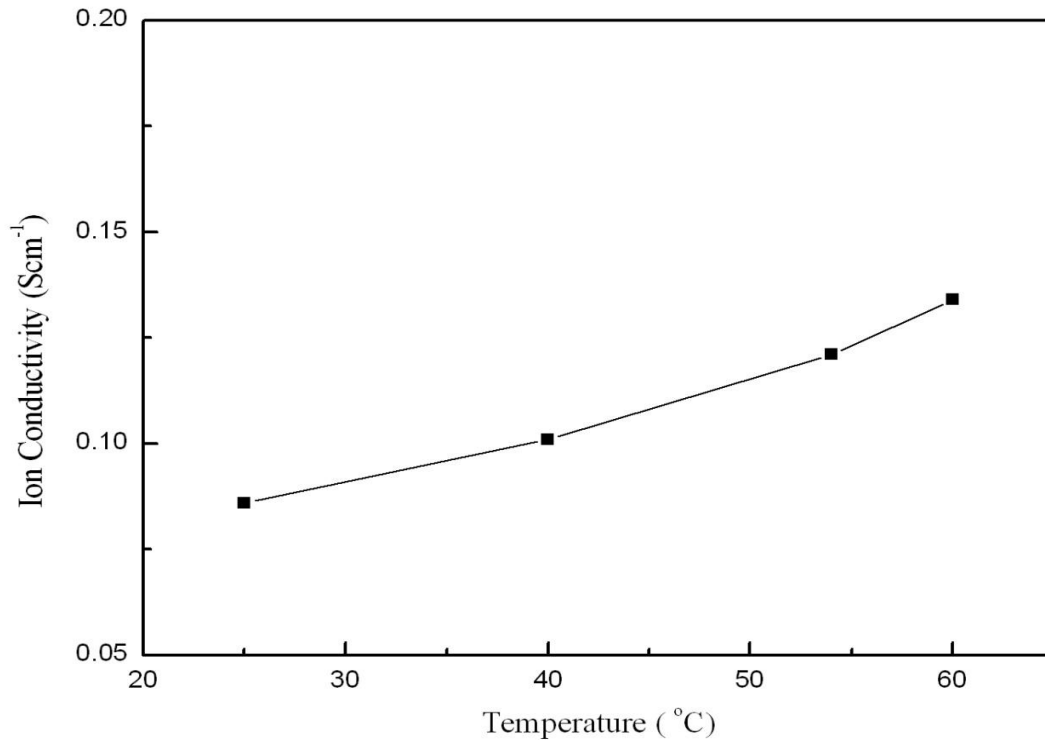


Figure 6-5 Conductivity of the PEO/GO membrane at a relative humidity of 100% from 25 °C to 60 °C

Furthermore, the DC electrical resistance of this PEO/GO membrane was greater than 20 M Ω at a room temperature 100% RH. The high resistance (low conductivity) also supported the formation of GO which had a reported electrical conductivity lower than $1 \times 10^{-9} \text{ S cm}^{-1}$ (10^7 fold lower when compared to graphite [1, 4]).

The polarisation and power density data obtained at different operating temperatures of GO/PEO membranes were shown in Figure 6-6. The open circuit potentials (OCV) for the fuel cell were relatively high, around 950 mV, at temperatures of 16 °C and 30 °C. The peak power densities were only 15 mW cm⁻² and 20 mW cm⁻² at 16 °C and 30 °C, respectively.

When the operation temperature was increased to 60 °C with RH 100%, the power density increased to 53 mWcm⁻² (Fig.5, c), nearly 2.5 times than that achieved at 30 °C which contributed to the higher temperature increasing the conductivity of the membrane. However, the OCV fell significantly to 760 mV from 950 mV, which was indicative of greater gas crossover, presumably associated with the softening of the membrane. Without optimizing the composition of catalyst layers, these power density results were attributed to high catalyst/membrane interfacial resistance. However, such performance still confirmed the feasibility of applying the PEO/GO composite membranes in fuel cells.

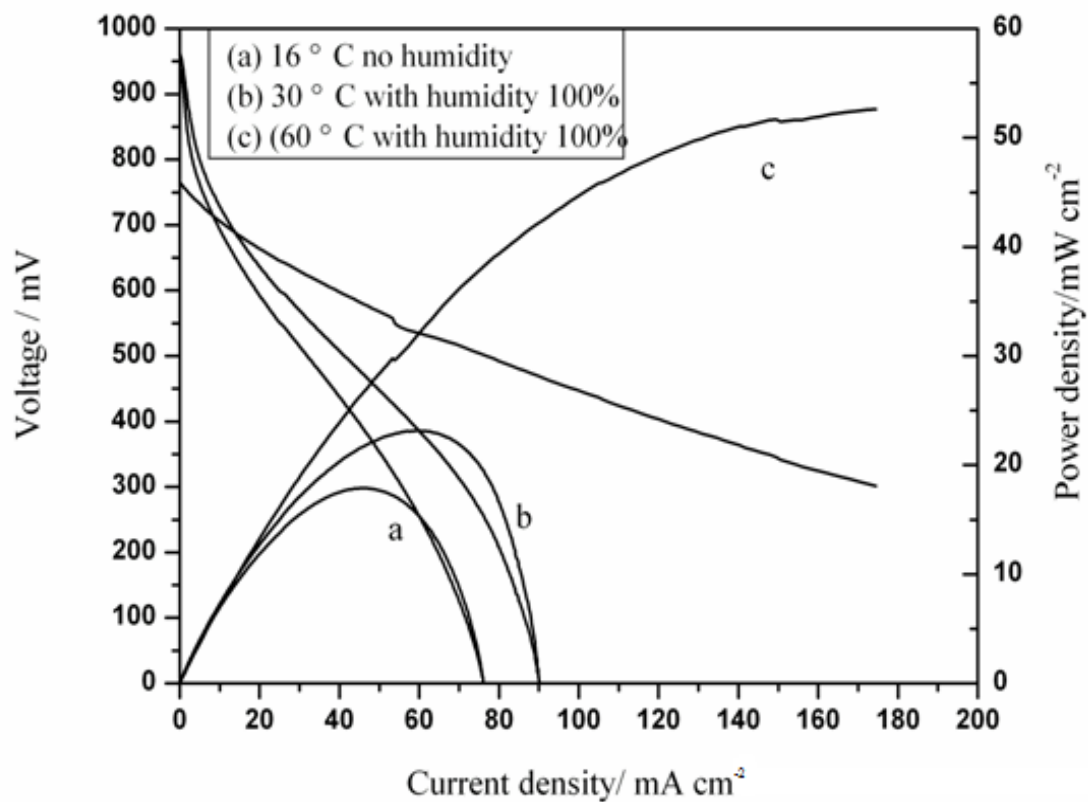


Figure 6-6 Polarisation and power density curves of the PEO/GO membrane in the fuel cell test. The Pt loading was 0.7 mg cm⁻² and H₂ and O₂ was used in the test without back pressure at 16 °C, 30°C, and 60°C.

6.2.2. Conclusions

PEO and GO were both hydrophilic and are highly compatible to form ionic conducting composite membranes for fuel cell applications. Proton exchange membranes could be prepared without polymer modifications. The key to this membrane's ion conductivity was the proton released from the COOH groups on the GO sheets in the PEO polymer matrix. Humidity was necessary for ionic transport in the membrane as water absorbed into the polymer acts as the medium for releasing protons. Ionic conductivity was also dependent on the temperature, which when increased may improve the release of protons from the COOH groups. However the higher temperatures, above 60 °C, caused deterioration in the membrane's mechanical property. The PEO/GO composite membrane had a proton conductivity of 0.09 S cm^{-1} at 60 °C, and gave a power density of 53 mW cm^{-2} in hydrogen PEMFC.

6.3 GO/PBI and functionalised GO/PBI composite membranes

The sulphonic acid moieties formed hydrophilic domains with a size of around 40 Å when in contact with water. The attempt to improve water retention ability of sulfonic acid groups would improve the conductivity. Recently, adding sulphonic acid groups to the GO composite as electrolyte has attracted attention. Kannan et al. reported the sulfonic acid-functionalised MWCNTs with Nafion[®] to enhance the performance of PEMFC [6], the GO and functional GO were evidenced to improve the conductivity and retain water. Also, in comparison to the carbon nanotube, GO was much cheaper and easier to get. So GO and functional GO were considered as candidates to be used in polymer membranes in order to improve conductivity and fuel cell performance. Ionic liquids (ILs) had good solubility in water and solvent and introduce a surface charge, so GO modification with ILs should create more stability and good dispersion in various matrices. Also Ionic liquid provided more proton transfer channels which would be beneficial to conductivity. The functional GO sheets were functionalised with 1-(3-aminopropyl) - 3-methylimidazolium bromide (IL-NH₂) combination with PBI membranes.

6.3.1. Results and discussion

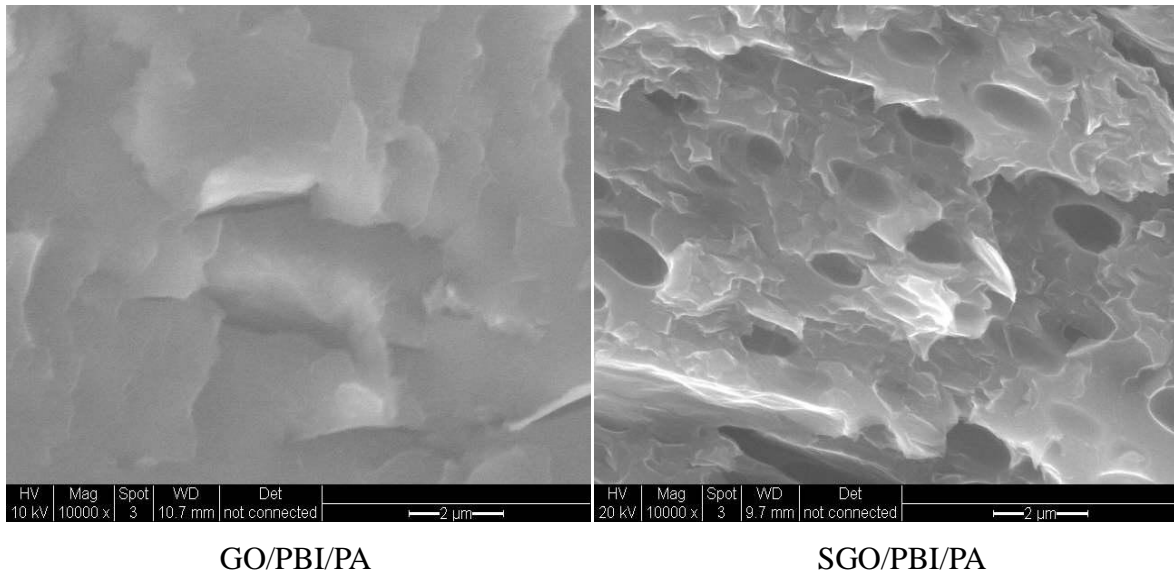
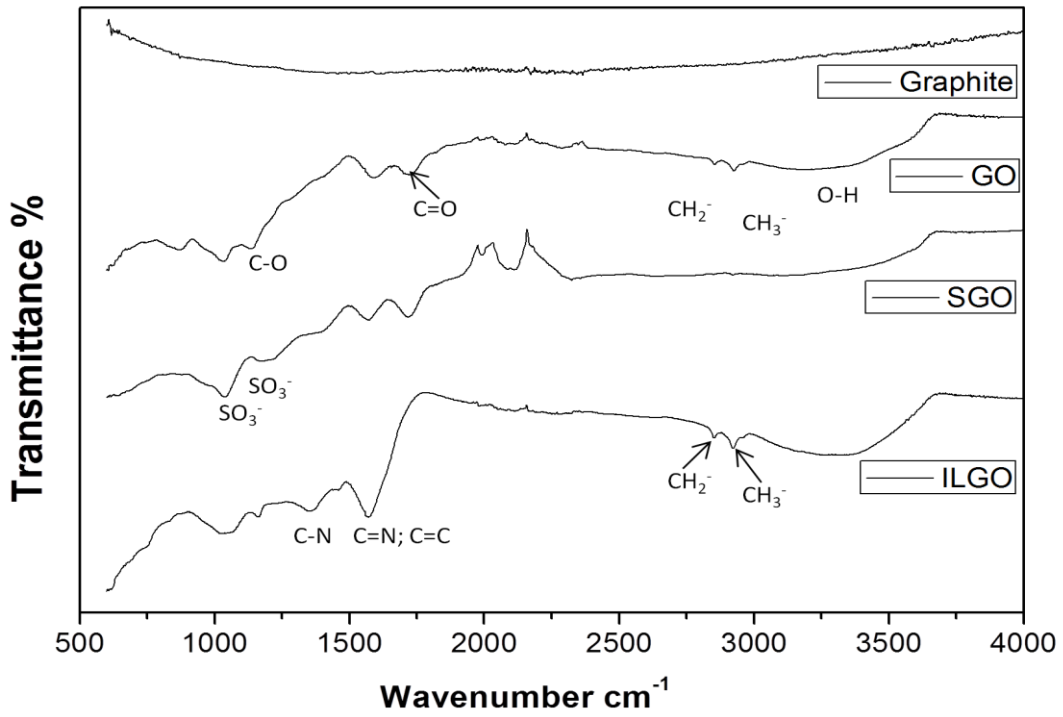
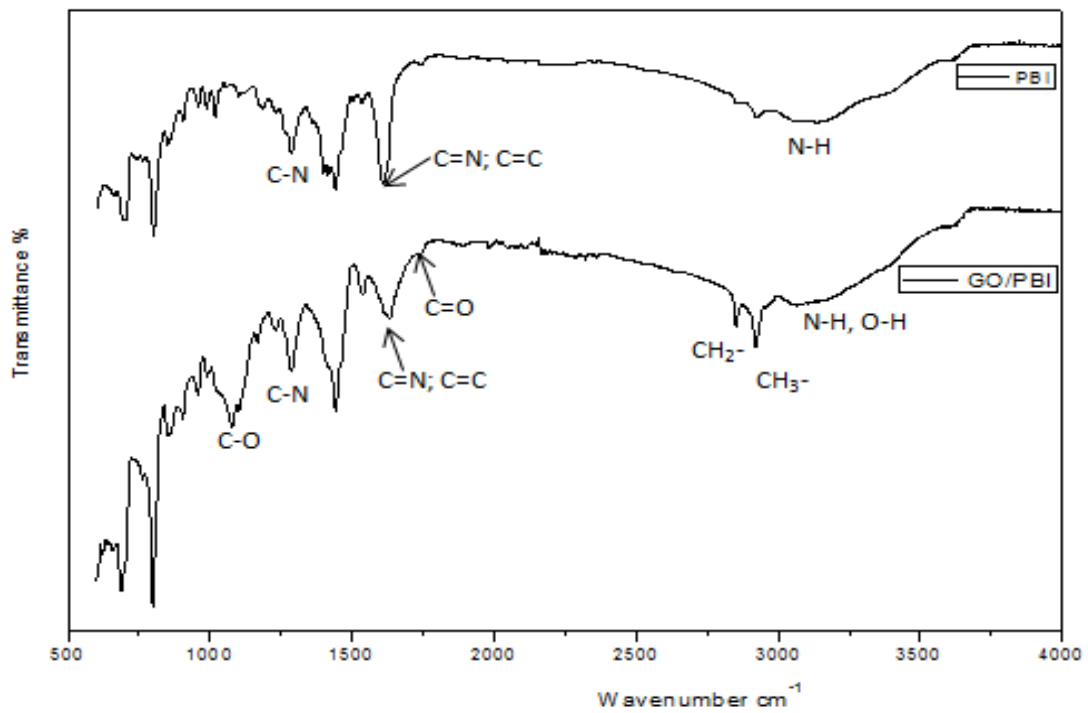


Figure 6-7 SEM images of GO/PBI/PA and SGO/PBI/PA

SEM observation was carried out after the membrane cast. Figure 6-7 shows SEM images of the cross-section of the GO/PBI and SGO/PBI composite membranes. The sheets in the membranes were dispersed through the cross section of the membrane. The GO, SGO and sheets should remain exfoliated in the polymer matrix and were tightly held in the PBI matrix according to the strong interfacial interactions. Therefore, the conduction paths were established through the PBI matrix over the whole membrane and these conduction paths provided a possible interpretation for the high conductivity of the composite membrane. Additionally, the membrane with SGO exhibited a more uniform morphology than the one with GO.



a)



b)

Figure 6-8 (a) Infrared spectra of Graphite, GO, SGO, and ILGO (b) Infrared spectra of PBI and GO/PBI

FTIR studies confirmed the successful oxidation of graphite to graphite oxide, as shown in Figure 6-8. The FTIR spectrum of GO and SGO in Figure 6-8 (a) showed the presence of different types of oxygen functionalities in graphite oxide at 3300 cm^{-1} (O-H stretching vibrations), at 1720 cm^{-1} (stretching vibrations from C=O), the two peaks at 2854 cm^{-1} and 2922 cm^{-1} correspond to symmetric Vs (CH₂) and asymmetric Vas(CH₂) while no significant peak was found in graphite (Figure 6-8). These results depict OH and other functionalities, such as COOH groups, in the resultant GO, which also confirmed the successful oxidation of graphite. Broadening occurred in -SO₃- symmetric stretching vibrations bands at 1040 cm^{-1} and asymmetric stretching of -SO₃- groups at 1174 cm^{-1} shown in SGO [7, 12].

The characteristic band of the carboxylic group in ILGO appeared at 1725 cm^{-1} (C=O stretching), the C-O vibrations of epoxy groups in GO appeared at 1153 cm^{-1} , and the CH₃(N) stretching, CH₂(N) stretching, and ring in-plane asymmetric stretching arising from the imidazolium ring at 1571 cm^{-1} and 1348 cm^{-1} , which confirmed the successful attachment of amine-terminated IL-NH₂ to GO nanosheets [12]. It indicated that IL was successfully grafted onto the GO.

As shown in fig 6-8 (b), comparing the PBI and GO/PBI composite, the stretching vibrations of C=O at 1720, C-O at 1077, CH₃- at 2921 and CH₂- at 2851 was appeared that corresponding to the GO structure, indicating the GO was mixed with PBI membrane to form the composite material.

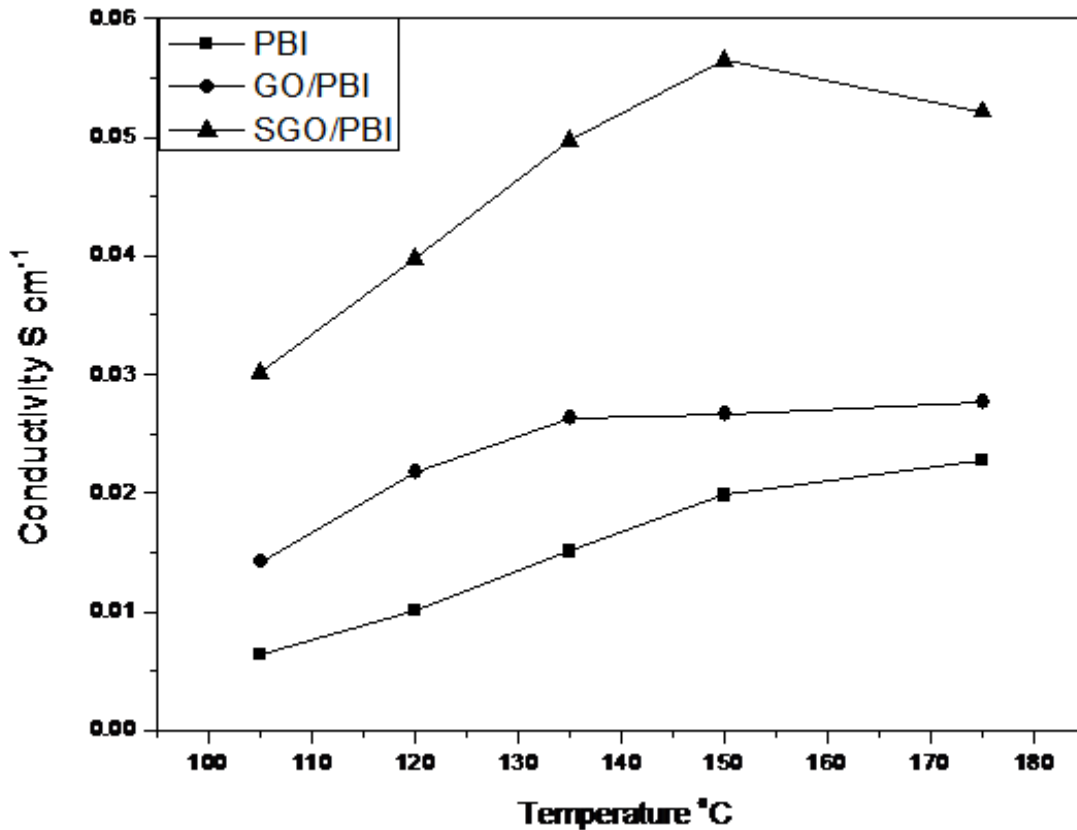


Figure 6-9 Conductivities of composite membranes loaded with H_3PO_4 PRU of 1.9 under anhydrous conditions

Figure 6-9 showed the conductivity data of the PBI, GO/PBI, and SGO/PBI membranes loaded with phosphoric acid (2 mol dm^{-3}) to achieve a PRU of 1.9 under anhydrous conditions. The conductivity of the PBI membrane was 0.023 S cm^{-1} at $175 \text{ }^\circ\text{C}$. The amount of “bonded acid” corresponded to two molecules of PA per repeat unit of PBI with two nitrogen sites for hydrogen bonding in a PBI monomer unit [13]. So the PA in membranes was mainly bonded acid that should remain inside the membranes and should not be easily removed during fuel cell operation.

The GO based membrane had greater conductivities than the pristine PBI membrane, and SGO gave even higher conductivities. For example, at 175°C , conductivity of PBI, GO/PBI, and SGO/PBI was 0.023 S cm^{-1} , 0.027 S cm^{-1} , and 0.052 S cm^{-1} as shown in Table 5-1. The improvement could be attributed to the combinations of the highly conductive GO and SGO in the PBI matrix. The conductivity of all membranes increased with temperature up to values of around $150 \text{ }^\circ\text{C}$. Overall the GO and SGO sheets improved the conductivity of PBI

composite membranes, with the latter giving values above 0.05 S cm^{-1} . The observed enhancement in conductivity could be explained by the increased SO_3H^- group content of the membrane due to the addition of SGO, which could possibly increase the number of channels available for proton transport by interconnecting some of the hydrophilic domains [6]. The GO and SGO enhanced the conductivities of the PBI with bonded acid which indicated that they were suitable candidates for fuel cells.

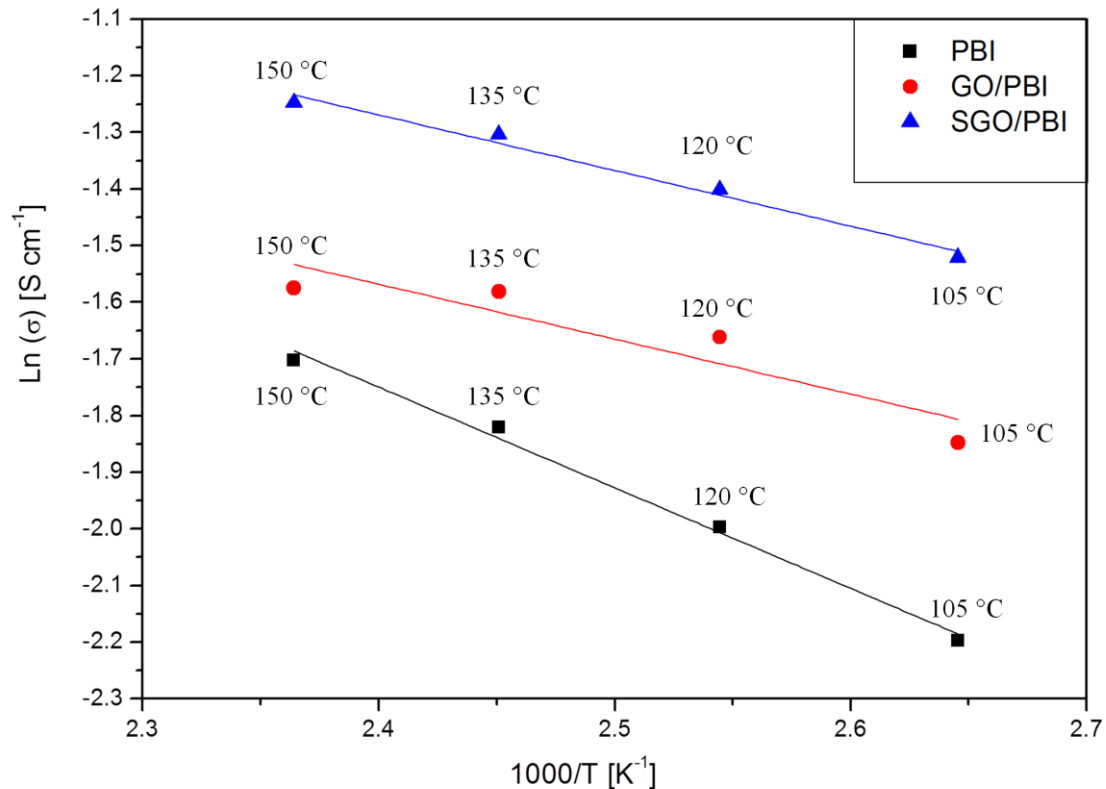


Figure 6-10 Arrhenius plots of PBI, 2 wt. % GO/PBI and 2 wt. % SGO/PBI composite membrane loaded with H_3PO_4 with acid loading of 1.9 PRU under anhydrous conditions

For a hopping-like conduction mechanism, the conductivity follows the Arrhenius law [13]:

$$\sigma = \sigma_0 \exp\left(\frac{-E_a}{RT}\right) = \frac{A}{T} \exp\left(\frac{-E_a}{RT}\right) \quad (6.1)$$

Where σ_0 and A are pre-exponential factors and E_a is the activation energy. The Arrhenius plots for acid loaded PBI and its composite membranes are illustrated in Figure 6-10.

Table 6-1 Activation energy and conductivity of the membrane at 175 °C

Membrane sample	Conductivity ($S\ cm^{-1}$)	Ea ($kJ\ mol^{-1}$)
PBI/PA	0.023	16.1
GO/PBI/PA	0.027	11.4
SGO/PBI/PA	0.052	9.3

Figure 6-10 showed the Arrhenius plots of the conductivity of the membranes, Ion transport activation energies (E_a) of membranes obtained by the Arrhenius equation are presented in Table 6-1. The Arrhenius behavior indicated the charge carriers are decoupled from the segmental movement of polymer chains [13, 14]. The activation energy is the barrier of the membrane that the proton conducting [13, 14]. The activation energy of the PBI/PA membrane was $16.1\ kJ\ mol^{-1}$, which was higher than that of GO and SGO loaded membranes. The lower activation energy requirement of the composite membrane indicated the proton conducting was easier to start, therefore the conductivity of composite membranes are higher than that of PBI membrane which was confirmed by the conductivity results.

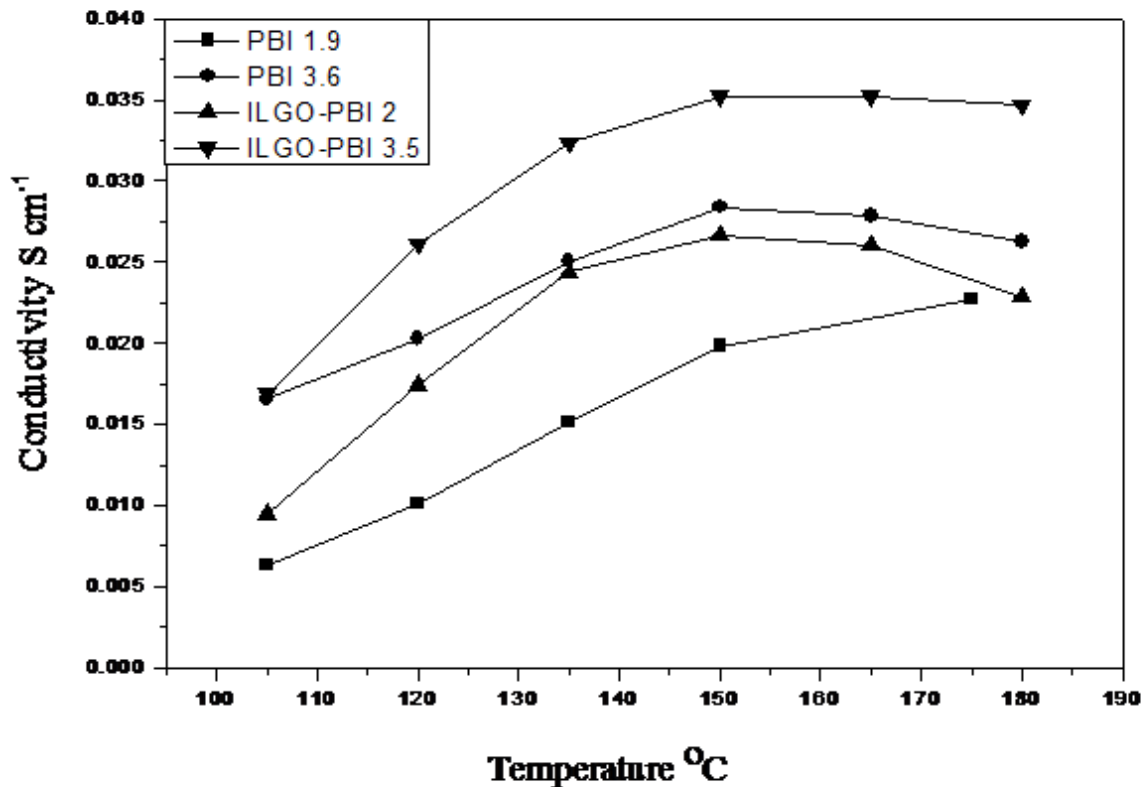
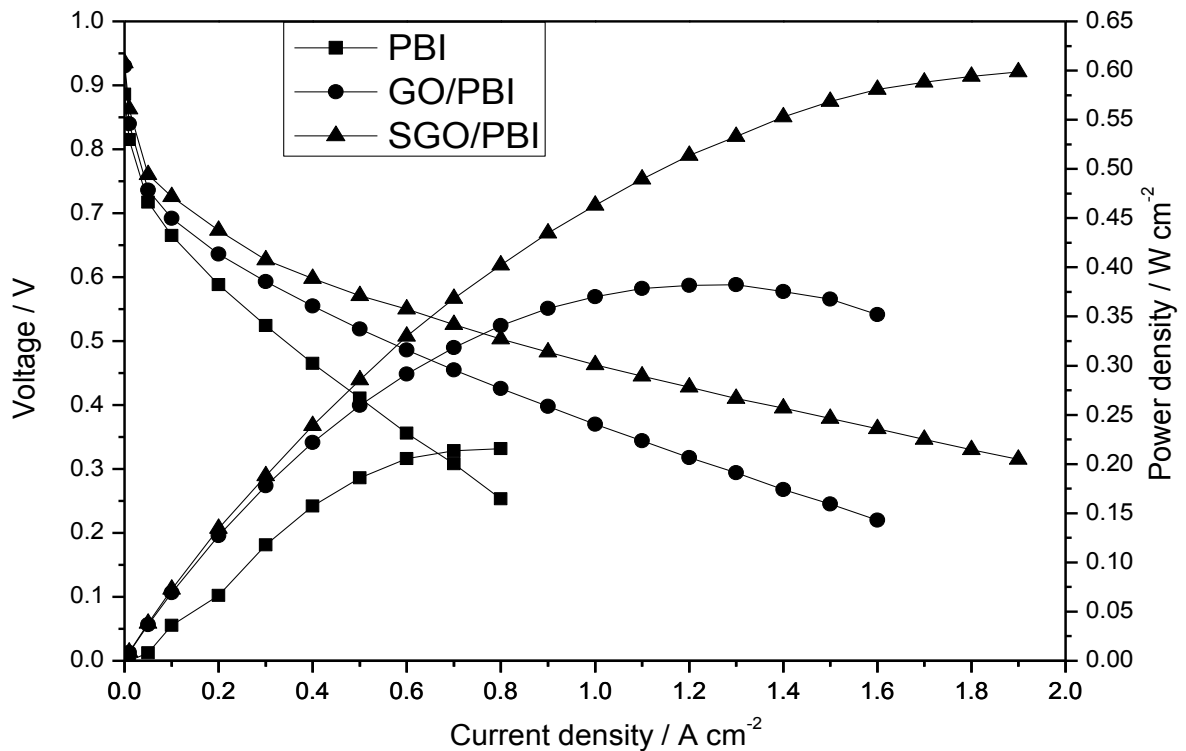
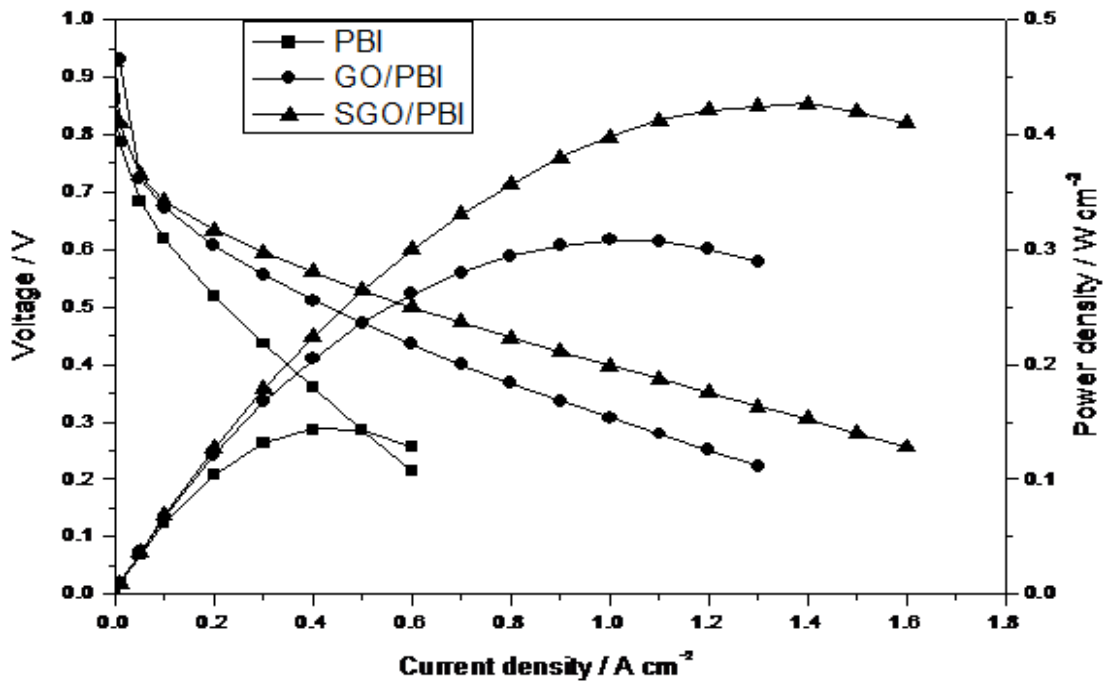


Figure 6-11 Conductivities of PBI and ILGO/PBI composite membranes loaded with similar PRU of 1.9 and 3.6 under anhydrous conditions

ILGO also showed a better conduction behaviour when it was added into the PBI membrane. The higher doping level of H_3PO_4 provided higher conductivity. The ILGO/PBI of 2 PRU showed a similar conductivity performance with the PBI membrane of PRU 3.6. The GO or functional GO as a filler used in the polymer matrix was an ideal way to reduce the doping level of the membrane. The ionic liquid group could form the bond with H_2PO_4^- which provides some defects for the proton transfer, so it is benefit to the proton conductivity that the ILGO/PBI shows better conductivity than pristine PBI. However, the proton conductivity of ILGO/PBI is less than the GO/PBI. This might come from the H^+ in GO, which can form hydrogen bonding with PA, be hindered by the large IL clusters. This is the main method for proton transport, so the proton conductivity was reduced. Otherwise, the GO was partly reduced to graphite which is not electric isolation when synthesized with IL. Therefore a short cut may form in the membrane that decreased the proton conductivity.



(a)



(b)

Figure 6-12 Polarisation and power density curves of a fuel cell operated at 175 °C with (a) H₂/O₂ atmospheric pressure and (b) H₂/Air atmospheric pressure. Pt loading: cathode 0.9 mg cm⁻²; anode 0.5 mg cm⁻²; anhydrous condition, H₃PO₄ PRU: 1.9, membrane thickness=70 μm

Fuel cell performance tests were carried out with H₂/O₂ and H₂/Air atmospheric pressure. The polarisation and power density curves of the H₂/O₂ and H₂/air fuel cells obtained at 175 °C under anhydrous conditions for PBI, GO/PBI and SGO/PBI membranes were shown in Fig. 6-12. The PBI based fuel cells exhibited significant activation polarisation, with overpotential of some 0.25 V at 0.1 A cm⁻², and the GO/PBI and SGO/PBI based fuel cells exhibited similar overpotentials of around 0.2 V at 0.1 A cm⁻². The performance of the cells with the GO/PBI and SGO/PBI composite membranes was significantly better than that with the PBI membrane. The peak power densities of PBI, GO/PBI, and SGO/PBI with oxygen were 0.22, 0.38 and 0.6 W cm⁻², respectively. The better performance was mainly attributed to the superior proton conductivity of the latter and also the strong acid and water retention properties of the composite membrane at low acid loading. Hydrogen bonds in GO which form acidic functional groups like carboxylic acid, and epoxy oxygen, could provide more facile hopping of protons to enhance the conductivity, and SO₃H⁻ group in SGO also benefit

the conductivity.

With atmospheric air, the OCVs of the membrane were above 0.9 V. The peak power density with the PBI membrane of 0.144 W cm^{-2} was much lower than obtained with higher PA acid loading (11 M) PBI membrane (0.34 W cm^{-2}) tested in the previous work [15]. The cell voltages produced with the GO/PBI composite membranes were greater than those with the PBI membrane at high-current densities. The SGO/PBI gave a peak power density of 0.43 W cm^{-2} . However, the GO/PBI and SGO/PBI with low PA loading levels gave a good performance which was even higher than that of greater (11.0 M) PA loaded PBI membrane, and indicated that the GO/PBI and SGO/PBI composite membranes were suitable for use with H_2 /Air fuel cells.

The results also confirmed that the Ohmic resistances of GO/PBI and SGO/PBI were less than that of the pristine PBI membrane. The voltage loss of the SGO/PBI membrane based fuel cell was 0.22 V from 0.6 to 1.6 A cm^{-2} . This was equivalent to a conductivity of 0.031 S cm^{-1} , which was in reasonable agreement with that of the membrane itself. In the case of the PBI membrane the voltage loss in the Ohmic region gave a conductivity of some 0.013 S cm^{-1} , in reasonable agreement with the measured membrane conductivity which was shown in Figure 6-9.

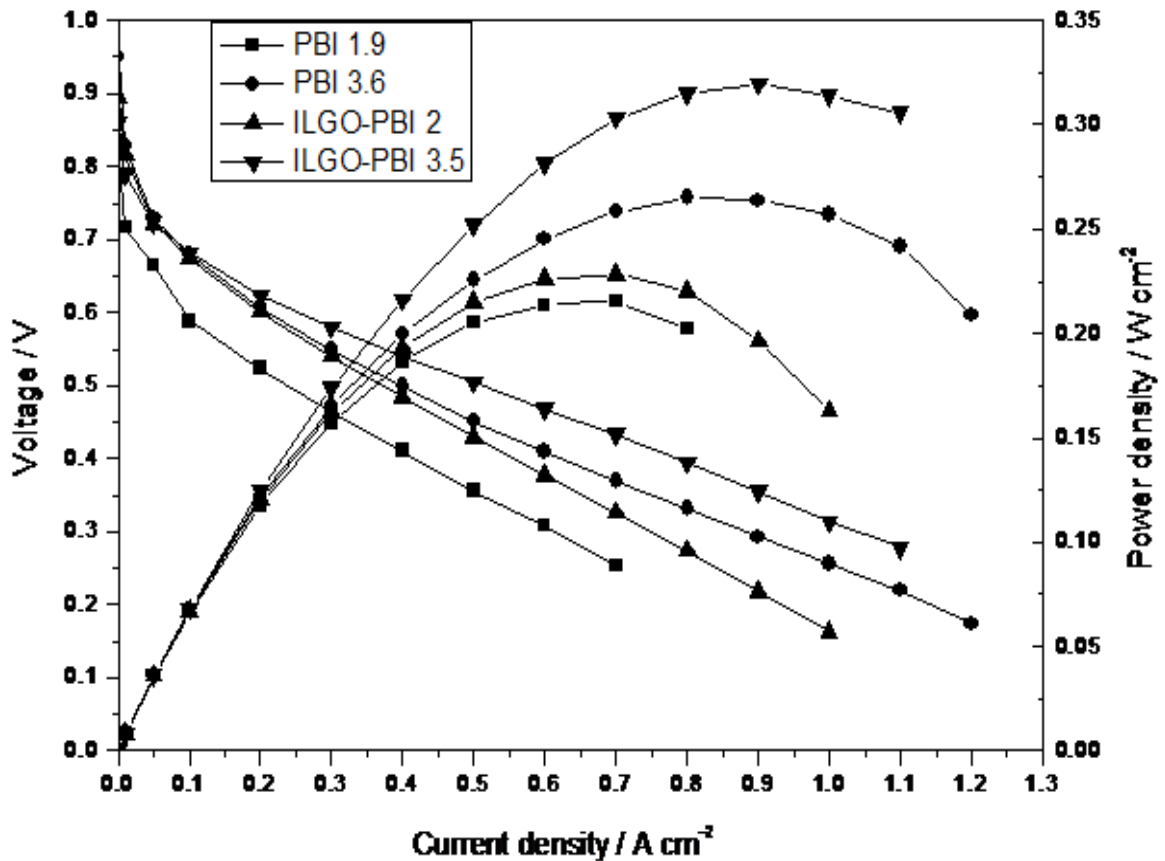


Figure 6-13 Polarisation and power density curves of a fuel cell operated at 175 °C with (a) H₂/O₂ atmospheric pressure. Pt loading: cathode 0.9 mg cm⁻²; anode 0.5 mg cm⁻²; anhydrous conditions, H₃PO₄ PRU: 1.9 and 3.5.

The fuel cell performance of ILGO/PBI composite membranes at different doping levels were both better than that with the PBI membrane. The membrane of higher doping level gave the better performance indicating that the H₃PO₄ was the main role for the conductivity. The better performance was mainly attributed to the superior proton conductivity of the ILGO and also the strong acid and water retention properties of the composite membrane. However, the performance of ILGO/PBI was worse than that of GO/PBI at low acid doping. This might be attributed to hydrogen bonds in GO which form acidic functional groups and could provide more facile hopping of protons to enhance the conductivity rather than ILGO. The H⁺ could release from carboxyl group in GO, so the GO could be both acceptor and donor for the proton, and the aminopropyl-methylimidazolium bonded with H₂PO₄⁻ formed a large group may cover the surface of GO which hinder the hydrogen bonding formation between carboxyl group and PA. This is one of the possible reasons that the ILGO/PBI had a lower conductivity than GO/PBI under the same condition. The other reason may be the GO partly

reduced to graphite which is electronic conductivity when synthesized with IL, and this ILGO had both proton and electron conductivity which had opposite affection for fuel cell performance.

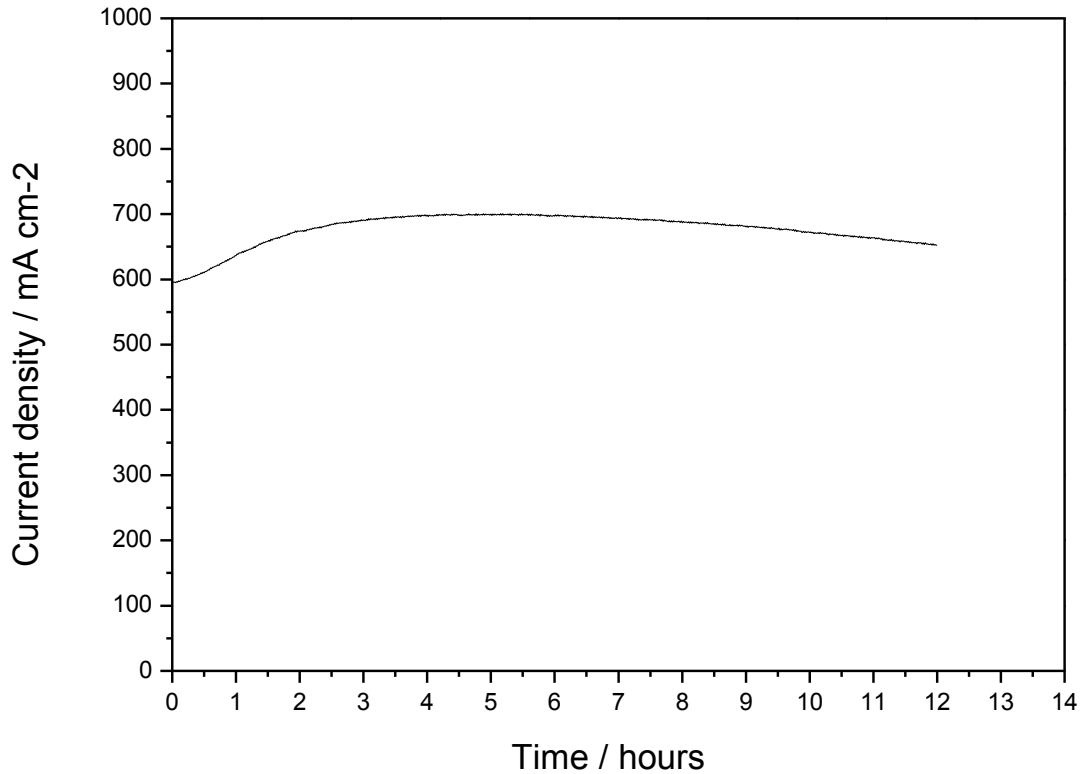


Fig. 6-14 Voltage response of a 12 h fuel cell life test under a constant voltage of -500 mV vs OCV at 150 °C with H₂/O₂ conditions

In order to initially assess the stability of the fuel cell, the durability of the resultant membrane was measured with Chronoamperometry for 12 h at 150 °C with H₂/O₂ at atmospheric conditions. Data presented in Fig. 6-14 showed that the performance of the fuel cell with the GO/PBI/H₃PO₄ composite membrane was stable in the tested range up to 12 hours. This result indicated that the GO was stable in fuel cell work conditions and the membrane was potentially stable during high temperature PEMFC applications although the long-term stability of the composite membrane still needed to be further investigated.

Overall, the new GO/PBI related composite membrane was a promising material for the PEMFC. There were some aspects which need further study to improve fuel cell performance. For example, from current densities 0 to 0.1 A cm⁻², there was an approximate 250 mV

voltage loss, indicating that the catalyst compositions in the MEA were not “optimal” for the fuel cell.

6.3.2 Conclusions

Inorganic-organic composite electrolytes, made from GO or SGO in PBI had been prepared for use in the PEMFC. The composite membranes, loaded with a low content of H_3PO_4 had higher conductivities than that of the phosphoric acid loaded PBI membrane. The GO/PBI, SGO/PBI, and ILGO/PBI composite membranes had proton conductivities of 0.027 S cm^{-1} , 0.052 S cm^{-1} , 0.025 S cm^{-1} at $175 \text{ }^\circ\text{C}$, respectively. In fuel cell tests the GO/PBI and SGO/PBI composite membranes gave a superior performance to that of a PBI/PA membrane with high loadings of PA. The peak power densities of GO/PBI, SGO/PBI were 380 mW cm^{-2} , 600 mW cm^{-2} and 320 mW cm^{-2} under H_2/O_2 conditions. The data indicated that the PBI composites with SGO, loaded with phosphoric acid may be potential membranes for high temperature PEMFC because of their high conductivity and fuel cell performance.

References

1. G. Eda, and M. Chhowalla, *Chemically derived graphene oxide: Towards large-area thin-film electronics and optoelectronics*, Adv. Mater., **2010**, 22 (22), 2392-2415.
2. I. Jung, D. Dikin, S. Park, W. Cai, S.L. Mielke, R.S. Ruoff, *Effect of water vapor on electrical properties of individual reduced graphene oxide sheets*, J. Phys. Chem. C, 2008, 112 (51), 20264-20268.
3. D. Cai, M. Song, and C. Xu, *Highly conductive carbon-nanotube/graphite-oxide hybrid films*, Adv. Mater., **2008**, 20 (9), 1706-1709.
4. Chen, D., L. Tang, and J. Li, *Graphene-based materials in electrochemistry*. Chemical Society Reviews, Chem. Soc. Reviews, **2010**, 39 (8), 3157-3180.
5. Bong Gill Choi, Jinkee Hong, Young Chul Park, Doo Hwan Jung, Won Hi Hong, Paula T. Hammond, and HoSeok Park, *Innovative Polymer Nanocomposite Electrolytes: Nanoscale Manipulation of Ion Channels by Functionalized Graphenes*, ACS Nano, **2011**, 5 (6), 5167-5174
6. R. Kannan, M. Parthasarathy, S.U. Maraveedu, S. Kurungot, V.K. Pillai, *Domain size manipulation of perfluorinated polymer electrolytes by sulfonic acid-functionalized MWCNTs to enhance fuel cell performance*, Langmuir, **2009**, 25 (14), 8299-8305.
7. Zarrin, H., Higgins, D., Jun, Y., Chen, Z., Fowler, M., *Functionalized graphene oxide nanocomposite membrane for low humidity and high temperature proton exchange membrane fuel cells*, Journal of Physical Chemistry C, **2011**, 115 (42), 20774-20781
8. W.S. Hummers Jr, and R.E. Offeman, *Preparation of graphitic oxide*, Chem. Soc., **1958**, 80 (6), 1339.
9. C. H. Manoratne, R. M. G. Rajapakse, M. A. K. L. Dissanayake, *Ionic Conductivity of Poly(ethylene oxide) (PEO)-Montmorillonite (MMT) Nanocomposites Prepared by Intercalation from Aqueous Medium*, Int. J. Electrochem. Sci., **2006**, 1, 32-46
10. R. Bissessur, P. K.Y. Liu, S. F. Scully, *Intercalation of polypyrrole into graphite oxide*, Synthetic Metals, **2006**, 156, 1023-1027.
11. H. K. Jeong, M. H. Jin, K. P. So, S. C. Lim, Y. H. Lee, *Tailoring the characteristics of graphite oxides by different oxidation times*, J. Phys. D: Appl. Phys., 2009, 42, 065418.
12. Yang, H., Shan, C., Li, F., Han, D., Zhang, Q., Niu, L, *Covalent functionalization of polydisperse chemically-converted graphene sheets with amine-terminated ionic liquid*, Chemical Communications, **2009**, (26), 3880-3882

- 13 He, R., Li, Q., Xiao, G., Bjerrum, N. J., *Proton conductivity of phosphoric acid doped Polybenzimidazole and its composites with inorganic proton conductors*, J. Mem. Sci., **2003**, 226 (1-2), 169-184
14. Li, M., Scott, K. Wu, X., *A poly (R₁R₂R₃)-N⁺/H₃PO₄ composite membrane for phosphoric acid polymer electrolyte membrane fuel cells*, Journal of Power Sources, **2009**, 194(2), 811-814
15. Xu, C., Wu, X., Wang, X., Mamlouk, M., Scott, K., *Composite membranes of polybenzimidazole and caesium-salts-of- heteropolyacids for intermediate temperature fuel cells*, Journal of Materials Chemistry, **2011**, 21 (16) , 6014-6019

Chapter 7: Functionalised PBI

7.1. Introduction

The PBI membrane was considered as a potential material for the PEMFC membrane. Furthermore, some functionalised groups such as $-\text{SO}_3$, $-\text{CH}_3$, and $-\text{CH}_2\text{-SiC}(\text{CH}_3)_3$ [1] were combined with PBI to improve conductivity, water retention and the mechanical strength of PBI.

In the present work, Quaternary Polybenzimidazole (QPBI) was synthesised that described in Chapter 3. The primary chemical structure and properties of the products were discussed in this chapter. Proton conductivity of H_3PO_4 loaded QPBI were studied.

7.2 Results and discussion

The NMR spectrum of synthesised QPBI dissolved in a solution of DMSO-d_6 was shown in Fig. 6-1. In the spectrum, the characteristics of PBI backbone were found. The peaks in the 4.05-4.25 ppm were assigned to the quaternary group and the peak of 3.26 was assigned to the $\text{CH}_2\text{-CH}_2\text{N}$ group [1- 3]. The peak assignments were consistent with the chemical structure of the quaternary group. The two peaks in the range of 1-1.1 ppm and 3.4-3.5 ppm were assigned to the $\text{N-CH}_2\text{-CH}_3$ structure, which were caused from some side reactions such as extra Chloro-N, N-dimethylethylamine hydrochlorid reacting with iodomethane.

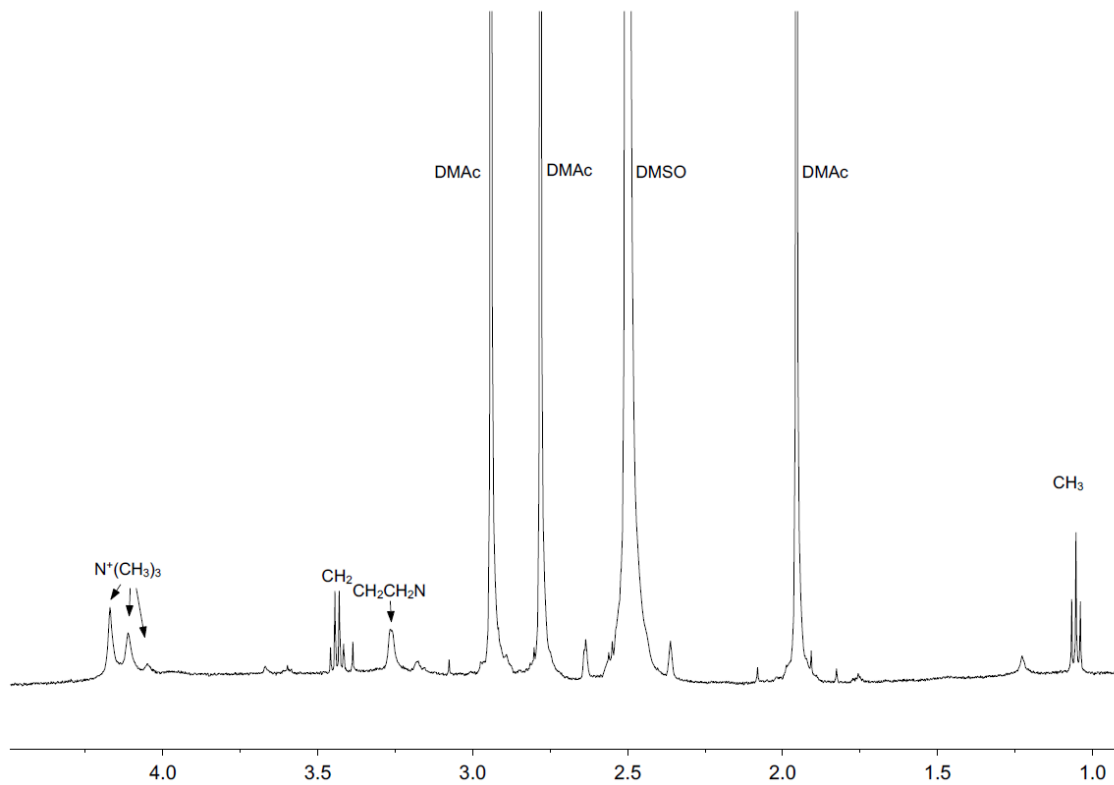
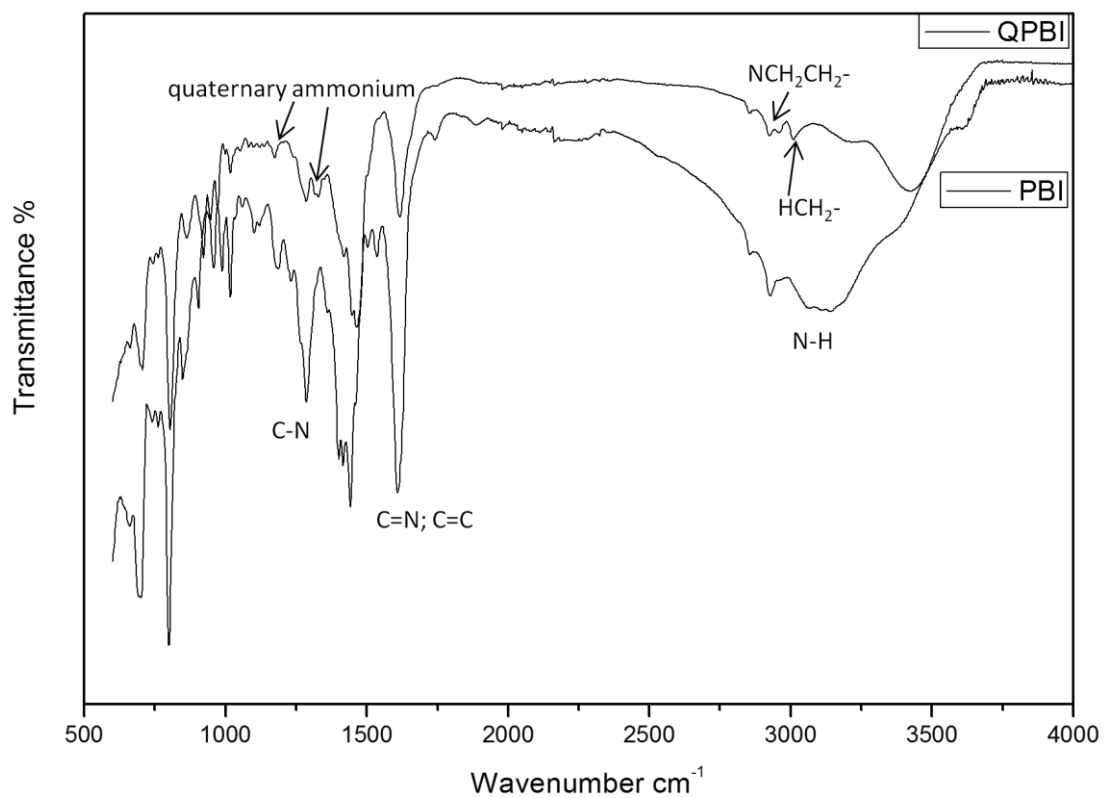
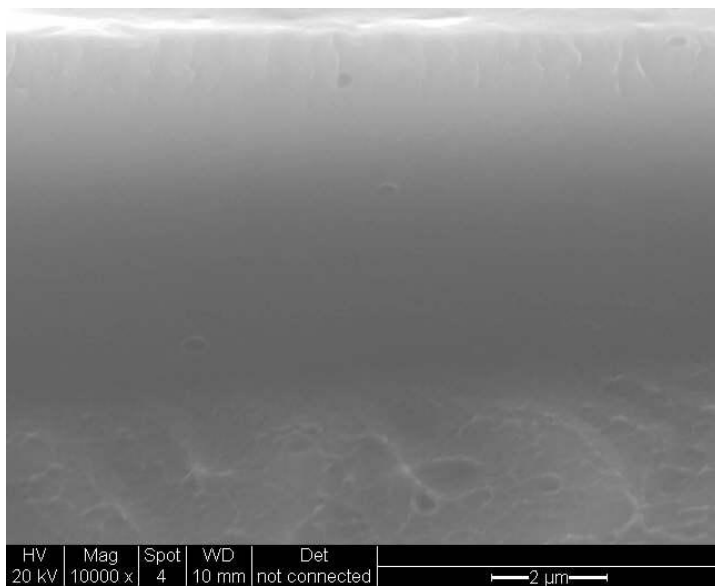
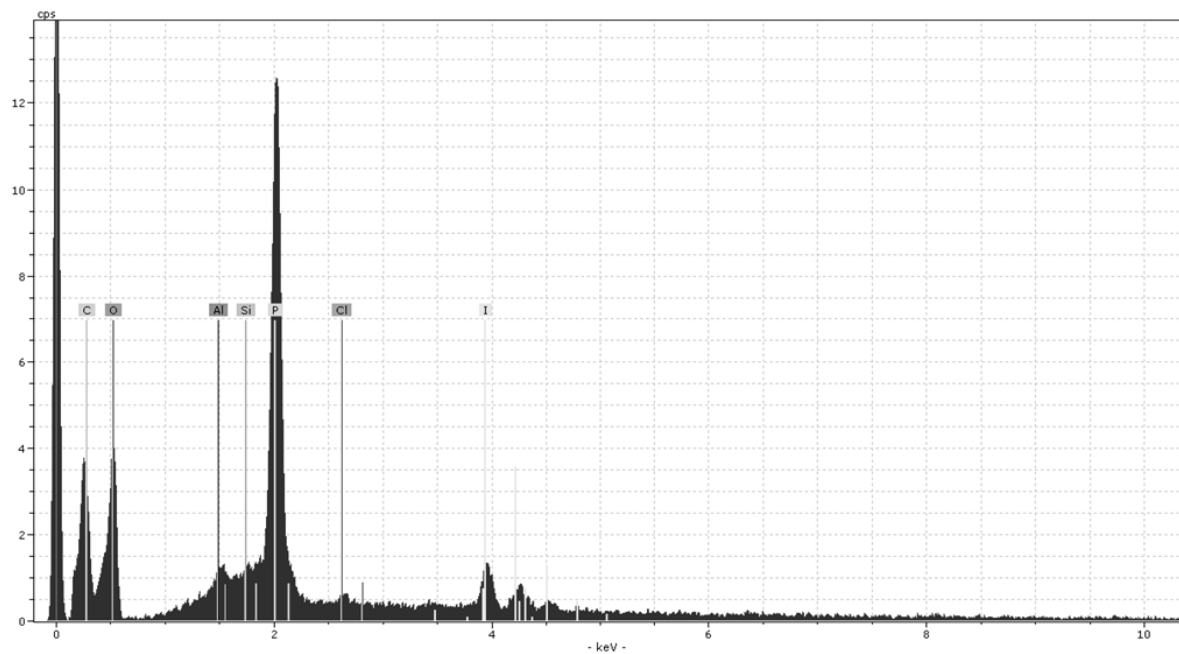
Figure 7-1 ^1H NMR spectra of QPBI

Figure 7-2 FT-IR spectra of QPBI

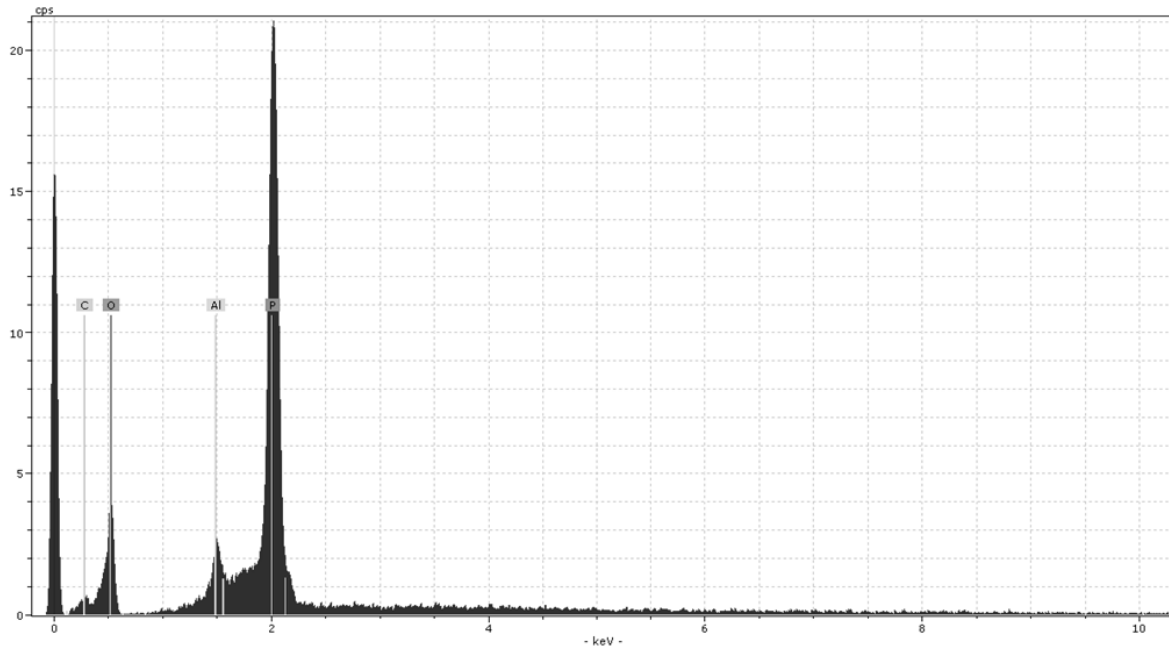
Fig. 7-2 showed the FT-IR spectra of the synthesised QPBI. The broad absorption band in the 3500–3000 cm^{-1} range was assigned to the N–H stretching of the imidazole rings and the pendant amino groups [3]. The shoulder peak at 1617 cm^{-1} and the strong absorption band at 1465 cm^{-1} were assigned to the C=N stretching and the in-plane deformation of the imidazole rings. The peaks of 2925 and 2854 cm^{-1} were attributed to HCH₂- and NCH₂CH₂- stretching which indicated that the synthesised QPBI is not fully quaternary. The small peaks at 1174 cm^{-1} and 1286 cm^{-1} were attributed to the quaternary ammonium group stretching vibration in QPBI [2, 3].



a)



b)



c)

Figure 7-3 EDX analysis for QPBI; before (a) and after (b) H_3PO_4 treatment

The SEM images (Fig. 7- 3a) of the membrane cross-section reveal a dense and non-porous structure after PA loading. As a fuel cell membrane, non-porous is a basic factor. Otherwise, the big crossover which is caused by H_2 gas directly going through the porous in the membrane will reduce the open circle voltage and further decrease the fuel cell performance.

In Fig. 7-3b the EDX analysis of QPBI showed C, Cl, and I elements at 0.25, 2.6, and 4.9 keV, respectively, which were contributed by QPBI and the ammonium group. The Al and Si element peaks were contributed by the sample holder. Fig. 6c showed the data for QPBI after loading with PA for 7days. The Cl⁻ and I⁻ element peaks were missing and the significant P element peak at 2.0 keV suggested a complete substitution of Cl⁻ and I⁻ to H_2PO_4^- . So, after PA loading there was no contribution to conductivity from HCl or HI acid. The conductivity followed the PA transport mechanism.

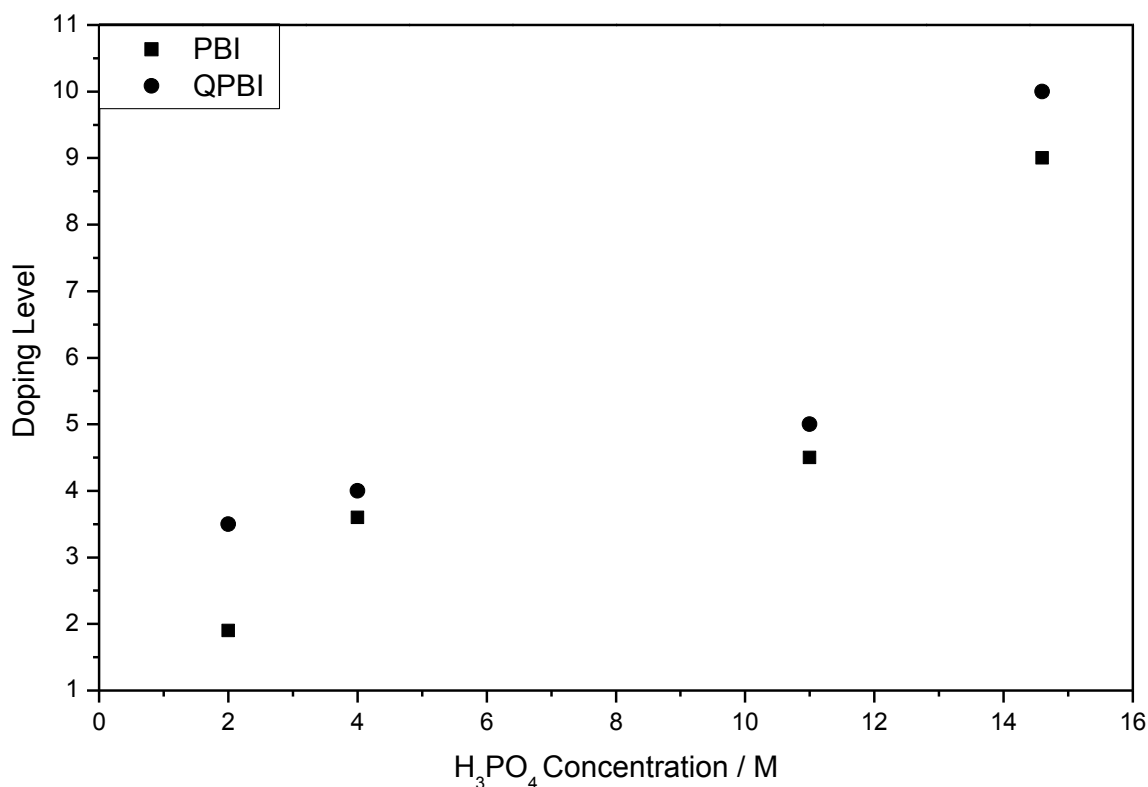


Figure 7-4 Variation in H₃PO₄ doping level of PBI and QPBI membranes in different H₃PO₄ concentrations at room temperature after 7 days

Fig. 7-4 showed the effect of PA concentration on the loading of acid in the PBI and QPBI membranes after 7 days of treatment. At the same phosphoric acid concentrations, QPBI had a higher acid loading than the pristine PBI. The higher PA loading in the QPBI compared to that for PBI achieved in low PA concentration was an attractive feature for membrane production. This higher PA loading was caused from the quaternary group enhancing the absorption capability of acid, because the quaternary group could form ionic bonds with PA rather than hydrogen bonds. So QPBI could reduce the acid loading amount and free acid content that would benefit the mechanical strength. The higher acid absorption capability from quaternary groups took more acid at the same acid concentration. This was also in agreement with experimental results. Also the volumetric swelling of QPBI at 85% H₃PO₄ was lower than for PBI as shown in Table 6-1. This less-compact packing of QPBI was caused by the higher acid loading, because there was already open space inside QPBI for adopting the acid.

Table 7-1 Volume swelling and mechanical strength of PBI and QPBI membrane

	PBI	QPBI
Volume Swelling (%)	90	40
Maximum load (MPa)	60	46

The mechanical strength of membranes without acid was measured at 42% relative humidity (RH) and room temperature (Table 1). The result of the tensile strength of PBI agreed with the literature (67.5 MPa) [4, 5]. The mechanical strength of QPBI membrane was weaker than that of the pristine PBI membrane. This reduction in mechanical strength was indicative of the dimethylethylene group introduced into PBI that changed the atomic packing in the macromolecular chain of QPBI.

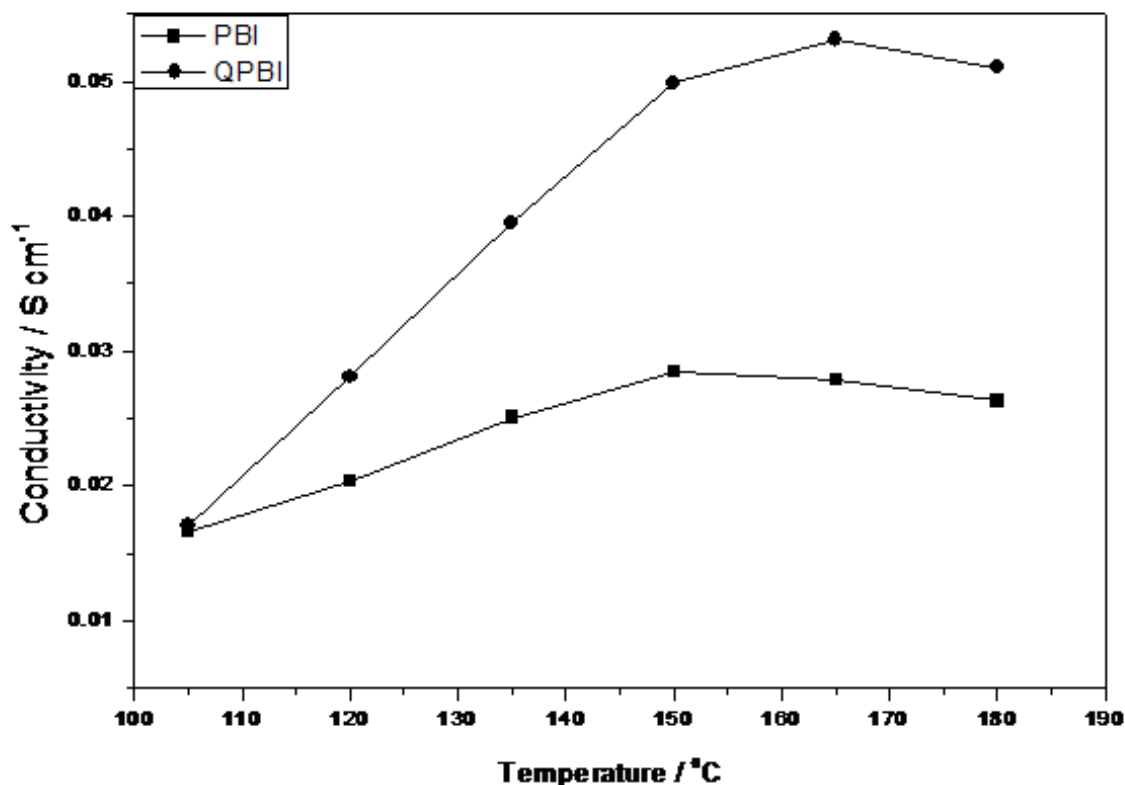


Figure 7-5 Conductivities of PBI and QPBI membrane loaded with H_3PO_4 . PRU of 3.6 and 3.5 respectively under anhydrous conditions

Fig. 7-5 showed the conductivity data of the PBI and QPBI membranes loaded with phosphoric acid to achieve a PRU of 3.5 under anhydrous conditions. After loading with the concentration of phosphoric acid (2.0 M H_3PO_4), the QPBI membrane showed a higher PA loading of 3.5. This was attributed to the ammonium group grafting onto the PBI chain which could form more hydrogen bonds. In comparison, the PBI was treated with a higher concentration of phosphoric acid to achieve a similar PA loading (3.6).

The QPBI membrane provided higher conductivity than that of PBI at the same doping level. For example, at 180°C, conductivity of PBI and QPBI were 0.026 S cm^{-1} , 0.051 S cm^{-1} . The improvement could be attributed to the fact that the ammonium group in quaternary PBI had stronger strength bonds to transfer the proton and higher acid absorption and retention capability which benefited proton transport. The ammonium group could also increase the number of channels available for proton transport by interconnecting some of the hydrophilic domains [6]. The QPBI exhibited enhanced conductivity compared to PBI with bonded acid which indicated that it was a suitable candidate for fuel cells. This indicated that PBI provided better mechanical properties although inferior conductivity than QPBI. A balance between conductivity and mechanical strength was required for a promising membrane in fuel cell applications.

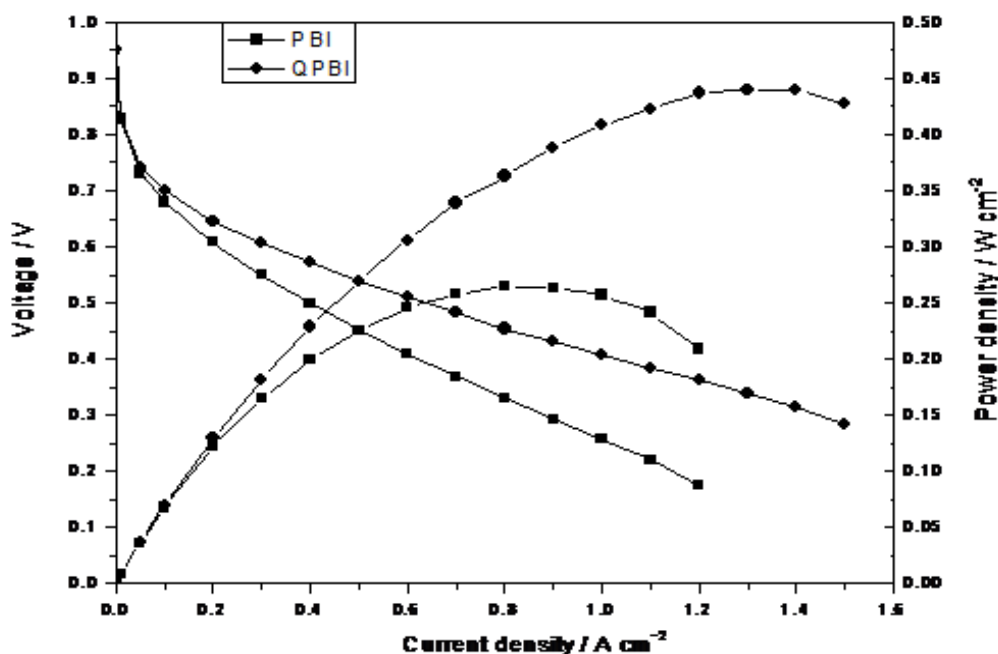


Figure 7-6 Polarisation and power density curves of a fuel cell operated at 175 °C with H_2/O_2 at pressure. Pt Loading is 0.5 mg cm^{-2} both anode and cathode

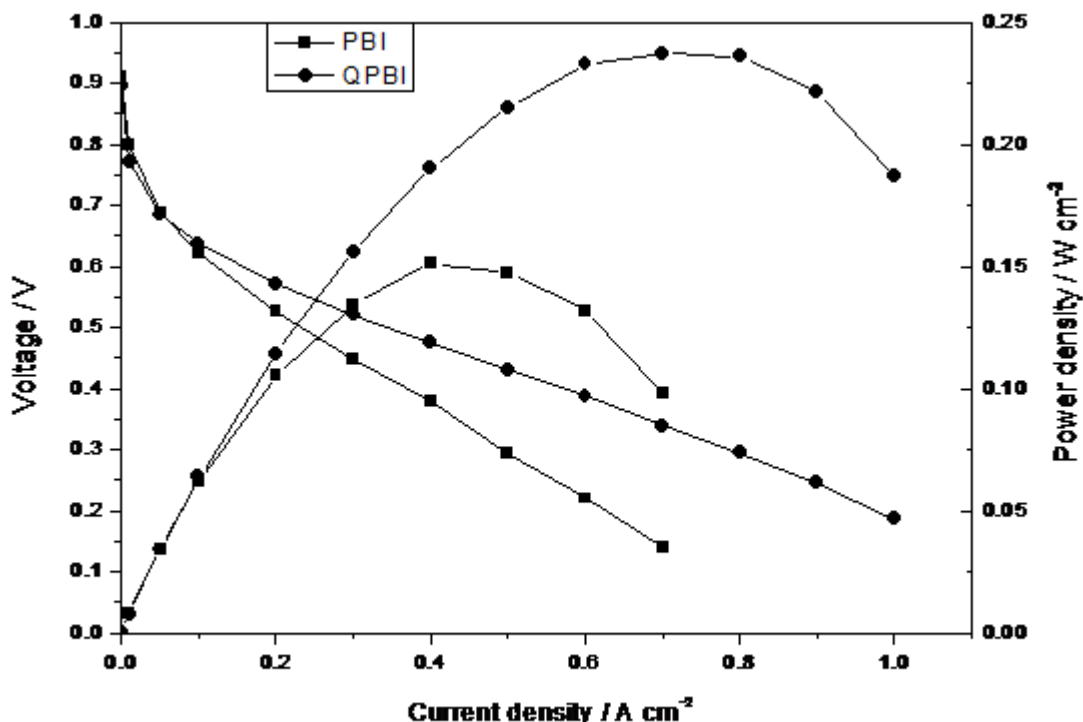
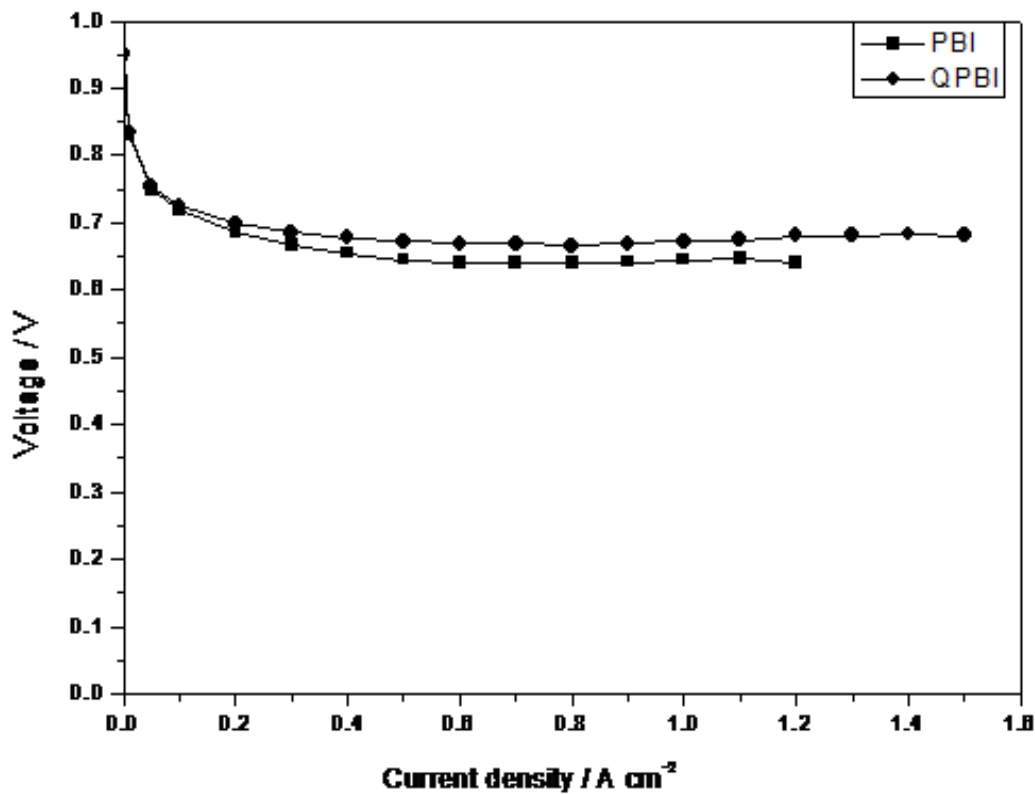


Figure 7-7 Polarisation and power density curves of a fuel cell operated at 175 °C with H₂/Air atmospheric pressure. Pt Loading is 0.5 mg cm⁻² both anode and cathode

Fuel cell performance tests were carried out with H₂/O₂ and H₂/Air at atmospheric pressure. The polarisation and power density curves of the H₂/O₂ and H₂/air fuel cells obtained at 175 °C under anhydrous conditions for PBI and QPBI membranes are shown in Fig. 7-6. The open circuit voltages (OCV) of all membranes were 0.95 V, which indicates that the membranes had low gas permeability [7]. The performance of the cells with the QPBI membranes was significantly better than that with the PBI membrane. The peak power densities of PBI and QPBI with oxygen were 0.265 and 0.44 W cm⁻², respectively. However, the PBI with high PA loading (11M PA) showed better performance than that with low PA loading [8-9] indicating that PA loading was a main factor in fuel cell performance. At the same output voltage of 0.5V, the current densities of the QPBI membrane was over 0.6 A cm⁻² higher than 0.4 A cm⁻² of PBI membrane at 175 °C. The better performance was mainly attributed to the superior proton conductivity of the QPBI which comes from the quaternary ammonium group and also the ammonium group has strong acid and water retention properties at low acid loading.

As expected, using air instead of O_2 would significantly reduce the performance as shown in Fig. 6-7. The OCVs of the membrane were around 0.9 V. The peak power density with the PBI membrane (0.151 W cm^{-2}) was lower than that obtained with the QPBI membrane (0.24 W cm^{-2}) with a similar PA loading. The cell voltages produced with the QPBI membranes were greater than those with the PBI membrane at high-current densities.

The internal resistance, as estimated from the voltage drop in the intermediate voltage range, gave a cell conductivity of around 0.0158 S cm^{-1} of QPBI. This conductivity was much less than that of the membrane itself and indicated significant voltage loss in the electrode layers. As few mobile PA was present in the membrane due to the low PA loading used, the electrode layer would have a relatively low ionic conductivity and thus catalyst utilisation in the electrode reactions would be relatively low.



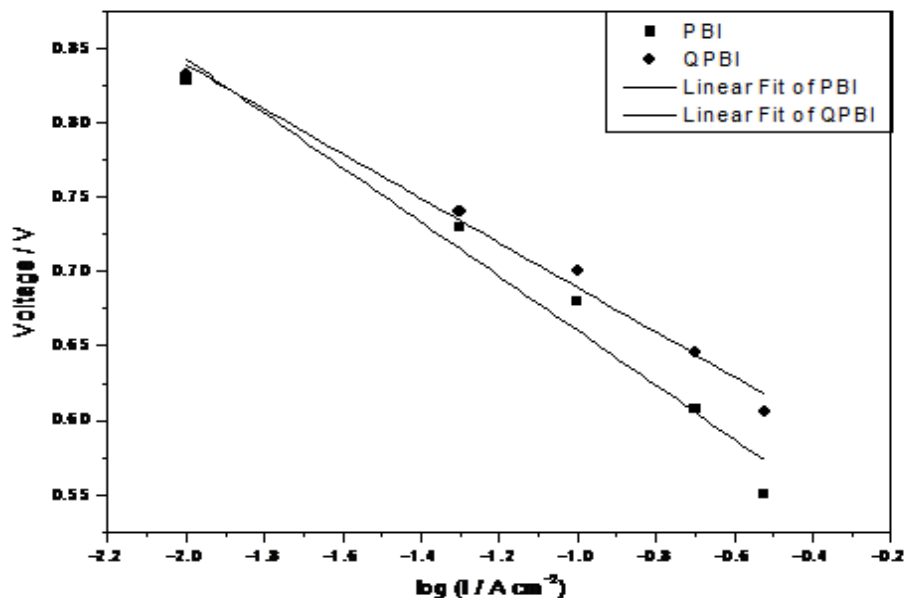


Figure 7-8 (a) IR corrected polarisation curves of PBI and QPBI membrane; (b) Tafel plots obtained from polarisation curves (I is current density)

Fig. 7-8 showed IR corrected polarisation curves of the fuel cells operated with H₂/O₂ at 175 °C. The voltage loss associated with electrode polarisation was small compared to that of the internal resistance in this region. The Tafel slope of PBI and QPBI were approximate 112 mV and 108 per decade, respectively. The value was close to the literature reported values (100 mV dec⁻¹) on ORR electrodes for phosphoric acid loaded PBI fuel cells [10].

7.3 Conclusion

A functionalised PBI with a quaternary ammonium group was successfully prepared and characterised for use in a high temperature PEMFC. The QPBI membranes, treated with the same content of H₃PO₄ had higher doping levels. The ionic conductivity of the QPBI membrane was 0.051 S cm⁻¹ at 150 °C which was two times that of the pristine loaded PBI (0.026 S cm⁻¹) with the same PA doping level. In fuel cell tests, power densities of 440 mW cm⁻² and 240 mW cm⁻² were achieved at 175 °C using oxygen and air, respectively. The data indicated that the quaternary ammonium group benefited from the conductivity of PBI and the QPBI membrane could be considered as a candidate membrane for high temperature PEMFC.

References

1. Kumbharkar, S.C., Kharul, U.K., N-substitution of polybenzimidazoles: Synthesis and evaluation of physical properties, *European Polymer Journal*, **2009**, 45, 3363–3371
2. Wen Z., Tang Y., Wang B., Wang H., *Study on synthesis and quaternary ammoniation of ABPBI*, China National Polymer academic conference, **2009**.
3. Xia, Z., Yuan, S., Jiang, G., Guo, X., Fang, J., Liu, L., Qiao, J., Yin, J., *Polybenzimidazoles with pendant quaternary ammonium groups as potential anion exchange membranes for fuel cells*, *Journal of Membrane Science*, **2012**, 390-391 , 152-159
4. Fuqiang Chu, Bencai Lin, Bo Qiu, Zhihong Si, Lihua Qiu, Zongzong Gu, Jianning Ding, Feng Yan and Jianmei Lu, *Polybenzimidazole/zwitterion-coated silica nanoparticle hybrid proton conducting membranes for anhydrous proton exchange membrane application*, *J. Mater. Chem.*, **2012**, 22, 18411-18417
5. He, R., Li, Q., Xiao, G., Bjerrum, N. J., Proton conductivity of phosphoric acid doped Polybenzimidazole and its composites with inorganic proton conductors, *J. Mem. Sci.*, **2003**, 226(1-2), 169-184
6. R. Kannan, M. Parthasarathy , S.U. Maraveedu , S. Kurungot , V.K. Pillai, Domain size manipulation of perfluorinated polymer electrolytes by sulfonic acid-functionalized MWCNTs to enhance fuel cell performance, *Langmuir*, **2009**, 25 (14), 8299-8305
7. Li M, Scott K, Wu X. A poly (R₁R₂R₃)-N⁺/H₃PO₄ composite membrane for phosphoric acid polymer electrolyte membrane fuel cells. *J Power Sources*, **2009**, 194(2), 811-814.
8. Justo Lobato, Pablo Cañizares, Manuel A. Rodrigo, Diego Ubeda, and F. Javier Pinar, *Promising TiOSO₄ Composite Polybenzimidazole-Based Membranes for High Temperature PEMFCs*, *ChemSusChem*, **2011**, 4(10), 1489-1497
9. Justo Lobato, Pablo Cañizares, Manuel A. Rodrigo, Diego Ubeda, F. Javier Pinar, *A novel titanium PBI-based composite membrane for high temperature PEMFCs*, *J. Membr. Sci.* **2011**, 369, 105-111
10. Liu, Z.; Wainright, J.S.; Savinell, R.F. *High-temperature polymer electrolytes for PEM fuel cells: Study of the oxygen reduction reaction (ORR) at a Pt–polymer electrolyte interface*. *Chem. Eng. Sci.* **2004**, 59, 4833–4838.

Chapter 8: Poly (tetrafluoroethylene) Support Composite Membranes

This chapter described research into a $C_{8x}H_{3-x}PMo_{12}O_{40}$ (CsPOMo)/ quaternary diazabicyclo-octane polysulfone with Poly-tetrafluoroethylene (QDPSU/PTFE) composite membrane with a low phosphoric acid loading. The membrane was characterised in terms of structure, proton conductivity and mechanical strength. Also, dimethylhexadecylamine partially quaternised poly (vinyl benzyl chloride) (qPVBzCl-) was synthesised as the substrate for the phosphoric acid loaded PTFE composite polymer membrane.

The composite membrane was synthesised and prepared as described in Chapter 4.

8. 1 Introduction

The premier works were based on PBI membranes, and quaternised polymers were also considered as a potential candidate membrane for intermediate temperature PEMFC. Poly $(R_1R_2R_3)^{N+}/H_3PO_4$ [1] and quaternary diazabicyclo-octane polysulfone/ H_3PO_4 [2] gave acceptable conductivity and performance for intermediate temperature fuel cells as discussed in Chapter 2. Although a number of novel quaternised materials have been developed, a number of challenges into the exploration of membranes with high fuel cell performance and mechanical strength still remained.

Good mechanical strength was an important property for membranes, as it benefited the working period in the fuel cells. However, quaternary ammonium (QA) groups in modified polymer materials significantly affected the resultant polymer physicochemical properties. This was due to reasons such as polymer chain rearrangements and crystal structure changes [2-7]. Therefore, besides ion conductivity, the stability and tensile strength are main factors in considering quaternised polymers as electrolyte membranes in PEMFCs. Polytetrafluoroethylene (PTFE) was a material that could increase the mechanical strength of the membrane.

8.2 Caesium Salt of Heteropolyacids/Quaternary diazabicyclo-octane Polysulfone/PTFE composite membranes

8.2.1 Results and Discussion

Fig. 8-1 showed an SEM image of the cross-section of the CsPOMo/PSU/PTFE/H₃PO₄ membrane. The dense structure of the composite membrane indicated that the pores of the PTFE membrane were filled with the CsPOMo and QDPSU. The distributions of caesium, phosphorous and molybdenum elements in the membrane were analysed using EDX and were shown in Fig. 8-2. Distribution of the CsPOMo and QDPSU was evidenced by the Cs, sulphur and fluorine elements. Phosphorous represented the H₃PO₄ loading in the membrane. As shown in Fig. 8-2, a homogenous structure of the composite membrane and a good dispersion were obtained.

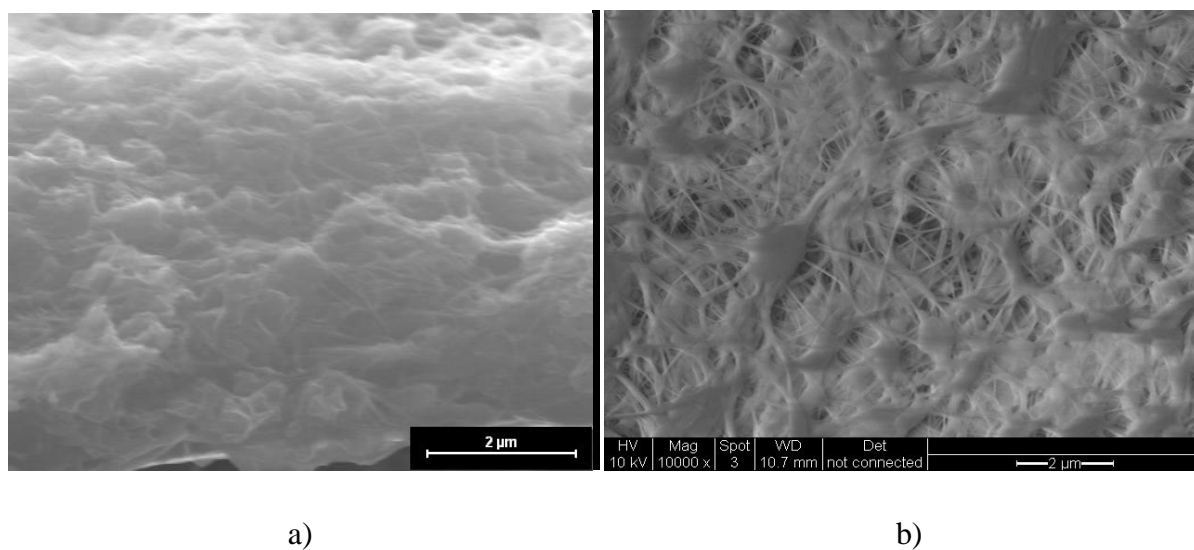
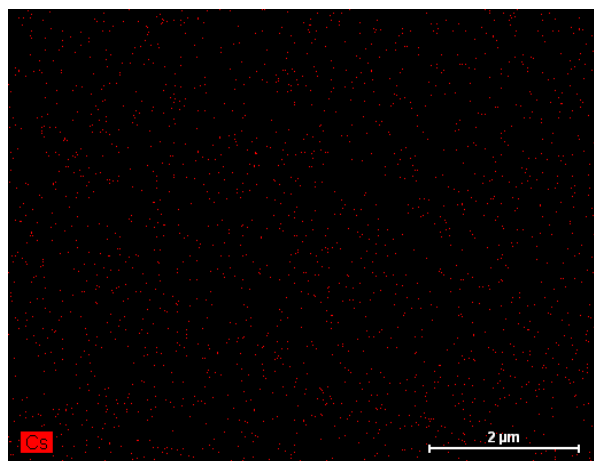
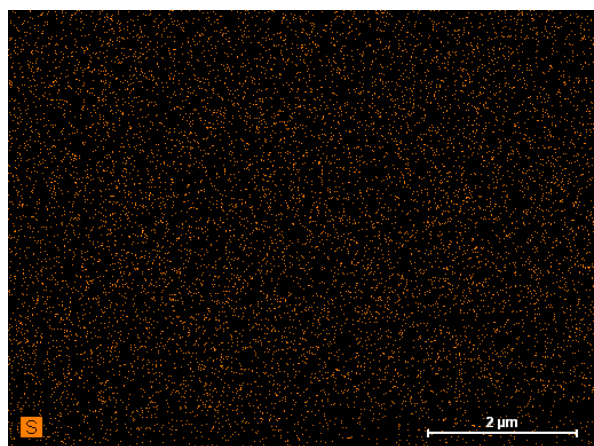


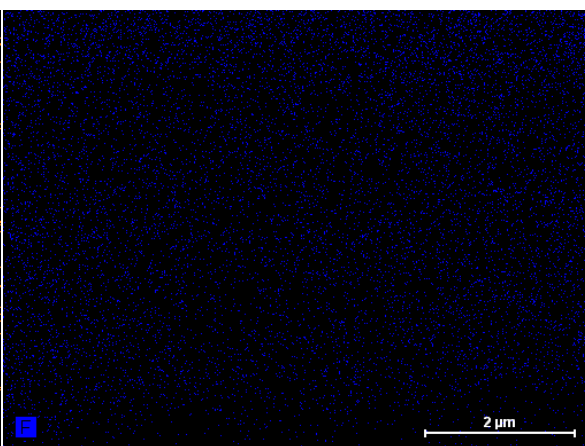
Figure 8-1 SEM of a) CsPOMo/QDPSU/PTFE/H₃PO₄ composite membrane and b) PTFE



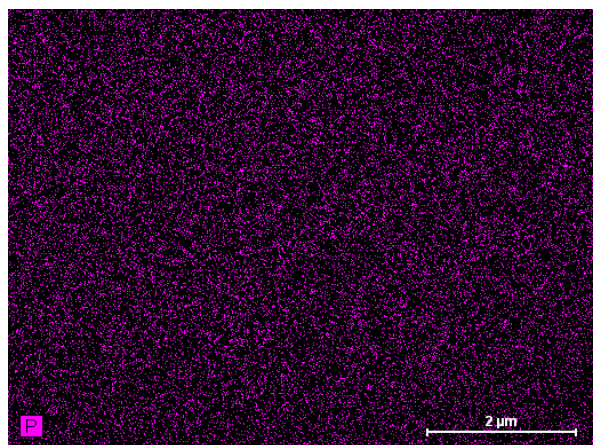
a)



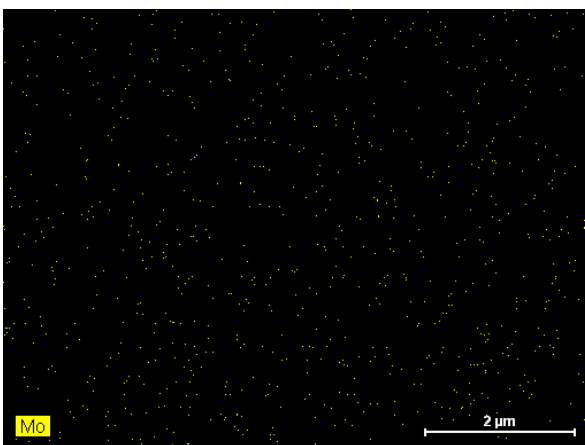
b)



c)



d)



e)

Figure 8-2 EDX analysis of CsPOMo/QDPSU/PTFE/H₃PO₄ composite membrane a) Cs, b) S, c) F, d) P, e) Mo

Fig. 8-3 showed the infrared spectra of CsPOMo-PSU-PTFE-H₃PO₄. The characteristic vibration bands of P=O (1065 cm⁻¹) in CsPOMo were apparent [9]. The small peaks at 2924 cm⁻¹, 1620 cm⁻¹ and the sharp peak at 1490 cm⁻¹ were attributed to quaternary ammonium group stretching vibration [2]. For the PA/QDPSU membrane, a significant vibration peak was found at 960 cm⁻¹ and was attributed by the P=O vibration. The data suggested the successful preparation of CsPOMo-PSU-PTFE-H₃PO₄ membranes.

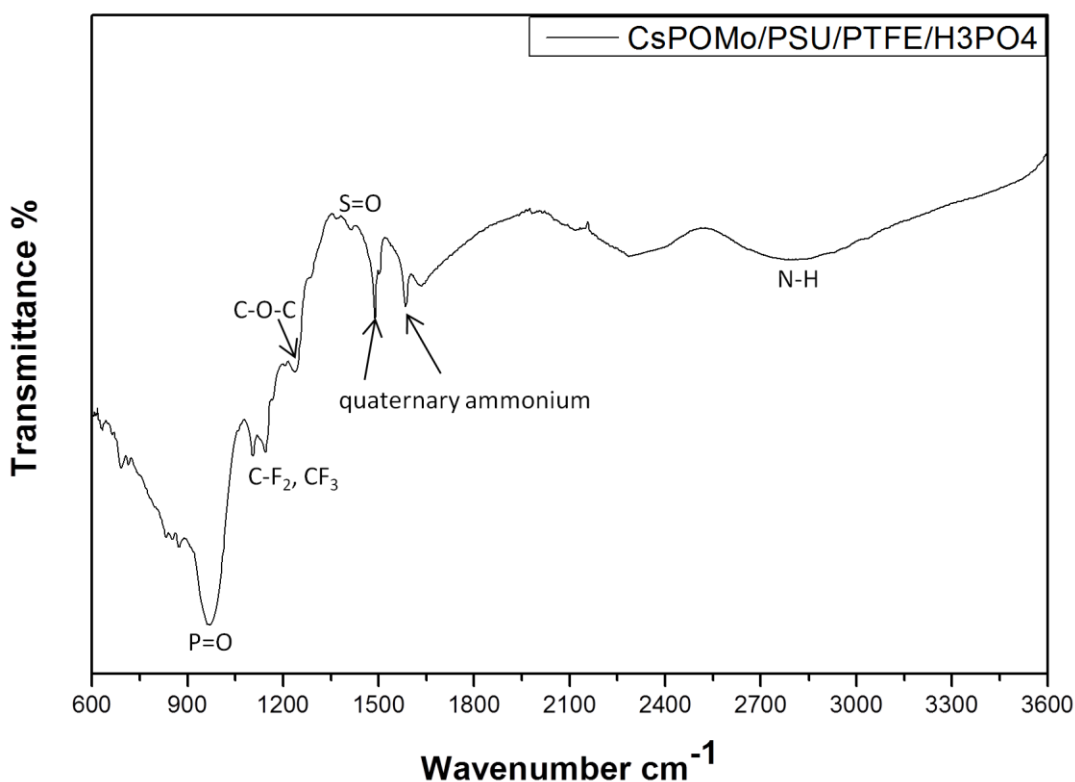


Figure 8-3 Infrared spectra of CsPOMo/PSU/PTFE/H₃PO₄ composite membrane

Fig. 8-4 showed conductivity data of the CsHPA/PSU/PTFE membrane loaded with phosphoric acid (PRU 1.8) at a relative humidity < 1%. In comparison to the PBI membrane with the same PA loading, the composite membrane had much higher conductivity. The conductivity of the composite membrane varied from 0.035 to 0.04 S cm⁻¹ in the temperature range of 105 to 150 °C. The highest conductivity of the PBI membrane was only 0.023 at 180 °C. The CsPOMo enhanced the conductivity of the membrane which might be due to the combination of the CsPOMo powder and the PSU/PTFE [9]. The combination of the hydrophobic PTFE substrate and hydrophilic (QDPSU) structure could improve water retention inside the membrane which could benefit conductivity [4]. The conductivities decreased when the temperature exceeded 150°C, which was caused by degradation of the

QDPSU. This indicated that the quaternary group was not stable in QDPSU over 150 °. However, it might be considered possible for this membrane to be used at 150 °C.

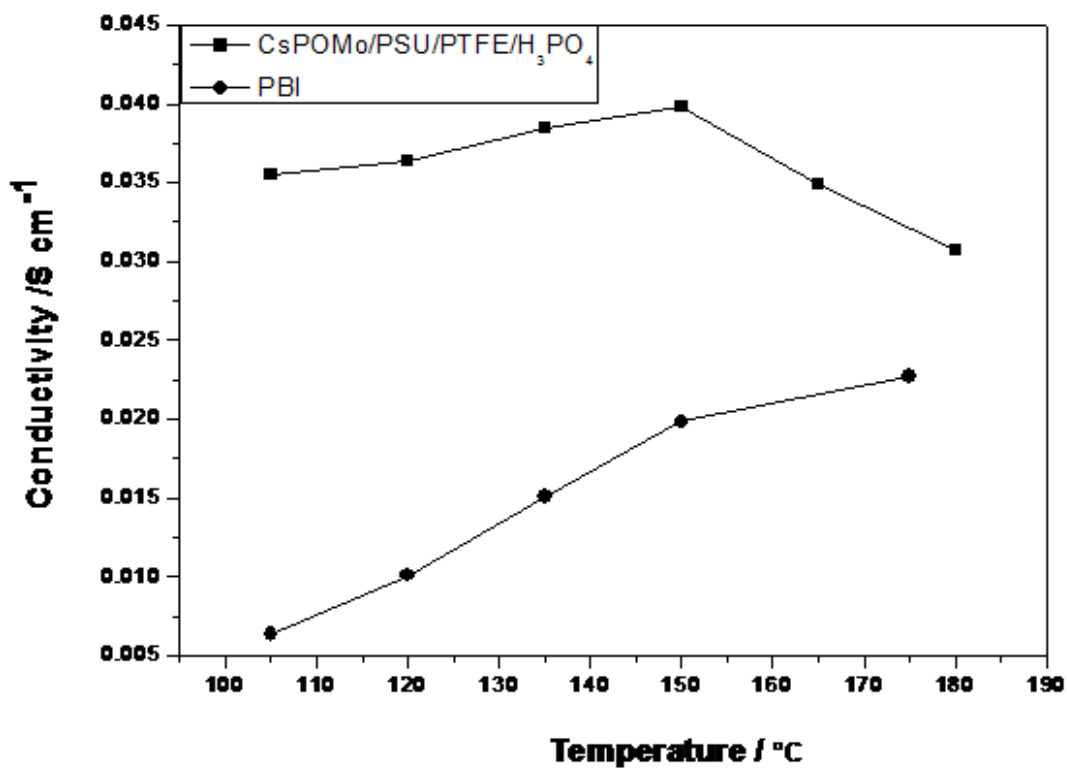


Figure 8-4 Conductivities of CsPOMo/PSU/PTFE composite membrane and PBI membrane loaded with H₃PO₄ (PRU 1.8) under relative humidity <1%

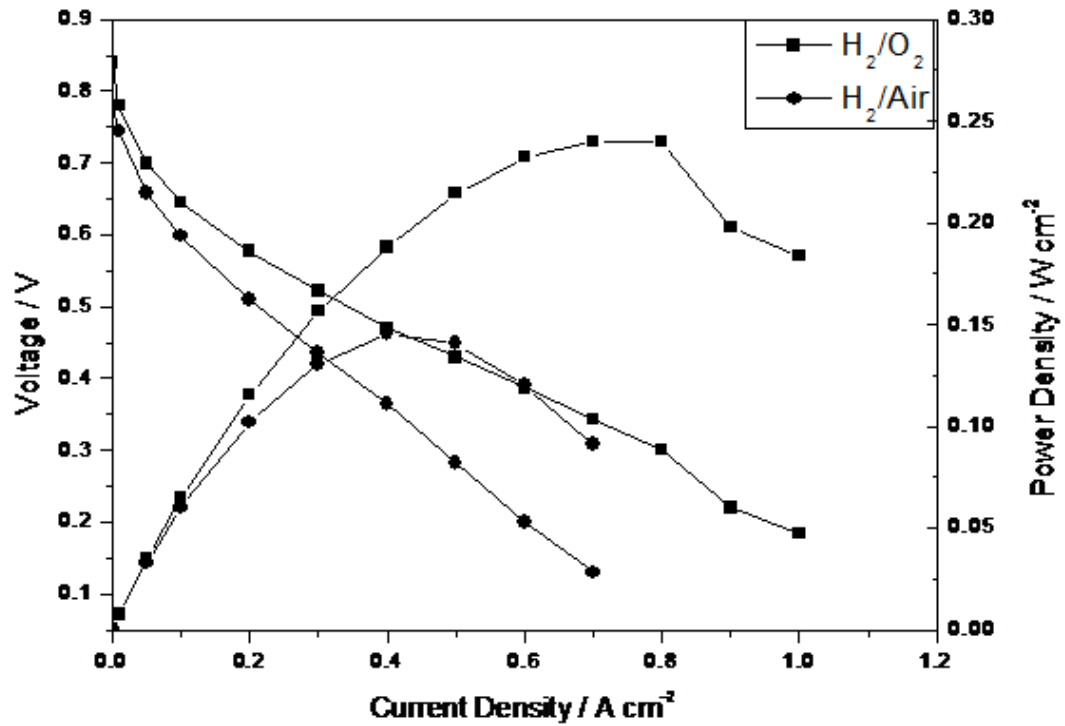


Figure 8-5 Polarisation and power density curves of a fuel cell operated at 150 °C with (a) H_2/O_2 and (b) H_2/air atmospheric pressure. Pt loading: cathode 0.4 mg cm^{-2} ; anode 0.2 mg cm^{-2} ; no gas humidity, H_3PO_4 PRU: 1.8, membrane thickness $28 \text{ }\mu\text{m}$. Gas rate: anode: $40 \text{ dm}^3 \text{ min}^{-1}$; cathode: $70 \text{ dm}^3 \text{ min}^{-1}$.

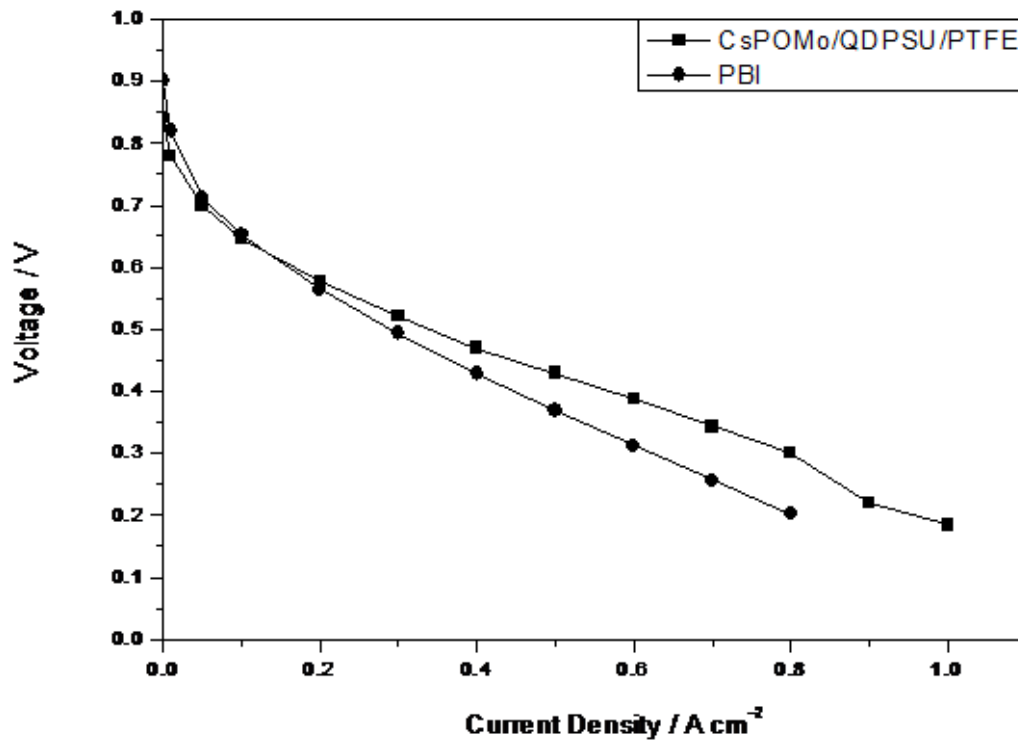
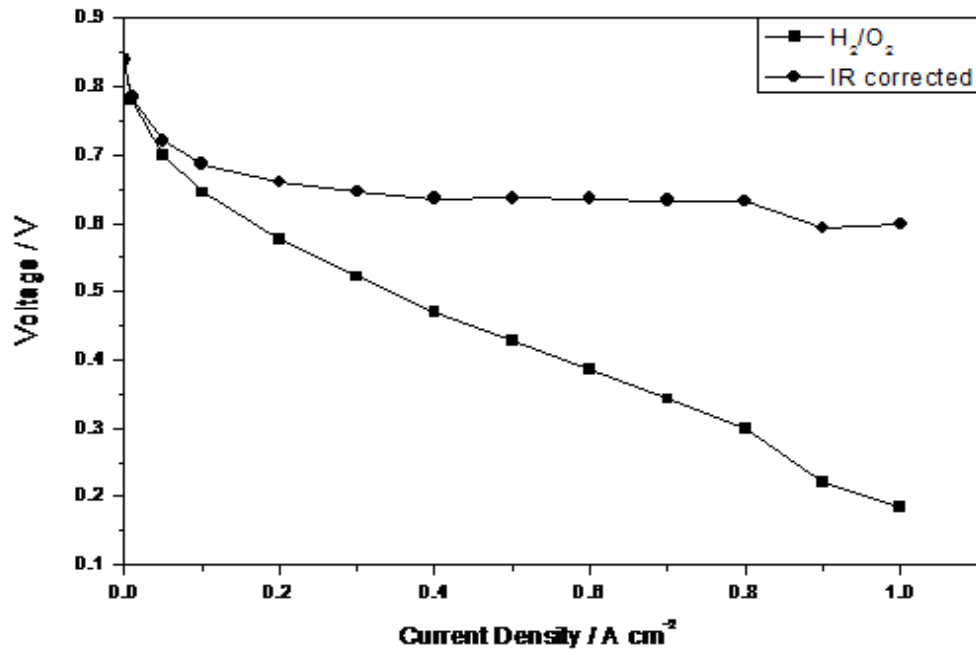
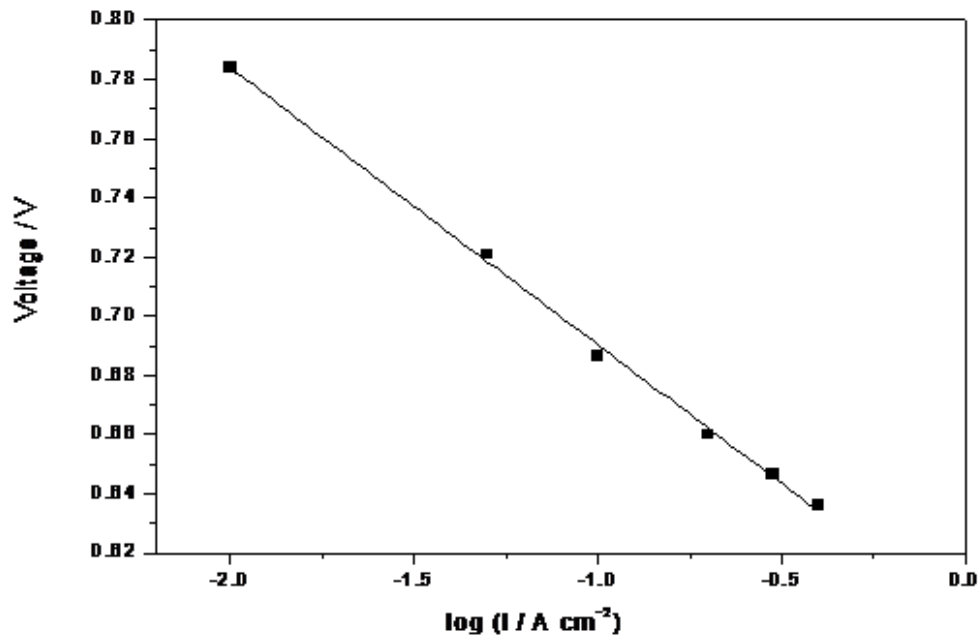


Figure 8-6 Polarisation curves of CsPOMo/QDPSU/PTFE and PBI fuel cell operated at 150 °C with H₂/O₂, at atmospheric pressure, humidity <1%.

The polarisation and power density curves of the H₂/O₂ fuel cell obtained at 150 °C at low humidity (< 1%) with the CsPOMo/PSU/PTFE membrane were shown in Fig. 7-5. Total Pt catalyst loading was relatively low at 0.6 mg cm⁻². The cell open circuit voltage was 0.85 V, which indicates that the relatively thin membrane (28 μm) was partially gas permeable. This probably resulted in some gas crossover and thus electrode polarisation was caused by mixed potentials at the electrodes. However, the thin membrane provided reasonably good conductivity. A peak power density of 240 mW cm⁻² was achieved with oxygen. This peak power was only slightly better than that with a low acid loading PBI membrane (220 mW cm⁻², doping level 1.9) used in previous work as shown in Fig. 7-6 [6]. The performance achieved by the composite membrane could be attributed to its greater proton conductivity and superior water retention properties on the membrane surface at low acid loading [4, 8]. The fuel cell with hydrogen and CO₂ free air gave a peak power density of 140 mW cm⁻² which was lower than that with oxygen, as would be expected from the lower partial pressure of oxygen with the former.



(a)



(b)

Figure 8-7 a) IR corrected polarisation curves of CsPOMo/PSU/PTFE b) Tafel plots obtained from polarisation curves in b). I is the current density.

The internal resistance, as estimated from the voltage drop in the intermediate voltage range, gave a cell conductivity of around 0.006 S cm^{-1} . This conductivity was much lower than that of the membrane itself and indicated significant voltage loss in the electrode layers (and other cell components). Furthermore, as Fig. 7-6 shows, there was an approximate 200 mV voltage loss from current densities of 0 to 0.1 A cm^{-2} .

IR correction based on the combined resistance of the membrane and electrode, was measured at the high current density region ($0.4\text{-}0.8 \text{ A cm}^{-2}$) with H_2/O_2 at $150 \text{ }^\circ\text{C}$ shown in Fig. 8-7. Compared to that of the internal resistance, the voltage loss associated with electrode polarisation was small in this region. From the plot of the IR corrected voltage vs $\log(\text{current density } I)$, the slope (Tafel type) of the line was approximately 98 mV per decade. The value was close to the literature reported values (100 mV dec^{-1}) on ORR electrodes for phosphoric acid loaded PBI fuel cells [9].

8.2.2 Conclusions

A thin CsPOMo/PTFE/QDPSU composite membrane was prepared and characterised for use in a high temperature PEMFC. The ionic conductivity of the composite membrane, loaded with a low content of H_3PO_4 , was 0.04 S cm^{-1} at $150 \text{ }^\circ\text{C}$. In fuel cell tests, power densities of 240 mW cm^{-2} and 140 mW cm^{-2} were achieved using oxygen and air, respectively. The data indicated that the CsPOMo/PTFE/QDPSU composite could be considered as a candidate membrane for high temperature PEMFC because of its acceptable conductivity and fuel cell performance with a low PA acid loading.

8.3 Dimethylhexadecylamine quaternized poly (vinyl benzyl chloride)/PTFE composite membrane

8.3.1 Results and discussion

Fig. 8-8 showed the thermogravimetric analysis (TGA) results of the H_3PO_4 doped PTFE/qPVBzCl⁻ composite membrane. From the curve there were mainly three steps for the weight loss: the first step, between the temperatures of 30°C to 100 °C, was the dehydration process of the composite membrane. The weight loss in this step was 10% which was mainly due to the free absorbed water in the membrane. The second step, with temperatures ranging from 250°C to 450 °C, was the degradation of the ionomer and PTFE. The third step, with temperatures of 550°C to 600 °C, was the carbonisation process. The composite membrane was stable in the intermediate temperature from 100°C to 200 °C, which was in a suitable fuel cell operation range.

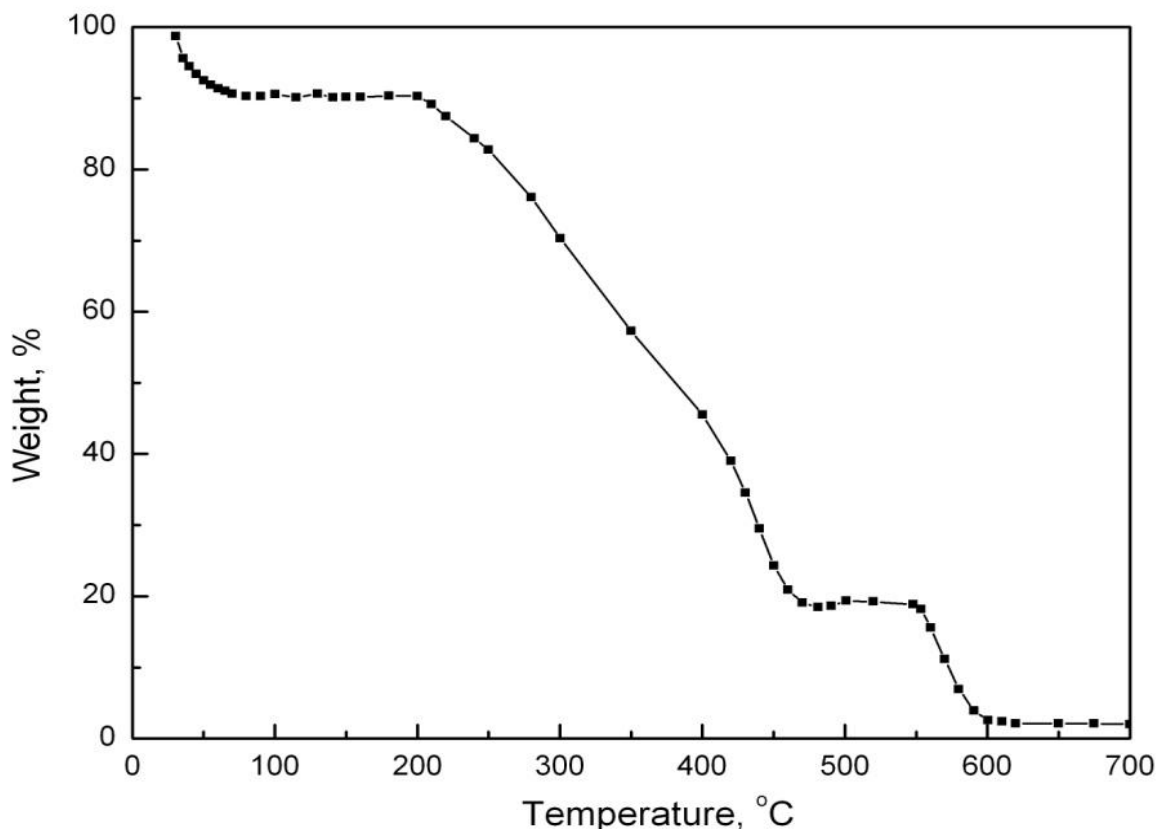


Figure 8-8 TGA analysis of the H_3PO_4 doped PTFE/qPVBz/Cl⁻ composite membrane

Figure 7-9 showed the tensile test results for the PTFE porous thin film, H_3PO_4 loaded PTFE/qPVBzCl⁻ composite membrane (PTFE/qPVBzCl⁻) and H_3PO_4 loaded qPVBzCl⁻ membranes. The H_3PO_4 loaded qPVBzCl⁻ membrane tensile strength was 9.55 MPa and Young's modulus was 0.1GPa. For the H_3PO_4 loaded PTFE/qPVBzCl⁻ membrane, the tensile stress was 56.23 MPa, and Young's Modulus was 0.25GPa. The fractured elongation was 23%. The PTFE, tensile strength was 51.20 MPa and Young's modulus was 0.131GPa. The H_3PO_4 loaded PTFE/qPVBzCl⁻ composite membrane had a better tensile strength than the PTFE thin film, which was a result of the contribution of the filled polymer qPVBzCl⁻. The membrane tensile strength was improved after the application of the PTFE thin film.

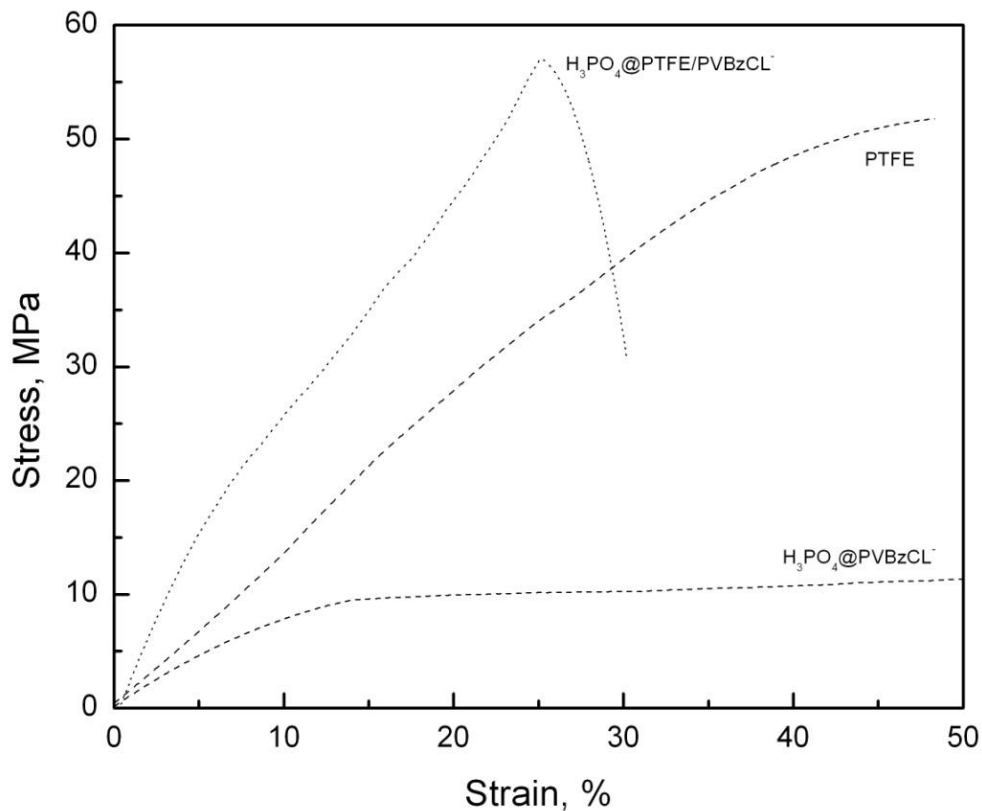


Figure 8-9 Stress-strain curves of the PTFE porous membrane, H_3PO_4 doped PTFE/qPVBzCl⁻ composite membrane and H_3PO_4 loaded qPVB/Cl⁻

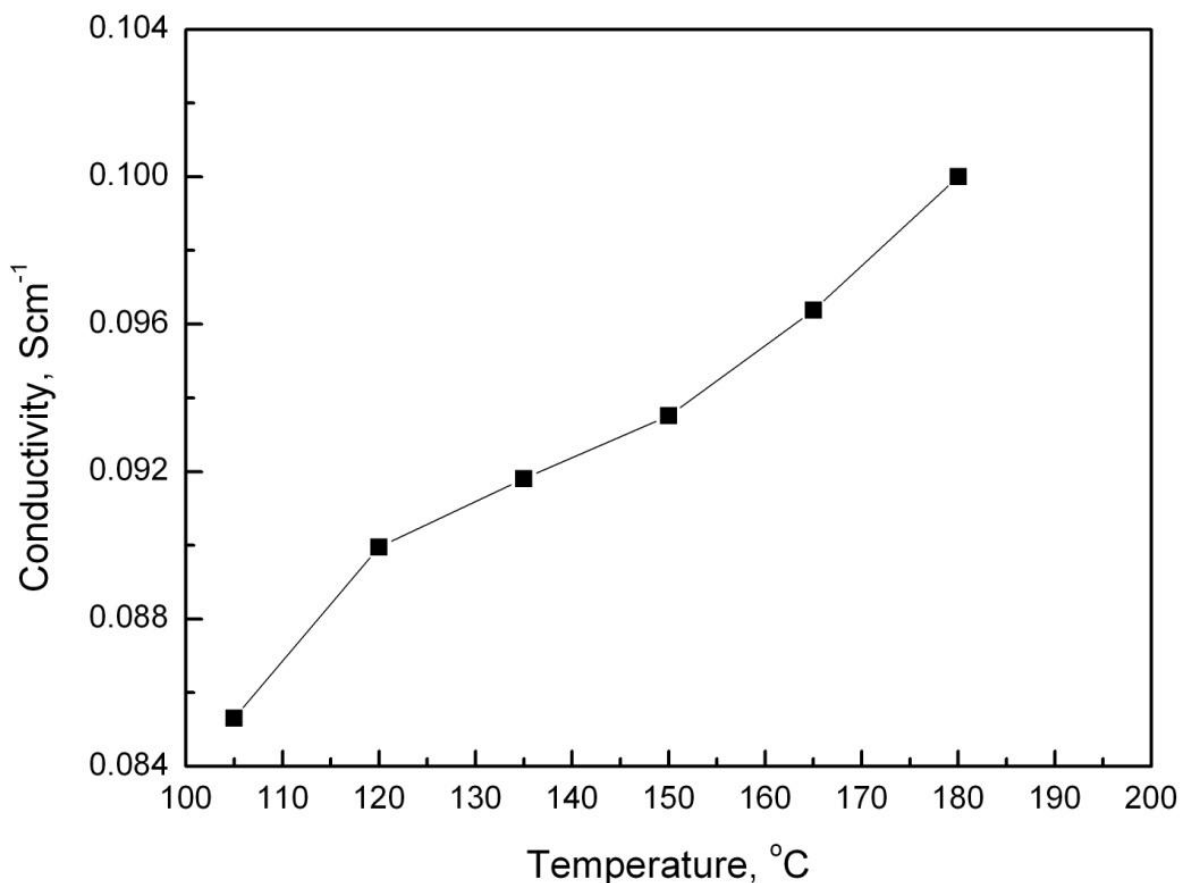


Figure 8-10 Proton conductivity-temperature relationship for the H₃PO₄ loaded PTFE/qPVBzCl⁻ membrane

Fig. 8-10 showed the conductivity data of the H₃PO₄ loaded PTFE/qPVBzCl⁻ membrane loaded with phosphoric acid (11 M) to achieve a PA loading of 5 at a relative humidity <1%. The conductivity of the membrane increased with increased temperature indicating good stability at intermediate temperatures. The peak conductivity was 0.1 S cm⁻¹ at 180 °C. The combination of hydrophobic (PTFE substrate) and hydrophilic (qPVBzCl⁻) structure would improve water retention inside the membrane which benefited conductivity [1, 2].

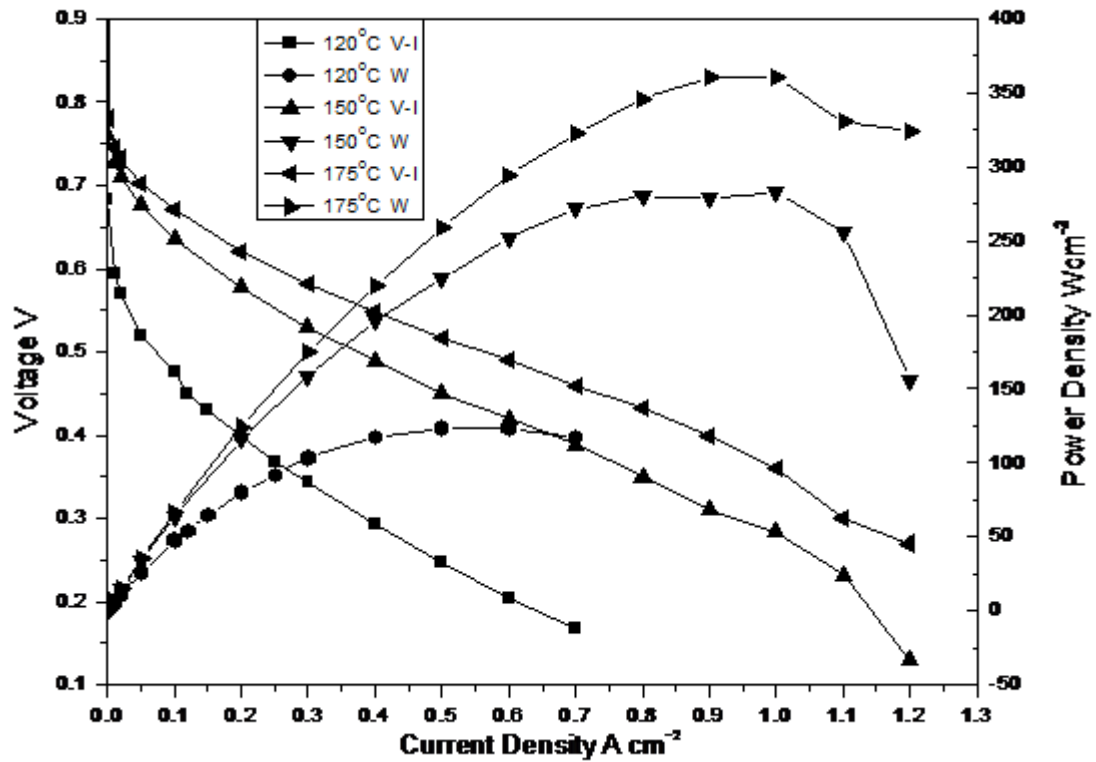


Figure 8-11 Polarisation curves of H_3PO_4 loaded PTFE/qPVBzCl⁻ membrane. H_2/O_2 was used without back pressure; Pt/C (0.5 mg cm^{-2})

The polarisation and power density curves of the H_2/O_2 obtained at 120 °C, 150 °C and 175 °C under low humidity conditions (<1%) for H_3PO_4 loaded PTFE/qPVBzCl⁻ membranes were shown in Fig.7.11. The fuel cell performance improved with the increasing temperature which was in agreement with the conductivity results. When the operating temperature increased from 120 °C to 175 °C, the OCV increased from 0.71 V to 0.85 V [3, 5, 7, and 13]. At 0.6 V, the fuel cell gave a 200 mA cm^{-2} current density and a 120 mA cm^{-2} power density at 175 °C. This voltage was a suitable value for fuel cell applications.

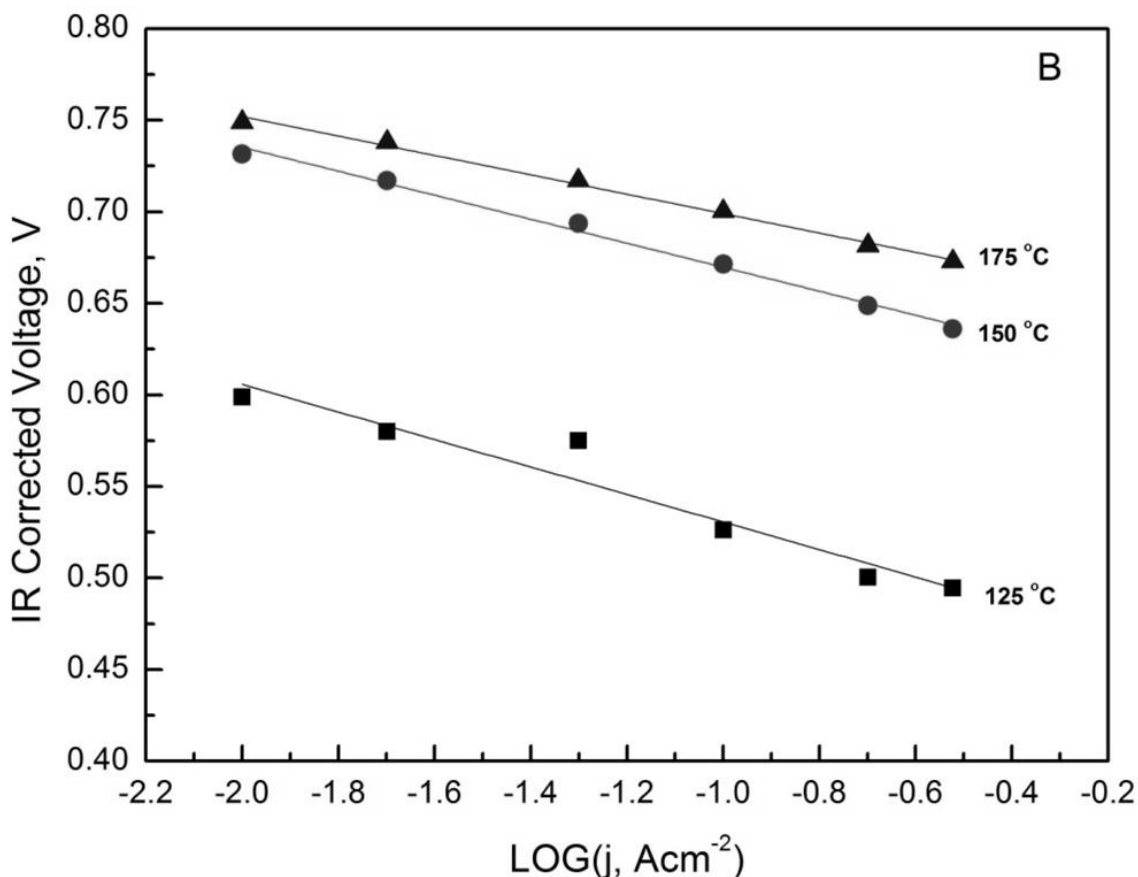


Figure 8-12 IR corrected V-I polarisation curves (A) and Tafel slopes (B) for different operation temperatures

Fig. 8-12 showed the Tafel plot of the IR corrected V-I curves. These results showed that the voltage loss was 72 mV, 60mV and 54mV per decade for temperature at 125 °C, 150 °C and 175 °C respectively. These values were less than the literature's reported values for the phosphoric acid loaded PBI fuel cells [4, 12]. The internal resistance, as estimated from the voltage drop in the intermediate voltage range, gave a cell conductivity of 0.018 S cm⁻¹ at 175 °C. This conductivity was much less than that of the membrane itself and indicated significant voltage loss in the electrode layers and other cell components.

8.3.2 Conclusions

N, N-Dimethylhexadecylamine partially quaternised poly (vinyl benzyl chloride) (qPVBzCl) was synthesised as the substrate for the phosphoric acid doping membrane through porous polytetrafluoroethylene (PTFE) thin film. qPVBzCl was successfully filled into the interconnected pores of the PTFE film to prepare the solid PTFE/qPVBzCl membranes. The

weight of the qPVB/Cl⁻ ionomer in the PTFE/qPVBzCl⁻ was 71% of the overall membrane weight. It could achieve phosphoric acid doping level 4.67 to 5.12. The H₃PO₄ loaded PTFE/qPVBzCl⁻ composite membrane tensile strength was greatly improved after the applications of the PTFE thin film and the membrane was stable in the intermediate fuel cell operation temperature from 100°C to 200 °C with peak conductivity of 0.1 Scm⁻¹ at 180 °C. A peak power density of 360 mW cm⁻² and limited current of 1.2 A cm⁻² was achieved at 175 °C.

References

1. Li, M.; Scott, K.; Wu, X. *A poly (R1R2R3)^{N+}/H₃PO₄ composite membrane for phosphoric acid polymer electrolyte membrane fuel cells*. J. Power Sources, 2009. 194(2), 811-814
2. Wang, X; Xu, C.; Golding, B.T.; Sadeghi, M.; Cao, Y.; Scott, K. *A novel phosphoric acid doped quaternary 1, 4-diazabicyclo-[2.2.2]-octane polysulfone membrane for intermediate temperature fuel cells*, Int. J. hydrogen energy, 2011, 36, 14, 8550-8556.
3. Cao Y., Wang X, Mamlouk M. and Scott K., *Preparation of alkaline anion exchange polymer membrane from methylated melamine grafted poly(vinylbenzyl chloride) and its fuel cell performance*, J. Mater. Chem., **2011**, 21, 12910-12916
4. Wang X., Li M., Golding B., Sadeghi M., Cao Y., Yu E., Scott K. *A polytetrafluoroethylene-quaternary 1,4-diazabicyclo-[2.2.2]-octane polysulfone composite membrane for alkaline anion exchange membrane fuel cells*, International Journal of Hydrogen Energy, **2011**, 36, 10022-10026
5. Li, Q.; Jensen, J. O.; Savinell, R. F.; Bjerrum, N. J. *High temperature proton exchange membranes based on polybenzimidazoles for fuel cells*, Prog. Polym. Sci., **2009**. 34(5), 449-477.
6. Xu, C.; Cao, Y.; Kumar, R.; Wu, X.; Wang, X; Scott, K. *A polybenzimidazole/sulfonated graphite oxide composite membrane for high temperature polymer electrolyte membrane fuel cells*, J. Mater. Chem., **2011**, 21, 6014.
7. Li, M., Scott, K., *A polytetrafluoroethylene/quaternized polysulfone membrane for high temperature polymer electrolyte membrane fuel cells*, Journal of Power Sources, **2011**, 196 (4) , 1894-1898
8. Chenxi Xu, Xu Wu, Xu Wang, M. Mamlouk and Keith Scott, *Composite membranes of polybenzimidazole and caesium-salts-of heteropolyacids for intermediate temperature fuel cells*, J. Mater. Chem., **2011**, 21, 6014
9. Liu, Z.; Wainright, J., Savinell R. *High-temperature polymer electrolytes for PEM fuel cells: study of the oxygen reduction reaction (ORR) at a Pt-polymer electrolyte interface*, Chem Eng Science. **2004**, 59, 4833-4838
10. Heo P., Kajiyama N., Kobayashi K., Nagao M., Sano M., and Hibino T. *Proton conduction in Sn_{0.95}Al_{0.05}P₂O₇-PBI-PTFE composite membrane*, Electrochemical and Solid-State Letters, **2008**, 11(6), B91-B95

11. Cho Y., Kim S., Kim T., Cho Y, Lim J., Jung N., Yoon W., Lee J., and Sung Y., *Preparation of MEA with the polybenzimidazole membrane for high temperature PEM fuel cell*, *Electrochemical and Solid-State Letters*, **2011**, 14 (3) B38-B40
12. Zecevic S., Wainright J., Litt M., Gojkovic S., Savinell R., *Kinetics of O₂ reduction on a Pt electrode covered with a thin film of solid polymer electrolyte*, *J Electrochem Soc.*, **1997**, 144(9):2973-2982

Chapter 9: Conclusion and Perspectives

9.1 Conclusions

Proton exchange membrane fuel cells (PEMFC) are currently based on high cost materials such as Nafion[®] membrane at low temperature. The high cost and challenges associated with low temperature operation conditions hinder the commercialization of fuel cells for future hydrogen economy. New materials for membrane and higher temperature (over 100°C) fuel cells offer advantages for operation.

Phosphoric loaded PBI offered proton conductivity operating in a range from 100-200 °C, using inorganic filler, and were considered a good option with polymer matrix to form a composite membrane for increasing conductivity. Heteropolyacid was a good conductor and can be transferred into relevant salts or introduced into other organic/inorganic systems for the development of novel proton conductors. The Cs-Heteropolyacid salt showed good conduction. The higher content of CsHPA in polymer provided the higher conductivity at a range of 10%-30%. The peak fuel cell power densities based on membranes of PBI, CsPOW/PBI, CsPOMo/PBI, CsSiOW/PBI, and CsSiOMo/PBI with a doping level of 6 were 0.43, 0.59, 0.63, 0.51, and 0.48 Wcm⁻² with atmospheric pressure oxygen, respectively. Under the same content (30%) in polymer, the CsPOMo showed the highest conductivity and fuel cell performance and CsSiOW provided the highest tensile strength. The CsHPA provided better conductivity than BmImHPA, indicating that Cs was better as a salt substitute with Heteropolyacid.

The GO/PBI, SGO/PBI, and ILGO/PBI composite membranes for a doping level of 1.9 H₃PO₄ PRU had proton conductivities of 0.027 S cm⁻¹, 0.052 S cm⁻¹, 0.025 S cm⁻¹ at 175 °C, respectively. The peak power densities of GO/PBI, SGO/PBI were 380 mW cm⁻², 600 mW cm⁻² and 320 mW cm⁻² under H₂/O₂ conditions. The GO and FGO added into PBI was a good way to improve the conductivity and reduce the PA loading. The caesium substitutes, heteropolyacid salt and graphite oxide, were good candidates using as inorganic filler in the PBI membrane for operation in a range of 100-200 °C.

A functionalised polymer (quaternary PBI) was effectively used to increase the conductivity and fuel cell performance. The quaternary ammonium PBI was used due to its higher acid absorption ability and water retention which benefits proton transport, and also the quaternary

group had a stronger bonding strength with PA. QPBI had a higher PA loading than PBI loading when treated with the same concentration of 2.0 M PA. The QPBI membrane showed 0.051 S cm^{-1} at $150 \text{ }^\circ\text{C}$ with PRU of 3.5. In fuel cell tests, power densities of 440 mW cm^{-2} and 240 mW cm^{-2} were achieved at H_2/O_2 and H_2/O_2 , respectively. Modified PBI with a functional group was another choice to improve conductivity of PBI, and the functional group may also work in other polymers such as PSU.

CsPOMo-PTFE-QDPSU and N, N-Dimethylhexadecylamine partially quaternized poly (vinyl benzyl chloride) (qPVBzCl)/PTFE composite membranes were prepared and characterised for use at a high temperature PEMFC. CsPOMo-PTFE-QDPSU (PRU 1.8) showed conductivity of 0.04 S cm^{-1} at $150 \text{ }^\circ\text{C}$ and power densities of 140 mW cm^{-2} at H_2/air at $175 \text{ }^\circ\text{C}$. PTFE/qPVBzCl/ H_3PO_4 of 5 PRU composite membranes had a peak power density of 360 mW cm^{-2} at $175 \text{ }^\circ\text{C}$. The PTFE provided the better mechanical strength, so the combination of the PTFE support frame with polymer or inorganic materials which had good conductivity but low mechanical strength is an ideal method to fit the commercial fuel cell. These studies provided a new approach for the phosphoric acid doping membrane development.

9.2 Future research recommendations

Recommendations on future work are addressed below:

1. Novel solid proton conductors such as $\text{Zr}(\text{HPO}_4)_2$ and CsHPO_4 as fillers combined with PBI to form composite membranes to reduce the requirements of free acid and moisture and to enhance the conductivity of PBI.
2. Stability and degradation studies of fuel cells based on acid loaded PBI over a longer times (over 1000 hours) operation test.
3. The properties including conductivity, mechanical strength, and gas permeability of PBI may also be improved by functionalised PBI structure, such as sulfonation, cross-linking and adding side chains and functional groups.
4. The electrode optimising based PBI system as well as including choosing the ionomer type and ratio. The novel preparation method such as catalyst coating on membrane method for MEA is also worth studying.

5. Novel polymers membrane materials for intermediate temperature PEM fuel cell. The polymer could be sulfonation polymer, quaternary polymer or polymer could form the hydrogen bond with phosphoric acid such as Polybenzoxazine [1], Polyphosphazene [2]. This synthesised polymer could also be combined with inorganic fillers to further improve the properties.
6. Develop membranes which can operate above temperatures of 200 °C. There would be no PA in this system due to the dehydration of PA at over 200 °C, such as CsHPO₄/GO and ionic liquid loaded PBI. More investigations are required to better understand the mechanism of ionic conduction in such materials to find optimising materials.
7. In order to minimise the resistance between electrodes and membranes, a catalyst ink with certain ionomer loading should be optimised. It is worth paying attention to the various conductivity ionomers (such as functionalised graphite oxide and ILHPA) and the amount of ionomers.

References

1. Kansiri Pakkethati, Ardia Boonmalert, Thanyalak Chaisuwan, Sujitra Wongkasemjit, *Development of polybenzoxazine membranes for ethanol–water separation via pervaporation*, *Desalination*, **2011**, 267 (1) , 73-81
2. Guo, Q., N. Pintauro, P., Tang, H., O'Connor, S., *nated and crosslinked polyphosphazene-based proton-exchange membranes*, *Journal of Membrane Science*, **1999**, 154 (2) , pp. 175-181

Appendix: List of Publications

Book chapter

1. Keith Scott, **Chenxi Xu**, Wu Xu, Yuancheng Cao, Ravi Kumar, *Applications of graphene and graphite oxide in fuel cell*, Invited chapter for the book of ***Innovative Graphene Technologies: Developments, Characterization and Evaluation***

Journal Papers

1. **Chenxi Xu**, Keith Scott, Qingfeng Li, Jingshuai Yang, Xu Wu, *Quaternary Polybenzimidazole Membrane for Intermediate Temperature Polymer Electrolyte membrane Fuel cells*, submitted to **Fuel Cells**
2. Keith Scott, **Chenxi Xu**, Xu Wu, *Intermediate Temperature Proton Conducting Membrane Electrolytes*, accepted by **Wiley Interdisciplinary Reviews: Energy and Environment**
3. Ravi Kumar, **Chenxi Xu** and Keith Scott, *Graphite oxide/Nafion composite membranes for polymer electrolyte fuel cells*, **RSC Advances**, 2012, 2 (23), 8777 – 8782
4. **Chenxi Xu**, Xu Wang, Xu Wu, Yuancheng Cao, Keith Scott, *A composites membrane of caesium salt of Heteropolyacid/quaternary diazabicyclo-octane polysulfone with Poly (tetrafluoroethylene) for intermediate temperature fuel cells*, **Membranes**, 2012, 2 (3), 384-394
5. Jingshuai Yang, Qingfeng Li, Lars N. Cleemann, **Chenxi Xu**, Jens Oluf Jensen, Chao Pan, Niels J. Bjerrum and Ronghuan He, *Synthesis and properties of poly(aryl sulfone benzimidazole) and its copolymers for high temperature membrane electrolytes of fuel cells*, **Journal of Materials Chemistry**, 2012, 22, 11185
6. **Chenxi Xu**, Yuancheng Cao, Ravi kumar, Xu Wu, Xu Wang, Keith Scott, *A Polybenzimidazole/ Sulphonated Graphite Oxide Composite Membrane for High Temperature Polymer Electrolyte membrane Fuel cells*, **Journal of Materials Chemistry**, 2011, 21 (30), 11359 – 11364
7. Xu Wang, **Chenxi Xu**, Bernard T. Golding, Masih Sadeghi, Yuancheng Cao, Keith Scott, *A novel phosphoric acid doped quaternary 1,4-diazabicyclo-[2.2.2]-octane polysulfone membrane for intermediate temperature fuel cell*, **International Journal of Hydrogen**

- Energy** 36 (14), 2011, pp. 8550-8556
8. Yuan-Cheng Cao, **Chenxi Xu (the equally first author)**, Xu Wu, Xu Wang, Lei Xing, Keith Scott, *A poly (ethylene oxide)/graphene oxide electrolyte membrane for low temperature polymer fuel cells*, **Journal of Power Sources**, 196 (2011) 8377–8382
 9. **Chenxi Xu**, Xu Wu, Xu Wang, Mohamed Mamlouk, and Keith Scott, *Composite membranes of Polybenzimidazole and Caesium-Salts-of-Heteropolyacids for Intermediate temperature fuel cells*, **Journal of Materials Chemistry**, 2011, 21, 6015-6019